


5-2018

# Liquefaction-induced Dragload and/or Downdrag on Deep Foundations within the New Madrid Seismic Zone

Ishimwe Elvis

University of Arkansas, Fayetteville

Follow this and additional works at: <http://scholarworks.uark.edu/etd>

 Part of the [Civil Engineering Commons](#), [Geophysics and Seismology Commons](#), [Geotechnical Engineering Commons](#), and the [Structural Engineering Commons](#)

---

## Recommended Citation

Elvis, Ishimwe, "Liquefaction-induced Dragload and/or Downdrag on Deep Foundations within the New Madrid Seismic Zone" (2018). *Theses and Dissertations*. 2766.  
<http://scholarworks.uark.edu/etd/2766>

This Dissertation is brought to you for free and open access by ScholarWorks@UARK. It has been accepted for inclusion in Theses and Dissertations by an authorized administrator of ScholarWorks@UARK. For more information, please contact [scholar@uark.edu](mailto:scholar@uark.edu), [ccmiddle@uark.edu](mailto:ccmiddle@uark.edu).

Liquefaction-induced Dragload and/or Downdrag on Deep Foundations within the New Madrid  
Seismic Zone

A dissertation submitted in partial fulfillment  
of the requirements for the degree of  
Doctor of Philosophy in Engineering

by

Elvis Ishimwe  
University of Arkansas  
Bachelor of Science in Civil Engineering, 2013  
University of Arkansas  
Master of Science in Civil Engineering, 2014

May 2018  
University of Arkansas

This dissertation is approved for recommendation to the Graduate Council.

---

Richard A. Coffman, Ph.D., P.E., P.L.S.  
Dissertation Director

---

Kyle Rollins, Ph.D.  
Committee Member

---

Christopher Liner, Ph.D.  
Committee Member

---

Michelle Bernhardt, Ph.D., P.E.  
Committee Member

## ABSTRACT

Deep foundation elements are typically used to transfer structural loads for multi-story buildings and large-span bridges to a competent soil layer when 1) the soil close to the ground surface has no sufficient bearing capacity, and when 2) liquefiable soils are encountered. The majority of the bridges constructed within seismic zones rely upon the stability of earthen embankments and deep foundation that are installed above or within liquefiable soil deposits. Despite large factor of safety values or different load and resistance factors being used to adequately design deep foundations within seismic areas, soil liquefaction may cause extensive damage to the structure by 1) reducing the axial geotechnical resistances, 2) reducing the lateral load capacity, 3) adding additional loads to the foundation (dragload), 4) inducing excessive foundation settlements (downdrag), and 5) causing lateral spreading on the soil surrounding the foundation.

The compressive movement of the soil caused by liquefaction affects the distribution of the load along a deep foundation. Dragloads are developed when the amount of the soil settlement is larger than the amount of foundation settlement. According to Muhunthan et al. (2017), the developed dragload may exceed the structural axial strength of the deep foundation in the extreme events. This additional load can significantly impact the axial behavior of a deep foundation. In addition, the liquefaction-induced settlements may affect serviceability of the structure by causing downdrag on the installed deep foundation element.

Many of the existing design methods to address dragload and downdrag are based on the consolidation phenomenon. Therefore, there is an immediate need for research to evaluate the impact of liquefaction-induced dragload and dragload on the performance of deep foundation elements constructed in earthquake prone areas. Full-scale axial load tests and full-scale blast-

induced liquefaction tests were performed around three drilled shaft foundations and three driven pile foundations to 1) evaluate the existing design methods, and 2) investigate the effects of liquefaction-induced dragload and downdrag on deep foundations. The tested foundations were constructed at the Turrell Arkansas Test Site (TATS), located within the New Madrid Seismic Zone (NMSZ), and Mississippi Embayment.

## ACKNOWLEDGMENTS

I would like to acknowledge my advisor Dr. Richard Coffman for his guidance, insightful criticisms, and for the opportunity to perform this research project. I would also like to acknowledge my committee members, Dr. Kyle M. Rollins, Dr. Michelle Bernhardt, and Dr. Christopher Liner for being extraordinary committee members. I would like to extend my acknowledgement to the following organizations, and companies for providing the labor, materials, and valuable information needed to make this research project possible:

- AFT Specialty Geotechnical Services
- Arkansas Department of Transportation (ARDOT)
- Chris-Hill Construction
- Deep Foundation Institute (DFI)
- Duane Houkom, Inc.
- Fugro (Loadtest, Inc.)
- GEI Consulting Engineers and Scientists
- GRL Engineers, Inc.
- International Construction Equipment (ICE)
- International Association of Foundation Drilling (ADSC-IAFD)
- Kolb Grading
- Missouri Department of Transportation (MODOT)
- McKinney Drilling Company
- Nucor-Yamato Steel
- Pile Driving Contractors Association (PDCA)
- Skyline Steel
- Texas Concrete Partners
- W&W AFCO Steel

In addition, I would like to thank my geotechnical research team: Sarah Bey, Cyrus Garner, Morgan Race, and Sean Salazar for their assistance and friendship. Finally, I would like to dedicate this dissertation to my loving, caring, and very supportive parents, Hanyurwimfura Pascal-Baylon and Ingabire Marie Rose.

## TABLE OF CONTENTS

<b>CHAPTER 1: Introduction</b> .....	<b>1</b>
1.1. Background.....	1
1.2. Need for the Research Study.....	1
1.3. Research Objectives.....	2
1.4. Scope of Work.....	3
1.5. Dissertation Overview.....	4
1.6. References.....	5
<b>CHAPTER 2: Controlled Blast Testing</b> .....	<b>8</b>
2.1. Chapter Overview.....	8
2.2. Controlled Blast Testing.....	8
2.3. Predicting Excess Porewater Pressure Ratio.....	12
2.3.1. Studer and Kok (1980).....	13
2.3.2. Veyera (1985).....	14
2.3.3. Hubert (1986).....	15
2.3.4. Charlie et al. (1992).....	15
2.3.5. Al-Qasimi et al. (2005).....	16
2.3.6. Charlie et al. (2013).....	16
2.3.7. Eller (2011).....	17
2.4. Predicting Blast-induced Peak Particle Velocity.....	17
2.5. Existing Threshold Values of PPV, $\epsilon_p$ and SD Required for Liquefaction.....	18
2.6. Liquefaction-induced Settlements in Saturated Sands.....	20
2.7. Chapter Summary.....	21
2.8. References.....	22
<b>CHAPTER 3: Design of Deep Foundation Elements and Analysis of Dragload and Downdrag</b> .....	<b>28</b>
3.1. Chapter Overview.....	28
3.2. Estimation of Geotechnical Axial Resistance.....	28
3.2.1. Unit Shaft and Toe Resistance in Cohesive Soils.....	29
3.2.2. Unit Shaft and Resistance in Cohesionless Soils.....	30
3.3. Prediction of Axial Resistance using Software Programs.....	31
3.3.1. FB-Deep.....	31
3.3.2. UNIPILE.....	32
3.4. Full-scale Axial Compression Load Testing of Deep Foundations.....	33

3.4.1. Conventional Top-Down Load Test .....	33
3.4.2. Bi-directional Load Cell Test.....	35
3.4.3. High Strain Dynamic Load Test .....	38
3.5. Development of Negative Shaft Resistance (Dragload) .....	40
3.5.1. Current Understanding of Dragload and Downdrag.....	41
3.5.2. Liquefaction-induced Dragload and Downdrag.....	44
3.5.2.1. Boulanger and Brandenberg (2004).....	44
3.5.2.2. Fellenius and Siegel (2008) .....	45
3.5.2.3. Rollins and Strand (2006) .....	47
3.5.2.4. Rollins and Hollenbaugh (2015).....	48
3.5.3. Liquefaction-induced Dragload and Downdrag Analysis in Design Codes .....	51
3.6. Chapter Summary .....	52
3.7. References.....	52
<b>CHAPTER 4: Turrell Arkansas Test Site Description .....</b>	<b>59</b>
4.1. Chapter Overview .....	59
4.2. Geology and NMSZ Faults .....	59
4.3. Evidence of Liquefaction within the NMSZ.....	63
4.4. Turrell Test Site Description.....	64
4.5. Geotechnical Site Characteristics .....	65
4.6. Chapter Summary .....	67
4.7. References.....	67
<b>CHAPTER 5: Predicted Geotechnical Axial Resistances and Dragloads .....</b>	<b>70</b>
5.1. Chapter Overview .....	70
5.2. Prediction of Axial Resistance and Dragload around Drilled Shafts.....	70
5.3. Dragload Analysis for Drilled Shafts.....	74
5.4. Prediction of Axial Resistance and Dragload around Driven Piles .....	75
5.5. Dragload Analysis for Driven Piles .....	78
5.6. Chapter Summary .....	79
5.7. References.....	79
<b>CHAPTER 6: Pilot Liquefaction Blast Test.....</b>	<b>81</b>
6.1. Chapter Overview .....	81
6.2. Abstract:.....	82
6.3. Background.....	82
6.4. Predicting Excess Porewater Pressure Ratio.....	84

6.5. Existing Threshold Values of PPV, $\epsilon_p$ and SD Required for Liquefaction.....	86
6.6. Controlled blasting Tests as Ground Improvement Method.....	87
6.7. Geotechnical Site Characteristics .....	88
6.8. Blast-induced Liquefaction Tests .....	90
6.9. Results and Discussion .....	92
6.9.1. Excess Porewater Pressure Ratio Results .....	92
6.9.2. Pre-and post-blast CPT Measurements.....	95
6.10. Proposed Empirical Model .....	97
6.11. Conclusions.....	100
6.12. Acknowledgements.....	100
6.13. References.....	100
<b>CHAPTER 7: Liquefaction-induced Dragload and Downdrag on Drilled Shaft Foundations</b> .....	<b>107</b>
7.1. Chapter Overview .....	107
7.2. Additional Information .....	107
7.3. Abstract .....	111
7.4. Introduction.....	112
7.5. Background.....	114
7.6. Geotechnical Site Characteristics .....	120
7.7. Testing Program.....	122
7.8. Blast-induced Liquefaction Test Results .....	125
7.8.1. Excess Porewater Pressure Ratio Results .....	125
7.8.2. Post-Blast Ground Surface Settlements .....	127
7.8.3. Pre-and Post-Blast Loads and Settlements Distribution Curves.....	128
7.9. Estimating Post-Blast Load and Resistance Distribution Curves .....	133
7.10. Conclusions.....	137
7.11. Acknowledgements.....	139
7.12. References.....	139
<b>CHAPTER 8: Liquefaction-induced Dragload and Downdrag on Driven Pile Foundations</b> .....	<b>144</b>
8.1. Chapter Overview .....	144
8.2. Abstract .....	145
8.3. Introduction.....	145
8.4. Background.....	146
8.5. Site Characteristics.....	149



8.6. Testing Program.....	150
8.6.1. Test Layout and Instrumentation .....	150
8.6.2. Blast-induced Liquefaction Tests .....	152
8.7. Test Results .....	153
8.7.1. Pre-Blast Axial Capacities Results .....	153
8.7.2. Excess Porewater Pressure Ratio Results .....	153
8.7.3. Post-blast Ground Surface Settlements.....	154
8.7.4. Pre-and Post-Blast Loads and Settlements Distribution Curves.....	155
8.8. Proposed Analytical Method.....	159
8.9. Conclusions.....	161
8.10. Acknowledgements.....	162
8.11. References.....	162
<b>CHAPTER 9: Conclusions and Recommendations .....</b>	<b>166</b>
9.1. Chapter Overview .....	166
9.2. Conclusion on Controlled Blast Testing (Pilot Liquefaction Test) .....	166
9.3. Conclusion on Liquefaction-induced Dragload around Deep Foundations.....	167
9.4. Recommendations.....	168
<b>APPENDIX A: Construction Procedures and Blasting Tests around Drilled Shafts and Driven Piles.....</b>	<b>170</b>
A.1. Overview.....	170
A.2. Construction of Drilled Shafts .....	170
A.3. Construction and Installation of Driven Piles .....	171
A.4. Test Instrumentation .....	178
A.5. Top Down Load Application .....	185
A.6. Controlled Blasting around Drilled Shafts and Driven Piles .....	187
A.7. References.....	189
<b>APPENDIX B: Geotechnical Site Investigation Information .....</b>	<b>191</b>
<b>APPENDIX C: Porewater Pressure Data.....</b>	<b>196</b>
<b>APPENDIX D: Alternative Approach for Liquefaction-induced Dragload .....</b>	<b>199</b>

## LIST OF FIGURES

Figure 2.1. Explosive charge weight as a function of radial distance (R) for determination of liquefaction based on excess porewater pressure ratio (modified from Studer and Kok 1980). ..	14
Figure 3.1. A schematic of an axially loaded deep foundation.....	29
Figure 3.2. A photograph of a dead weight being applied to a drilled shaft foundation (photo courtesy of Elvis Ishimwe). .....	34
Figure 3.3. A schematic of a platform loaded by concrete blocks (courtesy of Ganpati Construction Company). .....	34
Figure 3.4. A photograph of conventional static load test being conducted on a drilled shaft foundation [photograph by Bill Isenhower and presented in Brown et al. (2010)]. .....	35
Figure 3.5. Bi-directional load cell (O-Cell) installed within a drilled shaft foundation (courtesy of Loadtest. Inc.).....	36
Figure 3.6. Example of bi-directional load cell (O-Cell) test results: (a) measured upward and downward movement curves and (b) equivalent top-down load and settlement curve (modified from Brown et al. (2010). .....	38
Figure 3.7. (a) accelerometer, strain transducer, and WIFI transmitter utilized during pile dynamic tests [photograph Pile Dynamics presented in Hannigan et al. (2016)], and (b) pile driving analyzer (photo courtesy of Pile Dynamics, Inc.) .....	39
Figure 3.8. Example of CAPWAP output results (Coffman and Ishimwe 2017).....	40
Figure 3.9. Load and resistance distribution curves when the liquefied zone is located above the static neutral plane (from Fellenius and Siegel 2008). .....	45
Figure 3.10. Load and resistance distribution curves when the liquefied zone is located below the static neutral plane (from Fellenius and Siegel 2008). .....	46
Figure 3.11. Load and resistance distribution curves as obtained before and after blasting (from Rollins and Strand 2006). .....	47
Figure 3.12. Plan view of the testing site (Rollins and Hollenbaugh 2015). .....	49
Figure 3.13. Cross sectional layout of the testing site (from Rollins and Hollenbaugh 2015).....	49
Figure 3.14. Post-blast and predicted load and resistance distribution curves (from Rollins and Hollenbaugh 2015).....	50
Figure 4.1. Locations of Reelfoot rift boundaries and Mississippi Embayment (modified from Csontos and Arsdale 2008). .....	60

Figure 4.2. A schematic of the faults within the NMSZ (modified from Csontos and Arsdale 2008).	62
Figure 4.3. A photograph of a sand blow and sand dikes observed in the NMSZ (After USGS 2018).	63
Figure 4.4. (a) Site location map and (b) detailed site layout of the site (From Coffman 2015)..	65
Figure 4.5. Test site layout, including the locations of SPT, CPT soundings, drilled shafts, and driven piles.	66
Figure 4.6. Photographs of the MODOT CPT rig.	67
Figure 5.1. Load and resistance distribution curves along the (a) North, (b) Center, and (c) South drilled shaft foundation as obtained using AASHTO design guide method.	72
Figure 5.2. Load and resistance distribution curves along the (a) North, (b) Center, and (c) South drilled shaft foundation as obtained using FB-Deep program.	72
Figure 5.3. Distribution of (a) load and resistance and (b) drilled shaft-soil settlement around the North drilled foundation, as obtained using UNIPILE program.	73
Figure 5.4. Distribution of (a) load and resistance and (b) drilled shaft-soil settlement around the Center drilled foundation, as obtained using UNIPILE program.	73
Figure 5.5. Distribution of (a) load and resistance and (b) drilled shaft-soil settlement around the South drilled foundation, as obtained using UNIPILE program.	74
Figure 5.6. Load and resistance distribution curves along (a) steel H pile, (b) Steel pipe pile, and (c) pre-stressed concrete pile, as obtained using AASHTO design guide.	76
Figure 5.7. Load and resistance distribution curves along the (a) steel H pile, (b) Steel pipe pile, and (c) pre-stressed concrete pile, as obtained using FB-Deep program.	76
Figure 5.8. Distribution of (a) load and resistance and (b) drilled shaft-soil settlement around the steel H pile foundation, as obtained using UNIPILE program.	77
Figure 5.9. Distribution of (a) load and resistance and (b) drilled shaft-soil settlement around the steel pipe pile foundation, as obtained using UNIPILE program.	77
Figure 5.10. Distribution of (a) load and resistance and (b) drilled shaft-soil settlement around the pre-stressed pile foundation, as obtained using UNIPILE program.	78
Figure 6.1. (a) Interpreted soil profile (b) average cone tip resistance ( $q_c$ ), (c) average sleeve friction ( $f_s$ ), (d) relative density ( $D_r$ ) and (e) soil type behavior index ( $I_c$ ) at the TATS.	89
Figure 6.2. (a) Plan view and (b) cross-section with the locations of blast ring, explosive charges, piezometers, string potentiometers, and CPT soundings at the TATS.	91

Figure 6.3. Measured excess porewater pressure ratio values as a function of time, as obtained from inner and outer rings.....	93
Figure 6.4. Post-blast ground surface settlements as obtained from string potentiometers.....	94
Figure 6.5. Comparison between measured and predicted PPV values as a function of cubic root-scaled distances. ....	95
Figure 6.6. Pre-and post-blast CPT measurements from the northern testing location. ....	96
Figure 6.7. Pre-and post-blast CPT measurements from the western testing location. ....	96
Figure 6.8. Measured and predicted excess porewater pressure ratio values as a function of depth, as obtained using charge weight of 0.91 kg per deck per borehole, and Equations 2.2, 6.1, and 2.10, for determination of $R_u$ , SD, and PPV, respectively.....	98
Figure 6.9. Predicted excess porewater pressure ratio as a function of depth, as obtained using existing empirical equations and the new proposed equation (Equation 6.3) for inner and outer rings, respectively. ....	99
Figure 7.1. Plan view and a cross-section of the TATS with locations of explosive charges, piezoresistive piezometers, Sondex tube and CPT locations around drilled shaft foundations..	108
Figure 7.2. (a) Pre-and post-blast load and resistance distribution curves, (b) drilled shaft-soil settlement curves, as obtained from the South drilled shaft foundation. ....	108
Figure 7.3. Measured excess porewater pressure ratio values at different depths as a function of time following blasting around the South drilled shaft.....	109
Figure 7.4. Post-blast soil settlements following the third blast event around the South drilled shaft.....	110
<b>Figure 7.5.</b> (a) Water flowing to the ground and (b) ground settlement following blasting (Photography by the author). ....	110
Figure 7.6. A schematic of a typical deep foundation and the corresponding total resistance distribution curve. ....	115
Figure 7.7. A schematic of (a) an axially loaded drilled shaft foundation, (b) a drilled shaft foundation subjected to dragload and downdrag due to the settlement of the surrounding soil, (c) load and resistance distribution curves, and (d) drilled shaft-soil settlement distribution curves (modified from Fellenius 1984). ....	117
Figure 7.8. (a) Interpreted soil profile (b) cone tip resistance ( $q_c$ ), (c) SPT blow count ( $N_{60}$ ), (d) relative density ( $D_r$ ) and (e) soil type behavior index ( $I_c$ ) at the TATS.....	121
Figure 7.9. Plan view and a cross-section of the TATS with locations of drilled shaft foundations, explosive charges, piezometers, surveying stakes, Sondex tubes, and CPT soundings. ....	123

Figure 7.10. Measured excess porewater pressure ratio values at different depths, as a function of time for: (a) the first blast-induced liquefaction event around the North drilled shaft and (b) the second blast-induced liquefaction event around the South drilled shaft.....	125
Figure 7.11. Soil type behavior index ( $I_c$ ) obtained from the CPT soundings performed at the (a) the first and (b) second blast events.....	126
Figure 7.12. Post-blast soil settlements following liquefaction around (a) the North drilled shaft foundation and (b) the South drilled shaft foundation.....	128
Figure 7.13. Load shed as a function of depth as obtained for a) the North and b) the South drilled shaft foundation during the application of the beam blanks.....	129
Figure 7.14. (a) Pre- and post-blast load and resistance curves and (b) drilled shaft and soil settlement distribution curves, as obtained for the North drilled shaft foundation.....	130
Figure 7.15. (a) Pre-and post-blast load and resistance curves and (b) drilled shaft and soil settlement distribution curves, as obtained for the South drilled shaft foundation following blasting.....	132
Figure 7.16. (a) Analysis of an axially loaded drilled shaft foundation subjected to liquefaction. For load curve, $i$ sum starts from the top of the drilled shaft and progress to the toe location. For the resistance curve, $j$ sum starts from the toe location and progress to the top of the drilled shaft foundation. Predicted and measured load and resistance distribution curves as obtained for: (b) the North drilled shaft and (c) the South drilled shaft foundation. ....	135
Figure 7.17. (a) Measured load and resistance distribution and drilled shaft load-settlement curves as obtained for the a) North and b) South drilled shaft foundations. ....	136
Figure 8.1. A schematic of load and resistance distribution curves and pile-soil settlement distribution curves when the liquefied layer is located (a) above the neutral plane, and (b) below the neutral plane (modified from Fellenius and Siegel 2008).....	148
Figure 8.2. (a) Interpreted soil profile (b) average cone tip resistance ( $q_c$ ), (c) average SPT blow count ( $N_{60}$ ), and (d) relative density ( $D_r$ ) correlated from CPT soundings.....	150
Figure 8.3. (a) Plan view, and (b) cross-section of the testing site with locations of driven piles foundations, explosive charges, piezometers, surveying stakes, Sondex tubes, and CPT soundings. ....	151
Figure 8.4. Measured excess porewater pressure ratio values at different depths, as a function of time, as obtained following the: (a) first (b) second, and c) third blast events surrounding the steel H-pile, pipe pile, prestressed concrete pile, respectively. ....	154
Figure 8.5. Post-blast soil settlements following liquefaction, as obtained following the: (a) first, (b) second, and c) third blast events.....	155

Figure 8.6. Load distribution, as a function of depth, as observed for: a) Steel H-pile and b) steel pipe pile during the application of the beam blanks. The imbedded strain gauge data for the square concrete pile was not recovered due to weatherproofing problems within the communication cables for the strain gauges. ....	156
Figure 8.7. (a) Pre- and post-blast load and resistance distribution curves and (b) pile and soil settlement distribution curves, as obtained around the H-pile. ....	157
Figure 8.8. (a) Pre- and post-blast load and resistance distribution curves and (b) pile and soil settlement distribution curves, as obtained around the steel pipe pile. ....	158
Figure 8.9. (a) Pre- and post-blast load and resistance distribution curves and (b) pile and soil settlement distribution curves, as obtained around the pre-stressed pile (No after beam blanks curve due to weatherproofing problems within the communication cables for the strain gauges). ....	158
Figure 8.10. (a) Predicted and measured load and resistance distribution curves as obtained for: (a) steel H pile, (b) steel pipe pile, and (c) prestressed concrete pile. ....	161
Figure A.1. Photographs of (a) the installation of the rebar cage (b) the concrete being placed into a cased hole, and (c) a constructed drilled shaft foundation (north drilled shaft) at the Turrell Arkansas Test Site (Courtesy of Morgan Race). ....	171
Figure A.2. Schematic of the reinforcement details of the square pre-stressed, pre-cast concrete pile. ....	172
Figure A.3. Photographs of (a) a seven-wire 270 grade strand, (b) the W4.0 spiral wires being installed around the pre-stressed strands within the square pre-stressing bed prior to pre-stressing process and concrete placement, and (c) the concrete being placed into the pre-stressing bed (Photo by author). ....	173
Figure A.4. Photographs of (a) a slump test being conducted on the concrete mix, (b) the collected concrete cylinders (four-inch diameter and 8-inch long) acquired immediately after pouring the concrete into the pre-stressing bed, and (c) a test specimen (at failure) within a compression testing machine. (Photo by author). ....	174
Figure A.5. Photographs of (a) the steel pipe pile , and (b) pre-stressed pile being delivered at the TATS. ....	174
Figure A.6. Photographs of (a) Kobelco crane parts being delivered at the TATS, (b) a completed Kobelco crane with a boom before attaching the swinging leads and hammer system. ....	175
Figure A.7. Photographs of (a) a helmet being mounted to the ICE I-30 diesel hammer, and (b) the ICE-I-30 hammer being mounted to the swinging leads attached to the crane. ....	176
Figure A.8. Photographs of (a) two HP 14x117 sections being delivered on the testing site, (b) HP 14x117 being unloaded from the truck using the crane, (c) the mechanical splicer, and (d) the	

top segment of the H-pile being placed into the splicer and the welded to the bottom segment of the H-pile. .... 177

Figure A.9. Photographs of (a) the strain transducer, accelerometer, and WIFI transmitter utilized during pile dynamic load tests, (b) the Pile Driving Analyzer (PDA) being performed while driving the HP section. Fuel settings being changed during the installation of (c) the pipe pile and (d) the pre-stressed pile. .... 178

Figure A.10. Photograph of the linear vibrating wire strain gauge being mounted on the reinforcement cage (Photo courtesy of Sarah Bey, Bey 2014). .... 179

Figure A.11. Photographs of (a) the piezoresistive strain gauges assembly with end blocks and strain gauge cables attached on flange of the bottom segment of the H-pile, and (b) the protection angle iron covering the strain gauges (Photo courtesy by the author).. .... 180

Figure A.12. Photographs of (a) the strain gauge attached to sister bar and zip-tied on the 2-inch diameter PVC pipes, and (b) the strain gauge cables exiting from the completed pipe (Photo courtesy by the author). .... 181

Figure A.13. Photographs of (a) the piezoresistive strain gauges utilized for driven piles at the TATS, and (b) the sister bar strain gauge tied to a sister bar and attached to the spirals prior to the concrete pouring (Photo courtesy by the author). .... 181

Figure A.14. Photographs of (a) a typical piezoresistive piezometer utilized at the TATS, (b) the piezometers inserted within nylon cone tip and being saturated prior to installation, and (c) the piezometer component that includes, nylon cone tip, a retrieval cable, and an electric cable, attached on a push rod (Photo courtesy by the author). .... 182

Figure A.15. Photographs of (a) the installation of Sondex tube components, including the corrugated pipe metal clamps, PVC pipe (inserted within the corrugated pipe), (b) installed string potentiometers, (c) surveying stakes and automatic level utilized at the TATS, and (d) Leica digital level rods being attached at the top of the North drilled shaft foundation (Photo courtesy by the author). .... 184

Figure A.16. Photographs of the instantel minimize blast seismographs installed before blast-induced liquefaction tests (Photo courtesy by the author). .... 185

Figure A.17. Photographs of (a) beam blanks being placed at the top of the north drilled shaft, and (b) an axial load of 352.40 kips placed at the top of the North drilled shaft (Photo courtesy by the author). .... 186

Figure A.18. Photographs of (a) the crane that was used to move the beam blanks from a truck to the H pile, (b) the steel load distribution plate being reloaded from a truck, (c) the load distribution plate being placed at the top of the H-pile, and (d) the beam blanks being placed at the top of the H-pile (courtesy of Richard Coffman). .... 186

Figure A.19. Photographs of (a) the Dyno emulsion explosive, and (b) the charge being placed into the pre-drilled and cased hole (Photo courtesy by the author). .... 187

Figure A.20. (a) Explosive charge pattern for the three blast events, and (b) a photograph of the TATS before blasting the soil around the Center drilled shaft and the closed ended steel pipe pile.....	189
Figure B.1. Generalized soil profile, CPT measurements, total unit weight, relative density, shear strength, friction angle, SPT- $N_{60}$ and the soil index behavior correlated from these CPT measurements at the drilled shaft locations (data from Bey 2014).....	191
Figure B.2. Generalized soil profile, CPT measurements, total unit weight, relative density, shear strength, friction angle, SPT- $N_{60}$ and the soil index behavior correlated from these CPT measurements at the driven piles locations.....	192
Figure B.3. Pre-and post-blast CPT measurements from the northern testing location. ....	193
Figure B.4. Pre-and post-blast CPT measurements from the center testing location. ....	193
Figure B.5. Pre-and post-blast CPT measurements from the southern testing location. ....	194
Figure B.6. Generalized soil profile of the TATS and comparison between CPT data collected around drilled shaft and driven pile foundations. ....	195
Figure C.1. Measured excess porewater pressure as a function of time, as obtained from: (a) north, (b) center (c) south drilled shafts, respectively. ....	196
Figure C.2. Measured excess porewater pressure as a function of time, as obtained from: (a) steel H-pile, (b) Steel pipe (c) prestressed concrete pile, respectively.....	196
Figure C.3. Measured excess porewater pressure ratio as a function of depth, as obtained from: (a) north, (b) center (c) south drilled shafts, respectively. ....	197
Figure C.4. Measured excess porewater pressure ratio as a function of depth, as obtained from: (a) steel H-pile, (b) Steel pipe (c) prestressed concrete pile, respectively. ....	198
Figure D.1. A schematic of the alternative approach for liquefaction-induced dragloads. ....	199
Figure D.2. Developed Q-z, t-z curves, the amount of toe resistance, side resistance and the settlement developed around the North drilled shaft. ....	201
Figure D.3. Developed Q-z, t-z curves, the amount of toe resistance, side resistance and the settlement developed around the Center drilled shaft.....	202
Figure D.4. A comparison between the post-blast and predicted load and resistance distribution curves, as obtained for North drilled shaft.....	203
Figure D.5. A comparison between the post-blast and predicted load and resistance distribution curves, as obtained for Center drilled shaft. ....	203



## LIST OF TABLES

Table 2.1. Summary of existing empirical equation models to predict $R_u$ .....	13
Table 2.2. Summary of existing equation models to predict PPV.....	18
Table 2.3. Summary of existing thresholds of PPV, $\varepsilon_p$ , and SD required for liquefaction.....	19
Table 3.1. O-Cell load testing program instrumentation (after Miller 2003). ....	37
Table 5.1. Drilled shaft foundations properties. ....	70
Table 5.2. Magnitude of dragload and the neutral plane locations, as predicted using FB-Deep, UNIPILE and spreadsheet method.....	75
Table 5.3. Magnitude of dragload and the neutral plane locations for the piles at the TATS, as predicted using FB-Deep, UNIPILE, and spreadsheet method. ....	79
Table 8.1. A summary of CAPWAP results. ....	153

## LIST OF PUBLISHED PAPERS

Chapter 6: Ishimwe, E., Coffman, R.A., Rollins, K.M., (2018). “Predicting Blast-induced Liquefaction within the New Madrid Seismic Zone.” International Journal of Geomechanics. (Under second review).

Chapter 7: Ishimwe, E., Rollins, K.M., Coffman, R.A., (2018). “Dragload and Downdrag around Drilled Shafts following Blast-induced Liquefaction.” Journal of Geotechnical and Geoenvironmental Engineering (Under review).

Chapter 8: Rollins, K.M., Luke, I. K., Ishimwe, E., Coffman, R.A., (2018). “Analysis of Liquefaction-induced Dragload and Downdrag on Driven Pile Foundations.” Journal of Geotechnical and Geoenvironmental Engineering (Under review).

## CHAPTER 1: Introduction

### 1.1. Background

Liquefaction in loose, saturated sands has caused extensive damage to infrastructure (e.g., bridges abutments and embankments, roads, buildings, power, and water supplies) in nearly every historical earthquake event. In addition, soil liquefaction and the resulting loss of shear strength have led to landslides, lateral spreading at the location of bridge abutments and wharfs, and have caused failures of earthfill dams, loss of vertical and lateral bearing support for foundations due to excessive settlement. These catastrophic failures have caused economic losses in various areas in the world. For instance, more than 250 bridges were damaged by soil liquefaction phenomena during the 1964 Alaska earthquake. Most of the damage observed after the 1964 Alaska earthquake and after other earthquakes, including the 1964 Niigata earthquake, the 1989 Loma Prieta earthquake, the 2010 Maule earthquake, and the 2011 New Zealand earthquake was attributed to the soil liquefaction (Gallagher et al. 2007).

### 1.2. Need for the Research Study

The current knowledge regarding the development of dragload and downdrag that is presented in several standard design codes, is based on the soil settlement related to consolidation phenomena. For instance, several designers and researchers have performed field and laboratory tests (e.g., Bjerrum et al. 1969, Endo et al. 1969, Bozozuk 1972, Bozozuk 1981, Broms and Silberman 1964, Long and Healy 1974, Fellenius and Broms (1969), Fellenius 1972, 1979, and 1988, Davisson 1993, Briaud and Tucker 1997, Poulos 1997, Dumas 2000, Hannigan et al. 2005, Fellenius 2006, Fellenius and Siegel 2008, Siegel et al. 2013, Hannigan et al. 2016, Tan and Fellenius 2016) to address consolidation-dragload and downdrag in deep foundation design. Only a few research studies have been conducted to evaluate the liquefaction-induced dragload and downdrag (Boulanger and Brandenburg 2004, Rollins and Strand 2006, Fellenius

and Siegel 2008, Vijayaruban et al. 2015, Rollins and Hollenbaugh 2015, and Muhunthan et al. 2017).

The research discussed herein was required because there is an absence of test results to validate different aforementioned analytical and empirical methods that were developed to determine the behavior of deep foundations subjected to the dragload and/or downdrag induced by soil liquefaction. In addition, the analysis of post-liquefaction axial geotechnical resistance, of deep foundation elements in Northeast Arkansas, will provide insight into deep foundation behavior following an earthquake event. A comparison of the measured and predicted pre- and post-liquefaction axial geotechnical for full-scale driven pile and full-scale drilled shaft foundation elements will be presented and discussed in this document. Most importantly, the findings from this research will be transferred into suitable recommendations and approaches that the Arkansas Department of Transportation (ARDOT), and other state agencies, can use to design for liquefaction-induced dragload and downdrag.

### **1.3. Research Objectives**

The main objective of this research study is to determine the amount of liquefaction-induced dragload and/or downdrag, and utilized to quantify the effects of an earthquake on deep foundation elements installed within a potentially liquefiable soil deposit. The following specific tasks were to be completed to accomplish this research objective.

- Conduct a pilot blast-induced liquefaction test program to determine the blasting layout (the appropriate amount of explosive charges, the detonation delays, and the charge spacing) required to produce soil liquefaction for full-scale blast tests.
- Design different types of driven piles, including: the steel H-pile, steel pipe pile and pre-stressed, post-tensioned, concrete pile.

- Analyze the full-scale dynamic testing results that were obtained during pile driving and during restrike.
- Evaluate the full-scale blast-induced liquefaction test results around three different drilled shaft foundation elements and around the three aforementioned driven pile foundation elements.
- Determine the amount of liquefaction-induced dragload and downdrag, and evaluate the effect of liquefaction of deep foundation behavior.
- Determine the pre-and post-blast load and resistance distribution curves.
- Determine the driven pile or drilled shaft and soil settlement distribution curves.
- Evaluate the neutral plane approach, as recommended by Fellenius (1984, 2004) on liquefaction-induced dragload using the test results obtained from this research.

#### **1.4. Scope of Work**

The research project was divided into two phases: 1) a pilot blast-induced liquefaction test on soil with no deep foundation elements and 2) full-scale blast-induced liquefaction tests with the soil containing deep foundation elements. The primary purpose of the first phase was to 1) confirm liquefaction at the testing site, and 2) determine the blasting layout (the appropriate amount of explosive charges, the detonation delays, and the charge spacing) required to produce liquefaction at the testing site. The second phase consisted of the 1) installation of driven pile foundations, 2) installation of various devices into the surrounding soil, including Sondex tubes, piezometers, and, surveying stakes and digital rod levels), 3) performance of pre- and post-blast SCPT tests, 4) performance of pre-blast, full-scale axial load tests, and 5) performance of full-scale blast-induced liquefaction in the soil surrounding driven pile and drilled shaft foundations.

## 1.5. Dissertation Overview

This dissertation is divided into nine chapters. The introduction containing the research background, need for this research project, research objectives, and the scope of the research work is discussed in Chapter 1. The literature review of this research study is presented in Chapter 2 and 3. Specifically, a literature review on controlled blast tests or blast-induced liquefaction tests is presented in Chapter 2. A literature review of the design and full-scale load test of drilled shaft and driven piles foundation elements is presented in Chapter 3. The development of dragload and downdrag from consolidation and liquefaction, and the design recommendations are also discussed in Chapter 3. The geology, and the geotechnical site information of the TATS is discussed in Chapter 4. The prediction of axial resistance and dragloads around the drilled shaft and driven piles are presented and discussed in Chapter 5. A journal paper discussing the prediction of blast-induced liquefaction within the New Madrid Seismic Zone is presented herein as Chapter 5. The existing and new empirical methods used to predict the excess porewater pressure ratios and amount of explosive charge weight required during controlled blasting are also discussed in journey paper that is presented in Chapter 5. The effects on dragload and downdrag on drilled shaft foundations following liquefaction are discussed in journal paper presented in Chapter 7. A journal paper discussing the liquefaction-induced dragload and downdrag around driven piles is presented as Chapter 8.

The conclusions and recommendations developed based on the results obtained from the test results are presented in Chapter 9. Specifically, the conclusions on controlled blast tests (pilot liquefaction tests), are discussed in Section 9.2. The conclusions drawn from the blast-induced liquefaction test results are presented in Section 9.3. The overall recommendations regarding liquefaction-induced dragload and downdrag developed based on the obtained test results are discussed in Section 9.4. Finally, an overview of the general construction methods and

test instrumentation used for drilled shaft and driven pile foundation element at the TATS is presented in Appendix A.

## 1.6. References

- Bjerrum, L., Johannessen, I. J., and Eide, O., (1969). "Reduction of negative skin friction on steel piles to rock." *Proc. 7th ICSMFE, Mexico City, Vol. 2*, pp. 27-34.
- Briaud, J. L., and Tucker, L. (1997). "Design and Construction Guidelines for Downdrag on Uncoated and Bitumen-Coated Piles." NCHRP Report 393, Transportation Research Board, National Academy Press, Washington, D.C., pp. 198.
- Boulanger, R.W and Brandenberg, S.J. (2004). "Neutral plane solution for liquefaction-induced downdrag on vertical piles." *Proceedings, ASCE Geo-Trans conference, ASCE, Reston, VA*, 470-479.
- Bozozuk, M. (1981). "Bearing capacity of a pile preloaded by downdrag." *Proceedings of the 10<sup>th</sup> international conference on soil mechanics and foundations engineering, Mexico Cit, Vol. 2*: 631-636.
- Bozozuk, M., (1972). "Down drag measurement on 160-ft floating pipe test pile in marine clay." *Canadian Geotechnical Journal, Vol. 9, No. 2*, pp. 127-136.
- Broms, B. B. and Silberman, J. O., (1964). "Skin friction resistance for piles in cohesionless soil." *Sols-Soils, No. 10*, pp. 33-41.
- Dumas, C. (2000). "Soil downdrag on deep foundations." An overview of perspective proceedings of the 18<sup>th</sup> ASCE/PennDOT Geotechnical Seminar, Hershey, PA, 19p.
- Davisson, M. T. (1993). "Negative skin friction in piles and design decisions." *International Conference on Case Histories in Geotechnical Engineering. 7*.
- Endo, M., Minou, A., Kawasaki, T., and Shibata, T. 1969. Negative skin friction acting on steel piles in clay. *In Proceedings of the 8th International Conference on Soil Mechanics and Foundation Engineering, Mexico City, 25–29 August 1969. Mexico Geotechnical Society. Vol. 2*, pp. 85–92.
- Fellenius, B.H., and Broms, B. B. (1969). "Negative skin friction for long piles driven in clay." *Proc. 7th ICSMFE, Mexico City, Vol. 2*, pp. 93-98.
- Fellenius, B.H. (1972). "Reduction of negative skin friction with bitumen slip layers." *Discussion. Journal of the Geotechnical Engineering Division, ASCE, 101(GT4)*: 412–414.
- Fellenius, B.H. (1979). "Downdrag on bitumen coated piles." *Journal of Geotechnical Engineering, ASCE, 105 (GT10)*: 1262–1265.

- Fellenius, B.H., (1988). "Unified Design of Piles and Pile Groups." TRB Washington, Record 1169, pp. 75-82.
- Fellenius, B.H. (1991). *Foundation Engineering Handbook*, Chapter 13 - Pile Foundations. Second Edition. Van Nostrand Reinhold Publisher, New York, NY, pp. 511-536.
- Fellenius, B. H. (2004). "Unified Design of Piled Foundations with Emphasis on Settlement Analysis." *Proceedings of ASCE Conference Deep Foundations 2004*, pp. 253-275.
- Fellenius, B.H. (2006). "Results from long-term measurement in piles of drag load and downdrag" *Canadian Geotech. J.*, April 2006 43(4), 409-430.
- Fellenius, B. H. and Siegel, T.C. (2008). Pile drag load and downdrag in a liquefaction event *J. Geotech. and Geoenviron. Engrg.* ASCE, Reston, Virginia, 134 (9), 1412-1416.
- Gallagher, P. M., Pamuk, A. and Abdoun, T. (2007). "Stabilization of liquefiable soils using colloidal silica grout." *Journal of Materials in Civil Engineering*, Vol. 19, No.1, pp. 33-40.
- Hannigan, P.J., Goble, G.G., Thendean, G., Linkins, G.E. and Rausche, F. (2005). "Design and Construction, Vol. I and II. Federal Highway Report No. FHWA-HI-05, Federal Highway Administration, Washington, D.C.
- Hannigan, P.J., Robinson, B. R., Goble, G.G., Linkins, G.E. & Rausche, F., Becker, M. L. (2016). "Design and construction of driven pile foundations." FHWA-NHI-16-009, National Highway Institute, Federal Highway Administration, U.S. Department of Transportation, Washington, D.C.
- Long, R. L, Healy, K. A. (1974). "Negative Skin Friction on Piles." Final Report, JHR74-77. Project 73-1.
- Muhunthan, B., vijayathanan, N. V., and Abbasi, B., (2017). "Liquefaction-induced downdrag on drilled shafts." Washington State Department of Transportation. Final Research Report.
- Poulos, H. G. (1997). "Piles subjected to negative friction." *A procedure for design, Geotechnical Engineering*, 23-44.
- Rollins, K. M. and S. R. Strand (2006). Downdrag Forces Due to Liquefaction Surrounding a Pile. *Proceedings of the 8th U.S. National Conference on Earthquake Engineering*. Paper No. 1646, San Francisco, CA, April 18-22.
- Rollins, K.M. and Hollenbaugh (2015). "Liquefaction Induced Negative Skin Friction from Blast-induced Liquefaction Tests with Auger-cast Piles." *6<sup>th</sup> International Conference on Earthquake Geotechnical Engineering*, Christchurch, New Zealand.
- Siegel, T.C., Lamb, R., Dasenbrock, D., and Axtell, P.J. (2013). "Alternative Design Approach for Drag Load and Downdrag with the LRFD Framework." *Proceedings of the 38th Annual Conference on Deep Foundations 2013*, Phoenix, AZ, pp. 23-39.



Strand, S. R. (2008). "Liquefaction Mitigation Using Vertical Composite Drains and Liquefaction induced Downdrag on Piles: Implications for Deep Foundation Design," Ph.D. thesis, Department of Civil and Environmental Engineering, Brigham Young University, Provo, UT.

Tan, S. A., and Fellenius, B. H. (2016). "Negative skin friction pile concepts with soil-structure interaction." *Geotechnical Research*, 3(4), 137-147.

Vijayaruban, N. V., Muhunthan, B., and Fellenius, B.H. (2015). "Liquefaction-induced Downdrag on Piles and Drilled Shafts." 6<sup>th</sup> International Conference on Earthquake Geotechnical Engineering. Christchurch, New Zealand.

## CHAPTER 2: Controlled Blast Testing

### 2.1. Chapter Overview

A literature review on controlled blasting, production of excess porewater pressure development of existing threshold values required for liquefaction is provided in this chapter. A summary of the existing empirical and theoretical models used to predict blasting parameters (e.g., peak particle velocity, peak compressive strain and scaled distance) and blast-induced excess porewater pressure ratio is presented in this chapter. Likewise, the influence of soil parameters (e.g., unit weight, relative density and effective stress) and blasting parameters on excess porewater pressure development is discussed herein. In addition, the existing threshold values of peak particle strain, peak compressive strain and, scaled distance required for liquefaction are provided and discussed herein. In addition, the methods proposed for estimating post-liquefaction soil settlements in saturated sandy soils are discussed in Section 2.5.

### 2.2. Controlled Blast Testing

Controlled blasting has used as a ground improvement method in geotechnical engineering, to densify or compact loose saturated sandy soils through liquefaction (e.g., Lyman 1941, Ivanov 1967, Solymar 1984, Handford 1988, La fosse and Rosenvinge 1992, Kimmerling 1994, Narin van Court and Mitchell 1994, Gohl et al. 1994, Gohl et al. 1996, Gohl et al. 1998, Ashfold et al. 2000, Gohl et al. 2000, Gohl et al. 2001, Gallagher et al. 2007, Gohl et al. 2009, and Vega-Posada 2012). Like with in an earthquake event, ground shaking produced by explosives create energy that causes an increase in water pressure within the void space between the soil particles. As the porewater pressure increases, the soil structure collapses, and the soil starts to behave like a liquid. This phenomenon is known as “liquefaction.” This rearrangement of particles results a loss of effective stress and a decrease in shear strength due to the generation of the excess porewater pressure (Narin van Court 1997). After a certain time, depending upon

the soil type, the generated excess porewater pressure begins to dissipate. As the excess porewater pressure subsides, 1) the soil particles are rearranged, 2) a new granular skeleton is formed, and 3) the soil begin to compress (Mitchel 1981, Narin van Court 1997). As reported by Charlie et al. (1988), the excess porewater pressure dissipation is a function of the permeability of the material, the grain particle distribution, and the geometry of blasting layout (explosive charge weight, the detonation delay and blasting sequence, and the charge spacing).

Several research studies (e.g., Ivanov 1967, Lyakhov 1961, Puchkov 1962, Langleu et al. 1972, Banister and Ellett 1974, Damitio 1978, Dowding and Hryciw 1986) have been conducted using small and large explosives, with charge weights of less than 1000 kg, to evaluate liquefaction. The results obtained from these blasting tests were used to evaluate the influence of different parameters including, the amount of charge weight and the pattern and sequence detonation on soil liquefaction potential (Charlie et al. 1988). The influence of peak and residual porewater pressure, the duration of the excess porewater pressure generation, the amount of settlement and the ground acceleration associated with blast-induced soil liquefaction have also been investigated by various researchers (e.g., Florin and Ivanov 1961, Yamamura and Koga 1974, Arya et al. 1978, Studer and Kok 1980). In these aforementioned studies, little attention was paid to the porewater pressure generation. However, in some instances, the observation of geysers, sand boils, and springs were observed and recorded, indirectly indicating liquefaction at the testing sites (Charlie et al. 1988). For example, Kummenje and Eide (1961) performed blast testing to investigate sea-bottom sands; explosive charges varying from 0.07 to 2.4 kg were detonated at the depth of 10 m below the sea bed. From the testing results, an increase in porewater pressure was observed, and large settlements due the blasting were reported. Ivanov (1967) performed laboratory experiments using explosive charges ranging from 1.5 to 4.5 g,

placed at depths of 30-50 cm. Following the detonation of 10 to 15 explosives, an increase in porewater pressure was observed. Ivanov (1967) also conducted a field-scale experiment at Gorki, Russia, in fine grained sands with low relative density ranging from 10 to 20 percent deposited under the water table. For the Ivanov (1967) field-scale study a total of 5 kg of explosive charge was detonated at a depth of 4.9 m. This detonation caused the formation of geysers, the upward flow of water for 10 minutes, and the supports of a bridge, that was located 35 m away, sank into the sand due to the liquefaction.

Over three decades ago, controlled blast studies transitioned from being a ground improvement method to an in-situ testing known as “blast-induced liquefaction.” The blast-induced liquefaction has been used to physically model soil liquefaction without waiting an earthquake event to occur. Several research studies have been performed to assess liquefaction using controlled blasting tests (e.g., Sheriff et al. 1977, Charlie 1985, Charlie et al. 1988a, Charlie et al. 1992, Kimmerling 1994, Figueroa et al. 1994, Ferrito 1997, Gohl et al. 2001, Okamura and Soga 2006, Charlie and Doehring 2007, Rollins and Anderson 2008, Stuedlein et al. 2016, Amoroso et al. 2017, Bong and Stuedlein 2018). For example, Charlie et al. (1988) performed a controlled blast study using nuclear and high-energy chemical explosives to investigate the range of liquefaction based upon the energy of the explosive. In Delta, Canada, Gohl et al. (2001) conducted field liquefaction tests using two 6 kg explosive charges to liquefy a loose sandy silt soil. As reported by Gohl et al. (2001), delays were introduced to the detonation sequence to generate multiple blast pulses. The relationships between shear strain amplitude, number of strain cycles and residual pore pressure generation and post-cyclic soil deformations after the dissipation of excess porewater pressure are discussed by Gohl et al. (2001).

Other research experiments have been carried out to evaluate the effects of liquefaction on deep foundation performance (e.g., Ashford et al. 2000, Ashour and Norris 2003, Ashford et al. 2004, Rollins 2004, Rollins et al. 2004, Rollins and Strand 2006, Strand 2008, Rollins and Hollenbaugh 2015, Stuedlein et al. 2016, Amoroso et al. 2017). For instance, to understand the interaction between the soil and deep foundation while subjected to cyclic loading, various blast-induced liquefaction tests were conducted on Treasure Island, in California, as part of Treasure Island Liquefaction Test (TILT) project (Ashford et al. 2000, Ashour and Norris 2003, Ashford et al. 2004, Rollins 2004, and Rollins et al. 2004). Ashour and Norris (2003) provided a new analysis procedure for evaluating the lateral response of an isolated pile installed in liquefied sand at the Treasure Island site. Ashford et al. (2000) also performed, for the first time a blast-induced liquefaction tests on piles. The tests were performed at the Treasure Island site to evaluate the behavior of full-scale laterally loaded piles installed in liquefiable soils. Ashford et al. (2004) also performed a pilot liquefaction test at the Treasure Island to determine the required charge weight, delay, and pattern to induce liquefaction for full-scale testing of deep foundations. Ashford et al. (2004) concluded that controlled blasting techniques could be used to successfully induce liquefaction in well-defined or target layer below the ground surface. In addition, Rollins et al. (2005) also conducted a blast-induced liquefaction test and lateral load tests at the site located on the Treasure Island site to evaluate effect of liquefaction full-scale pile group. Camp et al. (2008) and (Rollins et al. 2008) performed blast-induced liquefaction tests in Charleston, South Carolina, to compare the pre-and post-cone penetration test results, and also to evaluate the lateral and dynamic load tests in liquefied sand for the Cooper Bridge.

### 2.3. Predicting Excess Porewater Pressure Ratio

As reported by Studer and Kok (1980), liquefaction occurs when the excess porewater pressure ( $R_u$ ) is equal to or greater than the unity ( $R_u \geq 1$ ). Specifically, liquefaction occurs when porewater pressure is equal to or exceed the initial grain-to-grain effective stress of the soil matrix (Larson-Robl 2016). In general,  $R_u$  can simply be defined as a ratio of the change in the porewater pressure ( $\Delta u$ ) to the initial vertical effective stress ( $\sigma_{vo}'$ ). Several empirical models have been developed from single and/or multiple denotations to predict  $R_u$  as a function of peak particle velocity (PPV), peak compression strain ( $\epsilon_p$ ), scaled distance (SD) [Kummeneje and Eide 1961, Studer and Kok 1980, Veyera 1985, Hubert 1986, Charlie et al. 1992, Rollins et al. 2004, Al-Qasimi et al. 2005, Eller 2011, Charlie et al. 2013, Larson-Robl 2016]. These empirical models can also be used to predict liquefaction susceptibility in loose, dense and very dense saturated soils. A summary of these empirical equations are summarized in Table 2.1 and discussed in the following subsections.

As reported by Charlie et al. (2013) and Larson-Robl (2016), there is a relationship between soil parameters (relative density and effective stress) and blasting vibration parameters (PPV and  $\epsilon_p$ ). As can be seen in Table 2.1, some of the aforementioned empirical models that are commonly used to predict  $R_u$  are only based on the blasting layout (charge weight and horizontal distance from explosive to the piezometer), and the in-situ conditions are not taken into considerations (Kummeneje and Eide 1961, Studer and Kok 1980, Charlie et al. 1992, and Rollins et al. 2004). To overcome these limitations, various researchers (e.g., Veyera 1985, Hubert 1986, Ali-Qasimi et al. 2005 Eller 2011, and Charlie et al. 2013) proposed empirical methods using PPV,  $\epsilon_p$ , relative density ( $D_r$ ), and effective stress ( $\sigma_{vo}'$ ) to predict pore pressure response required to attain liquefaction.

**Table 2.1.** Summary of existing empirical equation models to predict  $R_u$ .

Equation Number	Empirical Equations	Reference
2.1	$R_u = 65(SD)^{-2.2}(\sigma'_{vo})^{\frac{1}{3}}$	Kummeneje and Eide (1961)
2.2	$R_u = 1.65 + 0.64 \cdot \ln(1/SD)$	Studer and Kok (1980)
2.3	$R_u = 6.67 \cdot (PPV)^{0.33} \cdot (\sigma'_{vo})^{-0.31} \cdot (D_r)^{-0.179}$	Veyera (1985)
2.4	$R_u = 10.59 \cdot (\varepsilon_p)^{0.43} \cdot (\sigma'_{vo})^{-0.17} \cdot (D_r)^{-0.18}$	Hubert (1986)
2.5	$R_u = 3.9 \cdot (SD)^{-1.41}$	Charlie et al. (1992)
2.6	$R_u = 1.89 - 0.621 \ln(SD)$	Rollins et al. (2004)
2.7	$R_u = 1.13 \cdot (\sum PPV)^{0.54} \cdot \left(\frac{\sigma'_{vo}}{62.5kPa}\right)^{-\frac{1}{3}} \cdot \left(\frac{D_r}{43\%}\right)^{-\frac{1}{5}}$	Al-Qasimi et al. (2005)
2.8	$R_u = 134 \cdot (\varepsilon_p)^{1.2} \cdot (\sigma'_{vo})^{-1.78} \cdot (D_r)^{-0.08}$	Charlie et al. (2013)
2.9	$R_u = 1.747 - 0.512 \ln(SD) - 0.032(N_1)_{60} - 0.002\sigma'_{vo}$	Eller (2011)

Note:  $SD = R/W^{1/3}$ ; R = horizontal distance between charge and piezometer in m ; W = charge weight in kg  
 PPV = peak particle velocity in m/s  
 $\varepsilon_p$  = peak compressive strain in percent  
 $D_r$  = relative density in percent  
 $\sigma'_{vo}$  = In-situ vertical effective stress in kPa  
 $(N_1)_{60}$  = Corrected SPT blow count

### 2.3.1. Studer and Kok (1980)

The Studer and Kok (1980) empirical relation was developed by considering a single blast in saturated sandy soils. In this approach, the in-situ soil properties (relative density and effective stress) were not taken into consideration. This empirical relationship is previously presented in Table 2.1 as Equation 2.2, and is graphically shown in Figure 2.1. As previously mentioned,  $R_u$  have commonly been used as a threshold values to assess the liquefaction susceptibility. As shown in Figure 2.1, the  $R_u$  values less than 0.10 represent a safe zone for liquefaction,  $R_u$  values between 0.80 and 1.0 represent a dangerous zone, and the  $R_u$  values greater than or equal to 1.0 represent soil liquefaction.

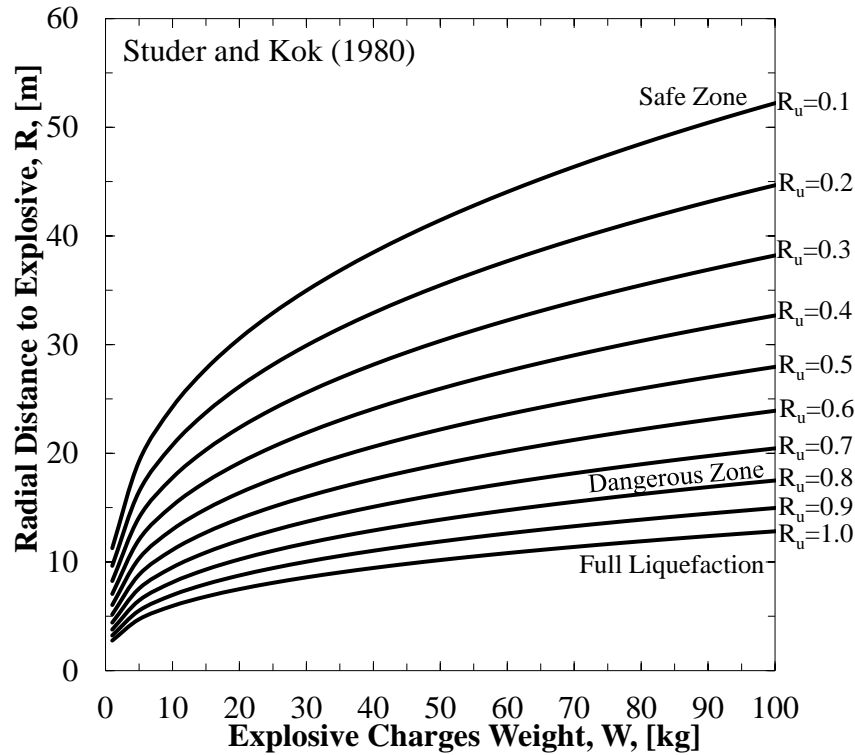


**Figure 2.1.** Explosive charge weight as a function of radial distance ( $R$ ) for determination of liquefaction based on excess porewater pressure ratio (modified from Studer and Kok 1980).

The term “SD” shown in the previous equations and used to predict PPV and  $R_u$ , has been defined as a ratio between the explosive distance [distance between the explosive charge location and the porewater pressure recorder (in meters)], and the squared or cubed root of explosive charge weight, (in kilograms of TNT), when square-root scaling or cube-root scaling methods are used. As reported by Kumar et al. (2014), in the case of a spherical charge, whose volume changes in a specified manner with a change of radius, cube-root scaling can be supported by dimensional analysis. Contrary, in the case of a cylindrical charge whose height changes in a specified manner with a change in radius, square-root scaling can be used.

### 2.3.2. Veyera (1985)

Veyera (1985) conducted one-dimensional laboratory shock loading tests on quartz sand. Liquefaction was observed under single compressive strains greater than 0.01 percent



corresponding to a peak particle velocity of 0.15 m/sec and peak stress of 500 kPa. The Veyera (1985) study was performed for soil with effective stresses values ranging from 86 to 690 kPa and relative densities ranging from 10 to 80 percent (Charlie et al. 1988a). The Veyera (1985) empirical equation to determine  $R_u$  as a function of compressive peak strain, effective stress and relative density is presented as Equation 2.3.

### **2.3.3. Hubert (1986)**

Huber (1986) also conducted a shock loading tests on a saturated Poudre Valley sand at relative densities of 20, 40, 60 and 80 percent under three effective stresses of 86, 172, 517kPa (Charlie et al. 1988a). Through a multivariate regression analysis of the test results, an empirical model (Equation 2.4) was developed. Liquefaction occurred after the first impact, when the peak compressive strain was greater than 0.2 percent. As reported in Charlie et al. (1988a), during Hubert (1986) research study, liquefaction could not be induced under multiple impacts if the strains were lower than 0.01 percent. Hubert (1986) also reported that the number of impacts required to induce liquefaction was a function of 1) strain amplitude, 2) initial effective stress, and 3) initial relative density.

### **2.3.4. Charlie et al. (1992)**

Charlie et al. (1992) performed a blast-induced liquefaction test on an alluvial sand deposit. The  $R_u$ , PPV, and residual porewater pressure were monitored and measured at various locations. Specifically, the measured PPV,  $\varepsilon_p$ , SD and threshold values of these parameters for inducing liquefaction were obtained. Charlie at al. (1992) reported that liquefaction occur when the PPV values exceeding 0.9 m/s in dense alluvial sand, and when the peak strains were less than 0.002% no significant residual porewater pressure occurred. The empirical equation for  $R_u$  that was determined from the experimental data is presented in Table 2.1 as Equation 2.5.

### 2.3.5. Al-Qasimi et al. (2005)

Al-Qasimi et al. (2005) conducted a series of blast-induced liquefaction tests on loose, saturated, sand at the Syncrude Canada Ltd. tailings site located in Alberta, Canada. Single and multiple explosives were detonated. Based on the experimental data obtained from this study, an empirical equation for  $R_u$  as a function of PPV,  $D_r$  and  $\sigma'_{vo}$  was developed (Equation 2.7). As reported by Al-Qasimi et al. (2005), excess porewater pressure ratio values greater than unity with the corresponding PPV values exceeding 0.65 m/s, SD less than  $6.3 \text{ m (kgTNT)}^{1/3}$ , and  $\epsilon_p$  exceeding 0.04 percent were produced from single detonation. Liquefaction was induced from multiple detonation with PPV values exceeding 0.13 m/s, SD values less than  $12.5 \text{ m (kgTNT)}^{1/3}$ , and  $\epsilon_p$  exceeding 0.008%. Al-Qasimi et al. (2005) also stated that multiple, millisecond delayed detonations induced liquefaction at lower PPV and at larger SD distances than the values produced by single detonations.

### 2.3.6. Charlie et al. (2013)

The results obtained from blast-induced pore pressure and liquefaction of saturated sand are presented in Charlie et al. (2013). An empirical equations of  $R_u$  (Equation 2.6) as a function of peak strain, relative density and effective stress, was developed for single detonations of spherically shaped explosives in water located over saturated sand at an initial effective stress of 18 kPa. Charlie et al. (2013) reported liquefaction for loose, dense, and very dense sand soil at the PPV values of 0.49, 0.52 and 0.71 m/s, and at SD less than 8.8, 9.8 and 8.2 m  $(\text{kgTNT})^{1/3}$ , respectively. Charlie et al. (2013) concluded that the PPV and  $\epsilon_p$  values that were required to induce liquefaction increases with relative density and effective stress.

### **2.3.7. Eller (2011)**

Through the use of data acquired from various case histories, Eller (2011) developed an empirical model, presented in Table 2.1 as Equation 2.9, to predict liquefaction and residual pore pressure for both single and multiple blast events. A review of the some of the existing empirical models used to predict pore pressure responses based on SD were also discussed in Eller (2011). Eller (2011) approach takes into consideration soil parameters such as vertical effective stress and blow count [SPT  $(N_1)_{60}$ ]. As reported by Eller (2011), it is should be anticipated to observe higher residual porewater pressures for multiple blasts than one large single blast with an equivalent scaled distance. Therefore, Eller (2011) recommended the use of multiple blasts in design of future blasting studies.

### **2.4. Predicting Blast-induced Peak Particle Velocity**

A large number of theoretical and empirical methods have been presented to determine blast-induced peak particle velocities (Drake and little 1983, Handford 1988, Jacobs et al. 1988, Charlie et al. 1992, Narin van Court 1997, Rollins et al. 2001, Wu et al. 2003, Al-Qasimi et al. 2005, Leong et al. 2007, Charlie et al. 2013, and Larson-Robl 2016). A summary of these empirical equations developed by various researchers are summarized in Table 2.2. It should be noted that the empirical equations, presented in Table 2.1 and other equations presented in the literature, are site-specific equations; however, Kumar et al. (2014) provided an empirical model (Equation 2.25) that considers the variation in soil properties including, unit weight ( $\gamma$ ), degree of saturation (S), Young's modulus (E) and scaled distance (SD). Kumar et al. (2014) also stated that the results obtained using the latter model are reasonable for fully saturated soils irrespective of soil type, and that the model typically predicts high values for partially saturated soils.

**Table 2.2.** Summary of existing equation models to predict PPV.

Equation Number	Empirical Equations	Reference
2.10	$PPV = 5.6(SD)^{-1.5}$	Drake and Lille (1983)
2.11	$PPV = 22(SD)^{-2.01}$	Handford (1988)
2.12	$PPV = 12.9(SD)^{-2.21}$	Jacobs et al. (1988)
2.13	$PPV = 8.75(SD)^{-0.74}$	Charlie et al. (1992)
2.14	$PPV = 0.264(SD)^{-0.74}$	Narin van Court (1997)*
2.15	$PPV = 1.7(SD)^{-1.36}$	Rollins et al. (2001)
2.16	$PPV = 0.198(SD)^{-0.688}$	Charlie et al. (2001)
2.17	$PPV = 2.733(SD)^{-2.34}$	Wu et al. (2003)
2.18	$PPV = 1.35(SD)^{-1.25}$	Ashford et al. (2004)
2.19	$PPV = 39.64(SD)^{-2.34}$	Al-Qasimi et al. (2005)
2.20	$PPV = 3.38(SD)^{-2.53}$	Leong et al. (2007)
2.21	$PPV = 14.5(SD)^{-1.45}$	Charlie et al. (2013); loose
2.22	$PPV = 13.6(SD)^{-1.45}$	Charlie et al. (2013); dense
2.23	$PPV = 12.3(SD)^{-1.5}$	Charlie et al. (2013); very dense
2.24	$PPV = (E/\gamma)^{0.229} SD^{-(1.6985-0.175 \cdot S)}$	Kumar et al. (2014)
2.25	$PPV = 121.3(SD)^{-1.49}$	Larson-Robl (2016), radial
2.26	$PPV = 67.1(SD)^{-1.21}$	Larson-Robl (2016), vertical
2.27	$PPV = 8.3(SD)^{-0.96}$	Larson-Robl (2016), transverse

Note:  $SD=R/W^{1/3}$ ; R=distance between charge and piezometer in m; W=charge weight in kg.

PPV=peak particle velocity in m/s

E=Young's modulus;  $\gamma$ =unit weight; S=degree of saturation

\* $SD=R/W^{1/2}$

## 2.5. Existing Threshold Values of PPV, $\epsilon_p$ and SD Required for Liquefaction

Although excess porewater pressure ratio have been commonly used as a threshold to assess the liquefaction potential, other blasting parameters including PPV,  $\epsilon_p$  and SD can be used as threshold limit for liquefaction. A summary of 24 existing threshold values reported in the literature are summarized in Table 2.3. For a very loose saturated cohesionless soil, Lykhov (1961) reported that liquefaction occurred at the PPV exceeding 0.11 m/s. A study conducted by

Puchkov (1962) reported a liquefaction at the SD values less than  $5 \text{ m/kg}^{1/3}$  with PPV exceeding  $0.08 \text{ m/s}$ .

**Table 2.3.** Summary of existing thresholds of PPV,  $\varepsilon_p$ , and SD required for liquefaction.

Reference	Soil Conditions	Scaled	Peak Particle	Peak Compressive
		Distance	Velocity	Strain
		SD	PPV	$\varepsilon_p$
		[ $\text{m/kg}^{1/3}$ ]	[m/s]	[%]
Lyakhov (1961)	Very loose	-	>0.11	-
Kummeneje and Eide (1961)	-	<4.3	-	-
Puchkov (1962)	Very loose	<5	>0.08	-
Ivanov (1967)	Very loose	<6-8	-	-
Studer et al. (1978)	-	2.9	-	-
Obermeyer (1980)	Hydraulic fill tailings	-	>0.02	-
Studer and Kok (1980)	-	<2.8	-	-
Long et al. (1981)	Loose	-	>0.05	-
Fragaszy et al. (1983)	-	2	-	-
Veyera (1985)	Loose	-	>0.4	>0.03
Hubert (1986)	Loose	-	>0.1	>0.01
Handford (1988)	Loose	-	>0.04	-
Charlie et al. (1992)	Dense	<3	>0.16	>0.01
Allen et al. (1997)	-	1.4	-	-
Walthan (2001)	-	2	-	-
Gohl et al. (2001)	Loose	-	-	>0.02
Pathirage (2000)	Loose	<6.7	>0.8	>0.06
Ashoford et al. (2004)	-	2.7	-	-
Al-Qasimi et al. (2005)	Loose	<6.3	>0.6	>0.04
Charlie and Doehring (2007)	-	3	>1.1	>0.07
Eller (2011)	Loose-medium dense	<20	-	-
Charlie et al. (2013)	Loose	<8.2	>0.49	>0.03
	Dense	<8.8	>0.52	>0.03
	Very dense	<9.8	>0.71	>0.04

According to Ivanov (1967), a very loose, saturated, sand experienced liquefaction at the SD values ranged from 6 to  $8 \text{ m/kg}^{1/3}$ . Charlie et al. (1992) observed liquefaction of dense alluvial sand with the PPV values exceeded  $0.16 \text{ m/s}$  with SD values less than  $3 \text{ m/kg}^{1/3}$  and when the peak strain values exceeded 0.01 percent. Charlie and Doehring (2007) performed an analysis of single underground explosions, using chemicals explosives, and reported that liquefaction can be induced when the SD values of  $3 \text{ m/kg}^{1/3}$ , and when the estimated peak

compressive strain exceed 0.07 percent and peak particle velocity exceed 1.1 m/sec were measured.

Charlie and Doehring (2007) also identified the SD of  $1 \text{ m/kg}^{1/3}$  as the upper bound maximum for liquefaction induced by surface explosives. These threshold values of PPV,  $\epsilon_p$  and SD and other values presented in the literature are summarized in Table 2.3. The thresholds of peak particle velocity and peak compressive strain that are required to induce liquefaction have been proven to be as function of the soil properties including soil density, effective stress and number of strain cycles, and lithification (Ali-Qasimi et al. 2005, Ashford et al. 2004, and Charlie and Doehring 2007).

## **2.6. Liquefaction-induced Settlements in Saturated Sands**

Earthquake-induced settlements have been observed after nearly every historical earthquake event. These liquefaction-induced settlements result in various destruction of infrastructure (e.g., buildings, roads, bridges, and underground lifelines). Several empirical methods have been developed to estimate the post-liquefaction settlement (e.g., Seed et al. 1975, Tokimatsu and Seed 1987, Ishihara et al 1990, Ishihara and Yoshimine 1992, Robertson and Wride 1998, Zhang et al. 2002, Lee 2007, Yi 2009 and Yi 2010). Most of the aforementioned methods are based on the SPT test (Tokimatsu and Seed 1987, Ishihara and Yoshimine 1992, and Lee 2007), and CPT test (Robertson and Wride 1998, Zhang et al. 2002, Idriss and Boulanger 2008, Yi 2009). The simplest and most widely used methods is the Tokimatsu and Seed (1987). However, the method requires the use of charts and diagrams (Lee 2007). For this research project, the simplified approach that was proposed by Lee (2017), is presented and discussed.

Lee (2007) proposed a simplified approach to estimate the earthquake-induced settlements in saturated sandy soils based on SPT-N value. The proposed approach has been

developed based on Tokimatsu and Seed (1987) approach, and the earthquake-induced settlement are predicted without using the charts, tables and diagrams (Lee 2007). In this approach, the liquefaction-induced settlement in saturated sandy soils is expressed as a function of volumetric strain and thickness of a given layer (Equation 2.28). The volumetric strain in Equation 2.9, is determined using Equation 2.2. As reported by Lee (2007), the approach provides a simple way to explore the level of risk of liquefaction based on the cyclic stress and SPT values.

$$S = \sum_{i=1}^n H_i \varepsilon_{vi} \quad \text{Equation 2.28}$$

Where  $H_i$  is the thickness for layer  $i$ ;  $\varepsilon_{vi}$  is the volumetric strain for layer  $i$  obtained using Equation 2.2,  $n$  is the number of soil layers.

$$\varepsilon_v = 10 \left[ (N_1)_{60} \right]^{-0.6} \quad \text{for } \frac{CSR}{(N_1)_{60}} > 0.01 \quad \text{Equation 2.19}$$

Where  $\varepsilon_v$  is the volumetric strain, and  $(N_1)_{60}$  is the normalized SPT-N,  $CSR_{7.5}$  is the Cyclic Stress Ratio (CSR) obtained using the following equation:

$$CSR_{7.5} = 0.65 \left( \frac{\sigma_v}{\sigma'_v} \right) \left( \frac{a_{\max}}{g} \right) \left( \frac{r_d}{MSF} \right) \quad \text{Equation 2.20}$$

Where  $CSR_{7.5}$  is the cyclic stress ratio with reference to earthquake magnitude of 7.5,  $\sigma_v$  is the total stress,  $\sigma'_v$  is the vertical effective stress at the certain depth,  $r_d$  is the stress reduction factor,  $MSF$  is the magnitude scaling factor,  $a_{\max}$  is the maximum horizontal acceleration at the ground surface, and  $g$  is the acceleration of gravity.

## 2.7. Chapter Summary

Various research studies have been conducted to improve an understanding pore pressure development and liquefaction development following controlled blast tests. The influence of

several soil parameters including peak particle velocity, peak strain and scaled distance on transient and residual porewater pressure responses have been presented and discussed. A review of the existing empirical models to 1) estimate  $R_u$  and PPV, and 2) the threshold values required for liquefaction are presented. Although, the aforementioned empirical models, presented in the literature, are site-specific equations, it has been proven that some of these equations predicts a accurate value of PPV and  $R_u$  for other locations than the locations for which the equations were developed.

## 2.8. References

- Amoroso et al. (2017). "The first Italian blast-induced liquefaction test (Mirabello, Emilia Romagna, Italy): description of the experiment and preliminary results." *Annals of Geophysics*, 60, 5, 2017; S0556; doi: 10.4401/ag-7415.
- Al-Qasimi, E.M.A., Charlie, W.A., and Woeller, D.J. (2005). "Canadian liquefaction experiment (CANLEX): Blast-induced ground motion and pore pressure experiments." *Geotechnical Testing Journal*, Vol. 28, No.1, 9-21.
- Allen, B. M., S. I. Drellack, and M. J. Townsend (1997), Surface effects of underground explosions, Rep. DOE/NV/11718-122, 140 pp., Nev. Oper. Off., U.S. Dep. of Energy, Las Vegas. (Available at <http://www.osti.gov>).
- Arya, A.S, Nandakumaran, P., Puri, V.K. and Mukerjee, S., (1978). "Verification of Liquefaction Potential by Field Blast Tests," 2<sup>nd</sup> International Conference on Microzonation for Safer Construction, American Society of Civil Engineers (ASCE) Earthquake Eng., Vol. 1, San Francisco, California, Nov. 26-Dec. 1, pp. 865-869.
- Ashford, S.A. and Rollins, K.M. (2002). "TILT: Treasure Island Liquefaction Test: Final Report." Report SSRP-2001/17, Department of Structural Engineering, University of California, San Diego.
- Ashford, S.A., Rollins, K.M., and Lane, J.D. (2004). "Blast-induced liquefaction for full-scale foundation testing." *Journal of Geotechnical and Geoenvironmental Engineering*. Vol. 130, No. 8, pp 798-806.
- Ashour, M., and Norris, G. (2003). "Lateral loaded pile response in liquefiable soil." *J. Geotech. Geoenviron. Eng.*, 129(5), 404-414.
- Banister, J.R., and Ellett, D.M., (1974). "Pore Pressure Enhancements Observed on Rio Blanco," Sandia National Laboratories, Report No. SLA-74-0328, Albuquerque, N.M., Aug., 47 p.



- Bong, T and Armin W. Stuedlein, A, W. (2018). "Effect of Cone Penetration Conditioning on Random Field Model Parameters and Impact of Spatial Variability on Liquefaction-Induced Differential Settlements." *Journal of Geotechnical and Geoenvironmental Engineering*, 2018, 144(5): 04018018.
- Bray, J.D., and Sancio, R.B. (2006). "Assessment of the liquefaction susceptibility of fine-grained soils." *Journal of Geotechnical and Geoenvironmental Engineering*. Vol. 132, No. 9, pp. 1165-1177.
- Charlie, W.A. (1985). "Review of present practices used in predicting the effects of blasting on pore pressure," U.S. Department of the Interior, Bureau of Reclamation. Report GR-85-9, 21 p.
- Charlie, W.A., Hubert, M.E., Schure, L.A., Veyera, G.E., Bretz, T.E., and Hassen, H.A. (1988a). "Blast induced liquefaction: summary of literature." Air Force Office of Scientific Research, Washington D.C., 316 p.
- Charlie, W.A., Doehring, D.O., Veyera, G.E., and Hassen, H.A. (1988b). "Blast induced liquefaction of soils: laboratory and field tests." Air Force Office of Scientific Research, Washington D.C., 184 p.
- Charlie, W.A., Jacobs, P.J., and Doehring, D.O. (1992). "Blast induced liquefaction of an alluvial sand deposit." *Geotechnical Testing Journal*. Vol. 15, No. 1, pp. 14-23.
- Charlie, W.A., and Doehring, D.O. (2007). "Groundwater table mounding, pore pressure, and liquefaction induced by explosions: energy-distance relations." *Reviews of Geophysics*. 45, RG4006. December 2007, pp. 1-9.
- Charlie, W. A., Bretz, T. E., Schure (White), L. A., and Doehring, D.O. (2013). "Blast-induced pore pressure and liquefaction of saturated sand." *Journal of Geotechnical and Geoenvironmental Engineering*, Vol. 139, No. 8, 1308-1389.
- Damitio, C., (1978). "Field Experience on Blast-Induced Liquefaction", Int. Workshop on Blast Induced Liquefaction, Dames and Moore, AFOSR, Maidenhead, U.K., Sept. 17-29, pp. 137-148.
- Dowding, C.H., and Hryciw, R.D., (1986). "A Laboratory Study of Blast Densification of Saturated Sand," *Journal of Geotechnical Engineering*, ASCE, Vol. 112, No. 2, Feb., pp. 187-199.
- Drake, J. L., and Little, C. D. (1983). "Ground shock from penetrating conventional weapons." Proc., Interaction of Non-Nuclear Munitions with Structures, U.S. Air Force Academy, Colorado Springs, CO, 1-6.
- Eller, J.M. (2011), "Predicting pore pressure in in-situ liquefaction studied using controlled blasting." Master's Thesis, Oregon State University.

- Ferrito, J.M. (1997). "Seismic design criteria for soil liquefaction." Technical Report TR-2077-SHR. Naval Facilities Engineering Center. 87p.
- Figuroa, J.L., Saada, A.S., Liang, L., and Dahisaria, N.M. (1994), "Evaluation of soil liquefaction by energy principles." *Journal of Geotechnical Engineering*, Vol. 120, No. 9, pp. 1554-1569.
- Florin, V.A., and Ivanov, P.L., (1961), "Liquefaction of Saturated Sandy Soils", 5th Int. Conf. on Soil Mechanics and Foundation Engineering, Vol. 1, Paris, France, July 17-22, pp. 107-111.
- Fragaszy, R. J., Voss, M. E., Schmidt, R. M., and Holsapple, K. S., 1983, "Laboratory and Centrifuge Modeling of Blast-induced Liquefaction," 8th International Symposium on Military Application of Blast Simulation, Spiez, Switzerland, pp. III.5-1–III.5-20.
- Gallagher, P. M., Pamuk, A. and Abdoun, T. (2007). "Stabilization of liquefiable soils using colloidal silica grout." *Journal of Materials in Civil Engineering*, Vol. 19, No.1, pp. 33-40.
- Gohl, W. B., Howie, J. A., and Everard, J. (1996). "Use of explosive compaction for dam foundation preparation." *Proc., 49th Canadian Geotechnical Conf., Vol. 2, Canadian Geotechnical Society, Richmond, BC, Canada, 758-793.*
- Gohl, W. B., Howie, J. A., Hawson, H. H., Diggle, D. (1994). "Field experience with blast densification." *Proc., 5th U.S. National Conf. on Earthquake Engineering, Vol. 4, Earthquake Engineering Research Institute, Oakland, CA, 221–231.*
- Gohl, W. B., Tsujino, S., Wu, G., Yoshida, N., Howie, J. A., and Everard, J. (1998). "Field application of explosive compaction in silty soils and numerical analysis." *Proc., Geotechnical Earthquake Engineering and Soil Dynamics III, GSP 75, ASCE, Reston, VA, 654–665.*
- Gohl, W. B., Jefferies, M. G., Howie, J. A., and Diggle, D. (2000). "Explosive compaction: Design, implementation and effectiveness." *Geotechnique*, 50(6), 657–665.
- Gohl, W.B., Howie, J. A., and Rea, C. E. (2001). "Use of controlled detonation of explosives for liquefaction testing." *Proceedings, Fourth Int. Conf. On Recent Advances in Geotechnical Earthquake Engineering and Soil Dynamics, San Diego, Calif. Paper no. 913.*
- Handford, G. T. (1988). "Densification of an existing dam with explosives." *Proc., Hydraulic Fill Structures, ASCE, New York, 750-762.*
- Hubert, M. E. (1986). "Shock loading of water saturated Eniwetok coral sand." M. S. thesis, Department of Civil Engineering, Colorado State University, Fort Collins, Co, 145-154.
- Ishihara, K. (1990). "Liquefaction and flow failure during earthquakes." *Géotechnique*, ICE, London, England, 43(3), 351–451.

- Ivanov, P. L. (1967). "Compaction of non-cohesive soils by explosions". Izdatel'stvo Literatury Po Stroitel'stvu, Leningrad, USSR.
- Jacobs, P. J. (1988). "Blast-induced liquefaction of an alluvial sand deposit," M.S. Thesis, Department of Civil Engineering, Colorado State University.
- Kimmerling, R.E. (1994). Blast Densification for Mitigation of Dynamic Settlement and Liquefaction – Final Report WA-RD 348.1. Washington State Department of Transportation. 135 pp.
- Kramer, S.L. (2008). "Evaluation of liquefaction hazards in Washington State." Final Research Report, Agreement T2695, Task 66, Liquefaction Phase III. Washington State Transportation Commission.
- Kumar, R., Choudhury, D., Bhargava, K. (2014). "Prediction of blast-induced vibration parameters for soil sites." International Journal of Geomechanics, Vol. 14, No. 3.
- Kummeneje, D., and Eide, O. (1961). "Investigation of loose sand deposits by blasting." Proc., 5th ICSMFE, ISSMFE, London, 491-497.
- Langley, N. P., Smith, C. R., and Pfefferle, W. (1972). "DIAL PACK event soil pore pressure and shear strength test." Aerospace Rep. No. TOR-0172 (S2970-20)-1. The Aerospace Corp., San Bernardino, CA, and Space and Missile Organization, U.S. Air Force Systems Command, Los Angeles.
- Larson-Robl, K. M. (2016). "Pore pressure measurement instrumentation response to blasting." M.S. Thesis, Mining Engineering, University of Kentucky.
- Lee, Y. (2007). "Earthquake-induced settlements in saturated sandy soils." ARPN Journal of Engineering and Applied Sciences.
- Leong, E. C., Anand, S., Cheong, H. K., and Lim, C. H. (2007). "Reexamination of peak stress and scaled distance due to ground shock." Int. J. Impact Eng., 34(9), 1487–1499.
- Long, J. H., Ries, E. R., and Michalopoulos, A. P. "Potential for Liquefaction Due to Construction Blasting," Proceedings, International Conference on Recent Advances in Geotechnical Engineering and Soil Dynamics, University of Missouri-Rolla, 1981, pp. 191-194.
- Lyman, A.K.B. (1942). Compaction of Cohesionless Foundation Soils by Explosives. Transactions ASCE (107) pp. 1330-1348.
- Lyakhov, G. M. (1961). "Shock Waves in the Ground and the Dilution of Water Saturated Sand." Zhurnal Prikladnoy Mekhanik Technicheskoy Fiziki, Moscow, 38-46.
- Mitchell, J.K. (2008). "Mitigation of Liquefaction Potential of Silty Sands." From Research to Practice in Geotechnical Engineering Congress 2008, pp 453-451.

- Narin Van Court, W.A., and Mitchell, J.K. (1994). "Explosive compaction: Densification of loose, saturated, cohesionless soils by blasting." Geotechnical Engineering Report No. UCB/GT/94-03. 116 p.
- Obermeyer, J. R., "Monitoring Uranium Tailings Dams During Blasting Program," Symposium on Uranium Mill Tailings Management, Colorado State University, November 1980, pp. 513-527.
- Pathirage, K. S., "Critical assessment of the CANLEX blast experiment to facilitate a development of an in-situ liquefaction methodology using explosives," *M.S. thesis*, Department of Civil Engineering, University of British Columbia, 2000.
- Puchkov, S. V. (1962). "Correlation between the velocity of seismic oscillations of particles and phenomenon of particles and liquefaction phenomenon of water-saturated sand." *Prob. of Eng. Seismology*, 6(21), 92–94 (in Russian).
- Rollins, K.M., Ashford, S. A., and Lane, J. D. (2001). "Full-scale lateral load testing of deep foundations using blast induced liquefaction." *Proc., 4<sup>th</sup> int. conf. on Recent Advances in Geotechnical Earthquake Engineering and Soil Dynamics*, Univ. of Missouri-Rolla, MO, 1-3.
- Rollins, K.M. (2004). "Liquefaction mitigation using vertical composite drains: Full-scale testing." *Final Report for Highway IDEA Project 94*. Transportation Research Board, February 2004, 105 p.
- Rollins, K.M., Lane, J.D., Nicholson, P.G., and Rollins, R.E. (2004). "Liquefaction hazard assessment using controlled-blasting techniques." *Proc. 11th International Conference on Soil Dynamics & Earthquake Engineering*. Vol. 2, pp. 630-637.
- Rollins, K.M., Lane, J.D., Dibb, E., Ashford, S.A., and Mullins, A.G. (2005a). "Pore pressure measurement in blast-induced liquefaction experiments." *Transportation Research Record 1936, Soil Mechanics 2005*, TRB, Washington D.C., pp. 210-220.
- Rollins, K.M. and Anderson, J.K.S. (2008). "Cone penetration resistance variation with time after blast liquefaction testing." *Procs. Geotechnical Earthquake Engineering and Soil Dynamics-IV*, Geotechnical Special Publication 181, ASCE, 10 p.
- Rollins, K.M. and Hallenbaugh (2015). "Liquefaction induced negative skin friction from blast-induced liquefaction tests with Auger-cast Piles." *6<sup>th</sup> International Conference on Earthquake Geotechnical Engineering*, Christchurch, New Zealand.
- Seed, H.B., Martin, P.P., and Lysmer, J. (1975). "The Generation and Dissipation of Pore Water Pressures During Soil Liquefaction." *Report Number UCB/EERC-75/26*, University of California at Berkeley, Berkeley, CA.
- Strand, S. R. (2008). "Liquefaction mitigation using vertical composite drains and liquefaction induced downdrag on piles: implications for deep foundation design." *PhD Thesis*, Brigham Young University.

- Studer, J., L. Kok, and R. W. Trense (1978), Soil liquefaction field test—Meppen Proving Ground 1978 free field response, paper presented at 6th International Symposium on Military Applications of Blast Simulation, Fr. Minist. of Def., Cahors, France.
- Studer, J. and Kok, L. (1980). “Blast-induced excess porewater pressure and liquefaction experience and application.” International Symposium on Soils under Cyclic and Transient Loading, Swansea, UK, pp. 581-593.
- Stuedlein, A.W., Gianella, T. N., and Canivan, G. (2016). “Densification of granular soils using conventional and drained timber displacement piles.” *J. Geotech. Geoenviron. Eng.*, 10.1061/(ASCE)GT.1943-5606.0001554, 04016075.
- Tokimatsu, K., and Seed, H.B. (1987). “Evaluation of settlements in sands due to earthquake shaking,” *Journal of Geotechnical and Environmental Engineering*, 103(8), 861-878.
- Vega-Posada, C. A. (2012). “Evaluation of liquefaction susceptibility of clean sands after blast densification.” Ph.D. dissertation, Northwestern Univ., Dept. of Civil Engineering, Evanston, IL, 209.
- Veyera, G. E. (1985). “Transient porewater pressure response and liquefaction in a saturated sand.” Ph.D. dissertation, Department of Civil Engineering, Colorado State University, Fort Collins.
- Walthan, T. (2001), The explosion crater at Fauld, *Mercian Geol.*, 15(2), 123–125.
- Yamamura, K. and Koga, Y., (1974). “Estimation of Liquefaction Potential by Means of Explosion Test,” Proc. of the 6th Joint Panel Conference of U.S. - Japan Cooperative Program in Natural Resources, National Bureau of Standards, Washington, D.C., Vol. 76, May. pp. 111-38-51.
- Yi, F. (2010). “Procedure to evaluate liquefaction-induced settlement based on shear wave velocity.” 9<sup>th</sup> US National and 10<sup>th</sup> Canadian Conference on Earthquake Engineering: Reaching Beyond Borders.
- Zhang, G., Robertson, P. K., and Brachman R. W.I. (2002). “Estimating liquefaction-induced ground settlements from CPT for level ground.” *Canadian. Geotech. J.*, NRC Canada, 39(5), 1168-1180.

## CHAPTER 3: Design of Deep Foundation Elements and Analysis of Dragload and Downdrag

### 3.1. Chapter Overview

The methodology for the design of two type of deep foundations, including drilled shafts and driven piles are discussed in this chapter. These design methodologies, are in accordance with the methods presented by the American Petroleum Institute (API), the American Association of State Highway and Transportation Officials (AASHTO) and the Federal Highway Administration (FHWA). A review of the common empirical and analytical equations used to calculate the nominal shaft resistance and toe resistance in cohesive and non-cohesive soil is presented in Section 3.2. In addition, the use of two software programs including, UNIPILE and FB-Deep to estimate the nominal resistance of a deep foundation is discussed in Section 3.3. Full-scale load tests and the instrumentation used to determine the amount of axial resistance are discussed in Section 3.4. A literature review on development of consolidation-induced dragload and downdrag, and the current understanding of these two phenomena is provided in Sections 3.5. An overview on liquefaction-induced dragload is discussed in Section 3.5.2. A discussion on liquefaction-induced dragload and downdrag in published design specifications is presented in Section 3.5.3.

### 3.2. Estimation of Geotechnical Axial Resistance

Deep foundations are used to support structural loads when shallow foundations do not provide adequate resistance to support the structure. The axial geotechnical resistance ( $R_t$ ), provided by a deep foundation to support a structure is divided into two components: shaft resistance,  $R_s$  and toe resistance,  $R_{toe}$  (Figure 3.1). As shown in Equation 3.1, the magnitude of the nominal total axial resistance of a deep foundation is determined by the summation of  $R_s$  and  $R_{toe}$ . Load and resistance factor design (LRFD) or allowable stress design (ASD) methodologies

can be applied to Equation 3-1 to compensate for uncertainties in material properties, construction tolerances, and variability in loads (Brown et al. 2010). Several empirical and analytical methods have been proposed to calculate the amount of unit shaft and toe resistances in cohesive and cohesionless soils.

$$R_t = R_s + R_{toe} = A_s f_s + A_g q_{toe} \quad \text{Equation 3.1}$$

Where  $R_t$  is the unfactored nominal total resistance,  $R_s$  is an unfactored total shaft resistance;  $R_{toe}$  is unfactored toe resistance,  $A_s$  is the surface area of a deep foundation,  $f_s$  = unit shaft resistance,  $A_g$  is the gross area of a deep foundation, and  $q_{toe}$  is the unit toe resistance.

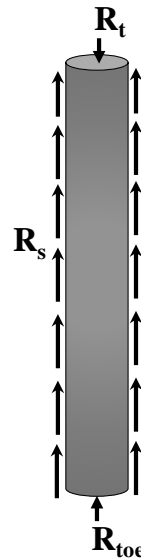


**Figure 3.1.** A schematic of an axially loaded deep foundation.

### 3.2.1. Unit Shaft and Toe Resistance in Cohesive Soils

For a deep foundation installed in cohesive soils, the nominal unit shaft resistance ( $f_s$ ) developed along a foundation, can be calculated using the total stress method known as “ $\alpha$ -method.” As reported in Hannigan et al. (2016), and presented in Equation 3.2, the approach is based on the assumption that the shaft resistance is independent of the vertical effective stress, and  $f_s$  is expressed as the product of the empirical adhesion factor ( $\alpha$ ) and the undrained shear strength ( $s_u$ ), as presented in Equation 3.2. For a foundation constructed in a cohesive soil, the

toe resistance is determined by using Equation 3.3. For cohesive soils, the  $f_s$  and  $q_{toe}$  have a limiting values of 380kPa (55psi) and 4000kPa (580 psi), respectively, as reported by O'Neill and Reese (1999).

$$f_s = \alpha \cdot s_u \quad \text{Equation 3.2}$$

The factor of adhesion,  $\alpha$  can be computer as follow:

$$\alpha = 0.55 \quad \text{for } s_u/P_a \leq 1.5$$

$$\alpha = 0.55 - 0.1 \cdot \left( \frac{s_u}{P_a} - 1.5 \right) \quad \text{for } 1.5 < s_u/P_a \leq 2.5$$

Where,  $P_a$  is the atmosphere pressure (101kPa or 14.7 psi).

$$q_{toe} = N_c s_u \quad \text{Equation 3.3}$$

Where  $N_c$  is the bearing capacity factor that is computed using the equations that were proposed by Fleming et al. (2009) and are presented as follows:

$$N_c = 9 \quad \text{for } h_{pen} \geq 3B,$$

$$N_c = 6 + \frac{h_{pen}}{B} \quad \text{otherwise.}$$

### 3.2.2. Unit Shaft and Resistance in Cohesionless Soils

For cohesionless soils (e.g., sands, gravels), the shaft resistance acting along a deep foundation can be calculated using the effective stress approach, known as “ $\beta$ -method.” Several empirical equations have been proposed for determining the  $\beta$  coefficient that is presented in Equation 3.4 (e.g., Chen and Kulhawy 2002, Tomlinson and Woodward 2008). However, a more reliable equation (Equation 3.5) that considers the in-situ conditions was recommended by Brown et al. (2010). Brown et al. (2010) approach was derived from the Chen and Kulwawy (2002) equations. In cohesionless soils, the toe resistance is computed using Equation 3.6.

$$f_s = \beta \sigma_v' \quad \text{Equation 3.4}$$



Where  $\beta$  is the shaft resistance coefficient that can be calculated using Equation 3.5, and  $\sigma'_v$  is vertical the effective stress.

$$\beta = \left(1 - \sin \phi'\right) \left(\frac{\sigma'_p}{\sigma'_v}\right)^{\sin \phi'} \tan \phi' \quad \text{Equation 3.5}$$

The following variables are used in Equation 3.5 can be determined as follows:

$$\sigma'_p = p_a (0.15(N_{60}))$$

$$\phi' = 27.5 + 9.2 \log[(N_1)_{60}]$$

Where  $\sigma'_p$  is the effective vertical preconsolidation stress,  $\phi'$  is the effective stress friction angle correlated from in-situ penetration tests or measured from triaxial tests,  $p_a$  is the atmosphere pressure, and  $N_{60}$  and  $(N_1)_{60}$  are N value corrected to 60 percent efficiency and the normalized SPT resistance, respectively.

$$q_{toe} = 1.2N_{60} \quad \text{Equation 3.6}$$

A thorough understanding on how load transfer from a deep foundation to soil during loading, and soil to foundation during soil settlement is required during the design of a foundation design. As reported by Fellenius et al. (1998), the amount of load transfer is governed by effective stress in the surrounding soil; the shaft and toe resistances are proportional to effective stress. Therefore, the  $\alpha$ -method and  $\beta$ -method are commonly recommended to be used to estimate the shaft resistance in cohesive and cohesionless soils, respectively.

### 3.3. Prediction of Axial Resistance using Software Programs

#### 3.3.1. FB-Deep

The FB-Deep, version 2.04, can be used to estimate static, axial, resistance of drilled shaft or driven pile foundation (s). The program was developed by the Bridge Software Institute at the University of Florida. The static, axial, resistance values obtained from FB-Deep are

determined by using the appropriate empirical equations provided in the FHWA design manuals (Brown et al. 2010). FB-Deep uses indirect methods (CPT and SPT data) for driven pile analysis. The SPT methodology is based on empirical correlations between CPT and SPT data for typical Florida soil types (Schmertmann 1978, Bloomquist et al. 1992). Three methods are included in FB-Deep program for CPT analysis: 1) the Schmertmann method developed by Schmertmann (1978), 2) the Laboratoire Central de Ponts et Chaussées (LCPC) method described in French highway department by Bustamante and Gianceselli (1982), and 3) The University of Florida (UF) method proposed in Florida Department of Transportation (FDOT) by Hu (2007). For drilled shaft foundation analysis, the axial capacity of a drilled shaft is predicted using the empirical equations provided in O'Neill and Reese (1999) in FHWA design manual. The methods proposed in McVay et al. 1999 are used to determine axial resistance of a drilled shaft installed in limestone. In addition, FB-Deep can also be utilized to predict the load-settlement curve for a drilled shaft foundation.

### **3.3.2. UNIPILE**

UNIPILE, version 5.0, was developed by Gouderault and Fellenius (2015) to estimate the nominal axial, static, geotechnical resistance and load-settlement curves for a single or a ground driven pile or drilled shaft foundations. The total resistance and load-settlement values, as obtained from UNIPILE, are predicted using indirect and direct methods. For indirect methods ( $\alpha$ -method or  $\beta$ -method), the soil strength parameters (e.g., unit weight, undrained shear strength, and friction angle) are correlated from CPT data. For direct methods, that includes: Eslami and Fellenius (CPTu), Schmertmann and Nottingham (CPT), deRuiter and Beringen-Dutch (CPT), Bustamante-LCPC (CPT), Decourt (SPT), O'Neil and Reese (SPT) or the Meyerhof (SPT) methods, are included in the program to estimate total resistance directly from CPT or SPT data. UNIPILE 5.0 is also capable of simulating a top-down and a bi-directional (O-cell) static load

test. In addition, the program is capable of performing the unified pile design method (Fellenius 1984, 1988, 2004) to assess consolidation-induced dragload and downdrag.

### **3.4. Full-scale Axial Compression Load Testing of Deep Foundations**

Determination of the total axial resistance and detailed information on load transfer under an axial load is one of the most important problems in foundation engineering (Goble and Hussein 1995). As reported by Brown et al. (2010) and Hannigan et al. (2016), the behavior of drilled shaft or driven pile foundations is highly dependent upon the local geology and the construction procedures. Therefore, it is essential for designers to perform at least one or more full-scale tests to ensure the use of reliable foundation design parameters, instead of the use of predicted parameters. According to Hannigan et al. (2016), static load testing is the most accurate method to measure the axial resistance and to evaluate the axial behavior of a deep foundation. Deep foundation elements can be tested in axially in compression or tension, or laterally. Four types of full-scale load test have been established and are commonly utilized to determine the axial resistance of a deep foundation. These tests include: conventional top-down loading testing, bi-directional load cell testing, static testing, and high strain dynamic load testing. Due the purpose of this research, only the topic of axial compression load tests is considered and discussed herein; only conventional top-down loading, bi-directional load, and high strain dynamic load tests are discussed.

#### **3.4.1. Conventional Top-Down Load Test**

As discussed by Brown et al. (2010), a conventional top-down load test is the most reliable test method to measure the performance of a drilled shaft foundation under axial load. The test consists of applying a static load on the top of the foundation. As stated by Kyfor et al. (1992), the load can be applied: 1) directly onto a platform on the drilled shaft head, as shown in Figure 3.2, 2) using a jack against a loaded platform, as illustrated in Figure 3.3, and 3) using a

jack against an anchored reaction beam system, as shown in Figure 3.4. The test pile or drilled shaft is typically instrumented with strain gauges to determine the load distribution during loading phase. The test is conducted in accordance with ASTM D-1143 (2013), and the tests can be performed during the design or construction stage.



**Figure 3.2.** A photograph of a dead weight being applied to a drilled shaft foundation (photo courtesy of Elvis Ishimwe).

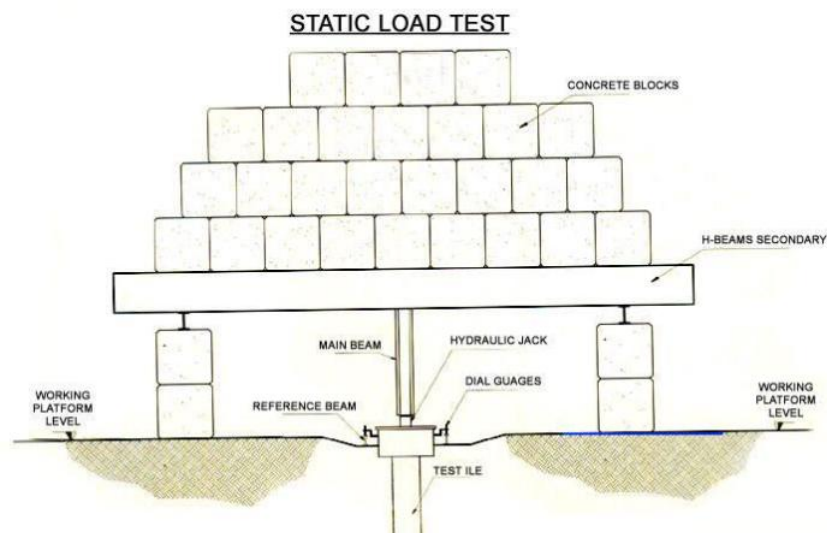


**Figure 3.3.** A schematic of a platform loaded by concrete blocks (courtesy of Ganpati Construction Company).

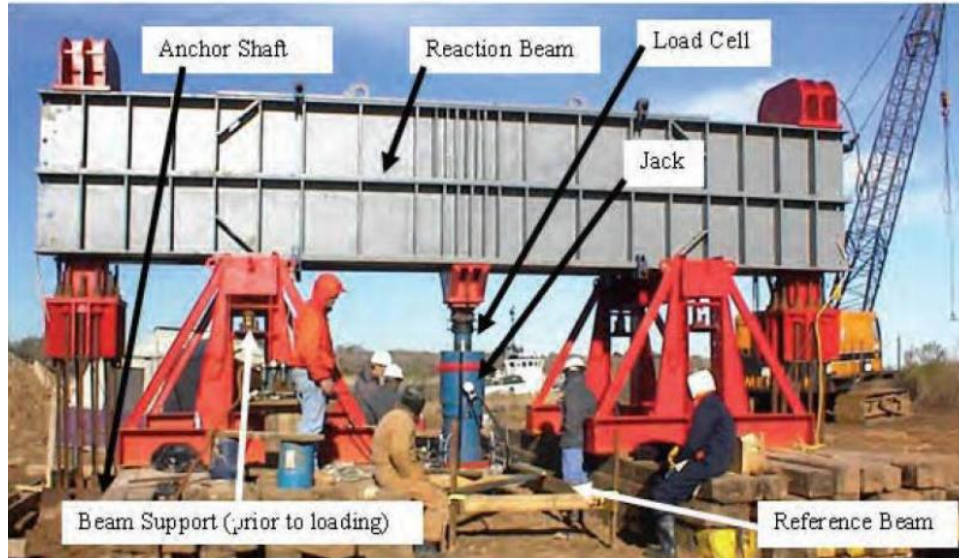


**Figure 3.4.** A photograph of conventional static load test being conducted on a drilled shaft foundation [photograph by Bill Isenhower and presented in Brown et al. (2010)].

As reported by Goble and Hussein (1995), various methodologies have been developed for performing static loading tests; the main difference relies on instrumentation, load application and interpretation of the test results. According to Brown et al. (2010), the testing cost may be reasonable for small diameter (3 to 4ft) drilled shafts. Brown et al. (2010) also stated that conventional top-down load test may not be economical tests for high load capacity and large diameter drilled shaft, because of the high load that are required to fully mobilize the shaft and toe resistance. Time, effort, level of safety and costs required to apply a static or dead weight load are some of the limitations of the top-down compression testing method.

### **3.4.2. Bi-directional Load Cell Test**

The bi-directional (O-cell) load test was developed by Jorj O. Osterberg to reduce the costs and other limitations associated with conventional top-down load test. The time and cost reduction are achieved by eliminating the use of a reaction beam system (static load frame, anchor system, hydraulic jack). As defined by Osterberg (1984) and Osterberg (1994), the O-cell test is a truly static load that uses shaft resistance to react against the toe resistance during the

application of the load from a hydraulic jack installed within a foundation. Typically, the hydraulic jack is installed at the toe or somewhere along the shaft (Figure 3.5) depending upon the soil conditions. Unlike the top-down test, the O-cell applies loads to the foundation in compression from the bottom of the foundation to the top.

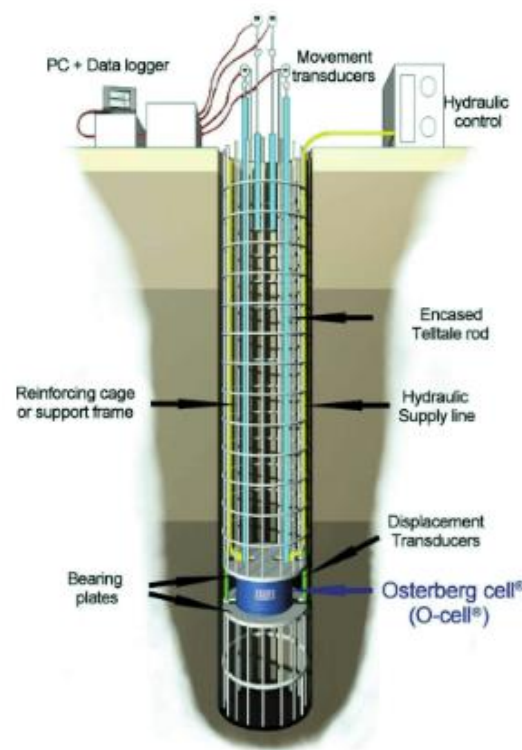


**Figure 3.5.** Bi-directional load cell (O-Cell) installed within a drilled shaft foundation (courtesy of Loadtest. Inc.).

During the test, the upper portion of the deep foundation is used as a reaction against the toe or the lower portion of the shaft (Brown et al. 2010). The O-cell test setup is shown in Figure 3.5 along with the instrumentation (Table 3.1) that is used during the test. As illustrated in Figure 3.5, the O-cell device consists of two bearing plates and one or multiple expandable hydraulic jacks casted within the test drilled shaft or pile. As shown Figure 3.5, a hydraulic supply line connected to the automatic pump is utilized to supply hydraulic pressure to the cell. In additional

to the O-cell device, other instrumentation are used during the test (Table 3.1). The location and the measurement component of each instrumentation are also presented in Table 3.1

**Table 3.1.** O-Cell load testing program instrumentation (after Miller 2003).

<b>Instrumentation</b>	<b>Load Test Location</b>	<b>Measurement Component</b>
Linear Vibrating Wire Transducers (LVWT)	Bottom plate of O-cell	Extension between the two plates of the O-cell
Linear Voltage Displacement Transducers (LVDT)	Reference beam or telltale of shaft	Vertical/horizontal movement of the top of the shaft
Strain Gauges	Various locations along the shaft	Strain/Stress within the shaft
Dial Gauges	Reference beam or telltale at top of shaft	Vertical/horizontal movement of the top of the shaft
Telltales	Extend from the bottom and/or top plate of the O-cell to the top of the shaft	Vertical movement of the O-cell and compression of the shaft

Like other static load tests, a load-settlement curve is obtained from bi-directional load measurements. The upward and downward loads are determined from the hydraulic jack at various times during testing. Likewise, to determine the load-settlement curve, the upward and downward movements are also obtained at various times from telltales installed at the top and bottom bearing plates, respectively. According to Brown et al. (2010), the O-cell test is typical terminated when: 1) the maximum axial resistance of the upper portion or bottom portion of the foundation has been achieved, and/or 2) the maximum expansion of the O-cells has been reached. An example of O-cell test results depicting the movement of the upper and bottom portion a drilled shaft is shown in Figure 3.6a. The equivalent top-down load-settlement curve is obtained from Figure 3.6a, by adding the shaft resistance (upward load) to the toe resistance (downward load) at the equal amount of movement (Figure 3.6b). The standard methods for performing an O-cell test and the procedures that must be followed to evaluate the results from the O-cell tests can be found in Brown et al. (2010).

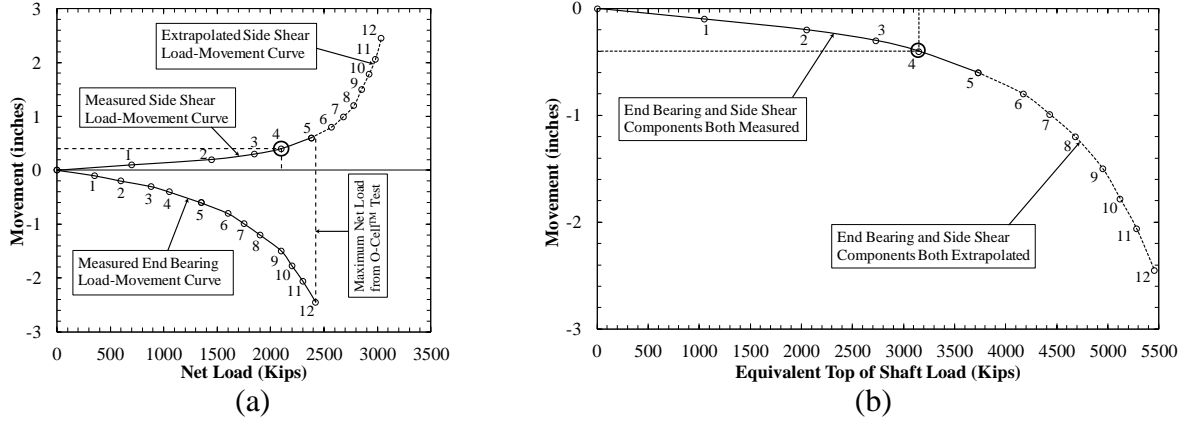


**Figure 3.6.** Example of bi-directional load cell (O-Cell) test results: (a) measured upward and downward movement curves and (b) equivalent top-down load and settlement curve (modified from Brown et al. (2010)).

### 3.4.3. High Strain Dynamic Load Test

According to Goble and Hussein (1997), the high strain dynamic load test was developed at the Case Institute of Technology, currently known as Case Western Reserve University by Goble et al. (1975) to evaluate the static axial capacity of piles from measurements of the force within the pile and the acceleration of the pile when subjected to hammer impacts. Dynamic tests can be conducted during the design and construction phases. As shown in Figure 3.7a, two types of instrumentation, including a strain transducer and accelerometer are mounted at a location near the pile head during pile installation or restruck with an impact hammer (Hannigan et al. 2016). The force obtained from the strain transducer is determined using Equation 3.7. The measured acceleration is integrated to obtain the velocity, and the force from acceleration is obtained using Equation 3.8.

$$F_{\varepsilon} = \varepsilon \cdot E \cdot A \quad \text{Equation 3.7}$$

$$F_V = \frac{vEA}{c} \quad \text{Equation 3.8}$$

Where  $F_{\varepsilon}$  is the force measurement obtained from strain transducer,  $\varepsilon$  is the strain from strain transducer,  $E$  is the elastic modulus of the deep foundation element,  $A$  is the gross area of the



deep foundation element,  $F_v$  is the force obtained from the accelerometer,  $v$  is the particle velocity integrated from the acceleration measurement,  $c$  is the compression wave speed within the deep foundation element.

The data obtained from strain and acceleration transducers are collected, stored and processed using a field laptop called the pile driving analyzer (PDA) as shown in Figure 3.7b. These high strain dynamic measurements can be used to: 1) evaluate pile driving and static resistances, 2) determine the pile driving stresses, 3) assess pile integrity, and 4) investigate hammer and driving system performance Goble and Hussein (1997). As reported by Hannigan et al. (2016), a signal matching software program known as the Case Wave Analysis Program (CAPWAP) is used to estimate the resistance of a deep foundation by using the force measurements obtained during the hammer impact. An example of CAPWAP results is provided in Figure 3.8. The basic concepts of wave mechanics and the interpretation of the dynamic load test results are discussed in detail by Hannigan et al. (2016).

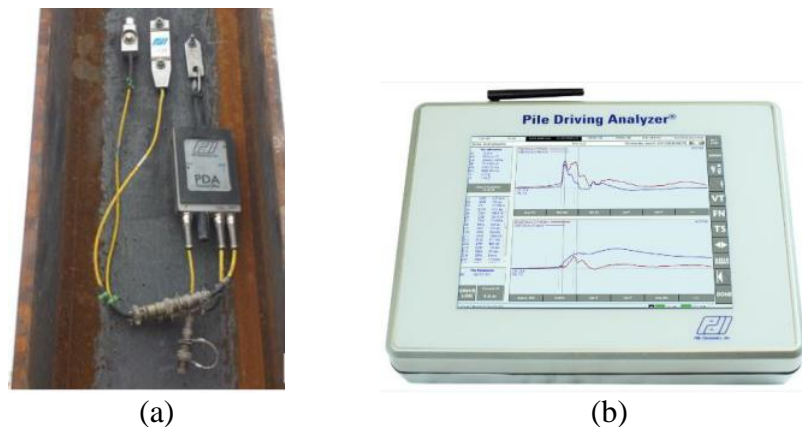


**Figure 3.7.** (a) accelerometer, strain transducer, and WIFI transmitter utilized during pile dynamic tests [photograph Pile Dynamics presented in Hannigan et al. (2016)], and (b) pile driving analyzer (photo courtesy of Pile Dynamics, Inc.).

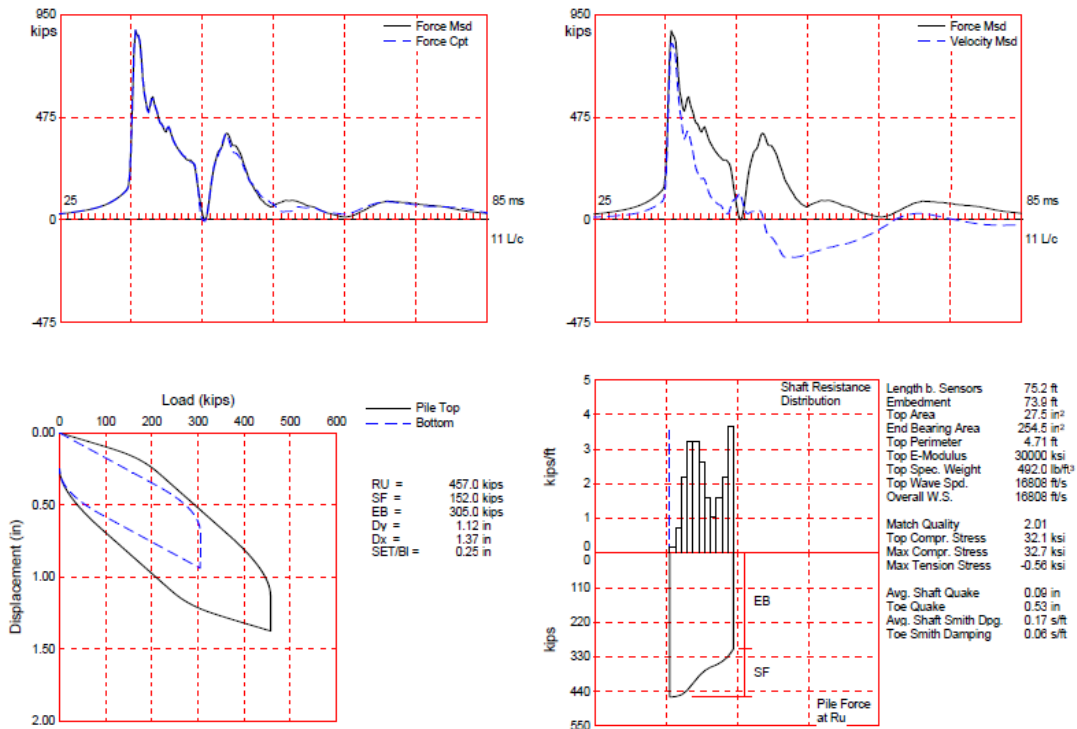


**Figure 3.8.** Example of CAPWAP output results (Coffman and Ishimwe 2017).

### 3.5. Development of Negative Shaft Resistance (Dragload)

As previously mentioned, the phenomenon of negative shaft resistance (NSF) or dragload on deep foundations has been addressed by several researchers (e.g., Bjerrum et al. 1969, Endo et al. 1969, Bozozuk 1970, 1972, 1981, Fellenius 1972, Long and Healy 1974, Fellenius 1984, Fellenius 2004, Poulos and Davis 1990, Davisson 1993, Briaud and Tucker 1997, Siegel et al. 2013). Various types of tests (field and laboratory centrifuge) have been conducted to evaluate the influence of this phenomenon on the performance deep foundation. Chellis (1951) was the first to report case histories when piles failed due the developed dragload. Little (1994) presented a review of the literature, including various field experiments, laboratory experiments, and theories regarding dragload. In addition, Briaud and Tucker (1997) provided case histories where dragloads have caused extensive damages to the actual structures. Briaud and Tucker (1997) also

reported that dragload forces have caused differential settlements, and extensive serviceability damage to various structures.

Most of the failures reported in Chellis (1951) and Briaud and Tucker (1997) were in either serviceability (excessive settlements) or structural strength limits. Fellenius (2006) also provided a summary of some the results of the tests performed since 1960s through 1990s to investigate the development of NSF on instrumented piles. In contrary, Fellenius (2004) and Kurns (2008) presented the positive aspects of dragload forces in piled foundations design. As stated the FHWA (Hannagan et al. 2016), the concept of accounting for dragload in deep foundation design is complicated. Various analytical methods for how designers should account for dragload and downdrag in engineering practice are discussed further in the next sections.

### **3.5.1. Current Understanding of Dragload and Downdrag**

The consideration of dragload when designing deep foundations is a topic of ongoing discussion. As agreed upon by several researchers, the developed dragloads due to the soil settlement act in the same direction as the axial load applied on the top of a deep foundation (e.g., dead load, live and transient load). From this understanding, the dragload should be accounted for as an extra axial load acting on the foundation, and only resistance at the toe and the positive shaft resistance support the applied structural loads. Several design approaches have been developed and recommended for the consideration of dragload and downdrag (Fellenius 1988, Fellenius 1989, Briaud and Tucker 1997, Poulos 1997, Dumas 2005, Hannigan et al. 2005, Fellenius and Siegel 2008, Siegel et al. 2013); some of these aforementioned analytical methods have been adapted by different design specification codes. For instance, the AASHTO (2014) and some other AASHTO based state highway design codes adopted Briaud and Tucker (1997) method. In the Briaud and Tucker (1997) method, the dragload is considered as a permanent load acting on the top of the pile. Therefore, the dragload is recognized under the geotechnical

strength limit state by AASHTO. Briaud and Tucker (1997) also reported the conditions by which the dragload and downdrag phenomena should be considered in the design. The appropriate equation (Equation 3.9), and load factors ( $\eta$ ,  $\gamma$ ,  $\gamma_p$ ,  $\phi_s$ , and  $\phi_p$ ) that are applied to the dragloads and to other forces acting on the deep foundation were presented in Brown et al. (2010). Further explanation of this concepts and design method can be found in FHWA construction procedures and LRFD Design Methods by Brown et al. (2010).

$$\sum \eta \gamma (Q_{str}) + \gamma_p (Q_n) = \sum \phi_s (Q_p) + \phi_p (Q_{eb}) \quad \text{Equation 3.9}$$

Where  $\eta$ ,  $\gamma$  and  $\gamma_p$  are the load factors for dead load and dragload, respectively.  $\phi_s$ , and  $\phi_p$  are the resistance factors for side resistance and end bearing capacity; respectively, when the dragload and downdrag are induced along the deep foundation.  $Q_{str}$  is structural load applied at the top of the foundation,  $Q_n$  is the developed dragload,  $Q$  is the positive side resistance, and  $Q_{eb}$  is the bearing capacity at toe location.

In contrast, some other federal highway design specification codes including: the FHWA manual (Hannigan et al. 2006), Canadian Foundation Engineering Manual (CFEM 1992), NCHRP-FHWA Report 343 (Barker et al. 1991) ASCE and US Army Corps of Engineers Technical Engineering Design Guides No. 1 and 7 (ASCE 1993 1994), the Australian Piling Standard (1995) and Hong Kong Foundation Design and Construction manual (Hong Kong Geotechnical Engineering Office, 2006) have recognized the concept of considering dragload using the neutral plane method by Fellenius (1984, 1988, 2004) approach. According to the Fellenius (1984, 1988, 2004) approach also known as “the unified pile design”, dragload and downdrag should only be considered to: 1) evaluate allowable and design loads, 2) check the structural axial capacity of the pile, 3) check the potential for excessive pile settlement. For the allowable load, only dead and live load are considered, not dragload, and the maximum load

located at the neutral plane (obtained using dragload and dead load, but no live load) should not exceed the axial structural capacity of the pile. Based on the experimental data obtained from the case histories, Fellenius (2006) concluded that the magnitude of the dragload is a settlement issue, not a bearing capacity issue, and the effects of dragload should be neglected while designing foundations. Fellenius (2006) stated that as the pile settles due to the axial load applied on the pile head, the positive shaft resistance are re-developed on portion of the pile located above the neutral plane, and the dragload are eliminated as the plunging continues. In addition, based on Fellenius (2006) approach, only dead and live loads should be considered when designing piled foundations.

The most recent FHWA Design and Construction of Driven Piles manual prepared by Hannigan et al. (2016) presented a design approach based on the modified neutral plane method that was introduced by Siegel et al. (2013). Hannigan et al. (2016) recommended that the developed dragload and downdrag should be considered for the structural strength and geotechnical service limit states, respectively. Specifically, dragload and downdrag are considered: 1) to evaluate allowable load and design loads, 2) to check the structural axial capacity ( $P_r$ ) of a given deep foundation (Equation 3.10), and 3) to check the potential for excessive settlement of a deep foundation. The site conditions and the requirements to implement the modified neutral plane method were discussed by Siegel et al. (2013) and Hannigan et al. (2016). The location of the neutral plane and the magnitude of the induced dragload are determined. The equation (Equation 3.10) presented by Hannigan et al. (2016) is then used to check the structural strength limit. In addition, designers are required to ensure that the magnitude of the ground settlement and downdrag are within the acceptable limit. The step by

step procedures for dragload analysis using this method are discussed in the FHWA manual by Hannigan et al. (2016) in Section 7.3.6.1.

$$1.25(Q_{str}) + \gamma_p(Q_n) < P_r \quad \text{Equation 3.10}$$

Where  $Q_{str}$  is the structural load,  $Q_n$  is the developed dragload,  $\gamma_p$  is the load factor for dragload,  $P_r$  is the structural axial capacity from a deep foundation.

### **3.5.2. Liquefaction-induced Dragload and Downdrag**

As previously mentioned, the post-liquefaction settlement caused by dissipation of porewater pressure can also lead to dragload and downdrag around a deep foundation. The possible mechanisms for deep foundation failure in liquefiable soils includes: 1) bending due to the liquefaction-induced lateral spreading, 2) collapse of foundations due to either reduction or increase of the toe and shaft resistances, and 3) punching due the excessive settlements. As reported by Dash et al. (2008), liquefaction-induced lateral spreading has been considered as the root cause of many pile foundation failures during earthquakes. However, liquefaction-induced dragload and downdrag has been reported as another possible mechanisms of deep foundation failure in liquefiable soils. Most of the research studies and analytical theories presented in the literature are based on consolidation-induced dragload and downdrag, and only few research studies have been performed to evaluate liquefaction-induced dragload and downdrag (e.g., Boulanger and Brandenburg 2004, Rollins and Strand 2006, Fellenius and Siegel 2008, Rollins and Hollenbaugh 2015).

#### **3.5.2.1. Boulanger and Brandenburg (2004)**

Boulanger and Brandenburg (2004) modified the traditional neutral plane method (Fellenius 1984) for liquefaction-induced dragload on vertical piles by accounting the variation of excess pore pressures and ground settlements over time as a liquefied layer reconsolidates.

Unlike the consolidation-induced dragload, the determination of the post-liquefaction settlements

requires 1) the excess porewater pressure isochrones over time, and 2) a relationship between the sand compressibility ( $m_v$ ) and the excess porewater pressure ratio ( $R_u$ ). Boulanger and Bandenberg (2004) provided an empirical relationship to determine the unit shaft resistance ( $f_s$ ), within a liquefied soil layer, as porewater pressure dissipates.

$$f_s = \sigma'_{vo} K_o \tan(\phi)(1 - R_u) \quad \text{Equation 3.11}$$

Where  $\sigma'_{vo}$  is the effective stress,  $\phi$  is the friction angle,  $K_o$  is the coefficient of lateral earth pressure at rest, and  $R_u$  is the excess porewater pressure ratio.

### 3.5.2.2. Fellenius and Siegel (2008)

Fellenius and Siegel (2008) applied the unified design method (Fellenius 1984, 2004, 2014), a method developed for consolidation-induced dragload and downdrag, to analyze the effect of liquefaction on an axially loaded driven pile. Fellenius and Siegel (2008) analyzed the load and distribution curves when the liquefiable layer was located: 1) above the static neutral plane (Figure 3-9), and 2) below the static neutral plane (Figure 3-10). As illustrated in Figure 3-9, there was no change on load and distribution curves when the liquefying layer was located above the static neutral plane.

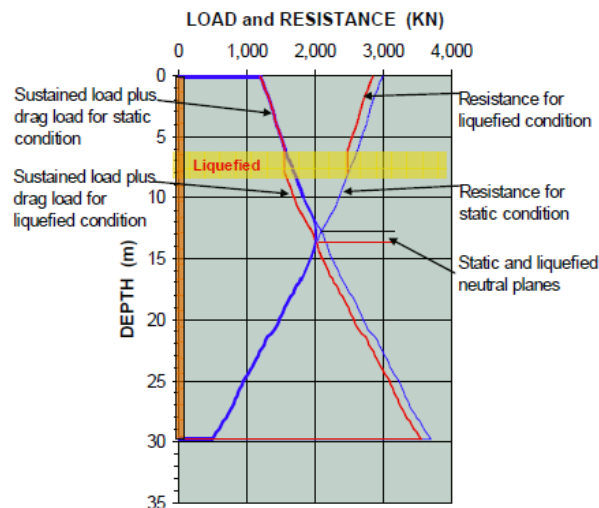


**Figure 3.9.** Load and resistance distribution curves when the liquefied zone is located above the static neutral plane (from Fellenius and Siegel 2008).

For this case, the loss of NSF within the liquefied zone will not affect the pile performance under an axial load. Contrary, different observations are obtained for the case where the liquefiable zone is located below the static neutral plane (Figure 3.10). After liquefaction, 1) the static neutral plane was re-located to the lower boundary of the liquefied zone, 2) an increase of dragload is observed, and 3) an increase in the mobilized toe resistance with the corresponding toe penetration (Fellenius and Siegel 2008). As stated by Fellenius and Siegel (2008), liquefaction of soils below the static neutral plane increases the axial compressive load in the pile and induces additional settlements. Therefore, Fellenius and Siegel (2008) recommended that for designers should consider the liquefaction-induced dragload for the structural design of pile section and settlement evaluation. Boulanger and Bandenberg (2004) and Fellenius and Siegel (2008) agreed that the problem of liquefaction-induced dragload is a settlement (downdrag) issue, not bearing capacity issue.

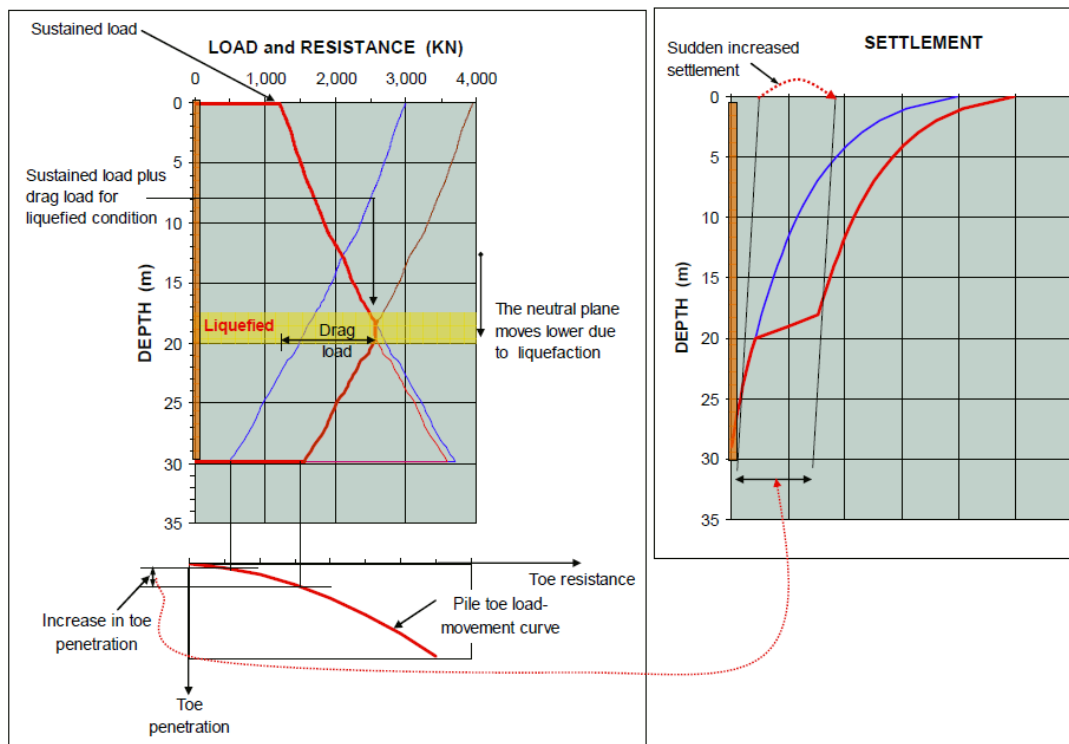


**Figure 3.10.** Load and resistance distribution curves when the liquefied zone is located below the static neutral plane (from Fellenius and Siegel 2008).



### 3.5.2.3. Rollins and Strand (2006)

Rollins and Strand (2006) performed a blast-induced liquefaction test, to evaluate the loss of NSF and the development of liquefaction-induced dragload on a 324 mm- diameter instrumented steel pipe pile with a 9.5 mm wall thickness. The test pile was driven close-ended with an embedment length of 21.3 m. The testing site was located near Vancouver, Canada, and the soil profile consisted of silty sand, clayey silts, and clean sands. The test pile was instrumented with strain gauges at the location shown in Figure 3.11. A load was applied on the top of the pile via a hydraulic jack and a reaction beam system to simulate the structural load. Liquefaction was induced by detonating small explosive charges installed around the test pile. The ground surface settlements were monitored using string potentiometers and the ground settlement as a function of depth was measured using a Sondex tube. The resistance distribution curve that was obtained during the pile loading is shown in Figure 3.11. The load and resistance distribution curves obtained after blasting and at the end of settlement are also presented in Figure 3.11.

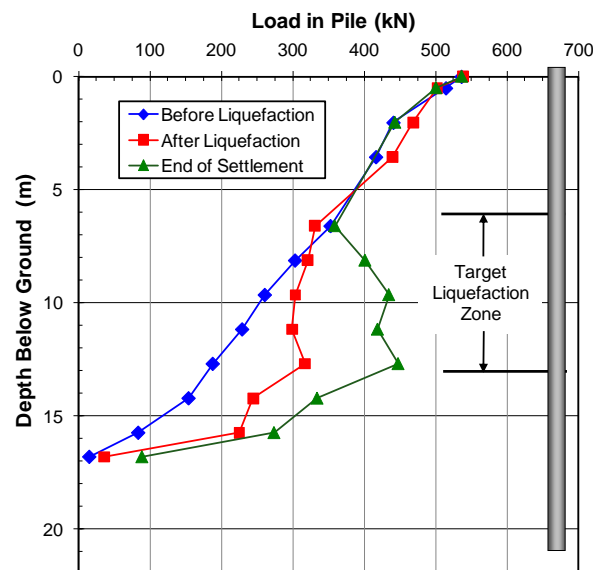


**Figure 3.11.** Load and resistance distribution curves as obtained before and after blasting (from Rollins and Strand 2006).

As shown in Figure 3.11, the applied load was transferred from pile to the soil and fully mobilized the shaft resistances to a depth of 13 m. As reported by Rollins and Strand (2006), the  $R_u$  values that were above the unit were observed; as the excess porewater pressure dissipated, the soil settled and the NSF, started to increase due to the decrease of porewater pressure. The developed dragloads were resisted by the positive shaft resistance and toe resistance below the neutral plane. At the end of excess porewater pressure dissipation, the average NSF within the liquefied layer, was approximately equal to 50% of the positive shaft friction before liquefaction (which is commonly assumed to be equal to zero). As noted in Rollins and Strand (2006), the use of hydraulic jacks prevented the ability to maintain a constant load on the pile head.

#### **3.5.2.4. Rollins and Hollenbaugh (2015)**

As noted in Rollins and Strand (2006), the use of hydraulic jacks prevented to maintain a constant load on the pile head. To overcome this problem, Rollins and Hollenbaugh (2015) performed a blast-induced liquefaction test around three 0.6 m diameter auger-cast piles in Christchurch, New Zealand. The site profile consisted of sandy silty and poorly graded clean sand. The three test piles were installed to depths of 8.5, 12 and 14 m below the ground surface. The plan view of the test piles and the location of the instrumentation used during testing are shown in Figure 3.12. The cross section of the testing site and the locations of the explosive charges, pore pressure transducers and strain gauges are presented in Figure 3.13. The ground surface settlement as a function of depth was measured using a Sondex profilometer installed at the location shown in Figure 3.13.

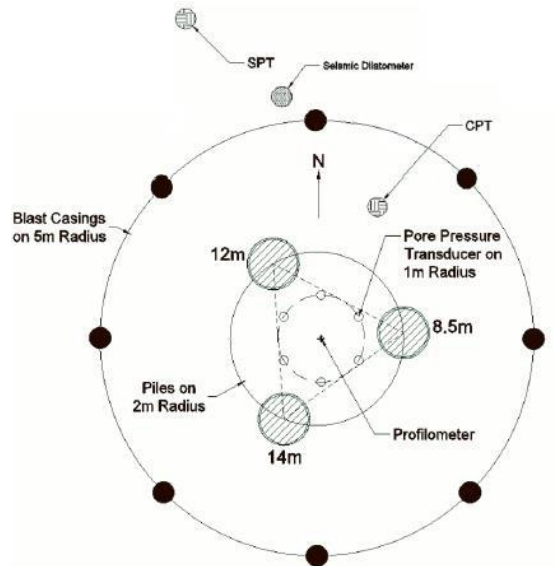


**Figure 3.12.** Plan view of the testing site (Rollins and Hollenbaugh 2015).

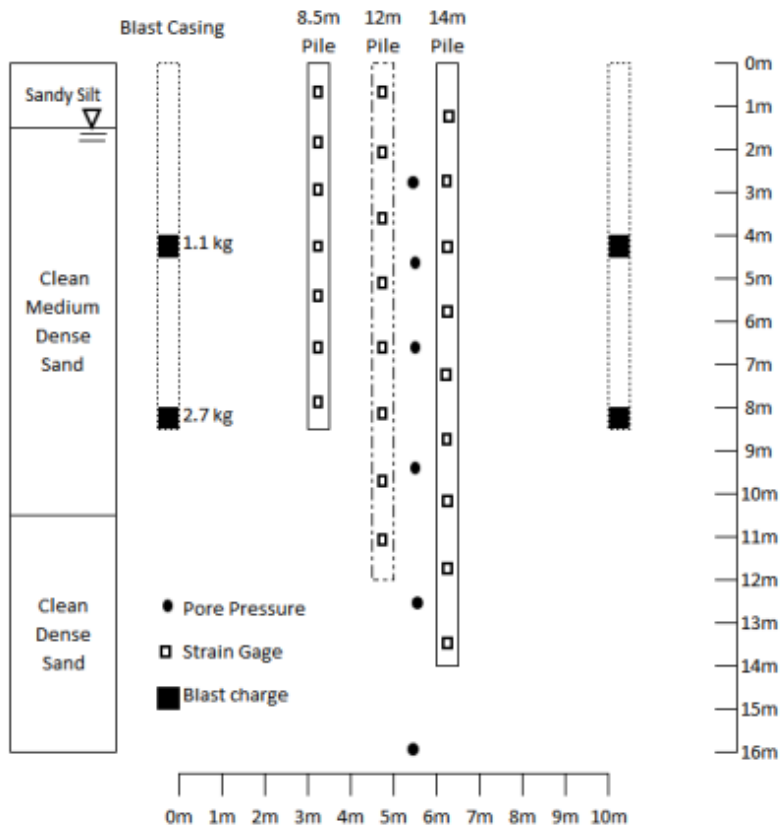


**Figure 3.13.** Cross sectional layout of the testing site (from Rollins and Hollenbaugh 2015).

Two sets of blasting tests were conducted at the testing site. The first set of blasting tests were performed with no load applied on the piles. The ground surface settlement as a function of depth was measured using a Sondex profilometer installed at the location previously shown in Figure 3.12. The measured and predicted load and resistance distribution curves of each pile are shown in Figure 3.14. As shown in Figure 3.14, the neutral plane location increased with the pile length, and the unit shaft resistance were between 50 and 70 percent of the unit shaft resistance predicted using the FHWA methods for drilled shaft foundations. At the end of excess porewater pressure dissipation, the average negative shaft resistance values were about 50 percent of the pre-blast positive shaft resistance. This was consistent with the observation obtained by Rollins and Strand (2006).

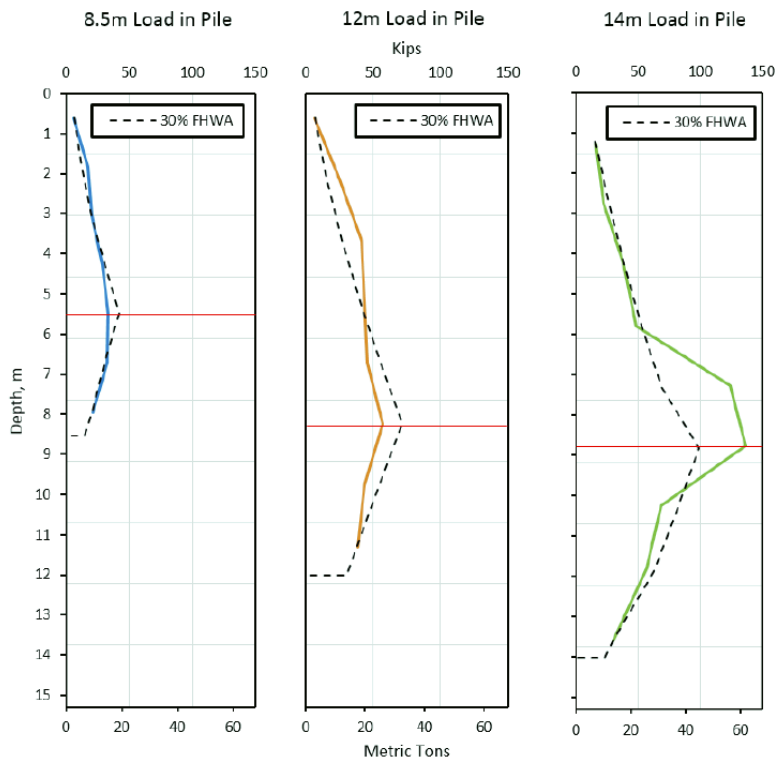


**Figure 3.14.** Post-blast and predicted load and resistance distribution curves (from Rollins and Hollenbaugh 2015).

### ***3.5.3. Liquefaction-induced Dragload and Downdrag Analysis in Design Codes***

The phenomenon of dragload induced due to the post-liquefaction settlements is addressed in few design specifications, including AASHTO and FHWA design manuals. For instance, Brown et al. (2010) stated that it is reasonable to assume that liquefaction-induced dragload and downdrag will occur after an earthquake event, as the excess porewater pressures dissipate. Brown et al. (2010) also proposed that foundation designers consider the dragload for the evaluation of strength and service limit states for drilled shaft foundations. The AASHTO (2014) method also account for the effects of dragload developed after seismic liquefaction. According to AASHTO, the dragload induced by seismic liquefaction are considered as Extreme Event I limit state, and the factored dragload is added to the factored loads (eg., live, dead and transient loads) for the structure. A load factor of 1.0 is recommended for liquefaction-induced dragload. Recently, FHWA by Hannigan et al. (2016) adapted Fellenius and Siegel (2008) for liquefaction-induced dragload. Like Fellenius and Siegel (2008) approach, Hannigan et al. (2016) also suggested to evaluate the structural design of the pile section and the settlement when liquefaction occurs below the static neutral plane.

In Washignton State Department of Transportation (WSDOT) final research report, Muhunthan et al. (2017) presented an analytical method to address the effects of liquefaction-induced downdrag on drilled shaft and driven pile foundations. The analytical method was based on the unified design method proposed by Fellenius and Siegel (2008) for liquefaction-induced dragload and downdrag around piles. The traditional unified design was modified to include the drilled shaft foundations and the potential for the presence of multiple liquefiable layers (Muhunthan et al. 2017). For the Muhunthan et al. 2017 research study, two important assumptions were made: 1) the soil settlement and pile settlment are equal at the neutral plane location, and 2) the shaft resistance within the liquiefied zone was zero. Muhunthan et al. (2017)

provided step-by-step analysis procedures to estimate the post-liquefaction load and resistance distribution curves for drilled shafts and driven piles. Muhunthan et al. (2017) applied the proposed analytical method to drilled shaft and driven pile foundations at the Juan Pablo II bridge to evaluate the impact of liquefaction on the foundations after the 2010 Maule earthquake in Chile. Unlike Fellenius and Siegel (2008), who located the neutral plane at a certain depth along the pile under static conditions (before liquefaction), Muhunthan et al. (2017), located the neutral plane at the top of the pile before liquefaction. The proposed method was able to estimate the liquefaction-induced downdrag at the Juan Pablo II bridge; however, there is a need of testing results to validate the aforementioned analytical methods.

### **3.6. Chapter Summary**

A literature review on the design of deep foundation, along with the empirical equations commonly used to estimate and measure the axial geotechnical resistance were provided in this Chapter. A brief review of existing empirical equations that are commonly used to calculate the nominal shaft and toe resistances in cohesive and non-cohesive soil were discussed. Results from different research projects on liquefaction-induced dragload and downdrag were discussed. A literature review on development of consolidation-induced dragload and downdrag, and the current understanding of these two phenomena was presented. The limitations of the existing design methods of deep foundations in liquefaction hazard areas were also discussed into detail.

### **3.7. References**

AASHTO (2012), LRFD Bridge Design Specifications: Parts 1 and 2. American Association of State Highway and Transportation Officials.

AASHTO (2014), "LRFD Bridge Design Specifications", American Association of State Highway and Transportation Officials, Seventh Edition, Washington, D.C.

American Petroleum Institute (API). (2003). Recommended Practice for Planning, Designing and Constructing Fixed Offshore Platforms – Load and Resistance Factor Design. API Recommended Practice 2A-LRFD (RP 2A-LRFD), First Edition, Reaffirmed 2003, 242p.

- ASTM D1143-07. (2014). Standard Test Methods for Deep Foundations Under Static Axial Compressive Load. Book of ASTM Standards, Vol. 4.08, ASTM International, West Conshohocken, PA, 15 p.
- Australian Piling Standard (1995). "Piling design and installation." Standard AS2159-1995, Australian Council of Standards, committee CE/18, Adelaide, Australia.
- Briaud, J.L., and Tucker, L. (1997). "Design and Construction Guidelines for Downdrag on Uncoated and Bitumen-Coated Piles." NCHRP Report 393, Transportation Research Board, National Academy Press, Washington, D.C., pp. 198.
- Brown, D. A., Turner, J.P. and Castelli R.J. (2010). "Drilled Shafts: Construction Procedures and LRFD Design Methods." FHWA-NHI-10-016, Geotechnical Engineering Circular (GEC) No. 10. U.S. Dept. of Transportation, Federal Highway Administration, 970 p.
- Boulanger, R.W and Brandenberg, S.J. (2004). "Neutral plane solution for liquefaction-induced downdrag on vertical piles." *Proceedings, ASCE Geo-Trans conference*, ASCE, Reston, VA, 470-479.
- Bozozuk, M. (1981). "Bearing capacity of a pile preloaded by downdrag." Proceedings of the 10<sup>th</sup> international conference on soil mechanics and foundations engineering, Mexico Cit, Vol. 2: 631-636.
- Bjerrum, L., Johannessen, I, J., and Eide, O., (1969). "Reduction of negative skin friction on steel piles to rock." Proc. 7th ICSMFE, Mexico City, Vol. 2, pp. 27-34.
- Bozozuk, M., (1972). "Down drag measurement on 160-ft floating pipe test pile in marine clay." Canadian Geotechnical Journal, Vol. 9, No. 2, pp. 127-136.
- Broms, B. B. and Silberman, J. O., (1964). "Skin friction resistance for piles in cohesionless soil." Sols-Soils, No. 10, pp. 33-41.
- Bustamante, M. and Gianselli, L., 1982. Pile bearing capacity predictions by means of static penetrometer CPT. Proceedings of the Second European Symposium on Penetration Testing, ESOPT II, Amsterdam, May 24-27, A.A. Balkema, Vol. 2, pp. 493-500.
- Canadian Geotechnical Society (1992). Canadian Foundation Engineering Manual, CFEM, third edition, BiTech Publishers, Vancouver. 512 p.
- Chellis, R. D. (1951), *Pile Foundations*, 1<sup>st</sup> Edition, McGraw-Hill Book Company, New York, New York.
- Chen, Y-J, and Kulhawy, F.H. (2002), "Evaluation of Drained Axial Capacity for Drilled Shafts," Geotechnical Special Publication No. 116, Deep Foundations 2002, M.W. O'Neill and F.C. Townsend, Editors, ASCE, Reston, VA, pp. 1200-1214.

- Dash, S.R, Bhattacharya, S. and Blakeborough, A.B. (2008): “Bending-Buckling interaction as a failure mechanism in seismically liquefiable deposits”, Technical Report of Oxford University. No 2302/08
- Davisson, M. T. (1993). “Negative skin friction in piles and design decisions.” International Conference on Case Histories in Geotechnical Engineering. 7.
- Decourt, L., 1982. Prediction of bearing capacity of piles based exclusively on N-values of the SPT. Proc. ESOPT II, Amsterdam, May 24-27, pp. 19-34.
- Decourt, L., 1989. The Standard Penetration Test. State-of-the-Art report. A.A. Balkema, Proc. of 12<sup>th</sup> International Conference on Soil Mechanics and Foundation Engineering, Rio de Janiero, Brazil, August 13-18, Vol.4, pp. 2405-2416.
- Decourt, L., 1995. Prediction of load-settlement relationships for foundations on the basis of the SPT. Proc. of the Conf. in honor of Leonardo Zeevaert, Mexico City, Oct. 28-Nov. 6, pp. 87-103.
- Decourt, L., 1999. Behavior of foundations under working load conditions. Proc. of 11th Pan-American Conference on Soil Mechanics.
- DeRuiter, J. and Beringen F.L., 1979. Pile foundations for large North Sea structures. Marine Geotechnology, 3(3) 267-314.
- Dumas, C. (2000). “Soil downdrag on deep foundations.” An overview of perspective proceedings of the 18<sup>th</sup> ASCE/PennDOT Geotechnical Seminar, Hershey, PA, 19p.
- Endo, M., Minou, A., Kawasaki, T., and Shibata, T. 1969. Negative skin friction acting on steel piles in clay. *In* Proceedings of the 8th International Conference on Soil Mechanics and Foundation Engineering, Mexico City, 25–29 August 1969. Mexico.
- Eslami, A., and Fellenius, B. H. (1997). Pile Capacity by Direct CPT and CPTu Methods Applied to 102 Case Histories. Canadian Geotechnical Journal, Vol. 34, No. 6, pp. 880-898.
- FB-Deep (2012). Bridge Software Institute, Gainesville, FL. Ver. 2.04.
- Fellenius, B.H., and Broms, B. B. (1969). “Negative skin friction for long piles driven in clay.” Proc. 7th ICSMFE, Mexico City, Vol. 2, pp. 93-98.
- Fellenius, B.H. (1972). “Reduction of negative skin friction with bitumen slip layers.” Discussion. Journal of the Geotechnical Engineering Division, ASCE, 101(GT4): 412–414.
- Fellenius, B.H. (1979). “Downdrag on bitumen coated piles.” Journal of Geotechnical Engineering, ASCE, 105 (GT10): 1262–1265.



- Fellenius, B.H., (1988). "Unified Design of Piles and Pile Groups." TRB Washington, Record 1169, pp. 75-82.
- Fellenius, B.H. (1991). *Foundation Engineering Handbook*, Chapter 13 - Pile Foundations. Second Edition. Van Nostrand Reinhold Publisher, New York, NY, pp. 511-536.
- Fellenius, B.H., (1998). "Recent advances in the design of piles for axial loads, dragloads, downdrag, and settlement." ASCE and Port of NY & NJ Seminar.
- Fellenius, B. H. (2004). "Unified Design of Piled Foundations with Emphasis on Settlement Analysis." Proceedings of ASCE Conference Deep Foundations 2004, pp. 253-275.
- Fellenius, B.H. (2006). "Results from long-term measurement in piles of drag load and downdrag" *Canadian Geotech. J.*, April 2006 43(4), 409-430.
- Fellenius, B. H. and Siegel, T.C. (2008). Pile drag load and downdrag in a liquefaction event *J. Geotech. and Geoenviron. Engrg.* ASCE, Reston, Virginia, 134 (9), 1412-1416.
- Fellenius, B.H. (2015). *Basics of Foundation Design*. Electronic Edition: [www.Fellenius.net](http://www.Fellenius.net), 432 pgs.
- Fleming, K., Weltman, A., Randolph, M. and Elson, K. (2009) *Piling Engineering*, 3rd ed. Taylor & Francis, New York.
- Goble, G. G., and Hussein, H. H., (1995). "Capacity evaluation methods of deep foundations: A critical review." GRL engineers, Cleveland, Ohio.
- Goudreault, P.A. and Fellenius, B.H., (2015). *UniPile Version 5 User Manual*, UniSoft Ltd., Ottawa, [[www.UniSoftLtd.com](http://www.UniSoftLtd.com)].
- Hannigan, P.J., Goble, G.G., Thendean, G., Linkins, G.E. and Rausche, F. (2005). "Design and Construction, Vol. I and II. Federal Highway Report No. FHWA-HI-05, Federal Highway Administration, Washington, D.C.
- Hannigan, P.J., Robinson, B. R., Goble, G.G., Likins, G.E. & Rausche, F., Becker, M. L. (2016). "Design and construction of driven pile foundations." FHWA-NHI-16-009, National Highway Institute, Federal Highway Administration, U.S. Department of Transportation, Washington, D.C.
- Hong Kong Geotechnical Office. (2006). "Foundation design and construction." Geo Publication No.1/2006, the Government of Hong Kong, Hong Kong.
- Hu, Z. (2007). "Updating Florida Department of Transportation's (FDOT) Pile/Shaft Design Procedures Based on CPT and DTP Data." Ph.D. thesis, Department of Civil Engineering, University of Florida.
- Ishihara, K. (1990). "Liquefaction and flow failure during earthquakes." *Géotechnique*, ICE, London, England, 43(3), 351-451.

- Kulhawy, F.H. and Chen, J. R. (2007). "Discussion of 'Drilled Shaft Side Resistance in Gravelly Soils' by Kyle M. Rollins, Robert J. Clayton, Rodney C. Mikesell, and Bradford C. Blaise," *Journal of Geotechnical and Geoenvironmental Engineering*, ASCE, Vol. 133, No. 10, pp. 1325-1328.
- Kyfor, Z.G., Schnore, A.S., Carlo, T.A. and Bailey, P.F. (1992). Static Testing of Deep Foundations. Report No. FHWA-SA-91-042, U.S. Department of Transportation, Federal Highway Administration, Office of Technology Applications, Washington, D.C., 174 p.
- Little, J. A. (1994), Downdrag of Piles: Review and Recent Experimentation, ASCE GSP 40, "Vertical and Horizontal Deformations of Foundations and Embankment", pp.1805-1826.
- Long, R. L, Healy, K. A. (1974). "Negative Skin Friction on Piles." Final Report, JHR74-77. Project 73-1.
- McVay, M.C., Schmertmann, J., Townsend, F, and Bullock, P., 1999. Pile freeze, a field and laboratory study. Final Report, Florida Department of Transportation, Research Center, Contract No. A-7967, 1,314 p.
- Meyerhof, G.G., 1951. The bearing capacity of foundations. *Geotechnique* 2(4) 301-332.
- Meyerhof, G.G., 1963. Some recent research on bearing capacity of foundations. *Canadian Geotechnical Journal* 1(1) 16-26.
- Meyerhof, G.G., 1976. Bearing capacity and settlement of pile foundations. The Eleventh Terzaghi Lecture, November 5, 1975. *ASCE Journal of Geotechnical Engineering* 102(GT3) 195-228.
- Muhunthan, B., vijayathan, N. V., and Abbasi, B., (2017). "Liquefaction-induced downdrag on drilled shafts." Washington State Department of Transportation. Final Research Report.
- Nottingham, L.C., 1975. Use of quasi-static friction cone penetrometer data to predict capacity of displacement piles. Ph.D. thesis, Dept of Civil Engineering, Univ. of Florida, 553 p.
- ODOT (Oregon Department of Transportation) (2015), "Standard Specifications for Highway Construction", 2015 Edition and related Standard Special Provisions.
- O'Neill, M.W., and Reese, L.C. (1999). "Drilled Shafts: Construction Procedures and Design Methods," Publication No. FHWA-IF-99-025, Federal Highway Administration, Washington, D.C., 758 p.
- Osterberg, J. O., (1984). "A New Simplified Method for Load Testing Drilled Shafts." *Foundation Drilling*, Vol. XXIII, No. 6 (July/August, 1984), International Association of Foundation Drilling (ADSC), 9 pgs.
- Osterberg, J. O. (1994). "Recent Advances in Load Testing Driven Piles and Drilled Shafts Using the Osterberg Load Cell Method", Geotechnical Division, Illinois Section, ASCE, 79 pp.

- Poulos, H. G. (1997). "Piles subjected to negative friction." A procedure for design, *Geotechnical Engineering*, 23-44.
- Rollins, K. M. and S. R. Strand (2006). Downdrag Forces Due to Liquefaction Surrounding a Pile. *Proceedings of the 8th U.S. National Conference on Earthquake Engineering*. Paper No. 1646, San Francisco, CA, April 18-22.
- Rollins, K.M. (2004). "Liquefaction Mitigation Using Vertical Composite Drains: Full Scale Testing." Final Report for Highway IDEA Project 94. Transportation Research Board, February 2004, 105 p.
- Rollins, K.M., Lane, J.D., Nicholson, P.G., and Rollins, R.E. (2004). "Liquefaction Hazard Assessment using Controlled-Blasting Techniques." *Proc. 11th International Conference on Soil Dynamics & Earthquake Engineering*. Vol. 2, pp. 630-637.
- Rollins, K.M., Lane, J.D., Dibb, E., Ashford, S.A., and Mullins, A.G. (2005a). "Pore Pressure Measurement in Blast-Induced Liquefaction Experiments." *Transportation Research Record* 1936, *Soil Mechanics* 2005, TRB, Washington D.C., pp. 210-220.
- Rollins, K.M. and Anderson, J.K.S. (2008). "Cone Penetration Resistance Variation with Time after Blast Liquefaction Testing." *Procs. Geotechnical Earthquake Engineering and Soil Dynamics-IV*, Geotechnical Special Publication 181, ASCE, 10 p.
- Rollins, K.M. and Hollenbaugh (2015). "Liquefaction Induced Negative Skin Friction from Blast-induced Liquefaction Tests with Auger-cast Piles." *6<sup>th</sup> International Conference on Earthquake Geotechnical Engineering*, Christchurch, New Zealand.
- Schmertmann, J.H., 1978. Guidelines for cone penetration test, performance, and design. U.S. Federal Highway Administration, Washington, Report FHWA-TS-78-209, 145 p.
- Siegel, T.C., Lamb, R., Dasenbrock, D., and Axtell, P.J. (2013). "Alternative Design Approach for Drag Load and Downdrag with the LRFD Framework." *Proceedings of the 38th Annual Conference on Deep Foundations* 2013, Phoenix, AZ, pp. 23-39.
- Skempton, A.W., (1951), "The Bearing Capacity of Clays", *Proc. Building Research Congress*, pp. 180-189
- Strand, S. R. (2008). Liquefaction Mitigation Using Vertical Composite Drains and Liquefaction induced Downdrag on Piles: Implications for Deep Foundation Design. Ph.D. thesis, Department of Civil and Environmental Engineering, Brigham Young University, Provo, UT.
- Tomlinson M. and Woodward, J. (2008) *Pile Design and Construction Practice*, 5th ed. Taylor & Francis, New York.
- Vijayaruban, N. V., Muhunthan, B., and Fellenius, B.H. (2015). "Liquefaction-induced Downdrag on Piles and Drilled Shafts." *6<sup>th</sup> International Conference on Earthquake Geotechnical Engineering*. Christchurch, New Zealand.

WSDOT (Washington State Department of Transportation) (2006). "Geotechnical Design Manual M 46-03.

## CHAPTER 4: Turrell Arkansas Test Site Description

### 4.1. Chapter Overview

The Turrell Arkansas Test Site (TATS) is located within the New Madrid Seismic Zone (NMSZ). A general review of the geologic and seismic nature of the NMSZ, and the evidence of earthquake-induced liquefaction features from the 1811-1812 New Madrid earthquakes sequence is presented in Section 4.2. A description of the results obtained from the geotechnical investigations tests that were completed at the TATS is also presented. The generalized soil profile of the TATS, as obtained based on the geotechnical investigations results is presented. Two types of penetration tests included: standard penetration test (SPT) and cone penetration testing (CPT) were performed at the TATS to 1) determine the engineering properties of the geomaterials that were required for deep foundation design. and 2) characterize the soil stratigraphy at the TATS. The results obtained from CPT soundings and correlated soil parameters are presented in Section 4.6.

### 4.2. Geology and NMSZ Faults

According to Johnston and Schweig (1996), in the winter of 1811 and 1812, a series of strong earthquakes that had estimated moment magnitude ranging from 7 to 8 occurred in the New Madrid Seismic Zone. As reported by United States Geological Survey (2009a), the perception of strong shaking during these earthquake events were estimated to be two to three time larger than the 1964 Alaska earthquake, and approximately ten times larger than the 1906 San Francisco earthquake. In addition, the NMSZ is considered as the most seismically active area in the central and eastern United States (Tuttle et al. 1999). Over more than four decades, various paleoseismic studies have been conducted to provide: 1) an evidence of the historical earthquake sequence, and 2) a better understanding on the geological and earthquake-induced

liquefaction features found in the NMSZ (e.g., Nuttli 1982, Penick 1981, Johnson 1996, Johnston and Schweig 1994, Tuttle et al. 2002, Csontos and Arsdale 2008).

The NMSZ is located in the central of the United States, within the Mississippi Embayment, as shown in Figure 4.4 on Page 65. The seismic zone includes southeastern Missouri, northeastern Arkansas, southern Illinois, southern Indiana, and western Kentucky. According to the USGS (2018), the Mississippi embayment is a broad trough filled with marine sedimentary rocks that date to 50-100 million years old and river sediments less than 5 millions years old. The upper 30 meters of sediment within the embayment includes sand, silt, and clay that is deposited by the Mississippi, Ohio, St. Francis, and White Rivers and their tributaries over the past 60,000 years. The Wisconsin valley deposits in the Mississippi embayment formed during the glacial period, from 10,000-60,000 years ago, and the Holocene meander belt deposits were laid down during the past 10,000 years.

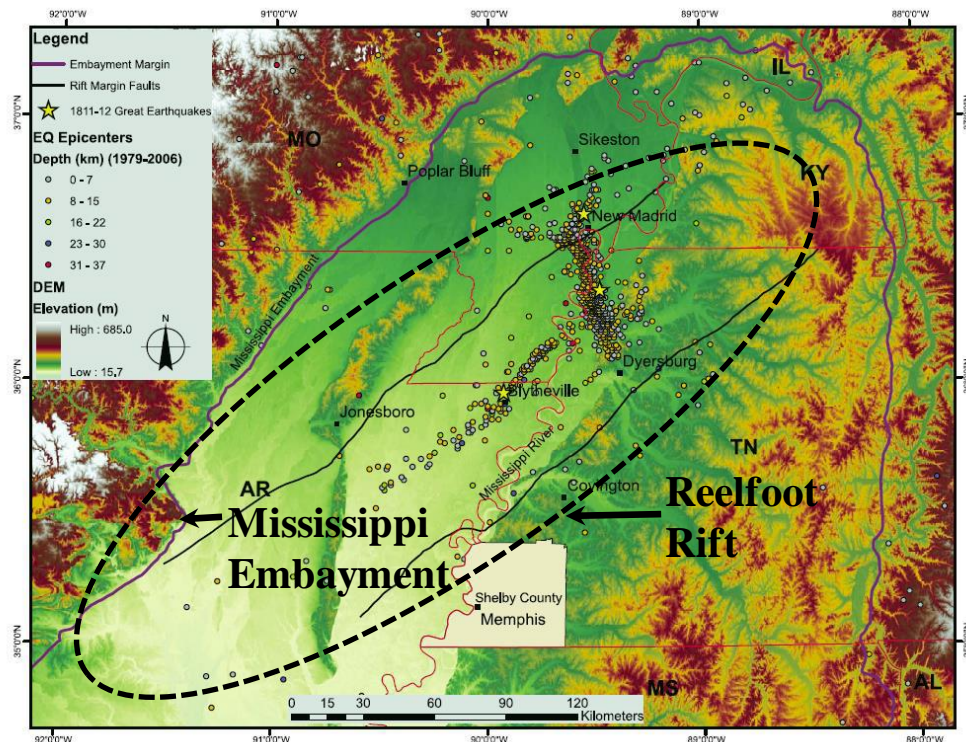


**Figure 4.1.** Locations of Reelfoot rift boundaries and Mississippi Embayment (modified from Csontos and Arsdale 2008).

The location of the 1811-1812 earthquakes are also shown in Figure 4.1. Most of the old and the new seismicity within the NMSZ have been attributed to reactivation of the Reelfoot rift faults (Zoback 1979, Kane et al. 1981, Braile et al. 1986, Thomas 1989, Dart and Swolfs 1998, and Csontos and Arsdale 2008). The geographical boundaries of the Reelfoot rift are shown in Figure 1. As can be seen in Figure 4.1, the most active fault within the NMSZ is the Reelfoot reverse fault between Dyersburg, Tennessee and New Madrid, Missouri (Van Arsdale et al. 1999). The Reelfoot rift is underlain by several Precambrian terranes that consists of granite, granite porphyry and dioritic gneiss (Thomas 1988, Dart 1992, Dart and Swolfs 1998, Csontos and Arsdale 2008). In addition, the tectonic features or other geological structures found in the Mississippi Embayment are associated with the Reelfoot rift faults. Several models have been developed and used to characterize and evaluate the faults within the NMSZ. For instance, Csontos and Arsdale (2008) conducted a three-dimensional analysis of 1704 earthquake hypocenters obtained between 1995 and 2006 to identify the fault geometry in the NMSZ. The locations of the analyzed earthquakes are also shown in Figure 4.1.

Csontos and Arsdale (2008) reported five important faults that include the New Madrid North, Risco, Axial, Reelfoot North and Reelfoot South faults. The outlined faults are shown in Figure 4.2. As reported by Csontos and Arsdale (2008), most of the earthquakes appear to align along with the fault planes, and a diffuse number of earthquakes exist where the axial fault divides the Reelfoot fault into Northern and Southern portions of the Reelfoot fault. Specifically, earthquakes have been reported between 4 and 14 km along the 30°-dipping Reelfoot North and above 4 km depth along the 44°-dipping Reelfoot South faults. The Reelfoot North and South these faults are aseismic with reverse displacement (Csontos and Arsdale 2008). Csontos and

Arsdale (2008) concluded that the faults in the NMSZ should be expected to be a right-lateral strike-slip fault zone with the exception being the Reelfoot fault that is a reverse fault.

A review on the formation of the aforementioned Reelfoot rift faults is discussed in detail by Csontos and Arsdale (2008). Tavakoli et al. (2010) also proposed a conceptual three-dimensional model of right-lateral strike-slip faulting to evaluate the occurrence of the 1811-1812 earthquakes in NMSZ. Using the proposed model, Tavakoli et al. (2010) observed a 240 km long deep-seated fault with the axis of Reelfoot rift and two parallel P shear faults that contributed to the deformation and stress concentration within the NMSZ. In addition, Tavakoli et al. (2010) reported that the surface deformation predicted using this model were in a good agreement with the observed seismicity patterns in the region. The estimated moment magnitudes, the duration with the estimated attenuation intensity of the 1811-1812 earthquakes were provided and discussed in detail by Johnston and Schweig (1996).

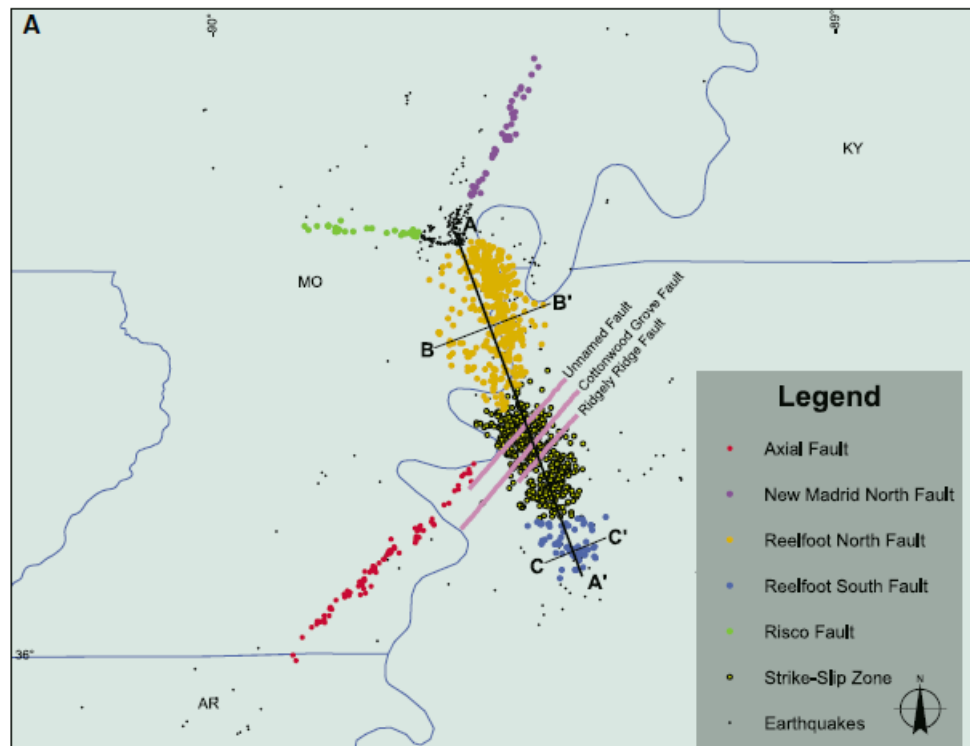


**Figure 4.2.** A schematic of the faults within the NMSZ (modified from Csontos and Arsdale 2008).



### 4.3. Evidence of Liquefaction within the NMSZ

The 1811-1812 earthquakes had strong ground motions that induced soil liquefaction due to the presence of deep, loose, saturated sandy soils of the Mississippi Embayment. This liquefaction caused ground deformations (lateral spread, open cracks, landslides) and the formation of earthquake-induced liquefaction features resulted from the generation and dissipation of porewater pressure during the strong shaking from the earthquake sequence. Sand blows (sand boils) and dikes are the most liquefaction features observed and analyzed in the NMSZ (Figure 4.3). For instance, large surficial sand blows with a thickness of between 1.0 to 1.5 m and 10 to 30 diameter can be easily identified on aerial photographs and on the ground within the NMSZ (Johnston and Schweig 1996).

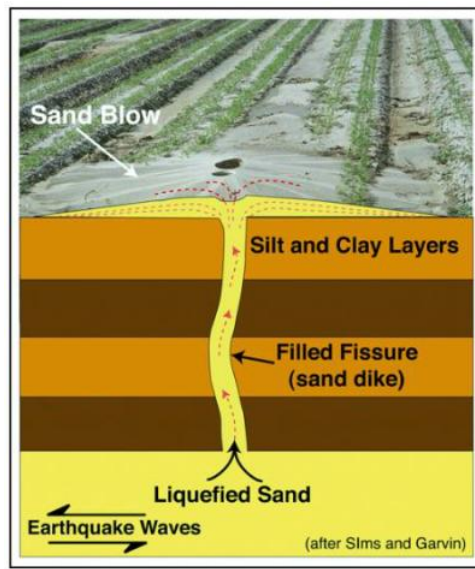


**Figure 4.3.** A photograph of a sand blow and sand dikes observed in the NMSZ (After USGS 2018).

As reported by Wolf et al. (2005), the liquefaction features within the NMSZ are identified by 1) examining the aerial photographs, and 2) by performing a field investigation. Several paleoseismologic studies of liquefaction features have been conducted to explain the occurrence of the 1811-1812 earthquakes sequences and to estimate the recurrence interval for

large earthquakes within the NMSZ (e.g., Johnston and Nava 1985, Obermeier 1989, Tuttle and Schweig 1996, Tuttle et al. 2002, Wolf et al. 2005, Tavakoli et al. 2010). Documentation about the ground deformations and damage following the 1811-1812 earthquakes was primarily obtained from eyewitness accounts and experiences reported by people who lived in this region when earthquakes occurred. The documentation related to the eyewitness accounts was compiled and reported by Nathan Moran at the Center for Earthquake Research and Information (CERI). Lyell (1849) was one of the first geologists who explored the NMSZ after the 1812 earthquakes. Lyell (1849) reported the fresh evidence of fissuring, sand blows, landslides, and sunken lands (Wesnousky et al. 1989). Usher (1837) and McGee (1892) also reported other descriptions of earthquake induced deformations that included the evidence for doming and uplift of young alluvial sediments in the NMSZ (Wesnousky et al. 1989). In addition, Fuller (1912) reported that fissuring in the ground surface was the most liquefaction feature that occurred within the New Madrid region. In brief, the documented occurrence of sand blows, sand dikes, lateral spread, and larger fissures of the ground surface provide the evidence that liquefaction occurred as a result of the 1811-1812 earthquake sequences.

#### **4.4. Turrell Test Site Description**

The Turrell Arkansas Test Site is located in Northeast Arkansas, within New Madrid Seismic Zone and within Mississippi Embayment, as illustrated in Figure 4.4a. The site is located approximately 50 miles Southeast of Jonesborough, Arkansas, and 30 miles Northwest of Memphis, Tennessee, at the intersection of Interstate 63 (now 555) and Interstate 55 (Figure 4.4b). The soil at the TATS is potentially liquefiable when subjected to the predicted earthquake. The with a design mean earthquake is an earthquake with a magnitude of 7.5, a peak ground

acceleration of 0.64g, and a seven percent probability of exceedance in 75 years (Race and Coffman 2013).

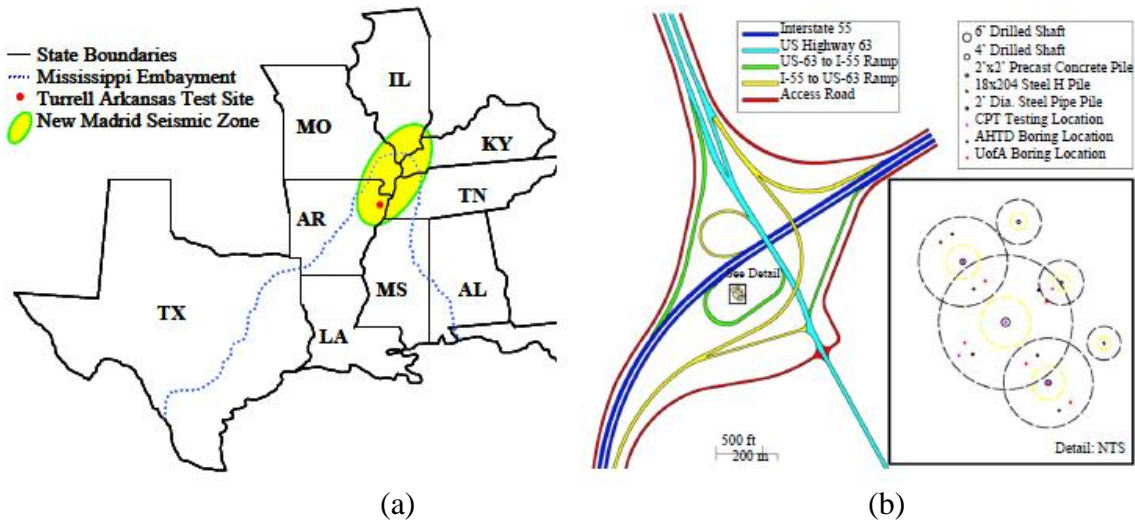


**Figure 4.4.** (a) Site location map and (b) detailed site layout of the site (From Coffman 2015).

#### 4.5. Geotechnical Site Characteristics

The engineering properties at the TATS were determined using various field and laboratory tests. Specifically, six SPT tests were conducted at the locations illustrated in Figure 4.5. The number of blows that were required to advance the sampler into the soil were recorded, and used to determine the correlated soil engineering parameters (e.g., unit weight, shear strength, and friction angle). Various laboratory tests were conducted on disturbed samples that were acquired from the SPT split-spoon sampler. Additional details relating to the soil sampling, drilling and laboratory testing results are provided in Bey (2014) and Race (2015).

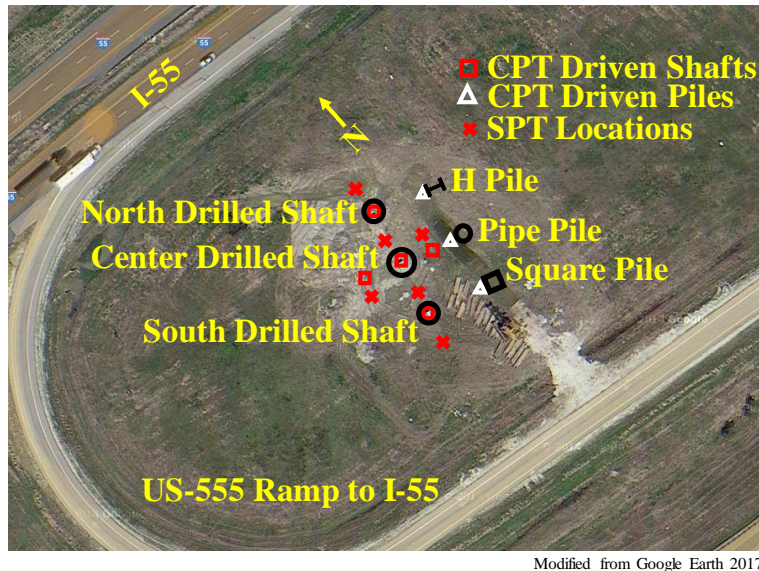


**Figure 4.5.** Test site layout, including the locations of SPT, CPT soundings, drilled shafts, and driven piles.

Prior to the construction phase, five CPT soundings were conducted at the locations of drilled shafts and driven piles section, as previously shown in Figure 4.5. The tests were conducted with the personnel from the MODOT using the five-channel cone mounted on the MODOT CPT rig (Figure 4.6). Cone tip resistance ( $q_t$ ), sleeve friction ( $f_s$ ), porewater pressure ( $u_2$ ), and shear wave velocity ( $V_s$ ) values as a function of depth that were measured, and are presented in Figures B.1 and B.2 for drilled shafts and driven piles locations, respectively. The soil engineering properties, including the total unit weight ( $\gamma$ ), relative density ( $D_r$ ), shear strength ( $c_u$ ), friction angle ( $\gamma$ ), SPT- $N_{60}$  and the soil index behavior correlated from these CPT measurements are also shown in Figures B.1 and B.2 in Appendix B, for drilled shafts and driven piles locations, respectively. Due to the New Madrid Seismic faults and the presence of loose and saturated soils, the TATS was determined to be liquefiable with a design mean earthquake magnitude of 7.5, a peak ground acceleration of 0.64 g, and a seven percent probability of exceedance in 75 years (Race and Coffman 2013).



**Figure 4.6.** Photographs of the MODOT CPT rig.

#### **4.6. Chapter Summary**

An overview on geologic and seismic nature of the NMSZ and the evidence of earthquake-induced liquefaction features from the 1811-1812 New Madrid earthquake sequence is presented herein. The site investigation techniques that were used to determine the geomaterial engineering properties and to characterize the soil subsurface at the TATS are outlined in this Chapter. A description of the CPT results and the correlated soil parameters obtained from the geotechnical investigations tests was also presented. The generalized soil profile developed using SPT, CPT, and laboratory test results was presented.

#### **4.7. References**

- Bey Sarah (2014) “Cost-benefit Analysis for Load Resistance Factor Design (LRFD) of Drilled Shafts in Arkansas.” M.S. Thesis, University of Arkansas, Fayetteville, Arkansas, pp.410.
- Csontos, R., Van Arsdale, R., Cox, R., and Waldron, B., 2008, Reelfoot rift and its impact on Quaternary deformation in the central Mississippi River valley: *Geosphere*, v. 4, p. 145–158, doi: 10.1130/GES00107.1.
- Dart, R.L., 1992, Catalog of pre-Cretaceous geologic drillhole data from the upper Mississippi embayment: A revision and update of Open-File Report 90-260: U.S. Geological Survey Open-File Report, 253 p.
- Fuller, M. L., (1912). “The New Madrid Earthquake.” U.S Geol. Surv. Bull 494. Wesnousky, S. G., Schweig, E. S, and Pezzopane, S. K. (1989). “Extent and Character of Soil

Liquefaction during the 1811-1812 New Madrid Earthquakes.” Center for Earthquake Research and Information. Memphis State University.

- Johnston, A. C., and S. J. Nava, 1985, Recurrence rates and probability estimates for the New Madrid seismic zone: *Journal of Geophysical Research*, 90, 6737–6753.
- Johnston, A.C., and Schweig, E.S. (1996). “The enigma of the New Madrid earthquakes of 1811–1812.” *Annual Review of Earth and Planetary Sciences*, Vol. 24, pp. 339-384.
- Kane, M.F., Hildenbrand, T.G., and Hendricks, J.D., 1981, Model for the tectonic evolution of the Mississippi embayment and its contemporary seismicity: *Geology*, v. 9, p. 563–568, doi: 10.1130/0091-7613(1981)9<563: MFTTEO>2.0.CO;2.
- McGee, W. J. (1892). “A fossil earthquake [abstract]. *Geol. Soc. Am. Bull.* 4: 411-415.
- Nathan, K. (2018). “Introduction: eye witness accounts”  
<<http://www.memphis.edu/cei/compendium/eyewitness.php>>
- Nuttli, O.W., 1982, Damaging earthquakes of the central Mississippi Valley, in McKeown, F.A., and Pakiser, L.C., eds., *Investigations of the New Madrid, Missouri, earthquake region: U.S. Geological Survey Professional Paper 1236-B*, p. 15–20.
- Obermeier, S. F., 1989, *The New Madrid earthquakes: An engineering-geologic interpretation of relict liquefaction features: U. S. Geological Survey.*
- Penick, J.L., 1981, *The New Madrid earthquakes: Columbia, University of Missouri Press*, 176 p.
- Race, M. L., Coffman, R. A., (2013), “Effect of Uncertainty in Site Characterization on the Prediction of Liquefaction Potential for Bridge Embankments in the Mississippi Embayment.” ASCE Geotechnical Special Publication No. 231, *Proc. GeoCongress 2013: Stability and Performance of Slopes and Embankments III*, San Diego, California, March, pp. 888-897.
- Race, M.L., Coffman, R.A., (2015). “Response of Drilled Shaft Foundation Constructed in Redrilled Shaft Excavation Following Collapse.” *Deep Foundations Institute Journal*. Vol. 9, No. 2, pp. 60- 73.
- Race, M.L., Bey, S.M., Coffman, R.A., (2015). “Statistical Analysis to Determine Appropriate Design Methodologies for Drilled Shafts Foundations.” *Geotechnical and Geological Engineering*. Vol. 33, Issue 3, pp 713-726.
- Race, M.L. (2015) “Amount of Uncertainty in the Methods Utilized to Design Shaft Foundations.” PhD. Thesis, University of Arkansas, Fayetteville, Arkansas, pp.325
- Schweig, E., and Ellis, M.A., 1994, Reconciling short recurrence intervals with minor deformation in the New Madrid seismic zone: *Science*, v. 264, p. 1308–1311, doi: 10.1126/science.264.5163.1308.

- Tuttle, M.P., Schweig, E.S., Sims, J.D., Lafferty, R.H., Wolf, L.W., and Haynes, M.L., 2002, The earthquake potential of the New Madrid seismic zone: *Seismological Society of America Bulletin*, v. 92, p. 2080–2089, doi: 10.1785/0120010227.
- Tavakoli, B., Pezeshk, S., and Randel, T. C. (2010). “Seismicity of the New Madrid Seismic Zone Derived from a Deep-Seated Strike-Slip Fault.” *Bulletin of the Seismological of America*. Vol. 100. No. 4, pp. 1646-1658.
- Tuttle, M. P., and E. S. Schweig, 1996, Recognizing and dating prehistoric liquefaction features: Lessons learned in the New Madrid seismic zone, central United States: *Journal of Geophysical Research*, 101, 6171–6178.
- United States Geological Survey (2009). “Earthquake Hazard in the New Madrid Seismic Zone Remains a Concern.” Fact Sheet 2009–3071. USGS, August 2009.
- United States Geological Survey (2018). “Science of the New Madrid Seismic Zone.” <<https://earthquake.usgs.gov/learn/topics/nmsz/1811-1812.php>>, February, 2018.
- Usher, F. C., (1837). “On the elevation of banks of the Mississippi in 1811.” *Silliman’s J. (Am. J. Sci., first series)* 31: 291-294.
- Van Arsdale, R.B., Cox, R.T., Johnston, A.C., Stephenson, W.J., and Odum, J.K., 1999, Southeastern extension of the Reelfoot fault: *Seismological Research Letters*, v. 70, p. 348–359.
- Wolf, L. W., Tuttle., M. P., Browning. S., and Park, S. (2006). “Geophysical surveys of earthquake-induced liquefaction deposits in the New Madrid Seismic Zone.” *Geophysics*, Vol. 71. No. 6.
- Zoback, M.D., 1979, Recurrent faulting in the vicinity of Reelfoot Lake, northwestern Tennessee: *Geological Society of America Bulletin*, v. 90, p. 1019–1024, doi: 10.1130/0016-7606(1979)90<1019: RFITVO>2.0. CO.

## CHAPTER 5: Predicted Geotechnical Axial Resistances and Dragloads

### 5.1. Chapter Overview

The amounts of axial resistance that were predicted using engineering properties that were presented in Chapter 4, two software programs (UNIPILE and FB-Deep), and the Microsoft® Excel spreadsheet method are discussed in Section 5.2 and 5.4 for drilled shafts and driven piles, respectively. The load and resistance distribution curves that were determined using the predictive results from the aforementioned software programs and the empirical methods (spreadsheet) are presented in Sections 5.3 and 5.5, for drilled shafts and driven piles, respectively. Discussions on the magnitude and the effects of the predicted dragloads on the axial performance of each foundation are also discussed in Sections 5.3, and 5.5, for drilled shafts and driven piles, respectively. In addition, drilled shaft/pile settlement and soil settlement distribution curves that were predicted using UNIPILE are also presented and discussed herein.

### 5.2. Prediction of Axial Resistance and Dragload around Drilled Shafts

Three drilled shaft foundations, with the properties summarized in Table 5.1, were designed and constructed at the TATS by Bey (2014) and Race (2015). Bey (2014) and Race (2015) used the FB-Deep and the engineering properties obtained from geotechnical investigation (Chapter 4) to design the drilled shafts. The drilled shafts were constructed in 2013. Further details on the construction and design methodologies of the North, Center and South drilled shafts can be found in Bey (2014) and Race (2015).

**Table 5.1.** Drilled shaft foundations properties.

	North Drilled Shaft	Center Drilled Shaft	South Drilled Shaft
Length, L [m]	28.0	20.0	27.6
Embedded Length, LE [m]	26.8	18.7	26.4
Diameter, D [m]	1.2	1.8	1.2
Area, A [m <sup>2</sup> ]	1.17	2.63	1.17
Modulus of Elasticity, E [MPa]	35.98	37.87	35.98



A photograph of the drilled shaft locations at the TATS was previously presented in Figure 4.5. For the spreadsheet method, the equations (Equations 3.1-3.6) that were previously discussed in Chapter 3 were used. The load and resistance distribution curves, and the drilled shaft/pile-soil settlement distribution curves were used to identify the location of the neutral plane and the corresponding dragloads. Step-by-step analysis procedures to identify the neutral plane location are presented in Chapter 7. The predicted load and resistance distribution curves, as estimated using the spreadsheet method, following the AASHTO design guide, for the north, center and south drilled shafts are shown in Figure 5.1.

The load and resistance distribution curves were estimated by inputting the correlated unit weight ( $\gamma$ ), blow count ( $N_{60}$  or  $N$ ) and undrained shear strength ( $c_u$ ) values within the respective software program (FB-Deep and UNIPILE). The plots obtained using the FB-Deep output data are shown in Figure 5.2. The predicted load and resistance distribution curves along with the drilled-shaft and soil settlement curves, as predicted using UNIPILE, are shown in Figures 5.3, 5.4 and 5.5 for the North, Center and South drilled shafts, respectively. The dragload values along with the corresponding neutral plane locations that were determined using the aforementioned methods are summarized in Table 5.2 on page 78. Dragload values were calculated by 1) applying a structural load of 352.40kips to the top of each drilled shaft foundation, and by 2) assuming that the amount of post-liquefaction soil settlement is larger than the settlements of each drilled shaft (4-inch).

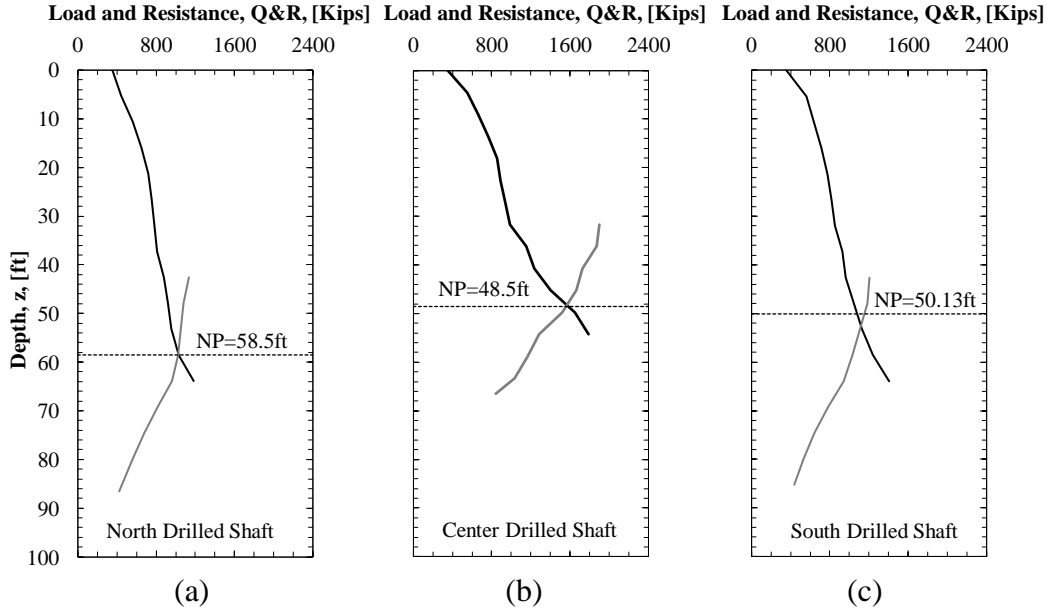


**Figure 5.1.** Load and resistance distribution curves along the (a) North, (b) Center, and (c) South drilled shaft foundation as obtained using AASHTO design guide method.

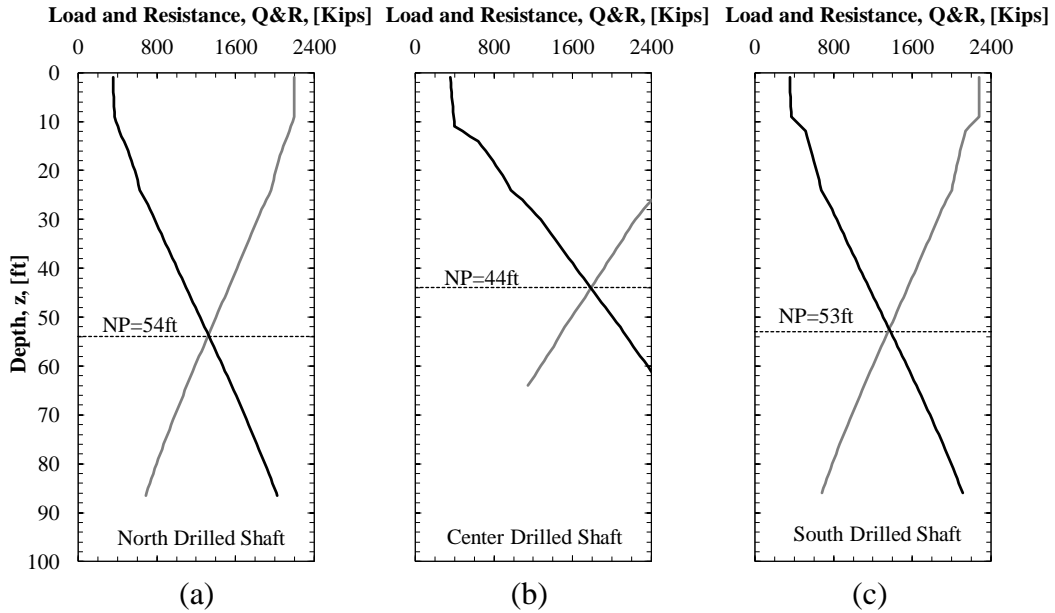


**Figure 5.2.** Load and resistance distribution curves along the (a) North, (b) Center, and (c) South drilled shaft foundation as obtained using FB-Deep program.

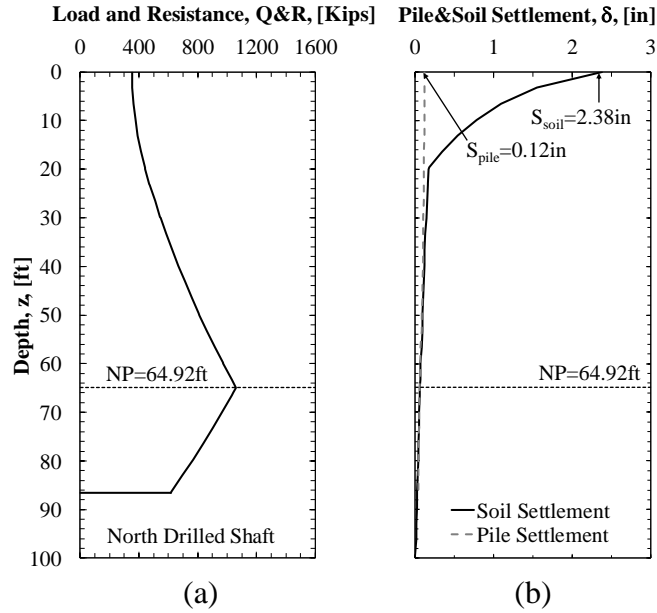


**Figure 5.3.** Distribution of (a) load and resistance and (b) drilled shaft-soil settlement around the North drilled foundation, as obtained using UNIPILE program.

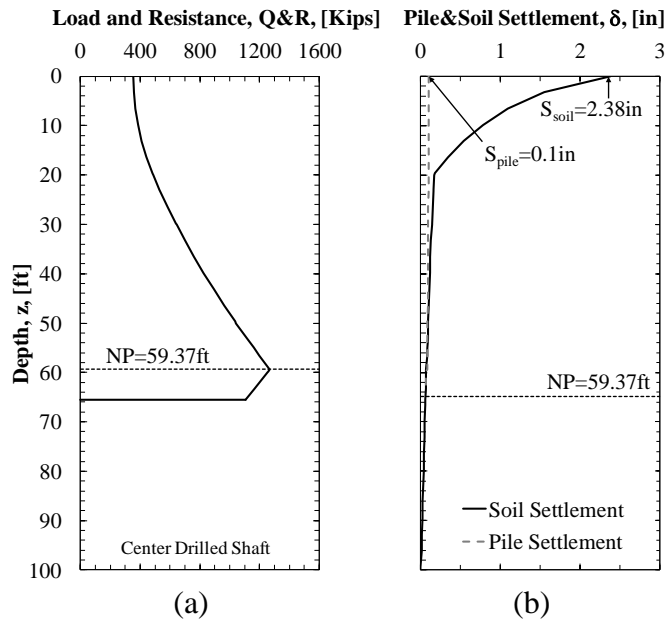


**Figure 5.4.** Distribution of (a) load and resistance and (b) drilled shaft-soil settlement around the Center drilled foundation, as obtained using UNIPILE program.

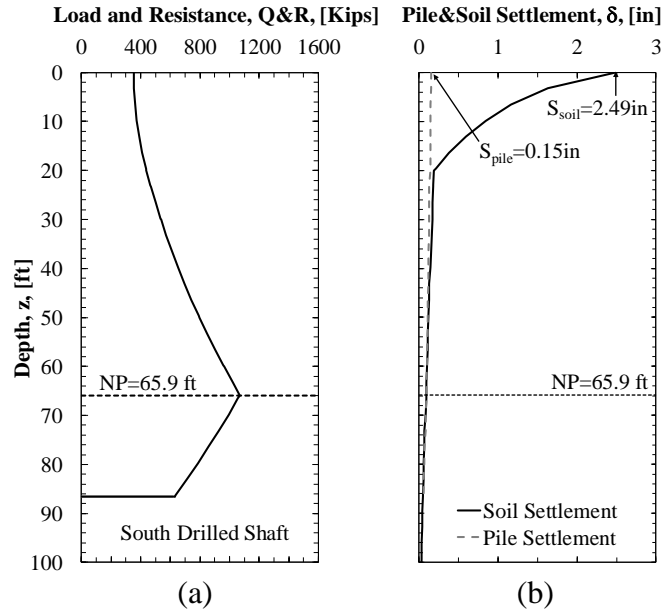


**Figure 5.5.** Distribution of (a) load and resistance and (b) drilled shaft-soil settlement around the South drilled foundation, as obtained using UNIPILE program.

### 5.3. Dragload Analysis for Drilled Shafts

The mechanism for the development of the negative shaft resistance (dragload) following liquefaction at the TATS was predicted. The effect of the liquefaction-induced dragload was assessed using the empirical equation proposed by Brown et al. (2010). As proposed by Brown et al. (2010), in FHWA design manual, the factored structural load applied to the top of the drilled shaft and the factored dragload must be less than the sum of factored positive shaft resistance and the factored toe resistance. For this analysis, the resistance factors for LRFD provided in Brown et al. (2010), were applied to the predicted shaft and toe resistances and predicted dragload (Table 5.2). Using Equation 3.9 on Page 42, the sum of the factored structural load and factored dragload exceeded the sum of the factored positive shaft and toe resistance for the three drilled shafts. Therefore, the drilled shafts were marked as inadequate (Table 5.2). on the contrary, the structural strength limit states were evaluated for each drilled shaft using Equation 3.10 on Page 43. For all drilled shaft, the factored structural resistance ( $P_r$ ) of each drilled shaft exceeded the combination of the factored dragload and factored structural load. The resistance provided in

Hannigan et al. (2016) were used for the structural strength limit states. As shown in Table 5.2, each of the drilled shaft foundations have sufficient (marked as “ADEQUATE” in Table 5.2) structural capacity to sustain the factored structural load and the induced dragloads. Although factored loads were used to evaluate the limit states, the load and resistance distribution curves presented herein (Figures 5.1 through 5.5) were obtained by using unfactored resistance values.

**Table 5.2.** Magnitude of dragload and the neutral plane locations, as predicted using FB-Deep, UNIPILE and spreadsheet method.

Foundation Type	Analysis Methods	Reference	Dragload DD [Kips]	Neutral Plane NP [ft]	Dragload Evaluation	
					Equation 3.9	Equation 3.10
North Drilled Shaft	Speadsheet	Brown et al. (2010)	668.44	58.5	<i>INADEQUATE</i>	ADEQUATE
	FB-Deep	Schmertmann (1967)	964.60	54	<i>INADEQUATE</i>	ADEQUATE
	UNIPILE	Fellenius 2016	708.01	64.92	<i>INADEQUATE</i>	ADEQUATE
Center Drilled Shaft	Speadsheet	Brown et al. (2010)	1219.99	48.5	<i>INADEQUATE</i>	ADEQUATE
	FB-Deep	Schmertmann 1967	1436.22	44	<i>INADEQUATE</i>	ADEQUATE
	UNIPILE	Fellenius 2016	914.95	59.37	<i>INADEQUATE</i>	ADEQUATE
South Drilled Shaft	Speadsheet	Brown et al. (2010)	758.67	50.13	<i>INADEQUATE</i>	ADEQUATE
	FB-Deep	Schmertmann 1967	1000.79	53	<i>INADEQUATE</i>	ADEQUATE
	UNIPILE	Fellenius 2016	708.01	65.9	<i>INADEQUATE</i>	ADEQUATE

#### 5.4. Prediction of Axial Resistance and Dragload around Driven Piles

Like for the drilled shafts, the amount of axial resistance was predicted for three driven piles. The mount of the axial resistance was obtained using the measured soil properties, software programs (UNIPILE and FB-Deep), and the Microsoft ® Excel spreadsheet method. The load and resistance distribution curves for each test pile, as obtained using spreadsheet method are presented in Figure 5.6. The plots obtained using the FB-Deep output data are shown in Figure 5.7. The load and resistance distribution curves and the pile-soil settlement curves, as predicted using UNIPILE, are shown in Figures 5.8, 5.9 and 5.10 for the H pile, pipe pile, and pre-stressed pile, respectively. The dragload values with the corresponding neutral plane locations estimated using the aforementioned methods are summarized in Table 5.3. An axial structural load of 117.76 kips was applied to the top of each test pile. Like with the drilled shafts, it was assumed that the soil surrounding each test pile undergoes settlement when subjected to

liquefaction, and settle more than the pile. As shown in Table 5.3, the dragload determined using the spreadsheet method were higher than the values obtained using both software programs.

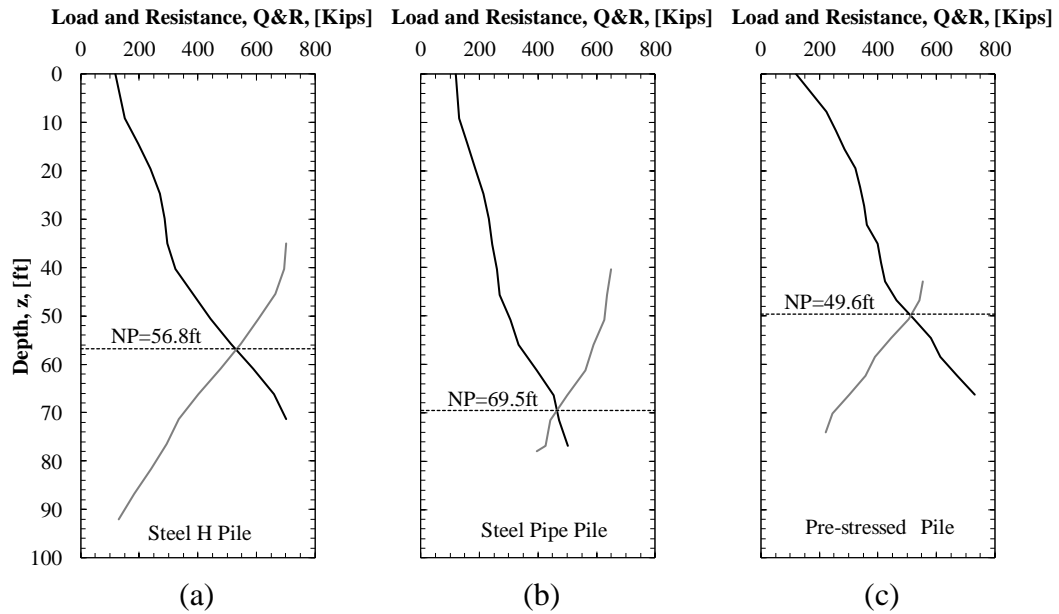


**Figure 5.6.** Load and resistance distribution curves along (a) steel H pile, (b) Steel pipe pile, and (c) pre-stressed concrete pile, as obtained using AASHTO design guide.

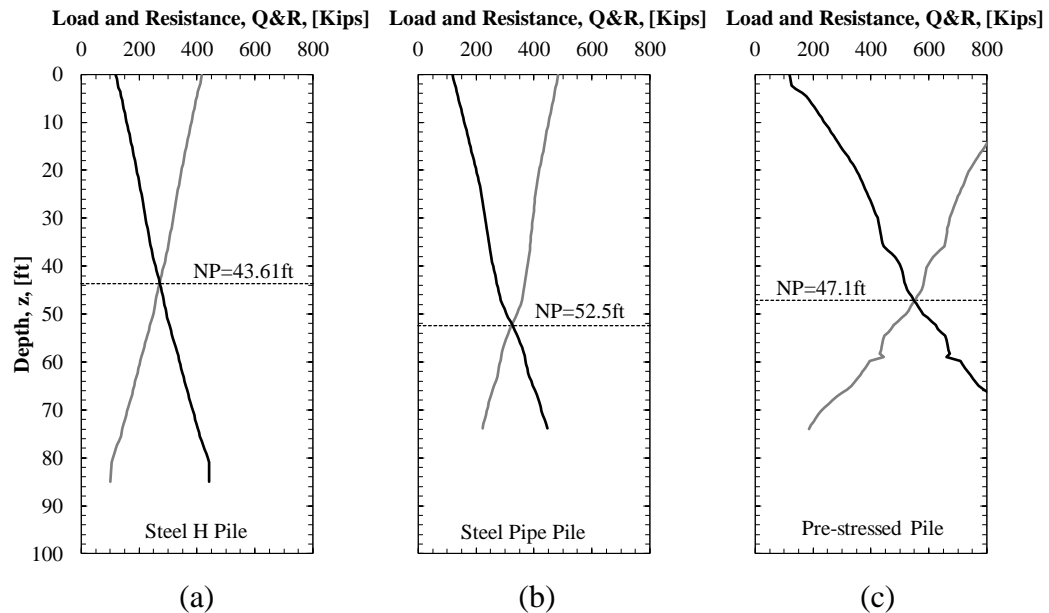


**Figure 5.7.** Load and resistance distribution curves along the (a) steel H pile, (b) Steel pipe pile, and (c) pre-stressed concrete pile, as obtained using FB-Deep program.

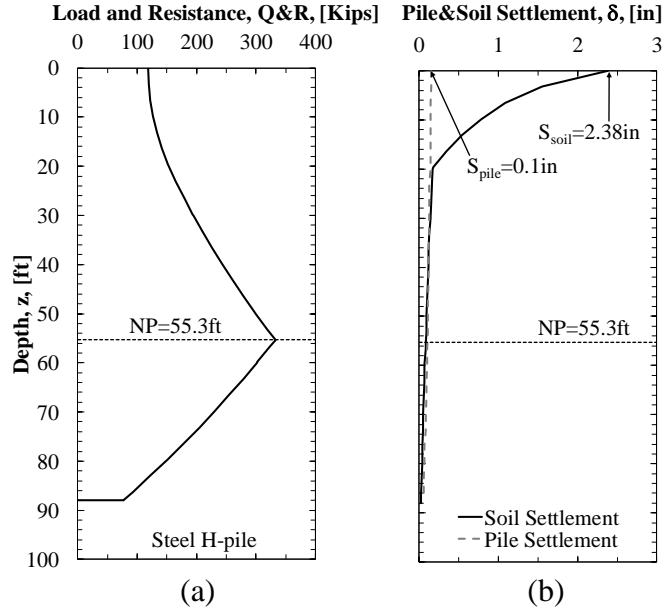


**Figure 5.8.** Distribution of (a) load and resistance and (b) drilled shaft-soil settlement around the steel H pile foundation, as obtained using UNIPILE program.

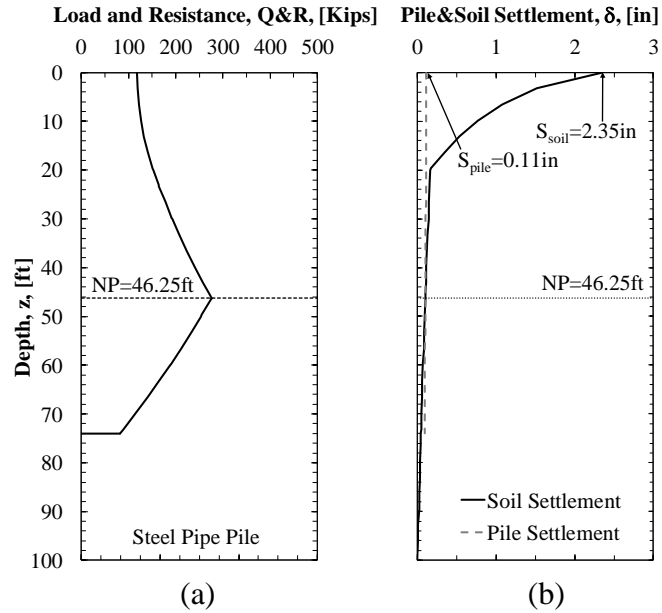


**Figure 5.9.** Distribution of (a) load and resistance and (b) drilled shaft-soil settlement around the steel pipe pile foundation, as obtained using UNIPILE program.

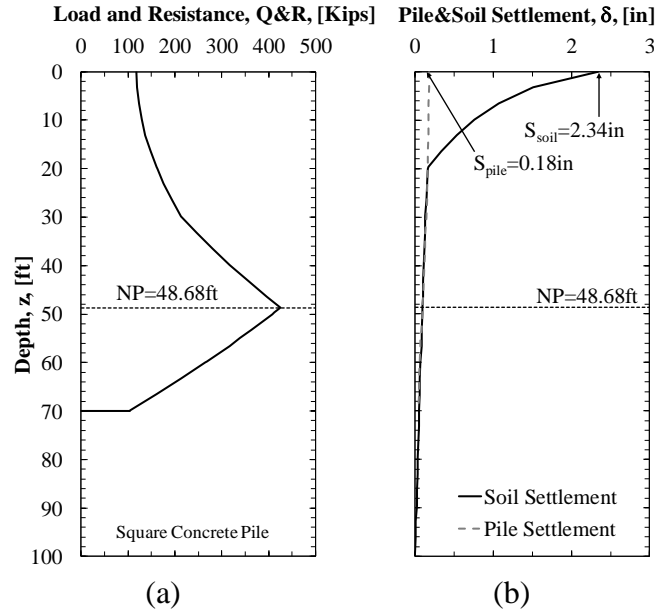


**Figure 5.10.** Distribution of (a) load and resistance and (b) drilled shaft-soil settlement around the pre-stressed pile foundation, as obtained using UNIPILE program.

### 5.5. Dragload Analysis for Driven Piles

Based on the site conditions that are documented herein, the dragload will accumulate along the pile after liquefaction. For the driven piles, an evaluation of limit states was performed after predicting the depth of the neutral plane and the amount of dragload developed around each test pile (Table 5.3). The effect of the predicted dragload, on the behavior of each test pile was also quantified using Equation 3.9 on Page 42, and Equation 3.10 on Page 43. As shown in Table 5.4, the sum of the factored structural load and factored dragload exceeded the sum of the factored positive shaft and toe resistance for the three test piles. However, the predicted values of shaft resistance, toe resistance and dragload satisfied Equation 3.10, with the exception of the steel pipe pile.



**Table 5.3.** Magnitude of dragload and the neutral plane locations for the piles at the TATS, as predicted using FB-Deep, UNIPILE, and spreadsheet method.

Foundation Type	Analysis Methods	Reference	Dragload DD	Neutral Plane NP	Dragload Evaluation	
					Equation 3.9	Equation 3.10
			[Kips]	[ft]		
Steel-H Pile	Spreadsheet	Brown et al. (2010)	415.52	56.8	<i>INADEQUATE</i>	<i>ADEQUATE</i>
	FB-Deep	Schmertmann 1967	143.03	43.61	<i>INADEQUATE</i>	<i>ADEQUATE</i>
Steel Pipe Pile	UNIPILE	Fellenius 2016	214.22	55.3	<i>INADEQUATE</i>	<i>ADEQUATE</i>
	Spreadsheet	Brown et al. (2010)	456.89	69.5	<i>INADEQUATE</i>	<i>INADEQUATE</i>
Square Pipe Pile	FB-Deep	Schmertmann 1967	203.28	52.49	<i>INADEQUATE</i>	<i>ADEQUATE</i>
	UNIPILE	Fellenius 2016	157.51	46.25	<i>INADEQUATE</i>	<i>ADEQUATE</i>
Square Pipe Pile	Spreadsheet	Brown et al. (2010)	370.91	49.6	<i>INADEQUATE</i>	<i>ADEQUATE</i>
	FB-Deep	Schmertmann 1967	433.52	47.1	<i>INADEQUATE</i>	<i>ADEQUATE</i>
	UNIPILE	Fellenius 2016	306.66	48.68	<i>INADEQUATE</i>	<i>ADEQUATE</i>

## 5.6. Chapter Summary

The predicted dragload, as obtained using the soil properties obtained from site investigation, software programs, and the spreadsheet method were discussed herein. In this chapter, the load and resistance distribution curves, as obtained using the aforementioned software programs and the empirical equations are presented. Following the approach outlined in FHWA design manuals by Brown et al. (2010), and Hannigan et al. (2016), the drilled shafts and driven pile were marked as inadequate when subjected to induced dragload. In contrast, all of the drilled shafts and driven piles were determined to be structurally adequate using the Hannigan et al. (2016) approach, with the exception of the steel pipe pile.

## 5.7. References

- Bey Sarah (2014) “Cost-benefit Analysis for Load Resistance Factor Design (LRFD) of Drilled Shafts in Arkansas.” M.S. Thesis, University of Arkansas, Fayetteville, Arkansas, pp.410.
- Brown, D. A., Turner, J.P. and Castelli R.J. (2010). “Drilled Shafts: Construction Procedures and LRFD Design Methods.” FHWA-NHI-10-016, Geotechnical Engineering Circular (GEC) No. 10. U.S. Dept. of Transportation, Federal Highway Administration, 970 p.
- FB-Deep (2016). Bridge Software Institute, Gainesville, FL. Ver. 2.04.
- Goudreault, P.A. and Fellenius, B.H., (2015). UniPile Version 5 User Manual, UniSoft Ltd., Ottawa, [www.UniSoftLtd.com].
- Hannigan, P.J., Robinson, B. R., Goble, G.G., Likins, G.E. & Rausche, F., Becker, M. L. (2016). “Design and Construction of Driven Pile Foundations.” FHWA-NHI-16-009, National

Highway Institute, Federal Highway Administration, U.S. Department of Transportation, Washington, D.C.

- Race, M. L., Coffman, R. A., (2013), “Effect of Uncertainty in Site Characterization on the Prediction of Liquefaction Potential for Bridge Embankments in the Mississippi Embayment.” ASCE Geotechnical Special Publication No. 231, *Proc. GeoCongress 2013: Stability and Performance of Slopes and Embankments III*, San Diego, California, March, pp. 888-897.
- Race, M.L., Coffman, R.A., (2015). “Response of Drilled Shaft Foundation Constructed in Redrilled Shaft Excavation Following Collapse.” *Deep Foundations Institute Journal*. Vol. 9, No. 2, pp. 60- 73.
- Race, M.L., Bey, S.M., Coffman, R.A., (2015). “Statistical Analysis to Determine Appropriate Design Methodologies for Drilled Shafts Foundations.” *Geotechnical and Geological Engineering*. Vol. 33, Issue 3, pp 713-726.

## CHAPTER 6: Pilot Liquefaction Blast Test

### 6.1. Chapter Overview

A free-field, pilot liquefaction test program was performed at the TATS. The main purpose of this investigation was to determine the blasting layout that was needed to produce liquefaction within the soil surrounding deep foundation elements. The results obtained from the installed porewater pressure transducers and pre- and post- blast cone penetration tests (CPT) are discussed. Based on the excess porewater pressure responses, liquefaction was only induced in the sand layer at the depth of 11.30m (37ft) where the  $R_u$  values were greater than the unity (1.06 and 0.95) for the piezometer that were located at that depth. Therefore, additional explosive charges were required to induce the entire target layer. The results obtained from the pre- and post-blast CPT tests were evaluated and discussed in this chapter. A new empirical model that takes into consideration the in-situ soil conditions at the TATS was developed and presented.

The paper enclosed in this chapter will be submitted within the International Journal of Geomechanics. The full reference is: Ishimwe, E., Coffman, R.A., Rollins, K.M., (2018). "Predicting Blast-induced Liquefaction within the New Madrid Seismic Zone." International Journal of Geomechanics. (Under second review).

## Predicting Blast-induced Liquefaction within the New Madrid Seismic Zone

**Elvis Ishimwe**, Graduate Research Student, University of Arkansas, Fayetteville, Arkansas, USA; email: eishimwe@email.uark.edu

**Richard A. Coffman**, Associate Professor, University of Arkansas, Fayetteville, Arkansas, USA; email: rick@uark.edu

**Kyle M. Rollins**, Professor, Brigham Young University, Provo, Utah, USA; email: rollinsk@byu.edu

### 6.2. Abstract:

A controlled-blasting testing program was performed to determine the blasting layout (the appropriate amount of explosive charges, the detonation delays, and the charge spacing), and to verify induced liquefaction of the soil deposit at a testing site located within the New Madrid Seismic Zone (NMSZ). The results obtained from the installed transducers and the pre- and post-blast cone penetration tests (CPT) are discussed. Although, the CPT were performed when the excess porewater pressures were dissipated, a review of CPT profiles after blasting showed no evidence of increase of cone tip resistance and sleeve friction. Due to the small amount of explosive charge weight that was used, the excess porewater pressure ratio values only increased above the unity at the depth of 11.30 m. A review of the existing empirical models used to predict blast-induced porewater pressure responses and liquefaction is presented. A new empirical model that accounts for the in-situ soil properties, to estimate the excess pore pressure ratio, was developed and presented herein.

**Keywords:** Charge weight; Blasting; Empirical models; Liquefaction; Excess porewater pressure ratio; Peak compressive strain; Peak particle velocity.

### 6.3. Background

Controlled blasting has been used 1) as ground improvement technique to densify loose, saturated granular soils (e.g., Lyman 1941, Ivanov 1967, Solymar 1984, Handford 1988, La fosse and Rosenvinge 1992, Kimmerling 1994, Narin van Court and Mitchell 1994, Raju and Gudehus 1994, Gohl et al. 1994, Gohl et al. 1996, Gohl et al. 1998, Gohl et al. 2000, Gohl et al. 2001,

Gohl et al. 2009, Vega-Posada 2012), 2) to physically model liquefaction for large full-scale testing (e.g., Charlie 1985, Charlie et al. 1988a, Charlie et al. 1992, Kimmerling 1994, Figueroa et al. 1994, Ferrito 1997, Okamura and Soga 2006, Charlie and Doehring 2007, Rollins and Anderson 2008), and 3) to evaluate the effects of liquefaction on deep foundation performance (e.g., Ashford et al. 2004, Rollins 2004, Rollins et al. 2004, Rollins and Strand 2006, Rollins and Hollenbaugh 2015). Controlled blasting can be performed on the ground surface and/or underground. For underground blasting, the energy generated from the explosion is typically considered as the key parameter that is required to induce liquefaction. Specifically, explosive charges create a blast wave that propagates through the soil, and generate enough excess porewater pressure to liquefy the target soil material. The dissipation of the generated blast-induced porewater pressures causes the liquefied soil material to compress or consolidate following blasting. As reported by Narin van Court and Mitchel (1994), for liquefaction to occur, the amount of energy generated from blasting must exceed the amount of energy required to resist soil liquefaction. This amount of required energy is not only a function of explosive weight, but also a function of the blasting geometry, the type of explosive, the charge spacing, the detonation time, the soil characteristics, and wave attenuation from the blasts.

Several laboratory and in-situ techniques have been previously performed, and various empirical models have been developed to evaluate soil liquefaction potential based on the blast-induced porewater pressure responses (Charlie 1985, Charlie et al. 1988a and 1988b, Figueroa et al. 1994, Ferrito 1997, Gohl et al. 2001, Youd et al. 2001, Ashford and Rollins 2002, Seed et al. 2003, Rollins et al. 2004, Al-Qasimi et al. 2005, Bray and Sancio 2006, Charlie and Doehring 2007, Kramer 2008, Rollins and Hollenbaugh 2015). However, many of the methods that have been developed are only applicable for relatively loose sands at shallow depth, and do not take

into account the in-situ soil properties such as: relative density, grain size distribution, permeability, and overburden effective stress. In addition, some of these methods are only applicable for certain types of soils (e.g., clean sands and silty sands).

#### **6.4. Predicting Excess Porewater Pressure Ratio**

The standard of practice that is currently used for Controlled Blast Testing relies upon using existing empirical models. Several empirical models have been developed from single and/or multiple denotations to predict  $R_u$  as a function of peak particle velocity (PPV), peak compression strain ( $\epsilon_p$ ), scaled distance (SD), and in-situ soil properties (Kummeneje and Eide 1961, Studer and Kok 1980, Veyera 1985, Hubert 1986, Charlie et al. 1992, Rollins et al. 2004, Al-Qasimi et al. 2005, Eller 2011, Charlie et al. 2013). These empirical equations were previously summarized in Table 2.1 on Page 13. The Studer and Kok (1980) approach (Equation 2.2 in Table 2.1) has been commonly used to develop most of the existing empirical methods to predict the amount of porewater pressure responses. The Studer and Kok (1980) relationship was originally developed by considering a single blast in saturated sandy soils. By using this approach, the excess porewater pressure ratio values are predicted using scaled distance, and in-situ soil properties are not taken into consideration.

The SD term, shown in Table 2.1, is defined as the distance between the explosive charge location and the piezometer (in meters) divided by squared or cubed root of the charge weight (in kilograms of TNT). As reported by Kumar et al. (2014), the cubic-root and square-root scaling methods can be used to determine SD in the case of spherical charges and cylindrical charges, respectively.  $R_u$  can also be obtained by dividing the change in the porewater pressure by the initial vertical effective stress. The  $R_u$  values have been commonly used as a threshold to evaluate the blast-induced liquefaction potential. For instance, Studer and Kok (1980) reported that  $R_u$  values that were less than 0.10 represented a safe zone for liquefaction,  $R_u$  values that were between

0.80 and 1.0 represented the dangerous zone, and  $R_u$  values that were greater than or equal to 1.0 represented full soil liquefaction. In addition, The Studer and Kok (1980) method, and other existing empirical models that have been used to predict porewater pressure responses (e.g., Lyakhov 1961, Jacobs et al. 1988, Charlie et al. 1992, Rollins et al. 2001, Larson-Robl 2016), were based only on the blasting layout (SD), and not on the in-situ soil conditions.

To minimize the uncertainties and limitations that were associated with not considering the in-situ soil properties, several researchers (Veyera 1985, Hubert 1986, Al-Qasimi et al. 2005, Eller 2011, Charlie et al. 2013) developed empirical models to predict the residual porewater pressure ratio and the initiation of liquefaction as a function of peak particle velocity, peak compressive strain, relative density ( $D_r$ ) and initial vertical effective stress ( $\sigma'_{vo}$ ), as previously presented in Table 2.1. The peak compressive strain, as presented in Table 2.1, is defined as the ratio of the peak particle velocity divided by the compression wave velocity ( $V_p$ ). As previously discussed, the Studer and Kok (1980) approach, and other empirical equations (e.g., Charlie et al. 1992, Ashford et al. 2004, Al-Qasimi et al. 2005), were developed from a single detonation. Due to this shortcoming, Eller (2011) established the following empirical relationship for multiple detonations (Equation 2.9), and that is a modified version of cubic-root scaling method.

$$SD = \frac{R_1 + R_2 + \dots + R_j}{\sum (W_1 + W_2 + \dots + W_j)^{1/3}} \quad \text{Equation 6.1}$$

Within Equation 6.1, R is the distance between the explosive charge location and the monitoring piezometer, W is the TNT-equivalent weight of the charge in kg, N is the number of blasts.

A large number of theoretical and empirical methods have been presented to determine blast-induced peak particle velocities (Drake and little 1983, Handford 1988, Jacobs et al. 1988, Charlie et al. 1992, Narin van Court 1997, Rollins et al. 2001, Wu et al. 2003, Al-Qasimi et al.

2005, Leong et al. 2007, Charlie et al. 2013, and Larson-Robl 2016). A summary of these empirical equations developed are presented in Table 2.2 on Page 18. It should be noted that the aforementioned empirical equations, and other equations presented in the literature, are site-specific equations. For PPV determination, only Kumar et al. (2014) provided an empirical model (Equation 2.24) that considers the variation in soil properties including, unit weight ( $\gamma$ ), degree of saturation (S), Young's modulus (E). Kumar et al. (2014) also stated that the results obtained using the latter model are reasonable for fully saturated soils irrespective of soil type, and the model predicts high values for partially saturated soils. In addition, Charlie and Doehring (2007) reported that the approach provided by Drake and Little (1983) predicts a reasonably accurate value of PPV for most of the testing sites.

#### **6.5. Existing Threshold Values of PPV, $\epsilon_p$ and SD Required for Liquefaction**

Besides  $R_u$  have being commonly used as a threshold to assess the liquefaction potential, various researchers (Lyakhov 1961, Kummeneje and Eide 1961, Puchkov 1962, Ivanov 1967, Studer et al. 1974, Obermeyer 1980, Studer and Kok 1980, Long et al. 1981, Fragaszy et al. 1983, Veyera 1985, Hubert 1986, Handford 1988, Charlie et al. 1992, Allen et al. 1997, Walthan 2001, Gohl et al. 2001, Pathirage 2000, Eller 2001, and Charlie et al. 2013) provided other blasting parameters (PPV,  $\epsilon_p$  and SD) to be used as threshold limits for liquefaction. For a very loose saturated cohesionless soil, Lyakhov (1961) reported that liquefaction occurred at the PPV values exceeding 0.11 m/s. A study conducted by Puchkov (1962) reported liquefaction at the SD values less than  $5 \text{ m/kg}^{1/3}$  with PPV exceeding 0.08 m/s. According to Ivanov (1967), a very loose saturated sand experienced liquefaction at the SD values ranging from 6 to  $8 \text{ m/kg}^{1/3}$ . Charlie et al. (1992) observed liquefaction of dense alluvial sand at PPV values exceeding 0.16 m/s with SD less than  $3 \text{ m/kg}^{1/3}$  and peak strain exceeding 0.01 percent. Charlie and Doehring



(2007) performed an analysis of single underground explosions using chemical explosives, and reported that liquefaction can be induced to the SD values of  $3 \text{ m/kg}^{1/3}$ , where the estimated peak compressive strain exceeds 0.07 percent and peak particle velocity exceeds 1.1 m/sec were measured. Charlie and Doehring (2007) also identified the SD of  $1 \text{ m/kg}^{1/3}$  as the upper bound maximum for liquefaction induced by surface explosives. These threshold values of PPV,  $\epsilon_p$  and SD and other values presented in the literature are previously summarized in Table 2.3 on Page 18. In addition, the presented threshold values have been proven to be as a function of the soil properties including soil density, effective stress and number of strain cycles, and lithification (Ali-Qasimi et al. 2005, Ashford et al. 2004, and Charlie and Doehring 2007).

#### **6.6. Controlled blasting Tests as Ground Improvement Method**

Ground improvement and the effects of blast-induced liquefaction on the in-situ soil properties have been evaluated by measuring the ground surface settlements and by investigating the pre- and post-blast CPT measurement. Several researchers (Solymar 1984, Dowding and Hryciw 1986, Gandhi et al. 1999, Liao and Mayne 2005, Camp et al. 2008, Narsilio et al. 2009, Gohl et al. 1996, Rollins and Anderson 2008, Finno et al. 2016) have assessed pre-and post-blast CPT data. Despite soil densification measured after the dissipation of the porewater pressure, no increase or a decrease of tip resistance have been observed from the aforementioned research studies.

The topic of using penetration tests, including CPT and standard penetration tests (SPT), to verify ground improvement or the effect of liquefaction on the soil resistances is a topic of ongoing discussion. Several research studies (Solymar 1984, Dowding and Hryciw 1986, Schmertman 1987, Mesri et al. 1990, Gohl et al. 1998, Camp et al. 2008, Gallant and Finno 2016, Finno et al. 2016) have been conducted to confirm why there is a little or no increase of penetration resistance after blasting. Finno et al. (2016) performed an extensive research study to

investigate the effect of free gas released from explosive on penetration resistance test results. Based on the post-blast field testing results, Finno et al. (2016) concluded that the gas released during blasting affect the mechanical behavior of soil. A detailed discussion of this theory and other proposed theories can be found in Finno et al. (2016). In contrast, Liao and Mayne (2005) conducted CPT soundings within the NMSZ, and concluded that the post-blast CPT measurements might be significantly affected by blast-induced liquefaction and time effects. A review of CPT profiles provided by Liao and Mayne (2005) showed a decrease of cone tip resistance, sleeve friction, and shear wave velocity values and at the testing site. These results were consistent with the observations presented in Camp et al. (2008).

A controlled blast test was conducted at the Turrell Arkansas Test Site (TATS) to 1) evaluate the effect of in-situ conditions on blast-induced excess porewater pressure responses and 2) predict liquefaction at the testing site located within the NMSZ. A review of the existing empirical models used to predict blast-induced porewater pressure responses and liquefaction is also presented here. A comparison of pre- and post-blast CPT data was also presented. Based on the results obtained from the TATS, new empirical model was developed to predict  $R_u$  and PPV. For the new empirical model for  $R_u$ , the contribution of PPV and  $\sigma'_{vo}$ , were taken into consideration for a certain range of  $D_r$  values.

### **6.7. Geotechnical Site Characteristics**

The TATS is located in Northeast Arkansas within the New Madrid Seismic Zone (NMSZ), and the Mississippi Embayment. The generalized soil profile, the average cone tip resistance ( $q_c$ ), average sleeve friction ( $f_s$ ), average relative density ( $D_r$ ) and soil type behavior index ( $I_c$ ), are presented in Figure 6.1. The  $D_r$  and  $I_c$  values were correlated from the CPT soundings data using Kulhawy and Mayne (1990) and Robertson and Cabal (2012), respectively. The soil profile consists of high plasticity clay, from the ground surface to a depth of 6.60 m,

underlain by a potentially liquefiable sand deposit. As illustrated in Figure 1, the liquefiable sand deposit consists of a silty sand layer (6.60 to 10.65 m), and a loose sand layer (10.65 to 25 m). The plasticity index (PI) within the clay layer ranged from 40 to 55 percent, with an average of fine content (FC) of approximately 97.67 percent. Although the groundwater table fluctuates with the river level of the Mississippi River, the groundwater table was encountered at the approximate depth of 7.01 m below the ground surface before blasting.

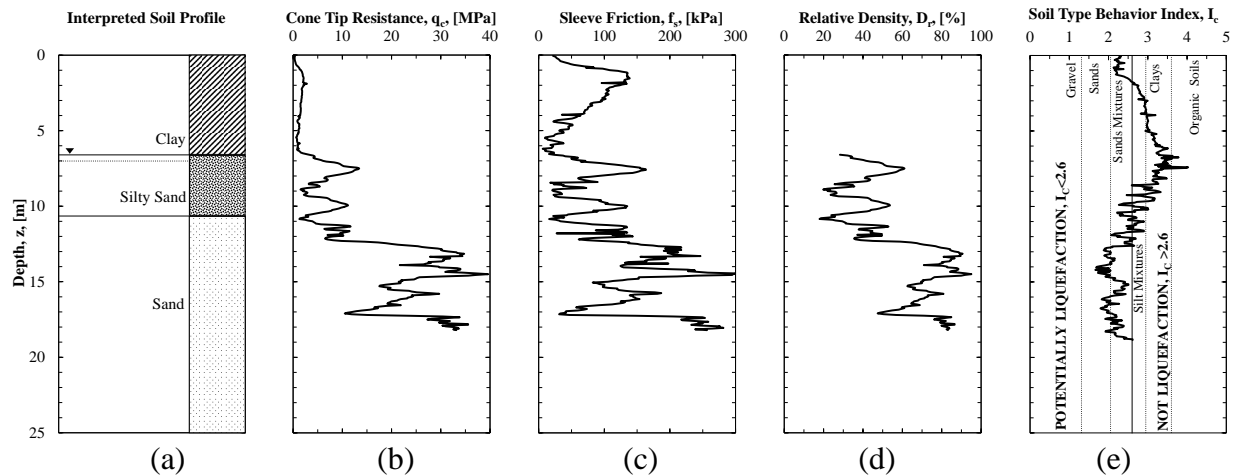


**Figure 6.1.** (a) Interpreted soil profile (b) average cone tip resistance ( $q_c$ ), (c) average sleeve friction ( $f_s$ ), (d) relative density ( $D_r$ ) and (e) soil type behavior index ( $I_c$ ) at the TATS.

Based on the liquefaction susceptibility chart that was developed from the  $I_c$  criteria (Figure 6.1e), as proposed by Robertson and Wride (1998), the soil types with calculated  $I_c$  values less than 2.6, were typically susceptible to liquefaction. At this site, the soil materials with  $I_c$  values less than 2.6 were observed below an approximate depth of 8 m. The values of  $I_c$ , PI, and FC observed at the depths above 8 m indicated that no liquefaction should occur within the upper soil layer. The liquefaction susceptibility at the TATS was first investigated by Race and Coffman (2013) following the procedures proposed by Idriss and Boulanger (2008). Using the results obtained from in-situ and laboratory tests, liquefaction was predicted to occur within the silty sand and the sand layers for the design mean magnitude of 7.5 and a peak ground acceleration of 0.64g that might be produced within the NMSZ (Race and Coffman 2013).

## 6.8. Blast-induced Liquefaction Tests

As previously indicated, several researchers, including Charlie et al. (1992), Al-Qasimi et al. (2005), Charlie et al. (2013), Charlie and Doehring (2007) provided guidance regarding the conditions required for the development of liquefaction (Tables 2.3). At the TATS, charge weight values of 1.0 kg and 0.82 kg per deck were estimated for inner and outer ring; respectively, by using the Drake and Little (1983), Eller (2011), and Studer and Kok (1980) equations to estimate PPV, SD and  $R_u$  required for liquefaction. The amount of explosive charge were also determined by considering 1) a SD value of 3 m/kg<sup>3</sup> as the upper bound, 2) PPV value of 1.1 m/s and a  $\epsilon_p$  value of 0.07 percent as lower boundaries, and 3) an  $R_u$  values equals to the unity for liquefaction to occur. These threshold values were selected based on the results obtained from the existing empirical models summarized in Tables 2.3. To prevent possible damage to the adjacent infrastructure, an average of 0.91 kg (2 lbs) per deck was detonated to induce liquefaction at the testing site.

A plan view and a cross-sectional layout of the testing site are shown in Figure 2. Prior to blasting, thirteen (13) porewater pressure transducers (piezometers) were installed at different depths around two circular arrays (inner and outer rings), as shown in Figure 2b. These piezometers were used to monitor the generation and dissipation of the excess porewater pressure responses as a function of time and depth during, and after blasting. The inner and outer rings of the piezometers were installed at a distance of 0.53 and 1.07 m from the center of blast ring, respectively. The piezometers were installed following the procedures provided in Rollins et al. (2005b). The PPV values were measured using seismographs located at the ground settlement. Four string potentiometers were installed inside the blast ring to monitor the ground surface movement associated with the excess porewater pressures dissipation following blasting. This blasting geometry design was similar to blasting layouts used by various researchers

(Ashford et al. 2004; Rollins 2004; Rollins et al. 2004; Rollins and Strand 2006; Rollins and Hollenbaugh 2015) to induce liquefaction around deep foundation elements.

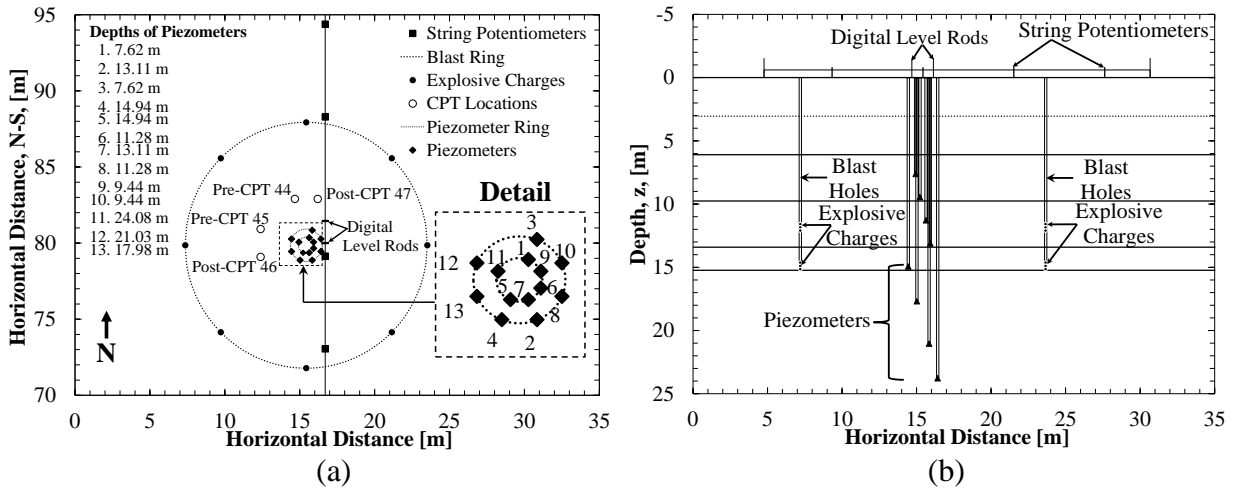


**Figure 6.2.** (a) Plan view and (b) cross-section with the locations of blast ring, explosive charges, piezometers, string potentiometers, and CPT soundings at the TATS.

Two decks of explosives charges were detonated to liquefy the soil material within the target layer (8 to 13 m). The explosive charges were placed in a circular array that consisted of the eight, pre-drilled and cased blast holes (Figure 6.2). The blast holes were drilled at a radial distance of 8.10 m from the center of the blast ring. As illustrated in Figure 6.2, the explosive charges were placed in two decks within each blast hole. The first deck contained 0.91 kg of explosive charge at a depth of 14.60 m. The second deck also contained 0.91 kg of explosive charge at a depth of 11.60 m below the ground surface. A total of 14.56 kg (1.82 per blast hole) of charge was detonated to liquefy the sand deposit between 7 and 13 m. The explosive charges that were installed, consisted of a mixture of ammonium nitrate, sodium nitrate, and aluminum. The charges were detonated one at a time, proceeding around the ring at the deepest deck (14.60 m) and then around the ring at the shallowest deck (11.60 m) to 1) minimize vibrations, and 2) to generate multiple blast pulses. The charges were sequentially detonated in counterclockwise

fashion around the blasting ring with a 500ms delay between the detonations of each individual charge.

Four CPT tests were performed to investigate the effects of blast-induced liquefaction on in-situ soil properties. Two series of CPT tests, referred as Pre-CPT 44 and Pre-CPT 45, were performed prior to blasting. These pre-blast CPT tests were also used to characterize the subsurface stratigraphy and to evaluate the soil liquefaction susceptibility. Two other CPT tests, referred as Post-CPT 46 and Post-CPT 47, were performed after blasting. A comparison of the cone tip resistance ( $q_c$ ) and sleeve friction ( $f_s$ ) measurements that were collected before and after blasting are presented and discussed in subsequent sections. As shown in Figure 6.2, the pre-and post-blast CPT tests were performed inside the blast ring.

## **6.9. Results and Discussion**

### **6.9.1. Excess Porewater Pressure Ratio Results**

The excess porewater pressure ratio time histories and the maximum  $R_u$  values recorded from the installed piezometers are presented in Figure 6.3. Although the blast charge weights used in this study were similar to the charges produced liquefaction at testing site in Vancouver, Canada (Strand 2008) and Christchurch, New Zealand (Wentz et al. 2015), the piezometers showed  $R_u$  values much smaller than required for liquefaction. As shown in Figure 3, the porewater pressures were instantaneously elevated immediately after blasting, and then gradually dissipated over a period of approximately 10 minutes. Maximum  $R_u$  of 1.17 and 1.05, indicating liquefaction, were from the piezometers located at a depth of 11.30 m in the outer and inner ring piezometers, respectively.  $R_u$  values of 0.46 and 0.43 were measured at a depth of 9.4 m for the piezometer located in the outer and inner ring, respectively.

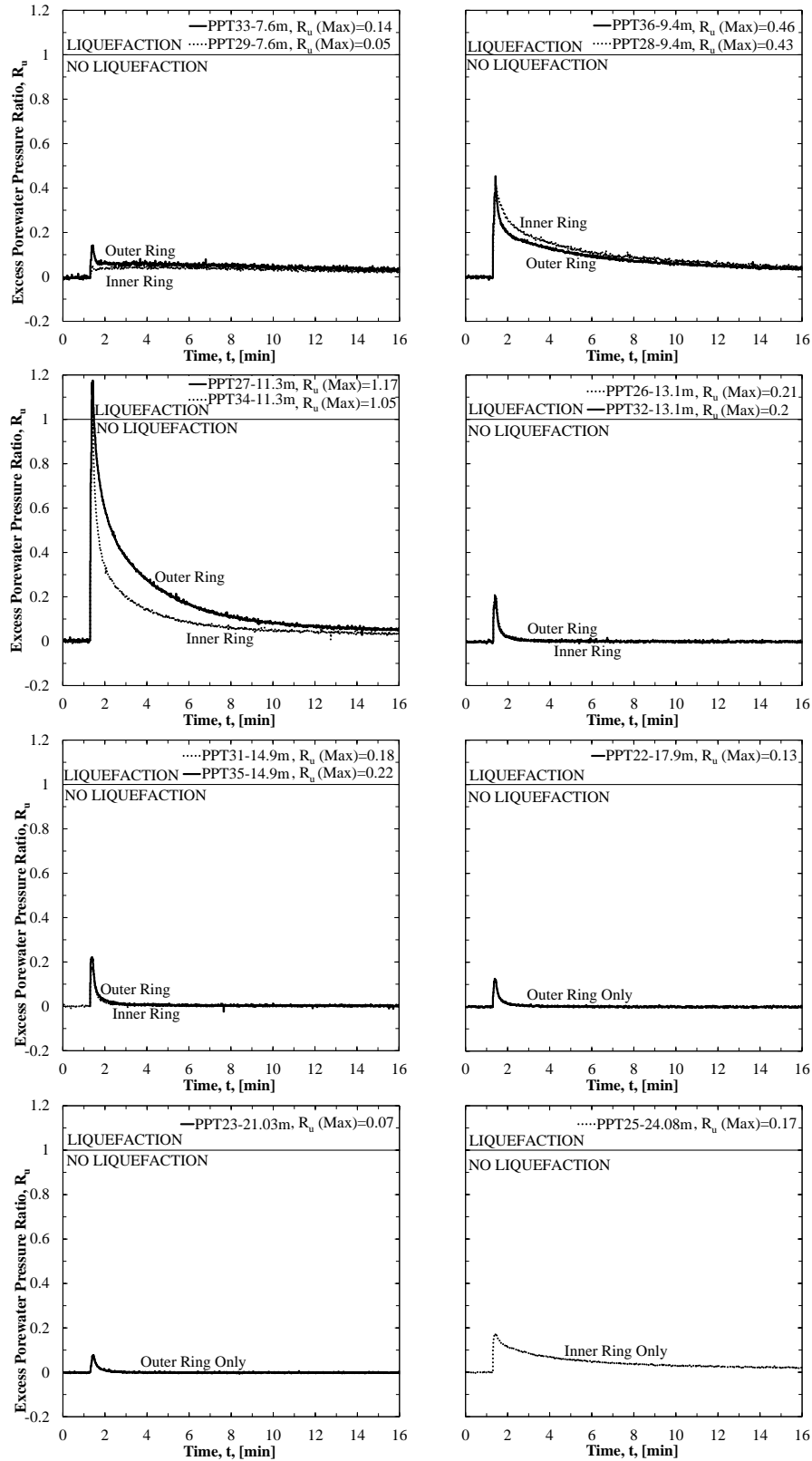


**Figure 6.3.** Measured excess porewater pressure ratio values as a function of time, as obtained from inner and outer rings.

The low  $R_u$  values that were observed from piezometers located at the depths of 7.60 m, 13.10 m, 14.90 m, 17.90 m, 21.03 m and 24.08 m were attributed to: 1) the generated vibrations and shock waves that were not being large enough to induce complete liquefaction, 2) the presence of the impermeable soil materials (clay and silty sand) that were observed at the depth of 7.60 m, 3) the higher relative density values that were observed at the depths of 13.10 m, 14.90 m, and 17.90 m, and 4) the piezometer devices located at 21.03 and 24.08 m being located farther away from explosive charges.

Based on video recordings and seismometer records, only 12 of the 16 individual 0.91 kg charges that were set to detonate (eight blast holes, two decks with 0.91 kg of charge per deck per blast hole), were detonated properly. Four of the charges completed a low-order detonation due to dynamic shock when the blasting cap fired. Based on discussions with the blasting contractor, lack of stemming and water hammer that developed following detonation of the lower deck of charges may have prevented the upper charges from detonating properly. It was believed that this low-order detonation may have also contributed to the low  $R_u$  measurements. The post-blast ground surface settlements are presented in Figure 6.4. A total ground settlement of 25.67 mm was measured inside of the blast ring. Due to the presence of impervious soil overlying the liquefied layer, sand boils and flowing of groundwater were not observed at the ground surface following blasting.

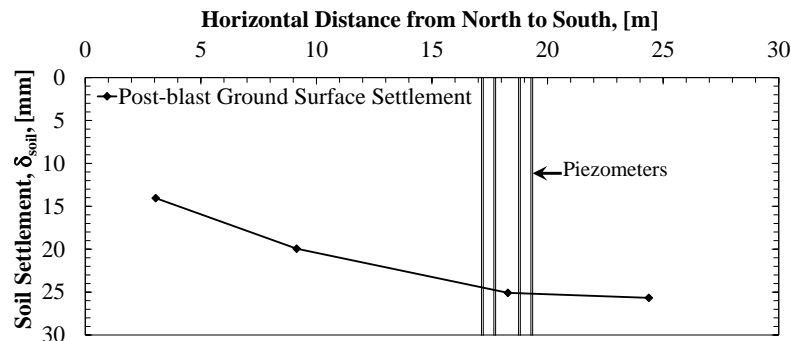


**Figure 6.4.** Post-blast ground surface settlements as obtained from string potentiometers.



Predicted PPV values obtained using existing empirical models and measured PPV values, as a function of the cubic-root-scaled distances are presented in Figure 5. The best-fit empirical equation developed from the TATS for PPV is provided as Equation 6.2:

$$PPV = 9.05(SD)^{-2.51} \quad \text{Equation 6.2}$$

Like lower than predicted excess porewater pressure ratio measurements, lower than expected peak particle velocity values were also measured at the TATS. As shown in Figure 6.5, the measured PPV values were also lower than most of the predicted PPV values, except the values obtained using Leong et al. (2007), and Wu et al. (2003). This difference can be attributed to 1) the presence of cohesive materials within the upper layer of the profile at the TATS, 2) a different blasting layout, and 3) variation of site conditions.

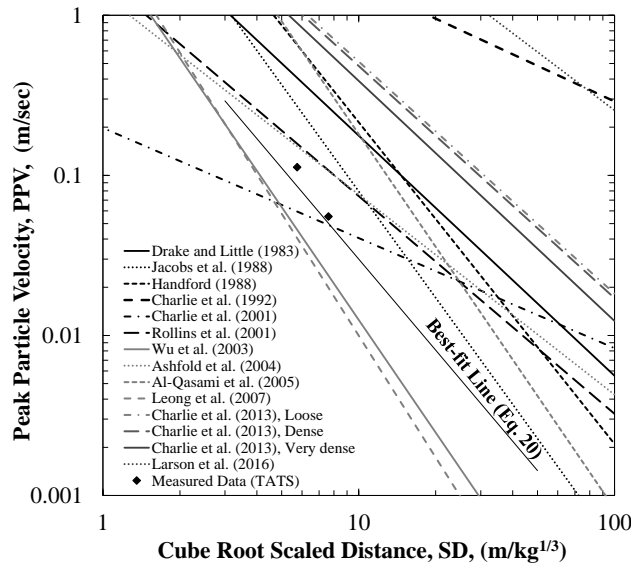


**Figure 6.5.** Comparison between measured and predicted PPV values as a function of cubic root-scaled distances.

### 6.9.2. Pre-and post-blast CPT Measurements

Results from the pre- and post-CPT tests that were obtained from the northern and western locations are shown in Figures 6.6 and 6.7, respectively. A slight decrease of tip resistance and sleeve friction was observed within the target layer. This decrease was observed

within the silty sand layer in the northern CPT soundings, and within silty sand and sand in the western CPT soundings. Some zones within the post-blast CPT profiles also showed a slight increase of both tip resistance and sleeve friction values. These slight increases were not consistent within the entire soil profile. Therefore, it is reasonable to attribute the decrease and/or increase of cone-penetration test results to 1) the soil variability and 2) CPT measurement errors for this specific site.

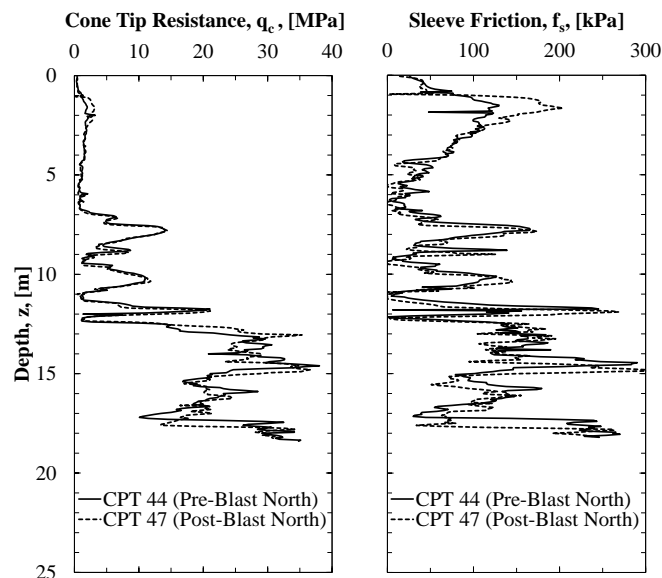


**Figure 6.6.** Pre- and post-blast CPT measurements from the northern testing location.

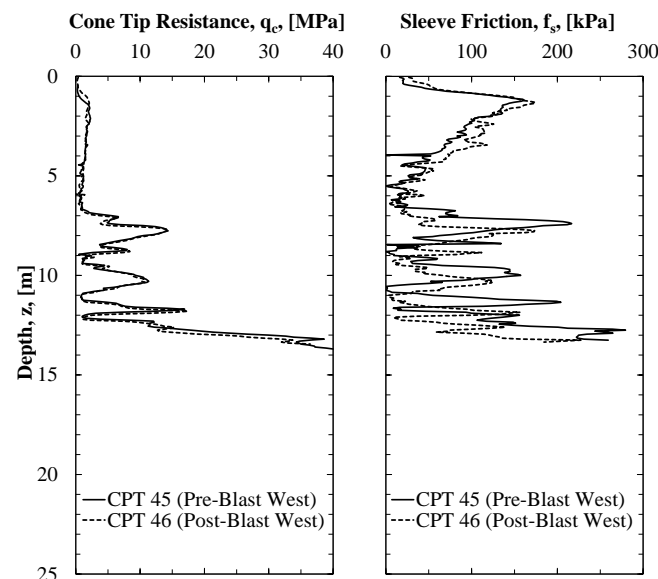


**Figure 6.7.** Pre- and post-blast CPT measurements from the western testing location.

Based on the piezometer measurements, the measured excess porewater pressure ratio were elevated for a period of 10 minutes. The post-CPT soundings were performed one hour after blasting. It is very possible that the porewater pressures were completely dissipated when the post-CPT soundings were acquired. This delay in the collection of the CPT data may have prevented capturing the complete decrease of tip resistance and sleeve friction values. As can be seen in Figures 6.6, and 6.7, despite the dissipation of excess porewater pressure and the post-blast settlement measurements, there was no evidence of the increase of tip resistance and sleeve friction data, as a result of excess porewater dissipation. This was consistent with the observations obtained within the NMSZ by Liao and Mayne 2005, and also discussed by other researchers (Solyman 1984, Dowding and Hryciw 1986, Gandhi et al. 1999, Camp et al. 2008, Narsilio et al. 2009, Gohl et al. 1996, Rollins and Anderson 2008, Gallant and Finno 2016, Finno et al. 2016). As discussed in Finno et al. (2016), due to the soil conditions at the TATS (higher fines content), the release of nitrogen gas may have also prevented an increase the increase of tip resistance measurements at the TATS.

#### **6.10. Proposed Empirical Model**

Liquefaction occurred at the testing site, as was evident from the observed excess porewater pressure ratio measurements and ground surface settlement measurements. However, the required amount of the explosive charges, that was predicted using existing equations (Equations 2.2, 6.1, and 2.10, for determination of  $R_u$ , SD, and PPV, respectively) did not produced enough energy to liquefy the entire target layer. This was mostly attributed to 1) not all of the explosive charges were detonated, and 2) in-situ soil properties not being considered into Equations 2.2, 6.1 and 2.10. Therefore, a site-specific, empirical model, that includes vertical effective stress and relative density was developed. The measured and predicted excess porewater pressure ratio values, determined using the existing empirical models that consider the

soil conditions (Veyera 1985, Hubert 1986, Al-Qasimi et al. 2005, and Charlie et al. 2013) are presented in Figure 6.8.

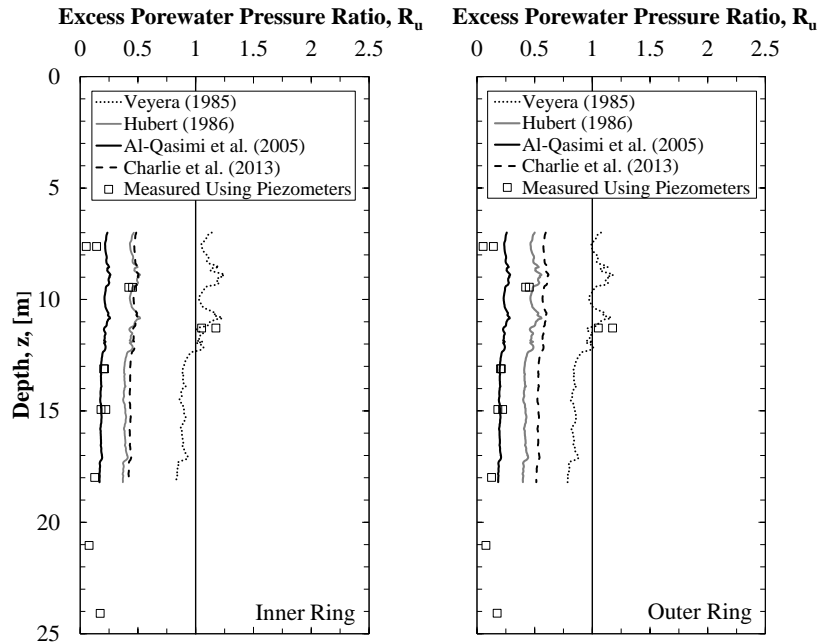


**Figure 6.8.** Measured and predicted excess porewater pressure ratio values as a function of depth, as obtained using charge weight of 0.91 kg per deck per borehole, and Equations 2.2, 6.1, and 2.10, for determination of  $R_u$ , SD, and PPV, respectively.

In general, the values estimated using the Al-Qasimi et al. (2005) method (Equation 2.7) were the most comparable to the measured results, within and below the target layer, except for the liquefied. The other methods over-predicted the  $R_u$  values. Therefore, the Al-Qasimi et al. (2005) was modified to incorporate the pre-blast in-situ soil properties that were acquired at this site. Specifically, the Al-Qasimi et al. (2005) model was modified by changing the leading coefficient ( $C_{Dr}$ ) to fit the measured and predicted  $R_u$  values into a linear equation. As previously shown in Table 2.1, within the Al-Qasimi et al. (2005) empirical model (Equation 2.7), the  $C_{Dr}$  equals to 1.13 for the entire soil profile. For the proposed model,  $C_{Dr}=3$  for  $D_r>55\%$  and  $C_{Dr}=12.5$  for  $D_r<55\%$ . The modified Al-Qasimi et al. (2005) equations that is expressed in terms of PPV, vertical effective stress (in kPa) and relative density (in percentage) is expressed as

Equation 6.3:

$$R_u = C_{Dr} (PPV)^{0.54} (\sigma_{vo}')^{-\frac{1}{3}} (D_r)^{-\frac{1}{5}} \quad \text{Equation 6.3}$$

The development of a proper empirical equation, for the testing site described herein, allowed for the calculation of the explosive charge weight that should have been used to liquefy the entire target layer (8 to 13 m). As shown in Figure 9, liquefaction was predicted to occur within silt sand and sand layers by using an explosive charge weight of 3.77 and 3.37 kg per borehole for the inner and outer ring, respectively. These explosive charge weight were determined using 1) the Eller (2011) equation (Equation 2.9) to calculate the SD values for multiple detonations, 2) the proposed PPV equation (Equation 6.2) to calculate the appropriate PPV values for the site, 3) the relative density and effective stress values from CPT correlations, and 4) the proposed empirical equation (Equation 6.3) to determine  $R_u$ , and 5) the  $R_u$  values being greater than or equals to unity for liquefaction to occur. Therefore, at least 3.77 kg of explosive charges per borehole were recommended for future blast testing at this site.

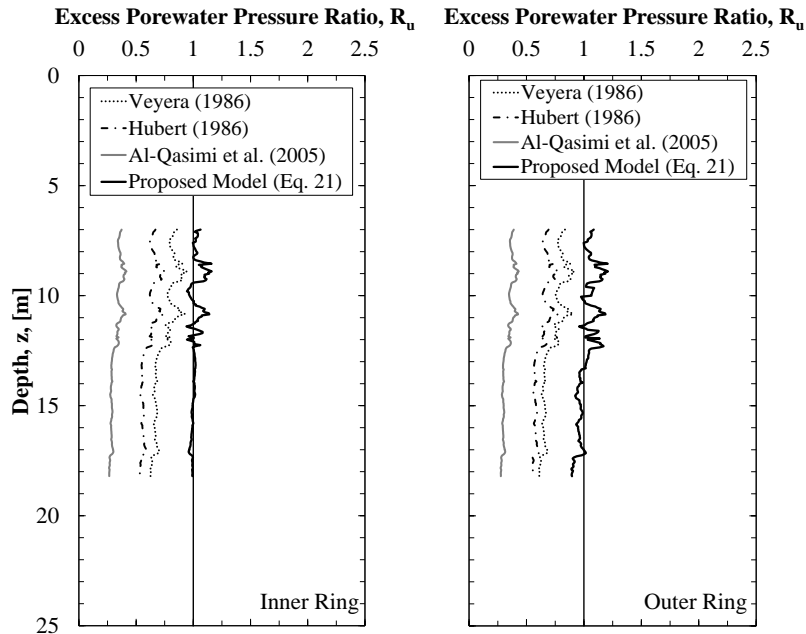


**Figure 6.9.** Predicted excess porewater pressure ratio as a function of depth, as obtained using existing empirical equations and the new proposed equation (Equation 6.3) for inner and outer rings, respectively.

### 6.11. Conclusions

A proper empirical equation for predicting the excess porewater pressure ratio at the TATS was developed. CPT tests were not able to verify the effect of blasting on penetration resistances of the soil at the testing site. Although blast-induced liquefaction may contribute to the changes of both tip resistance and sleeve friction, a review of the post-CPT profiles showed no evidence of increase of tip resistance and sleeve friction due densification. The changes of tip resistance and sleeve friction values that were observed in post-blast CPT data were associated to the soil variability and CPT measurement errors. Therefore, in the case of verifying ground improvement or post-blast densification, it is recommended to measure pre-and post-blast ground settlements instead of penetration test results.

For the future blasting tests, it is recommended that the blast boreholes contain one deck of explosives rather than multiple decks of explosives to avoid improper detonations. In addition, because the in-situ properties (vertical effective stress, particle size distribution, relative density, permeability and drainage) affected the amount of excess pore pressure responses, these parameters should be accounted for in the blasting design. For the sites within the NMSZ and other sites with similar soil conditions, it is recommended to use the threshold values provided in herein and Equations 6.2 and 6.3 to estimate the PPV and the  $R_u$  values, respectively.

### 6.12. Acknowledgements

The authors thank the Arkansas State Highway and Transportation Department, the Missouri Department of Transportation, Duane Houkom, Inc., and Loadtest, Inc., for financial and/or in kind contributions to the scope work described herein.

### 6.13. References

Al-Qasimi, E.M.A., Charlie, W.A., and Woeller, D.J. (2005). "Canadian liquefaction experiment (CANLEX): Blast-induced ground motion and pore pressure experiments." Geotechnical Testing Journal, Vol. 28, No.1, 9-21.

- Allen, B. M., S. I. Drellack, and M. J. Townsend (1997), Surface effects of underground explosions, Rep. DOE/NV/11718-122, 140 pp., Nev. Oper. Off., U.S. Dep. of Energy, Las Vegas. (Available at <http://www.osti.gov>)
- Ashford, S.A. and Rollins, K.M. (2002). "TILT: Treasure Island Liquefaction Test: Final Report." Report SSRP-2001/17, Department of Structural Engineering, University of California, San Diego.
- Ashford, S.A., Rollins, K.M., and Lane, J.D. (2004). "Blast-induced liquefaction for full-scale foundation testing." *Journal of Geotechnical and Geoenvironmental Engineering*. Vol. 130, No. 8, pp 798-806.
- Bray, J.D., and Sancio, R.B. (2006). "Assessment of the liquefaction susceptibility of fine-grained soils." *Journal of Geotechnical and Geoenvironmental Engineering*. Vol. 132, No. 9, pp. 1165-1177.
- Camp, W. M., Mayne, P. W., and Rollins, K. M. (2008). "Cone penetration testing before, during, and after blast-induced liquefaction." ASCE, Sacramento, CA, 10.
- Charlie, W.A. (1985). "Review of present practices used in predicting the effects of blasting on pore pressure," U.S. Department of the Interior, Bureau of Reclamation. Report GR-85-9, 21 p.
- Charlie, W.A., Hubert, M.E., Schure, L.A., Veyera, G.E., Bretz, T.E., and Hassen, H.A. (1988a). "Blast induced liquefaction: summary of literature." Air Force Office of Scientific Research, Washington D.C., 316 p.
- Charlie, W.A., Doehring, D.O., Veyera, G.E., and Hassen, H.A. (1988b). "Blast induced liquefaction of soils: laboratory and field tests." Air Force Office of Scientific Research, Washington D.C., 184 p.
- Charlie, W.A., Jacobs, P.J., and Doehring, D.O. (1992). "Blast induced liquefaction of an alluvial sand deposit." *Geotechnical Testing Journal*. Vol. 15, No. 1, pp. 14-23.
- Charlie, W.A., and Doehring, D.O. (2007). "Groundwater table mounding, pore pressure, and liquefaction induced by explosions: energy-distance relations." *Reviews of Geophysics*. 45, RG4006. December 2007, pp. 1-9.
- Charlie, W. A., Bretz, T. E., Schure (White), L. A., and Doehring, D.O. (2013). "Blast-induced pore pressure and liquefaction of saturated sand." *Journal of Geotechnical and Geoenvironmental Engineering*, Vol. 139, No. 8, 1308-1389.
- Drake, J. L., and Little, C. D. (1983). "Ground shock from penetrating conventional weapons." Proc., Interaction of Non-Nuclear Munitions with Structures, U.S. Air Force Academy, Colorado Springs, CO, 1-6.

- Dowding, C. H., and Hryciw, R. D. (1986). "A laboratory study of blast densification of saturated sand." *J. Geotech. Eng.*, 10.1061/(ASCE) 0733-9410(1986)112:2(187), 187–199.
- Eller, J.M. (2011), "Predicting pore pressure in in-situ liquefaction studied using controlled blasting." Master's Thesis, Oregon State University.
- Ferrito, J.M. (1997). "Seismic design criteria for soil liquefaction." Technical Report TR-2077-SHR. Naval Facilities Engineering Center. 87p.
- Figueroa, J.L., Saada, A.S., Liang, L., and Dahisaria, N.M. (1994), "Evaluation of soil liquefaction by energy principles." *Journal of Geotechnical Engineering*, Vol. 120, No. 9, pp. 1554-1569.
- Fragaszy, R. J., Voss, M. E., Schmidt, R. M., and Holsapple, K. S., 1983, "Laboratory and Centrifuge Modeling of Blast-induced Liquefaction," 8th International Symposium on Military Application of Blast Simulation, Spiez, Switzerland, pp. III.5-1–III.5-20.
- Finno, R. J., Gallant, A. P., and Sabatini, P. (2016). "Evaluating ground improvement after blast densification: Performance at the Oakridge landfill." *J. Geotech. Geoenviron. Eng.*, 10.1061/(ASCE)GT.1943-5606.0001365, 04015054.
- Gallagher, P. M., Pamuk, A. and Abdoun, T. (2007). "Stabilization of liquefiable soils using colloidal silica grout." *Journal of Materials in Civil Engineering*, Vol. 19, No.1, pp. 33-40.
- Gallant, A. P., and Finno, R. J. (2016). "Stress Redistribution after Blast Densification." *J. Geotech. Geoenviron. Eng.*, 10.1061/(ASCE)GT.1943-5606.0001365, 04015054.
- Gandhi, S., Dey, A., and Selvam, S. (1999). "Densification of pond ash by blasting." *J. Geotech. Geoenviron. Eng.*, 10.1061/ (ASCE)1090-0241 (1999)125:10(889), 889–899.
- Gohl, W. B., Howie, J. A., and Everard, J. (1996). "Use of explosive compaction for dam foundation preparation." *Proc.*, 49th Canadian Geotechnical Conf., Vol. 2, Canadian Geotechnical Society, Richmond, BC, Canada, 758–793.
- Gohl, W. B., Howie, J. A., Hawson, H. H., Diggle, D. (1994). "Field experience with blast densification." *Proc.*, 5th U.S. National Conf. on Earthquake Engineering, Vol. 4, Earthquake Engineering Research Institute, Oakland, CA, 221–231.
- Gohl, W. B., Tsujino, S., Wu, G., Yoshida, N., Howie, J. A., and Everard, J. (1998). "Field application of explosive compaction in silty soils and numerical analysis." *Proc.*, Geotechnical Earthquake Engineering and Soil Dynamics III, GSP 75, ASCE, Reston, VA, 654–665.
- Gohl, W. B., Jefferies, M. G., Howie, J. A., and Diggle, D. (2000). "Explosive compaction: Design, implementation and effectiveness." *Geotechnique*, 50(6), 657–665.



- Gohl, W.B., Howie, J. A., and Rea, C. E. (2001). "Use of controlled detonation of explosives for liquefaction testing." Proceedings, Fourth Int. Conf. On Recent Advances in Geotechnical Earthquake Engineering and Soil Dynamics, San Diego, Calif. Paper no. 913.
- Handford, G. T. (1988). "Densification of an existing dam with explosives." Proc., Hydraulic Fill Structures, ASCE, New York, 750-762.
- Hubert, M. E. (1986). "Shock loading of water saturated Eniwetok coral sand." M. S. thesis, Department of Civil Engineering, Colorado State University, Fort Collins, Co, 145-154.
- Idriss, I.M. and Boulanger, R.W. (2008). Soil Liquefaction during Earthquakes. Earthquake Engineering Research Institute MNO-12, 235p.
- Ivanov, P.L. (1967). Compaction of Noncohesive Soils by Explosions (translated from Russian). National Technical Information Service Report No. TT70-57221. U.S. Department of Commerce, Springfield, VA, 211 pp.
- Jacobs, P. J. (1988). "Blast-induced liquefaction of an alluvial sand deposit," M.S. Thesis, Department of Civil Engineering, Colorado State University.
- Johnston, A.C., and Schweig, E.S. (1996). "The enigma of the New Madrid earthquakes of 1811–1812." Annual Review of Earth and Planetary Sciences, Vol. 24, pp. 339-384.
- Kummeneje, D., and Eide, O. (1961). "Investigation of loose sand deposits by blasting." Proc., 5th ICSMFE, ISSMFE, London, 491–497.
- Kimmerling, R.E. (1994). Blast Densification for Mitigation of Dynamic Settlement and Liquefaction – Final Report WA-RD 348.1. Washington State Department of Transportation. 135 pp.
- Kramer, S.L. (2008). "Evaluation of liquefaction hazards in Washington State." Final Research Report, Agreement T2695, Task 66, Liquefaction Phase III. Washington State Transportation Commission.
- Kulhawy, F. H., and Mayne, P. W. (1990). "Manual on estimating soil properties for foundation design." Electric Power Research Institute, EL-6800 Research Project 1493-6 Final Rep., 2-24 and 2-33.
- Kumar, R., Choudhury, D., Bhargava, K. (2014). "Prediction of blast-induced vibration parameters for soil sites." International Journal of Geomechanics, Vol. 14, No. 3.
- La Fosse, U., and Rosenvinge, T. V., IV (1992). "Densification of loose sands by deep blasting." Proc., Grouting, Soil Improvement and Geosynthetics, ASCE, Reston, VA, 954–968.
- Larson-Robl, K. M. (2016). "Pore pressure measurement instrumentation response to blasting." M.S. Thesis, Mining Engineering, University of Kentucky.

- Leong, E. C., Anand, S., Cheong, H. K., and Lim, C. H. (2007). "Reexamination of peak stress and scaled distance due to ground shock." *Int. J. Impact Eng.*, 34(9), 1487–1499.
- Liao, T., and Mayne, P. W. (2005). "Cone penetrometer measurements during Mississippi embayment seismic excitation experiment." *Earthquake Eng. Soil Dyn.*, 133(158), 1–12.
- Long, J. H., Ries, E. R., and Michalopoulos, A. P. "Potential for Liquefaction Due to Construction Blasting," *Proceedings, International Conference on Recent Advances in Geotechnical Engineering and Soil Dynamics, University of Missouri-Rolla, 1981*, pp. 191-194.
- Lyman, A. K. B. (1941). "Compaction of cohesionless foundation soils by explosives." *Trans. ASCE*, 107, 1330–1348.
- Lyakhov, G. M. (1961). "Shock Waves in the Ground and the Dilution of Water Saturated Sand." *Zhurnal Prikladnoy Mekhanik Technicheskoy Fiziki, Moscow*, 38–46.
- Mesri, G., Feng, T. W., and Benak, J. M. (1990). "Postdensification penetration resistance of clean sands." *J. Geotech. Eng.*, 10.1061/(ASCE) 0733-9410(1990)116:7(1095), 1095–1115.
- Mitchell, J.K. (2008). "Mitigation of Liquefaction Potential of Silty Sands." *From Research to Practice in Geotechnical Engineering Congress 2008*, pp 453-451.
- Narin Van Court, W.A., and Mitchell, J.K. (1994). "Explosive compaction: Densification of loose, saturated, cohesionless soils by blasting." *Geotechnical Engineering Report No. UCB/GT/94-03*. 116 p.
- Narsilio, G. A., Santamarina, J. C., Hebel, T., and Bachus, R. (2009). "Blast densification: Multi-instrumented case history." *J. Geotech. Geoenviron. Eng.*, 10.1061/(ASCE)GT.1943-5606.0000023, 723–734.
- Obermeyer, J. R., "Monitoring Uranium Tailings Dams During Blasting Program," *Symposium on Uranium Mill Tailings Management, Colorado State University, November 1980*, pp. 513-527.
- Okamura, M., and Soga, Y. (2006). "Effects of pore fluid compressibility on liquefaction resistance of partially saturated sand." *Soils Found.*, 46(5), 695–700.
- Pathirage, K. S., "Critical assessment of the CANLEX blast experiment to facilitate a development of an in-situ liquefaction methodology using explosives," *M.S. thesis, Department of Civil Engineering, University of British Columbia, 2000*.
- Puchkov, S. V. (1962). "Correlation between the velocity of seismic oscillations of particles and phenomenon of particles and liquefaction phenomenon of water-saturated sand." *Prob. of Eng. Seismology*, 6(21), 92–94 (in Russian).

- Raju, V. R., and Gudehus, G. (1994). "Compaction of loose sand deposits using blasting." Proc., 13th Int. Conf. on Soil Mechanics and Foundation Engineering, ASCE, Reston, VA, 1145–1150.
- Ranjan, K. D., (2015), "Engineering geological issues after Gorkha Earthquake 2015 in Nepal- a preliminary understanding." 10<sup>th</sup> Asian Regional Conference of IAEG, Kyoto, Japan.
- Race, M. L., Coffman, R. A., (2013), "Effect of uncertainty in site characterization on the prediction of liquefaction potential for bridge embankments in the Mississippi Embayment." ASCE Geotechnical Special Publication No. 231, Proc. Geo-Congress 2013: Stability and Performance of Slopes and Embankments III, San Diego, California, March, pp. 888-897.
- Robertson, P.K. & Wride, C.E., (1998), "Evaluating cyclic liquefaction potential using the cone penetration test." Canadian Geotechnical Journal, Vol.35, pp.442-459.
- Robertson, P.K. and Cabal, K.L. (2012). "Guide to Cone Penetration Testing for Geotechnical Engineering", Prepared for Gregg Drilling & Testing Inc., 5th Edition, 2012, 130 p.
- Rollins, K.M., Ashford, S. A., and Lane, J. D. (2001). "Full-scale lateral load testing of deep foundations using blast induced liquefaction." Proc., 4<sup>th</sup> int. conf. on Recent Advances in Geotechnical Earthquake Engineering and Soil Dynamics, Univ. of Missouri-Rolla, MO, 1-3.
- Rollins, K.M. (2004). "Liquefaction mitigation using vertical composite drains: Full-scale testing." Final Report for Highway IDEA Project 94. Transportation Research Board, February 2004, 105 p.
- Rollins, K.M., Lane, J.D., Nicholson, P.G., and Rollins, R.E. (2004). "Liquefaction hazard assessment using controlled-blasting techniques." Proc. 11th International Conference on Soil Dynamics & Earthquake Engineering. Vol. 2, pp. 630-637.
- Rollins, K.M., Lane, J.D., Dibb, E., Ashford, S.A., and Mullins, A.G. (2005a). "Pore pressure measurement in blast-induced liquefaction experiments." Transportation Research Record 1936, Soil Mechanics 2005, TRB, Washington D.C., pp. 210-220.
- Rollins, K. M. and S. R. Strand (2006). "Downdrag Forces Due to Liquefaction Surrounding a Pile". Proceedings of the 8<sup>th</sup> U.S. National Conference on Earthquake Engineering. Paper No. 1646, San Francisco, CA, April 18-22.
- Rollins, K.M. and Anderson, J.K.S. (2008). "Cone penetration resistance variation with time after blast liquefaction testing." Procs. Geotechnical Earthquake Engineering and Soil Dynamics-IV, Geotechnical Special Publication 181, ASCE, 10 p.
- Rollins, K.M. and Hallenbaugh (2015). "Liquefaction induced negative skin friction from blast-induced liquefaction tests with Auger-cast Piles." 6<sup>th</sup> International Conference on Earthquake Geotechnical Engineering, Christchurch, New Zealand.

- Seed, R.B., Cetin, K.O., Moss, R.E.S., Kammerer, A.M., Wu, J., Pestana, J.M., and Riemer, M.F. (2003). "Recent advances in soil liquefaction engineering and seismic site response evaluation: Unified and consistent framework." Proceedings: Fourth International Conference on Recent Advances in Geotechnical Earthquake Engineering and Soil Dynamics and Symposium in Honor of Professor W.D. Liam Finn, San Diego.
- Sherif, M. A., Ishibashi, I., and Tsuchiya, C. (1977). "Saturation effects on initial soil liquefaction." *J. Geotech. Eng.*, 103(GT8), 914–917.
- Schmertmann, J. H. (1987). "Discussion of 'time-dependent strength gain in freshly deposited or densified sand.'" *J. Geotech. Eng.*, 10.1061/ (ASCE)0733-9410(1987)113:2(173), 173–175.
- Solyman, Z. V. (1984). "Compaction of alluvial sands by deep blasting." *Can. Geotech. J.*, 21(2), 305–321.
- Strand, S. R. (2008). "Liquefaction mitigation using vertical composite drains and liquefaction induced downdrag on piles: implications for deep foundation design." PhD Thesis, Brigham Young University.
- Studer, J., L. Kok, and R. W. Trense (1978), Soil liquefaction field test—Meppen Proving Ground 1978 free field response, paper presented at 6th International Symposium on Military Applications of Blast Simulation, Fr. Minist. of Def., Cahors, France.
- Studer, J. and Kok, L. (1980). "Blast-induced excess porewater pressure and liquefaction experience and application." International Symposium on Soils under Cyclic and Transient Loading, Swansea, UK, pp. 581-593.
- Vega-Posada, C. A. (2012). "Evaluation of liquefaction susceptibility of clean sands after blast densification." Ph.D. dissertation, Northwestern Univ., Dept. of Civil Engineering, Evanston, IL, 209.
- Veyera, G. E. (1985). "Transient porewater pressure response and liquefaction in a saturated sand." Ph.D. dissertation, Department of Civil Engineering, Colorado State University, Fort Collins.
- Walther, T. (2001), "The explosion crater at Fauld", *Mercian Geol.*, 15(2), 123–125.
- Wentz, F.J., van Ballegooy, S., Rollins, K.M., Ashford, S.A., and Olsen, M.J. (2015). "Large scale testing of shallow ground improvements using blast-induced liquefaction." 6<sup>th</sup> International Conference on Earthquake Geotechnical Engineering, Christchurch, New Zealand.
- Youd, T.L., et al. (2001). "Liquefaction resistance of soils: Summary report from the 1996 NCEER and 1998 NCEER/NSF workshops on evaluation of liquefaction resistance of soils." *Journal of Geotechnical and Geoenvironmental Engineering*. ASCE, Vol. 127, No.10, pp. 817-833.

## CHAPTER 7: Liquefaction-induced Dragload and Downdrag on Drilled Shaft Foundations

### 7.1. Chapter Overview

Blast-induced liquefaction tests were performed on two drilled shaft foundations constructed at the TATS. The tests were conducted to 1) evaluate the loss of shaft resistance, and to 2) assess the effect of liquefaction-induced dragload on the behavior of the drilled shaft foundations following liquefaction. Prior to blasting, 1567.34kN of static dead load was applied to top of each drilled shaft to simulate the factored structural load capacity. Following blasting, the excess porewater pressure, the ground settlement as a function of time, and soil settlements as a function of time and depth were monitored. The results of the ground settlements, caused by porewater pressure dissipation; the drilled shaft settlements are presented and discussed herein. An increase in side resistance following blasting was observed. This increase was attributed to the increase of effective stress as porewater pressure dissipated. The pre-and post-liquefaction load and settlement distribution curves along with the drilled shaft-soil settlement curves for each drilled shaft during initial loading and following blasting are discussed herein.

The paper enclosed in this chapter will be submitted within Journal of Geotechnical and Geoenvironmental Engineering. The full reference is: Ishimwe, E., Rollins, K.M., Coffman, R.A., (2018). "Dragload and Downdrag around Drilled Shafts following Blast-induced Liquefaction." Journal of Geotechnical and Geoenvironmental Engineering (Under review).

### 7.2. Additional Information

As previously mentioned in Chapter 5, three drilled shafts that included: the north, center and south drilled shafts were tested during blast tests (Figure 7.1), and three blast events were performed at the TATS. However, only two drilled shafts, North and Center drilled shafts (Figure 7.1) were discussed in the journal paper presented in this Chapter. This was due to the

constrained project timeline of full-scale blast-induced liquefaction field work, and the data acquisition system was disconnected when the excess porewater were still dissipating. As shown in Figure 7.2a, tests around the South drilled shaft were terminated when the neutral plane was still on the top of the drilled shaft. An increase of the load with time was also observed around this drilled shaft foundation.

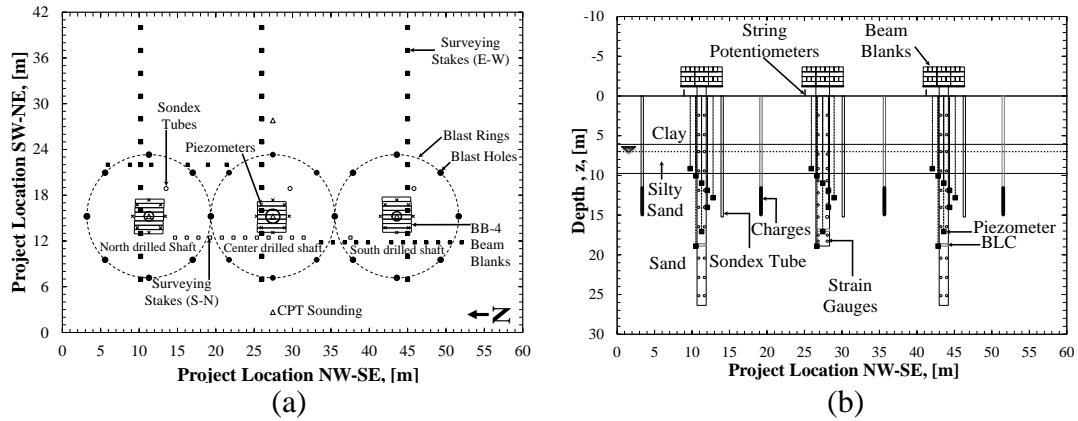


**Figure 7.1.** Plan view and a cross-section of the TATS with locations of explosive charges, piezoresistive piezometers, Sondex tube and CPT locations around drilled shaft foundations.

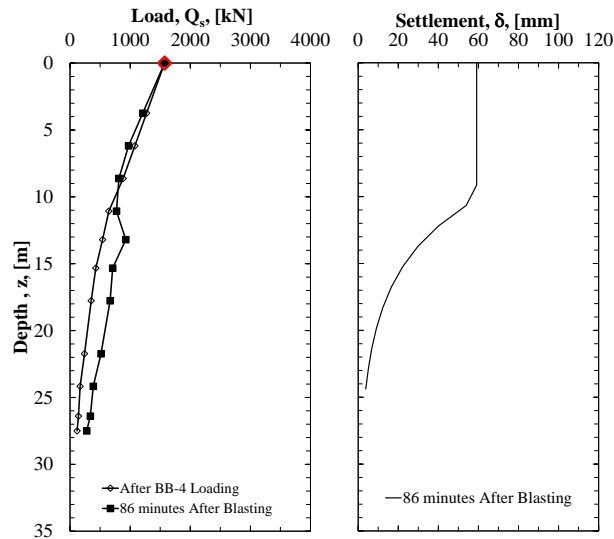


**Figure 7.2.** (a) Pre- and post-blast load and resistance distribution curves, (b) drilled shaft-soil settlement curves, as obtained from the South drilled shaft foundation.

A ground settlement of 59.13 mm was measured from the Sondex tube that was installed near the shaft (Figure 7.2b). For completeness, the porewater pressure responses and the ground

settlements as obtained from the South drilled shaft, are shown in Figures, 7.3 and 7.4, respectively. As shown in Figure 7.3, several piezometers were damaged during the retrieval process from the center drilled shaft. Therefore, only two piezometers were utilized around the south the drilled shaft. Although one of the two piezometers showed a  $R_u$  value less than the unity, different observations including water flowing to the ground surface and significant ground surface indicated that the site profile at this location was liquefied. The water started to flow to the ground at the locations near the piezometer boreholes and blast holes for a period of 5 to 10 minutes after blasting. These observations including water flowing on the ground surface and the ground surface settlements are shown in Figure 7.4 and 7.5. As anticipated, the presence of the clay prevented the formation of the sand boils.

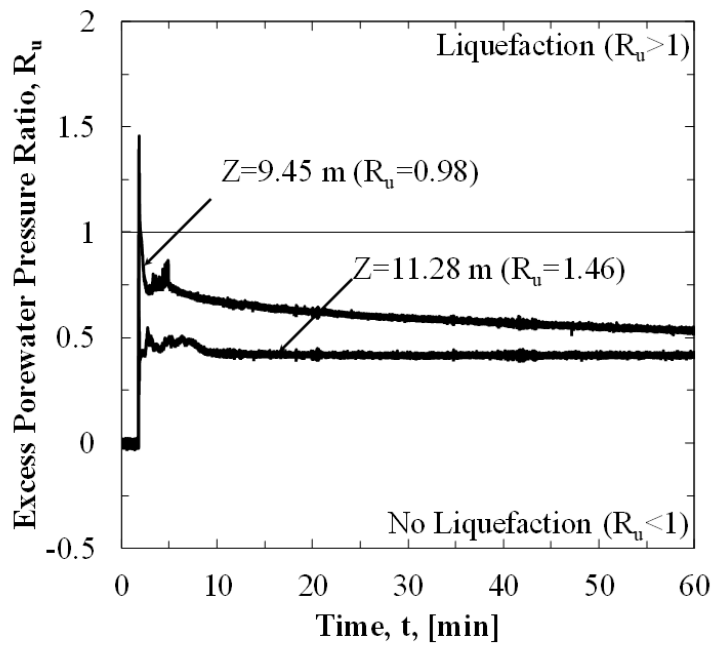


**Figure 7.3.** Measured excess porewater pressure ratio values at different depths as a function of time following blasting around the South drilled shaft.

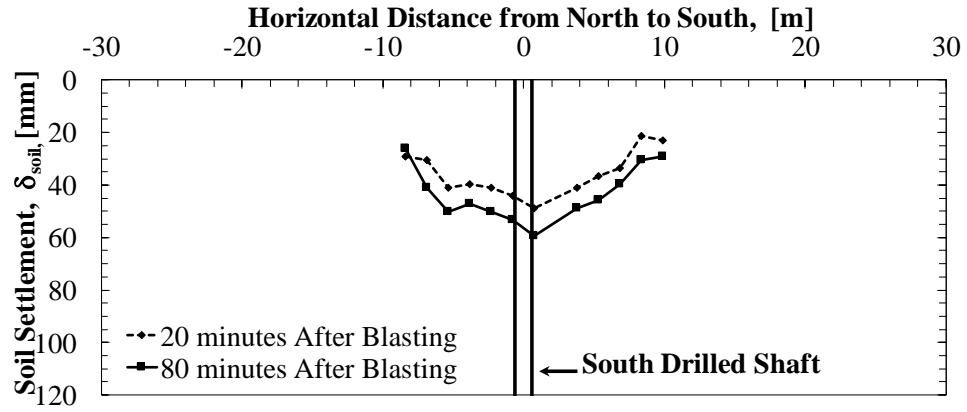


**Figure 7.4.** Post-blast soil settlements following the third blast event around the South drilled shaft.

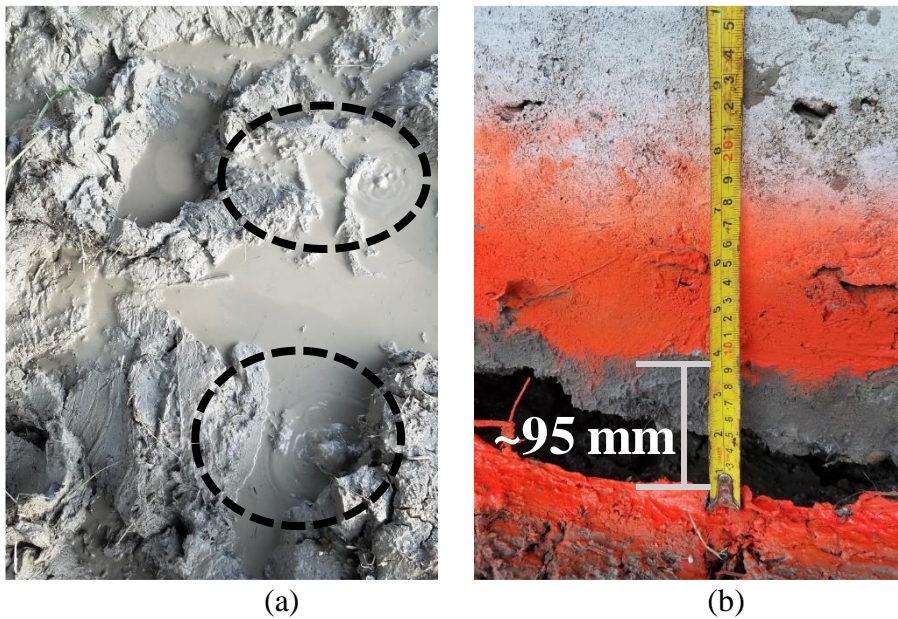


**Figure 7.5.** (a) Water flowing to the ground and (b) ground settlement following blasting (Photography by the author).



## Dragload and Downdrag around Drilled Shafts Following Blast-induced Liquefaction

Elvis Ishimwe<sup>1</sup>, Richard A. Coffman<sup>2</sup>, and Kyle M. Rollins<sup>3</sup>

<sup>1</sup>Graduate Student, University of Arkansas, Fayetteville, Arkansas, USA; email: eishimwe@email.uark.edu

<sup>2</sup>Associate Professor, University of Arkansas, Fayetteville, Arkansas, USA; email: rick@uark.edu

<sup>3</sup>Professor, Brigham Young University, Provo, Utah, USA; email: rollinsk@byu.edu

### 7.3. Abstract

Blast-induced liquefaction and full-scale axially loading tests were performed around two drilled shaft foundations constructed at the Turrell Arkansas Test Site, located within the New Madrid Seismic Zone. The drilled shafts were instrumented with strain gauges to provide the data necessary to evaluate the behavior of the axially loaded deep foundation elements when subjected to liquefaction. The liquefaction-induced dragloads and downdrag were measured, and the progression of the neutral plane was monitored, as the excess porewater pressure dissipated. The load and resistance distribution curves as a function of depth and time, and drilled shaft settlement curves for each drilled shaft during pre-loading and following blasting were obtained and are discussed. The post-blast resistance values that were measured immediately after blasting were approximately 30-percent of the measured pre-blast positive shaft resistance values. The shaft resistance within liquefied layer reduced from being 100-percent resisting shaft resistance to approximately 70-percent contributing shaft resistances. A design methodology to facilitate proper design of drilled shafts within deep soil deposits located in seismic areas is presented.

**Keywords:** Earthquake; Drilled shaft; Dragloads; Downdrag; Liquefaction; Deep foundation; Seismic design.

#### 7.4. Introduction

Deep foundations are typically used to transfer structural loads to competent soil layers when 1) the soil close to the ground surface has insufficient bearing capacity, and when 2) liquefiable soils are encountered. The majority of the bridges constructed within seismic zones rely upon the stability of deep foundations that are installed above or within liquefiable soil deposits. Despite large factor of safety values or different load and resistance factors being employed during the design of the deep foundations within seismic areas, soil liquefaction may cause extensive damage to infrastructure. The damage may result from: 1) a reduction in the end bearing and shaft resistances, 2) a reduction in the lateral load capacity, 3) the additional of extra loads to the foundation (dragload), 4) excessive foundation settlements (downdrag), and 5) lateral spreading of the soil surrounding the foundation.

The development of consolidation-induced dragload and downdrag around different types of deep foundation elements have been discussed by several researchers (e.g., Bjerrum et al. 1969, Endo et al. 1969, Bozozuk 1972, Bozozuk 1981, Broms and Silberman 1964, Long and Healy 1974, Fellenius and Broms 1969, Fellenius 1972, 1979, and 1988, Davisson 1993, Briaud and Tucker 1997, Poulos 1997, Dumas 2000, Hannigan et al. 2005, Fellenius 2006, Fellenius and Siegel 2008, Siegel et al. 2013, Hannigan et al. 2016, and Tan and Fellenius 2016). However, the phenomenon of liquefaction-induced dragload and downdrag has only been discussed in a few and more recent research studies (Boulanger and Brandenberg 2004, Rollins and Strand 2006, Fellenius and Siegel 2008, Vijayaruban et al. 2015, Rollins and Hollenbaugh 2015, and Muhunthan et al. 2017). In addition, the current state of knowledge about the development of dragload and/or downdrag that is presented in several design code specifications including those developed by the American Association of State Highway and Transportation Officials (AASHTO) and the Federal Highway Administration (FHWA), is mostly based on the soil

settlement related to consolidation phenomena instead of being related to liquefaction phenomena. Knowledge is lacking on how to address the dragload and downdrag caused by the post-liquefaction settlements, and the seismic effects of these two phenomena on deep foundation elements.

Consideration of the dragload and downdrag in deep foundation design has become a complicated topic over the last four decades. Deep foundation designers and researchers have recommended different design approaches on how to address the dragload and downdrag in deep foundation design (e.g., Endo et al. 1969, Fellenius 1988, Briaud and Tucker 1997, Poulos 1997, Dumas 2000, Hannigan et al. 2005, Fellenius and Siegel 2008, Siegel et al. 2013, Hannigan et al. 2016). Some of these recommended design approaches have been adopted in various design specifications. For instance, the FHWA design manual for drilled shaft foundation by Brown et al. (2010) and AASHTO (2012) design code and both recommend the neutral plane methodology described in the Briaud and Tucker (1997). These code-based design methods of deep foundations and other AASHTO based state highway design codes; including Washington State Department of Transportation (WSDOT 2006), Missouri Department of Transportation (MODOT 2005), and Oregon Department of Transportation (ODOT 2015), required designers to add a factored dragload component to the axial load imposed by the structure. According to Brown et al. (2010), the combination of the factored structural axial loads and the developed dragload should not exceed the sum of the factored value of the shaft and toe resistances.

In contrast, as reported by Fellenius and Siegel (2008), the Canadian Foundation Engineering Manual (1992), the Australian Piling Standard (1995), and the Hong Kong Foundation Design and Construction Manual (2006) have adopted the unified pile design method or the neutral plane approach described in Fellenius (1988, 2004). The FHWA design manual,

for driven piles by Hannigan et al. (2016) also adopted the neutral plane method that was first developed by Fellenius (1988), and modified by Siegel et al. (2013). To evaluate the existing design methods and to investigate the effects of liquefaction-induced dragload and downdrag on deep foundations, blast-induced liquefaction tests were performed around two drilled shaft foundations installed at the Turrell Arkansas Test Site (TATS). The two drilled shaft foundations were instrumented with strain gauges to measure the load distribution along the shaft prior to and after blasting. Different devices were installed into the surrounding soil to monitor the ground movement as a function of time and depth. The blast-induced liquefaction test results, including the pre- and post-blast load and resistance distribution curves and drilled shaft-soil settlement curves, are presented herein.

## 7.5. Background

As illustrated in Figure 1, the total nominal axial resistance ( $R_t$ ) provided by a deep foundation is divided into two components of resistance: shaft resistance ( $R_s$ ) and toe resistance ( $R_{toe}$ ). For a deep foundation, the total nominal resistance is generally determined using Equation 7.1. The resistance distribution curve, shown in Figure 7.6, is simply obtained by subtracting the cumulative shaft resistance to the ultimate resistance or by adding the toe resistance to the cumulative shaft resistance. When designing a deep foundation, the total nominal resistance and the corresponding resistances (shaft and toe) are usually factored to evaluate the Load and Resistance Factor Design (LRFD) strength limit states or for Allowable Stress Design (ASD) to ensure an adequate factor of safety (F.S) of the foundation.

$$R_t = R_s + R_{toe} = A_s f_s + A_g q_{toe} \quad \text{Equation 7.1}$$

Where  $R_t$  = unfactored total resistance;  $R_s$  = unfactored total shaft resistance;  $R_{toe}$  = unfactored toe resistance;  $f_s$  = unit shaft resistance;  $A_s$  = surface area of a drilled shaft;  $A_g$  = gross area of a deep foundation;  $q_{toe}$  = unit toe resistance.

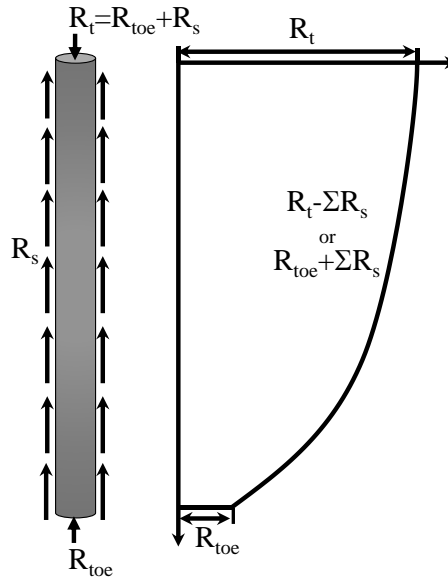


**Figure 7.6.** A schematic of a typical deep foundation and the corresponding total resistance distribution curve.

Several theoretical methods have been developed to determine unit shaft resistance and toe resistance (e.g., Skempton 1951, Meyerhof 1956, Tomlinson 1994, Kraft et al. 1981, O'Neill and Reese 1999, Brown et al. 2010). Some of these methods have been recommended in different design manuals (e.g., American Petroleum Institute 1993, FHWA 1999, AASHTO 2007, 2012 and 2014) to determine the total resistance provided by a drilled shaft or any other type of deep foundation in cohesive and cohesionless soils. The  $\alpha$ -method (total stress method) and  $\beta$ -method (effective stress method) are commonly used to estimate the shaft resistance in cohesive and cohesionless soils, respectively. For cohesive soils, the unit shaft and toe resistances are obtained using Equations. 7.2 and 7.3, respectively.

$$f_s = \alpha S_u$$

Equation 7.2

$$q_{toe} = N_c s_u \quad \text{Equation 7.3}$$

Where  $s_u$  = undrained shear strength;  $\alpha$  = a dimensionless factor relating unit shaft resistance to the undrained shear strength; and  $N_c$  = bearing capacity factor. The equations to determine the  $\alpha$ -coefficient and the  $N_c$  factor values are presented in Brown et al. (2010).

The shaft and toe resistances of a drilled shaft in cohesionless soils can be determined using the  $\beta$ -method (Equation 7.4), and toe resistance can be calculated using Equation 7.5. Various researchers (e.g., Skempton 1951, Fellenius 1991, O'Neill and Reese 1999, Kulhawy and Chen 2007) have proposed different methodologies to determine the  $\beta$ -coefficient. However, the Kulhawy and Chen (2007) approach is preferable because the method takes into consideration of the soil strength and variation of in-situ stresses in determining the  $\beta$ -coefficient.

$$f_s = \beta \sigma'_v \quad \text{Equation 7.4}$$

$$q_{toe} = 1.2N_{60} \quad \text{Equation 7.5}$$

Where  $\beta$  = shaft resistance coefficient, that can be obtained using the equations presented in O'Neill and Reese (1999) and Brown et al. (2010);  $\sigma'_v$  = vertical effective stress; and  $N_{60}$  = SPT-N value.

Typically, the positive shaft resistance ( $R_p$ ) and toe resistances ( $R_{toe}$ ) act upward (positive) to support the structural loads capacity ( $Q_{str}$ ) acting on the top of a drilled shaft foundation (Figure 7.7a). When a drilled shaft or other type of deep foundation is installed into a compressive soil (e.g., loose sand, soft clay, or recent fill), the soil that surrounds the deep foundation may move downward after installation. This compressive soil movement may be caused by 1) porewater pressure dissipation due to consolidation or liquefaction, 2) application of a surcharge on the soil adjacent to the deep foundation, 3) placement of a fill on the ground

surface, or 4) reconsolidation of the soil due to the deep foundation construction process. When soil settles more than the deep foundation, the induced soil movement may cause the positive shaft resistances acting upward along the foundation-soil interface to change direction and act in the downward (negative) direction (Fellenius 1984). In the event of a change in direction, negative shaft resistance ( $R_n$ ) are developed along a portion or along the entire foundation length (Figure 7.7b).

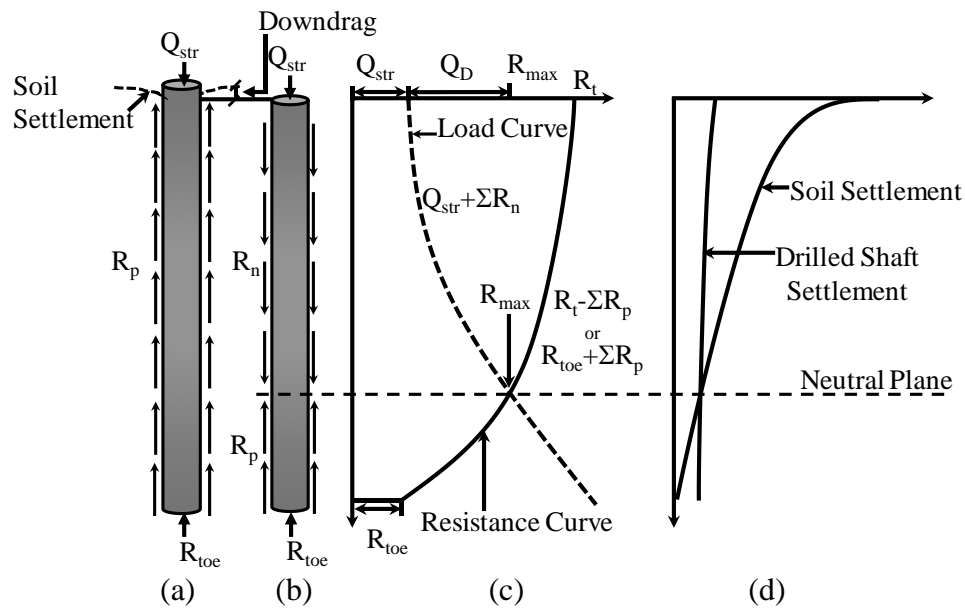


**Figure 7.7.** A schematic of (a) an axially loaded drilled shaft foundation, (b) a drilled shaft foundation subjected to dragload and downdrag due to the settlement of the surrounding soil, (c) load and resistance distribution curves, and (d) drilled shaft-soil settlement distribution curves (modified from Fellenius 1984).

Load and resistance distribution curves (Figure 7.7c) and drilled shaft-soil settlement distribution curves (Figure 7.7d), as a function of depth, are developed to evaluate the effects of the negative shaft resistance on the behavior of a given deep foundation element. The load curve, shown in Figure 7.7c, is obtained by adding the unfactored structural dead load ( $Q_{str}$ ) to the cumulative unfactored negative shaft resistance ( $\sum R_n$ ). The resistance curve, shown in Figure 7.7c, is determined by adding the unfactored toe resistance to the cumulative unfactored positive shaft resistance ( $\sum R_p$ ). As report by Brown et al. (2010), the load and resistance distribution

curves are obtained by assuming a full mobilization of shaft and toe resistance at relatively small shaft movements (10.16 to 12.70mm movement). In addition, as reported by Briaud and Tucker (1997), the amount of soil settlement must exceed the amount of foundation settlement by at least 101.6 mm (0.4 inches) for dragload to develop on a foundation.

As illustrated in Figure 7.7b, the movement of a drilled shaft foundation, due to the soil settlement, is called “downdrag.” The location of the boundary between load and resistance curves is called the “neutral plane.” The dragload ( $Q_D$ ) is defined as the accumulation of the negative shaft resistance ( $\sum R_n$ ) acting above the neutral plane location (Figure 7.7c). The neutral plane location can also be obtained from the combined plots of drilled shaft settlement and soil settlement (Figure 7.7d). As shown in Figure 7.7d, the drilled shaft and the surrounding soil settle equally at the neutral plane location. It is necessary for foundation designers to know the location of the neutral plane location because the forces (load and resistance) acting on the deep foundation are in equilibrium at the location of the neutral plane. In addition, the maximum axial load on the foundation ( $R_{max}$ ), which is the sum of unfactored structural load and the developed dragload, occurs the location of the neutral plane.

As previously illustrated in Figure 7.7c, the amount of load within the drilled shaft increases along the load curve until the location of the neutral plane is reached, and then decreases along the resistance curve below the neutral plane until the location of the toe of the drilled shaft. In addition, the developed negative shaft resistances act in the same direction as axial loads from the structure. Based on this concept, the dragloads should be considered for evaluation of geotechnical strength limit states, and should be accounted for as an additional axial load acting on the deep foundation. Consequently, an increase in the number of deep foundations or an increase in the length or diameter of the deep foundations may be required to



increase the geotechnical capacity to 1) resist the existing and the additional axial load (dragload), and 2) prevent extreme or differential downward movements of the foundation (downdrag).

As previously mentioned, the topic of liquefaction-induced dragload on deep foundation has been addressed by few authors including, Boulanger and Brandenburg 2004, Rollins and Strand 2006, Fellenius and Siegel 2008, Vijayaruban et al. 2015, Rollins and Hollenbaugh 2015, and Muhunthan et al. 2017, Boulanger and Brandenburg (2004) presented a modified neutral plane method for liquefaction-induced dragload on vertical piles by accounting for the variation of excess pore pressures and ground settlements over time, as a liquefied layer reconsolidates overtime. As presented in Equation 7.6, Boulanger and Brandenburg (2004) provided an empirical relationship to determine the shaft resistance ( $f_s$ ), within a liquefied soil layer as the excess porewater pressure dissipates. Within the Equation 7.6,  $\sigma'_v$  is the vertical effective stress,  $K_o$  is the coefficient of lateral earth pressure at rest,  $\phi$  is the friction angle, and  $R_u$  is the excess porewater pressure ratio.

$$f_s = \sigma'_{vo} K_o \tan(\phi)(1 - R_u) \quad \text{Equation 7.6}$$

In the absence of test results, Boulanger and Brandenburg (2004) concluded that the pile movement would be as large as the ground settlement if the combination of the structure load capacity and the developed dragload exceed the combination of the positive shaft resistance and the toe resistance. Therefore, the dragload phenomena should be considered when evaluating the serviceability limit states, not for the geotechnical strength limit state. Fellenius and Siegel (2008) applied the unified design method, a method that was developed for consolidation-induced dragload (not for seismic induced dragload), to analyze the dragload induced by seismic liquefaction. Again, 1) the absence of test results to validate the method, and 2) consideration of

the unit shaft resistance ( $f_s$ ) within the liquefied layer being equal to zero led Fellenius and Siegel (2008) to conclude that dragload will have only a minor effect on the deep foundation (if the liquefiable layer is located above neutral plane). According to Fellenius and Siegel (2008), the presence of dragload prior to liquefaction and liquefaction below the neutral plane will increase the axial compressive load within the pile and result in additional thus settlement resulting in less dragload. Therefore, Boulanger and Brandenberg (2004) and Fellenius and Siegel (2008) agree that the problem of liquefaction-induced dragload is a settlement (serviceability) issue, not a geotechnical axial capacity issue.

## 7.6. Geotechnical Site Characteristics

The TATS is located in Northeast Arkansas, within the New Madrid Seismic Zone (NMSZ) and within the Mississippi Embayment. The NMSZ has been the source of several historic earthquake events. Each of these previous earthquakes had strong ground motions that induced soil liquefaction due to the presence of deep, loose, saturated, sandy, soils deposited within the Mississippi Embayment (Johnston and Schweig 1996). A detailed geotechnical investigation that involved laboratory testing (soil strength and index property tests) and in-situ testing was performed at the TATS. The in-situ testing included, standard penetration testing (SPT) and cone penetration testing (CPT). The in-situ tests were performed to 1) determine the subsurface geotechnical engineering properties, and to 2) evaluate the soil liquefaction potential at the TATS. A detailed discussion regarding the soil investigation can be found in (Race and Coffman 2013, Bey 2014, Race and Coffman 2015, and Race et al. 2015). The generalized soil profile of the TATS is shown in Figure 7.8a. The average measured cone tip resistance ( $q_c$ ) and the average SPT corrected blow count ( $N_{60}$ ) values are shown in Figures 7.8b and 7.8c, respectively. The average relative density ( $D_r$ ) and soil type behavior index ( $I_c$ ), as correlated

from the CPT soundings data, as obtained using Kulhawy and Mayne (1990) and Robertson and Cabal (2012), are also shown in Figures. 7.8d and 7.8e, respectively.

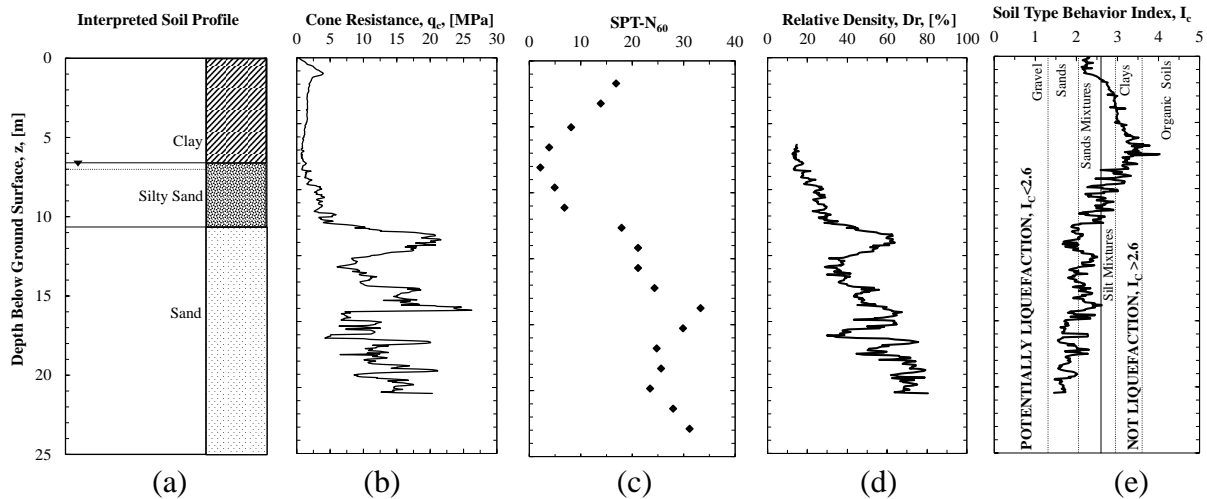


**Figure 7.8.** (a) Interpreted soil profile (b) cone tip resistance ( $q_c$ ), (c) SPT blow count ( $N_{60}$ ), (d) relative density ( $D_r$ ) and (e) soil type behavior index ( $I_c$ ) at the TATS.

Based on the geotechnical investigation information, the generalized soil profile at the TATS consist of high plasticity clay, from ground surface to a depth of 6.1 m. The clay was underlain by a silty sand layer from 6.10 to 9.8 m. The silty sand layer was underlain by a potentially liquefiable sand deposit, and the groundwater table was located approximately 7.0 m below the ground surface. Based on the liquefaction susceptibility chart (Figure 8e) that was developed from the  $I_c$  criteria, as proposed by Robertson and Wride (1998), the soil types with calculated  $I_c$  values less than 2.6, were typically susceptible to liquefaction, soils with  $I_c$  values less than 2.6 were observed below a depth of 11.4 m.

The liquefaction susceptibility at the TATS was first investigated by Race and Coffman (2013) following the procedures proposed by Idriss and Boulanger (2008). Using the results obtained from SPT, CPT, and laboratory testing, Race and Coffman (2013) concluded that the site was susceptible to liquefaction. Liquefaction was predicted to occur within the silty sand and within the sand layers for the design mean magnitude of 7.5 and peak acceleration of 0.64g that

might be produced within the NMSZ (Race and Coffman 2013). Unlike the soil profile at the previous locations of blast-induced liquefaction tests like Treasure Island, Vancouver, New Zealand and Charleston (South Carolina), which generally consisted of shallow, loose, clean sands, the liquefiable sand deposit at the TATS was overlain by a high plasticity clay.

### **7.7. Testing Program**

The two instrumented drilled shaft foundations that were tested at the TATS included a 1.2 m-diameter drilled shaft and a 1.8 m-diameter drilled shaft. A plan view and a cross-sectional layout of the testing site that included, the locations of the drilled shaft foundation, are shown in Figure 7.9. Specifically, the 1.2 m-diameter drilled shaft, hereafter referred to as the North drilled shaft, was constructed on the North side of the testing site. The 1.8 m-diameter drilled shaft, hereafter referred to as the South drilled shaft was installed on the South side of the TATS. The designed total length of the North drilled shaft was 27.6 m, with an embedded length of 26.4 m. The total length of the South drilled shaft was 21.18 m with, an embedded length of 20 m. The O'Neill and Reese (1999) methods were used during design to determine the shaft and toe resistances of the drilled shaft foundations within the cohesion and cohesionless materials that are present at the TATS. The design procedures for both of the drilled shaft foundation can be found in Bey (2014) and Race (2015).

As illustrated in Figure 7.9b, each drilled shaft was instrumented with ten sets of diametrically opposed linear vibrating wire strain gauges. Two sets of these strain gauges were located within the clay layer, two sets of the strain gauges within the silty sand layer, and the other six sets of the strain gauges were located within the sand layer. The strain gauges were attached to the rebar cage before placing the cage into the open excavation. The load capacity of each drilled shaft foundation was verified through the use of a permanently installed 50 cm

diameter bi-directional load cell (BLC). The BLC tests were performed by Bey (2014) to determine the amount of load transfer from shaft to the soil. The construction of the drilled shaft foundation, the documented installation, testing using BLC devices and strain gauges were discussed in detail in Bey (2014), Race (2015), and Race and Coffman (2015).

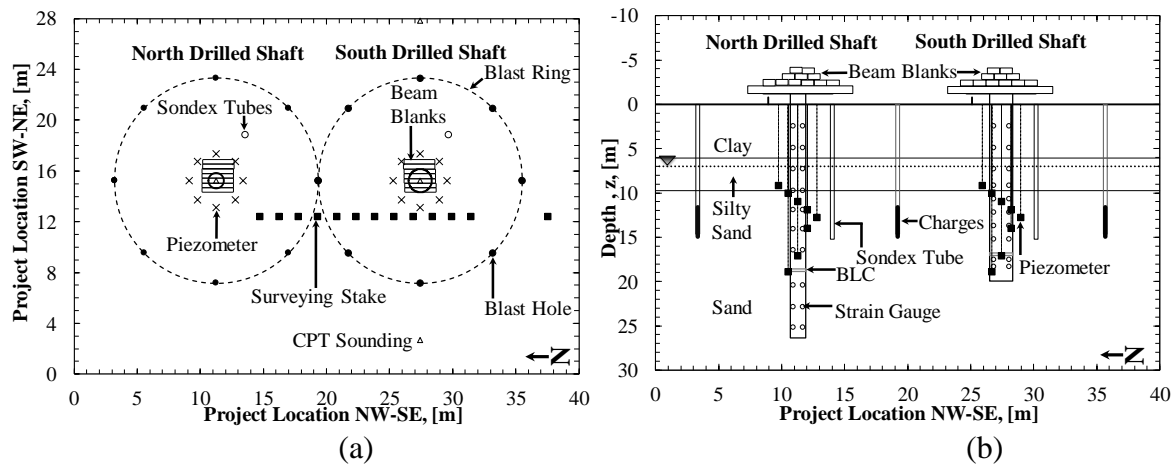


**Figure 7.9.** Plan view and a cross-section of the TATS with locations of drilled shaft foundations, explosive charges, piezometers, surveying stakes, Sondex tubes, and CPT soundings.

Additional pre-blast static testing consisted of applying a static dead-weight of 1567.3 kN on the top of each drilled shaft to simulate the unfactored axial load capacity of the superstructure. As previously illustrated in Figure 7.9, the static weight was generated by stacking a total of steel beam blanks on the top of the drilled shaft foundations before the detonation of the explosive charges. Digital level indicators were attached to the exposed side on the head of each drilled shaft head to monitor the movement of each drilled shaft during loading and after blasting. Eight porewater pressure transducers (piezometers) were installed at various locations and depths shown in Figure 7.9. These piezometers were used to monitor the generation and dissipation of the excess porewater pressure responses prior to, during, and after blasting. The piezometers were installed following the procedures provided in Rollins et al. (2005b). Surveying stakes were installed around each drilled shaft foundation to measure the

ground surface movement. Sondex tubes were also installed at a distance of 4.3 m from the center of each drilled shaft to determine the vertical soil settlement, as a function of time and depth. The positions of the surveying stakes and Sondex tubes are also presented in Figure 7.9.

#### Blast-induced Liquefaction Tests

Upon the completion of pre-blast full-scale tests and the installation of the aforementioned instrumentation, liquefaction was induced by detonating the charge explosives. Two blast events were performed to liquefy the soil at the TATS. The first blast event was performed around the North drilled shaft. During this event, 3.63 kg (8 lbs) of explosive charges were placed into each of the eight, pre-drilled blast holes that were located at a radial distance of 8.1 m from the center of the each drilled shaft foundation (Figure 7.9a). The charges in each blast hole were placed into one deck at a depth of 14.94 m below the ground surface, as shown in Figure 7.6b. The second event was conducted around the South drilled shaft. For this event, 5.4 kg (12 lbs) of explosive charge was placed into each of the eight, pre-drilled and cased blast holes at the depth of 14.94 m; the boreholes were located at a distance of 8.1 m from the center of the blast ring (Figure 7.9a). These explosive charge weight values were selected based on the results obtained from a pilot liquefaction test that was performed 14 months prior to these blast events. The charges that were utilized consisted of a mixture of ammonium nitrate, sodium nitrate, and aluminum. These explosive charges were detonated around the blasting ring with a 500 ms time delay between the detonations of the charge in each the individual charged boreholes. Blasting started from the one of blast holes and proceeded in counterclockwise around the blasting ring until the final charge in the ring was detonated.

## 7.8. Blast-induced Liquefaction Test Results

### 7.8.1. Excess Porewater Pressure Ratio Results

Time history plots of the measured excess porewater pressure ratio ( $R_u$ ) values that include the maximum measured  $R_u$  values are presented in Figure 7.10. Following the first blast event, maximum  $R_u$  values that were greater than unity were observed at the depths of 10.06 m, 10.97 m, 11.89 m and 14.02 m, and maximum  $R_u$  values greater than 0.8 were observed in piezometers at depths of 9.14 and 12.80 m (Figure 7.10a). Two piezometers were damaged during the installation of the piezometers for the second blast tests. As a result, the  $R_u$  values obtained from the six piezometers that functioned are presented in Figure 7.10b. During the second blast event,  $R_u$  values greater than unity were observed in three piezometers located at the depths of 9.14 m, 10.97 m, and 14.63 m (Figure 7.10b).

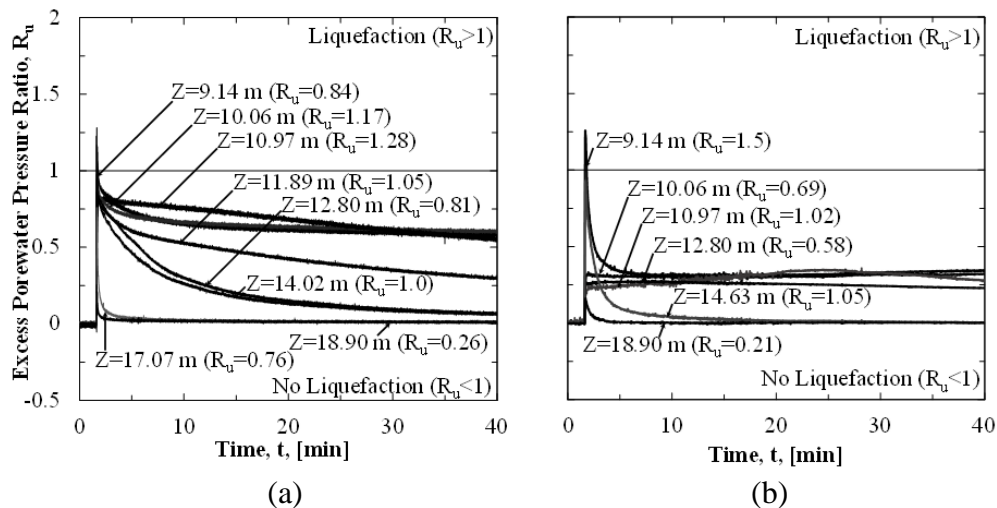


**Figure 7.10.** Measured excess porewater pressure ratio values at different depths, as a function of time for: (a) the first blast-induced liquefaction event around the North drilled shaft and (b) the second blast-induced liquefaction event around the South drilled shaft.

The excess porewater pressures were elevated immediately after blasting and dissipated as a function of time after each blast event. The excess porewater pressures from the second blast were observed to dissipate faster than the excess porewater pressures that were generated during the first blast. For example, a  $R_u$  value of 0.72 was measured, at the depth of 9.14 m, five

minutes after the first blast, and two minutes after the second blast. The delays in the dissipation of excess porewater pressure following the first blast event were attributed to the presence of less permeable materials (more clay and silt mixture soils) that was observed around the installed piezometers surrounding the North drilled shaft (Figure 7.11 a). The higher than expected rates of porewater pressure dissipation observed after the second blast, were associated with the presence of loose silty and sandy materials in the soil deposit around the locations of the piezometers used during the second blast event surrounding the south drilled shaft (Figure 7.11b).

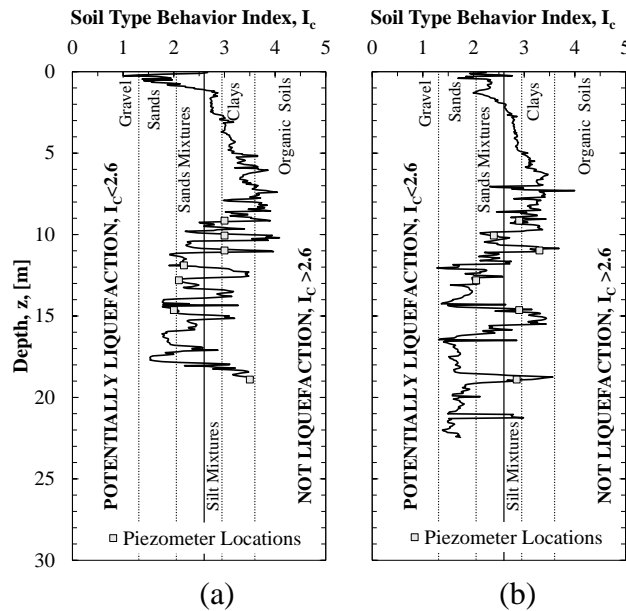


**Figure 7.11.** Soil type behavior index ( $I_c$ ) obtained from the CPT soundings performed at the (a) the first and (b) second blast events.

After each blast, the porewater pressure dissipated quickly in the piezometers that were located at the bottom of the liquefied layer. A delay in the porewater pressure dissipation was observed in the piezometer readings for the piezometers located at the top of the liquefied layer. This delay was attributed to the presence of the clay material above the silty sand layer. These observations were consistent for each of the blast tests. Following the two blast events, the  $R_u$  remained low at the depths of 17.07 and 18.90 m. These low  $R_u$  values were attributed to 1) the



higher relative density values that were observed at these depths, and 2) the amount of the energy that was generated by explosive charges was not enough to liquefy the soil at this depth.

Although some of the installed piezometers showed a  $R_u$  value less than unity, other observations indicated that the soil at the TATS liquefied. For instance, 1) water was observed to flow to the ground surface after blasting, and 2) ground surface settlement was observed. Due to the presence of the clay cap at the TATS, the pressurized ground water only flowed to the ground at the locations near the piezometer boreholes and blast holes. As anticipated, the presence of the clay cap also prevented the formation of sand boils.

### ***7.8.2. Post-Blast Ground Surface Settlements***

The ground surface settlement readings, at distinct times following each blast event, are provided in Figure 7.12. As was anticipated, the largest ground movements occurred near the location of the drilled shaft foundations. Based on the surveying data, ground surface settlement values of 57.91 and 98.08 mm were measured at times of 190 minutes and 327 minutes following the North drilled shaft and South drilled shaft, respectively. As shown in Figure 7.12, an increase in the ground surface settlements with time was observed. This increase in the ground surface settlement was due to the densification of the sand layer caused by the dissipation of the excess porewater pressures. As anticipated, the ground surface settlement values measured after the second blast event, in which a larger total amount of explosive charge was detonated, were greater than the observed ground surface settlement values following the first event. According to the data that were collected from the digital indicators after loading and during blast, the vertical movement of the top of the North drilled shaft and South drilled shaft were 6.27 and 24.51 mm, respectively. Based on these measurements, the soil settled more than the drilled shafts; therefore, liquefaction induced dragload and downdrag were anticipated to develop on the drilled shaft foundations.

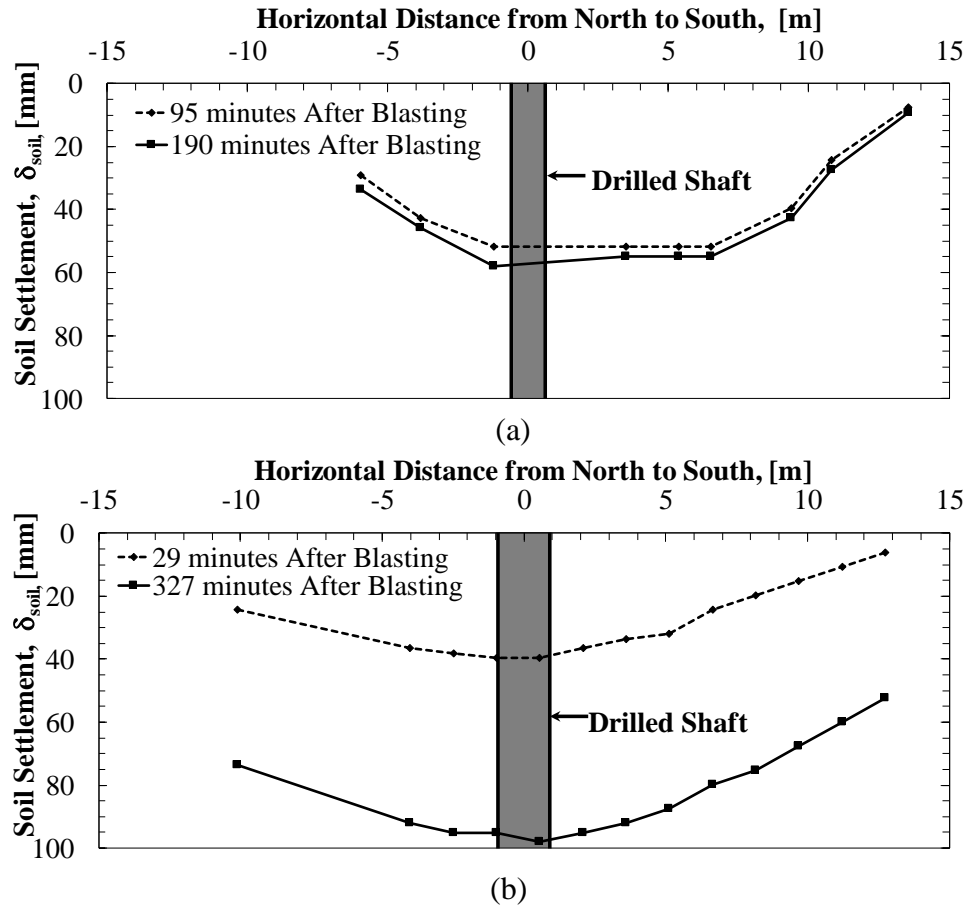


**Figure 7.12.** Post-blast soil settlements following liquefaction around (a) the North drilled shaft foundation and (b) the South drilled shaft foundation.

### 7.8.3. Pre-and Post-Blast Loads and Settlements Distribution Curves

The amount of load shed, as a function of depth, as related to the application of the static load (blank beams) to the top of each drilled shaft, was measured (Figure 7.13). The applied load (1567.3 kN) represented only about 19 and 16 percent of the ultimate total resistance that was obtained from BLC test that were previously performed on the North drilled shaft and the South drilled shaft, respectively. As shown in Figure 7.13, the applied load was transferred from the shaft to the surrounding soil and mobilized the shaft resistances from the ground surface to the toe location. As shown in Figure 7.13a, the soil from the ground surface to a depth of 10.97 m were mobilized (nearly 40 percent of the total length of the North drilled shaft) for the North drilled shaft. Due to the geometry and soil conditions around the South drilled shaft, the applied

static from beam blanks load mobilized the entire length of the South drilled shaft (Figure 7.13b). The total movements of the North drilled shaft and South drilled shaft after loading were 5.55 and 1.50 mm, respectively. These drilled shaft movements were less than the amount of movement proposed by Brown et al. (2010).

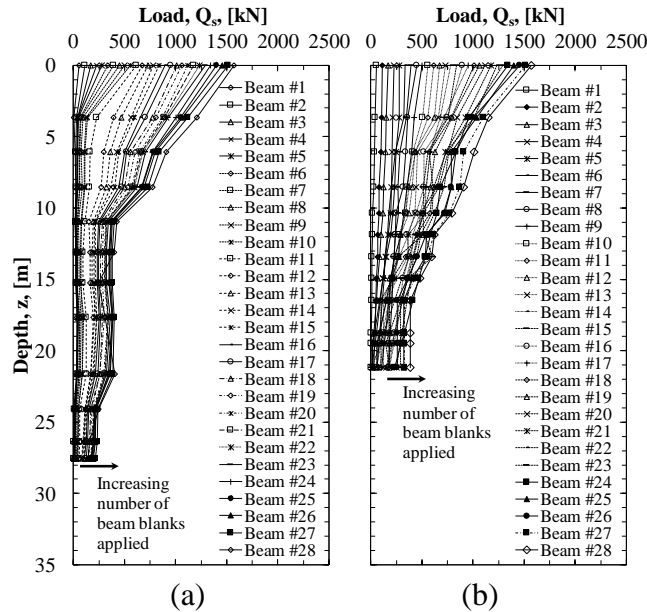


**Figure 7.13.** Load shed as a function of depth as obtained for a) the North and b) the South drilled shaft foundation during the application of the beam blanks.

As shown in Figure 7.13, during the application of static load to the top of each drilled shaft (prior to blasting), no negative shaft resistances were developed, the maximum load in each drilled shaft and the corresponding neutral plane were located at the top of each of the drilled shaft. As the excess porewater pressures, that were generated by blasting, began to dissipate, the surrounding soil settled, and the load distribution along the shaft increased due to the development of negative shaft resistances. The downward movement of the soil surrounding the drilled shaft foundation also affected the axial load distribution by mobilizing the shaft resistance and toe resistance as a function of time.

The post-blast load and resistance distribution curves that was recorded during the 200 minutes monitoring period, for the North drilled shaft, are shown in Figure 7.14a. The settlement

of the soil and the settlement of the drilled shaft, as a function of depth and time are shown in Figure 7.14b. For the first 5 to 10 minutes, an increase of shaft and toe resistances along the shaft was observed; however, no negative shaft resistances were developed during this period. During the initial time period (5 minutes), the neutral plane was still located at the top of the drilled shaft (head), and the applied loads were supported by the positive shaft resistances in the clay layer and the structure axial capacity provided by the drilled shaft.

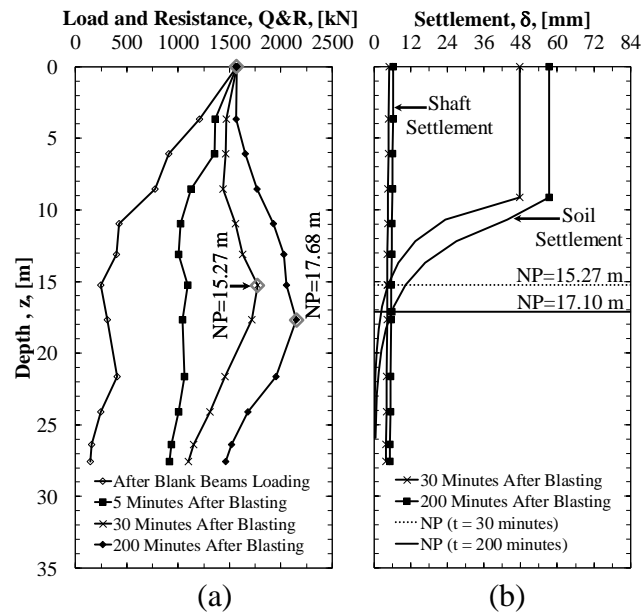


**Figure 7.14.** (a) Pre- and post-blast load and resistance curves and (b) drilled shaft and soil settlement distribution curves, as obtained for the North drilled shaft foundation.

After a period of 30 minutes following blasting, the neutral plane moved from the top of the drilled shaft to a depth of 15.27 m (near the bottom of the liquefied layer), in response to the increased in effective stress after liquefaction. The progression of the neutral plane, as the North drilled shaft and the surrounding soil settled as a function time, can also be easily identified in Figure 7.14. The soil was observed to settle more than the drilled shaft with corresponding values of 47.63 and 4.83 mm, respectively (30 minutes after blasting). The dragload developed after 30 minutes was 206.45 kN, and the neutral plane and dragload continued to move downward, and to increase as a function of time, respectively. After 200 minutes, the load and

resistance curves showed the neutral plane at a depth of 17.68 m with a corresponding dragload of 585.60 kN. However, according the drilled shaft and soil settlement distribution curves, the neutral plane was located at 17.10 m. This difference between the locations of the neutral plane was attributed to 1) difficulty in obtaining readings from the Sondex tubes, 2) load only being determined at the specific locations of the strain gauges, and 3) The Sondex tubes being located at a distance of 4.3 m away from the drilled shaft location.

The load and resistance distribution curves at various times following the second blast event around the South drilled shaft are shown in Figure 7.15. The neutral plane around the South drilled shaft also remained at the top of the drilled shaft for a period of 5 minutes following the blast. After a period of 60 minutes, the neutral plane moved to a depth of 13.41 m with a dragload of 390.61 kN, and then moved to a depth of 14.94 m with a dragload of 637.18 kN after a period of 165 minutes following blasting. The neutral plane locations, as determined from the drilled shaft and soil settlement curves, are also shown in Figure 7.15b. Based on the drilled shaft-soil settlement distribution curves, the neutral plane was located at 13.92 and 14.94 m, after a period 60 and 165 minutes after blasting, respectively. As was observed in the blast event around the North drilled shaft, an increase in the negative shaft resistance lowered the neutral plane to a depth below the liquefied layer for the South drilled shaft.

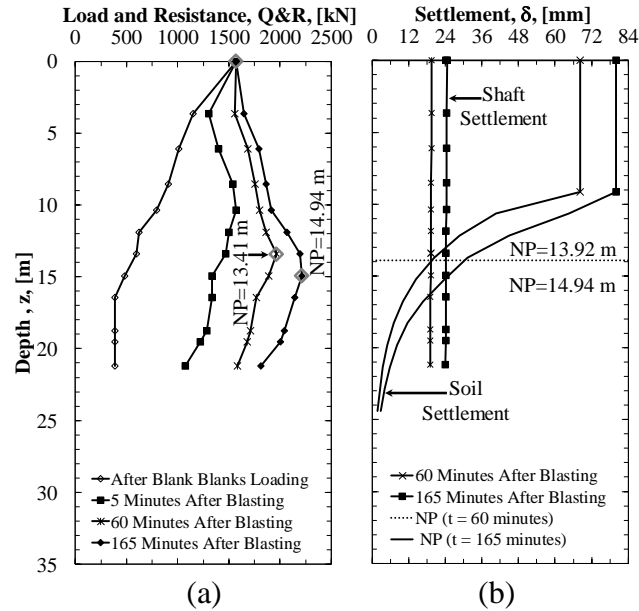


**Figure 7.15.** (a) Pre- and post-blast load and resistance curves and (b) drilled shaft and soil settlement distribution curves, as obtained for the South drilled shaft foundation following blasting.

As shown in Figures 7.14b and 7.15b, the amount of settlement observed within the clay layer was constant as a function of depth, and began to increase gradually with time in the liquefied layer. The soil settlement began significantly to decrease with depth within the silty sand and sand layers. As anticipated, the amount of settlement of each of the drilled shaft foundations was equal to the amount of the settlement of the surrounding soil at the neutral plane location. As previously discussed, the excess porewater dissipated from the bottom of the liquefied layer to the top. Therefore, the soil should also have more settlement at the top of the liquefied layer than the bottom of the liquefied layer, as was observed. As shown in Figure 7.14a and 7.15a, toe resistances from each drilled shaft were increased as the effective stresses increased after each blast event. As a result, this increase of the negative shaft and toe resistances also may have contributed to the settlements (downdrag) of the drilled shafts by increasing the toe penetration.

Based on the results obtained from full-scale blast-induced liquefaction studies, the amount of shaft resistance that was lost within the liquefied layer was determined by examining the load shed curves developed prior to and after liquefaction. Several researches have claimed to a complete loss of shaft resistances within the liquefied zone (Boulanger and Branderberg 2004, Fellenius and Siegel 2008), while others have claimed that the shaft resistance within liquefied zone is reduced by approximately 50-percent (Rollins and Stand 2006, Rollins and Hollenbaugh 2015). At the TATS, the shaft resistances did not decrease to zero after blasting. Instead, the post-blast shaft resistances measured after blasting were approximately 30-percent of the pre-blast positive shaft resistances. In addition, the shaft resistance within the liquefied layer reduced from being 100-percent resisting shaft resistance to approximately 70-percent contributing shaft resistances due to liquefaction.

### 7.9. Estimating Post-Blast Load and Resistance Distribution Curves

The recommended procedures of determining the load and resistance distribution curves were previously shown in Figure 7.7. However, for liquefaction-induced dragload and downdrag, the equations shown in Figure 7.7 were modified to estimate the post-induced load and resistance curves at the TATS. Specifically, the load and resistance distribution curves that were obtained by following the procedures illustrated in Figure 7.7, were fitted to the measured post-load and resistance distribution curves by multiplying the unfactored incremental shaft resistance by 30-percent. Equations 7.7 and 7.8 were developed and used to predict the post-liquefaction load and resistance distribution curves, respectively. As can be seen in Equation 7.7, the drilled shaft self-weight was taken into consideration for load curve.

$$Q_i = Q_{str} + \Sigma(0.3(f_{s,i} \cdot A_i)) + W_i \quad \text{Equation 7.7}$$

Where,  $Q_i$  = the unfactored load in the drilled shaft foundation as a function of depth, for the  $i^{\text{th}}$  element with the first  $i$  element being at the ground surface;  $Q_{\text{str}}$  = the unfactored structural load applied on the drilled shaft head;  $f_{s,i}$  = the unfactored shaft resistance of the  $i^{\text{th}}$  element;  $A_i$  = the surface area for the  $i^{\text{th}}$  element; and  $W_i$  = the weight of the  $i^{\text{th}}$  element of the drilled shaft foundation.

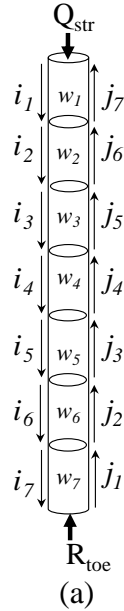
$$R_j = R_{\text{toe}} + \Sigma(0.3(f_{s,j} \cdot A_j)) \quad \text{Equation 7.8}$$

Where,  $R_j$  = the unfactored resistance in the drilled shaft foundation, as a function of depth, for the  $j^{\text{th}}$  element with the first  $j$  element being at the toe of the drilled shaft foundation,  $R_{\text{toe}}$  = the unfactored end bearing resistance at the toe of the drilled shaft foundation,  $f_{s,j}$  = the unfactored skin friction of the  $j^{\text{th}}$  element; and  $A_j$  = the surface area for the  $j^{\text{th}}$  element. The variables in Equations 7.7 and 7.8, are schematically shown in Figure 7.16a.

The predicted load and resistance curves that were obtained using the Equations 7.7 and 7.8 for the North drilled shaft and South drilled shaft, are shown in Figures 7.16b and 7.16c, respectively. The predicted locations of the neutral plane are also shown in Figures 7.16b and 7.16c. The difference between the measured and predicted neutral plane locations can be attributed to various factors such as variation in soil conditions, time effect, accuracy in correlating the CPT measurements to the soil parameters (e.g., unit weight, undrained shear strength, friction angle), and the load within the drilled shaft foundation only being measured at the location of the strain gauges. Although several methods (Seed et al. 1975, Tokimatsu and Seed 1987, Ishihara et al 1990, Robertson and Wride 1998, Zhang et al. 2002) exist to predict the soil settlement following liquefaction, the best method for identifying the location of the neutral plane is through the use of developed loads in the drilled shaft foundation.



**Load Curve ( $Q_i$ ):**  
 $i$  sum starts at the top and progress to the toe location



**Resistance Curve ( $R_j$ ):**  
 $j$  sum starts at the toe location and progress to the top of the drilled shaft.

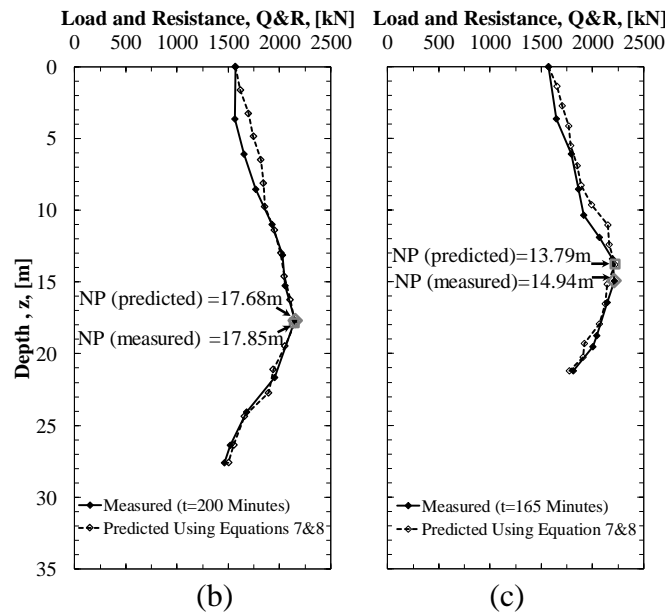


**Figure 7.16.** (a) Analysis of an axially loaded drilled shaft foundation subjected to liquefaction. For load curve,  $i$  sum starts from the top of the drilled shaft and progress to the toe location. For the resistance curve,  $j$  sum starts from the toe location and progress to the top of the drilled shaft foundation. Predicted and measured load and resistance distribution curves as obtained for: (b) the North drilled shaft and (c) the South drilled shaft foundation.

As recommended in Brown et al. (2010), an evaluation of limit states of a drilled shaft foundation under dragload requires 1) establishing the location of the neutral plane location, and 2) an analysis of the drilled shaft load-settlement curve. At the TATS, the pre- and post-load and resistance curves and the load settlement curves obtained from the BLC testing were used to

analyze the effect of liquefaction on a drilled shaft foundation, as shown in Figure 7.17. The drilled shaft load-settlement curves obtained during the application of blank beams on the top of each drilled shaft is shown in Figure 7.17. As previously discussed, the amount of the applied load was not enough to fully mobilize the shaft and resistances of each drilled shaft. The resistance curves derived from the load transfer obtained during BLC testing are also shown in Figure 7.17.

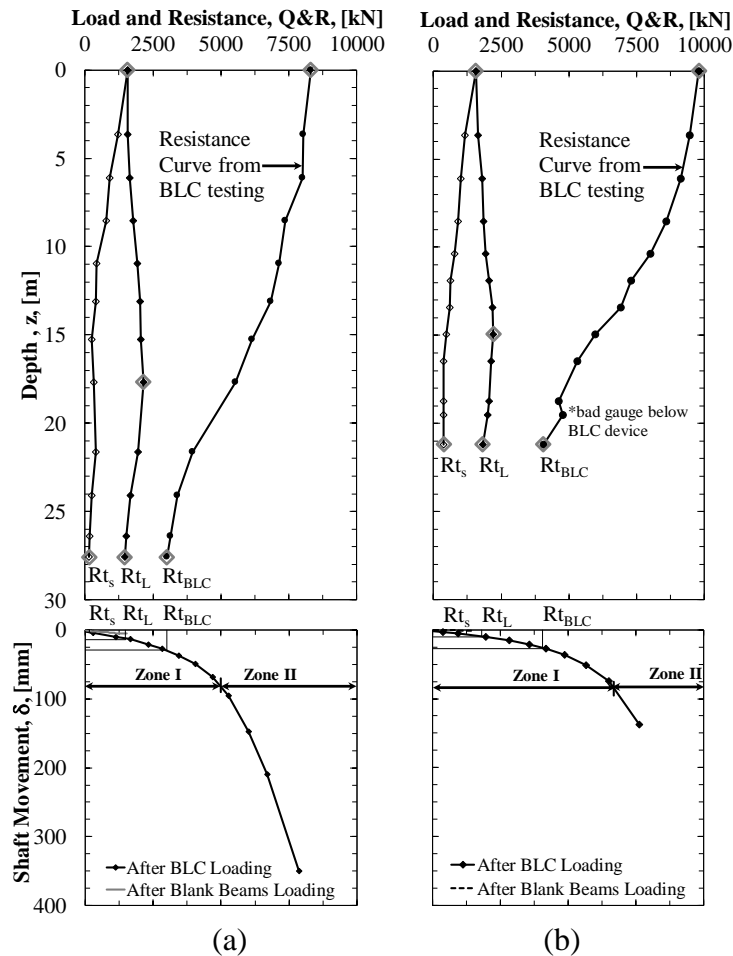


**Figure 7.17.** (a) Measured load and resistance distribution and drilled shaft load-settlement curves as obtained for the a) North and b) South drilled shaft foundations.

For the dragload to occur at the TATS, the settlement of the soil surrounding a drilled shaft had to exceed the drilled shaft settlement. Otherwise, the dragload would be eliminated as the drilled shaft start to plunge. Based on the drilled shaft load-settlement curves (Figure 7.17),

the potential for dragload load to develop is greater in Zone I, and no dragload would happen in Zone II due to the drilled shaft plunging (excessive downward movement of a foundation with small change in the load). Dragloads were developed around the drilled shafts at the TATS because 1) the soil liquefied and settled more than the drilled shaft foundations, and 2) the toe resistances mobilized during the application of static load ( $R_{ts}$ ), during liquefaction ( $R_{tL}$ ), and the total toe resistance measured from BLC tests ( $R_{tBLC}$ ) were in Zone I, as illustrated in Figure 7.17.

If excessive large drilled shaft settlements (downdrag) caused by the loss of shaft resistance and/or the developed dragloads had occurred, the drilled shafts would have begun plunging (moving from Zone I to Zone II) until sufficient toe resistance was developed to support the induced dragload and the applied load. In this case, the unfactored liquefaction-induced dragload should be included in the evaluation of serviceability limit state, and designers have to ensure that the induced downdrag are within the acceptable limits. Under most conditions, most of the drilled shaft foundations are typically designed using factored loads ( $\gamma$ ) or factor of safety (F.S), and bear on competent material. Therefore, the design capacity ( $R_t/F.S$  or  $\gamma R_t$ ) exists at some value in Zone I on the load-settlement curve. A drilled shaft foundation that is constructed under these two conditions, as most drilled shafts are designed, has a potential for structural collapse due to the loss of shaft resistance and the developed dragload. It is recommended for a foundation designer to combine the unfactored structural axial load with the liquefaction-induced dragload for evaluating the structural strength limit state for a drilled shaft foundation.

## 7.10. Conclusions

Blast-induced liquefaction tests were performed around two-instrumented drilled shaft foundations. The soil surrounding the drilled shaft foundations was liquefied, as was evident

from the following observations that occurred after blasting: 1) downward movement of the ground surface, 2) downward movement of the soil as a function of depth, 3) development of excess pore water pressure, and 4) increased load on the individual foundations as a function of depth until the depth of the neutral plane. Based on the results obtained from the testing program described herein, following conclusions were inferred:

1. Blast-induced liquefaction tests were successful to induced dragload and downdrag on the drilled shaft foundations constructed at the TATS.
2. During the application of static load to the top of each drilled shaft foundation, no negative shaft resistances were developed. The maximum load ( $R_{max}$ ) and the corresponding neutral plane were located at the top of the drilled shaft before liquefaction.
3. A small relative movement (less than 6 mm) mobilized the shaft resistance along drilled shaft foundation.
4. The post-blast shaft resistances measured immediately after blasting were approximately 30-percent of the pre-blast positive shaft resistances.
5. The shaft resistance with liquefied layer reduced from being 100-percent resisting shaft resistance to approximately 70-percent contributing shaft resistances.
6. The neutral plane that was initially at the top of the foundation moved the bottom of the liquefied layer due to liquefaction. The neutral plane moved due to 1) the reduction of the shaft resistance and 2) the developed negative shaft resistance (dragload).
7. The neutral plane locations can be determined from post-liquefaction load distribution and/ or from the drilled shaft and settlement distribution curves. However, due to the difficulties associated with measuring the soil settlement as a function of depth and time, the load and resistance distribution method is more reliable.
8. For a drilled shaft foundation installed in earthquake prone areas, liquefaction-induced dragload should be considered and combined with other loads acting on the drilled shaft head for evaluation of structural strength limit states and serviceability limit state.

## 7.11. Acknowledgements

The authors thank the Arkansas State Highway and Transportation Department, the Missouri Department of Transportation, McKinney Drilling Company, Chris-Hill Construction, Texas Concrete Partners, PDCA, Duane Houkom, Inc., Loadtest, Inc., GEI Consulting Engineers and Scientists, DFI, ADSC, PDCA, Kolb Grading, GRL Engineers, Inc., ICE, AFT Specialty Geotechnical Services, Skyline Steel, W&W AFCO Steel, and Nucor-Yamato Steel, for financial and/or in kind contributions to the scope work described herein.

## 7.12. References

- AASHTO (2007). LRFD Bridge Design Specifications. American Association of State Highway and Transportation Officials, 4<sup>th</sup> Ed., Washington, D.C., USA.
- AASHTO (2012). LRFD Bridge Design Specifications: American Association of State Highway and Transportation Officials Parts 1 and 2. American Association of State Highway and Transportation Officials. Sixth Edition, Washington, D.C.
- AASHTO (2014), “LRFD Bridge Design Specifications”, American Association of State Highway and Transportation Officials, Seventh Edition, Washington, D.C.
- American Petroleum Institute (API). (1993). Recommended Practice for Planning, Designing and Constructing Fixed Offshore Platforms – Load and Resistance Factor Design. API Recommended Practice 2A-LRFD (RP 2A-LRFD), First Edition, Reaffirmed 2003, 242p.
- Australian Piling Standard (1995). “Piling design and installation.” Standard AS2159-1995, Australian Council of Standards, committee CE/18, Adelaide, Australia.
- Briaud, J. L., and Tucker, L. (1997). “Design and Construction Guidelines for Downdrag on Uncoated and Bitumen-Coated Piles.” NCHRP Report 393, Transportation Research Board, National Academy Press, Washington, D.C., pp. 198.
- Brown, D. A., Turner, J.P. and Castelli R.J. (2010). “Drilled Shafts: Construction Procedures and LRFD Design Methods.” FHWA-NHI-10-016, Geotechnical Engineering Circular (GEC) No. 10. U.S. Dept. of Transportation, Federal Highway Administration, 970 p.
- Bey, S. (2014) “Cost-benefit Analysis for Load Resistance Factor Design (LRFD) of Drilled Shafts in Arkansas.” M.S. Thesis, University of Arkansas, Fayetteville, Arkansas, pp.410.
- Boulanger, R.W and Brandenberg, S.J. (2004). “Neutral plane solution for liquefaction-induced downdrag on vertical piles.” Proceedings, ASCE Geo-Trans conference, ASCE, Reston, VA, 470-479.

- Bozozuk, M. (1981). "Bearing capacity of a pile preloaded by downdrag." Proceedings of the 10<sup>th</sup> international conference on soil mechanics and foundations engineering, Mexico Cit, Vol. 2: 631-636.
- Bjerrum, L., Johannessen, I, J. and Eide, O. (1969). "Reduction of negative skin friction on steel piles to rock." Proc. 7th ICSMFE, Mexico City, Vol. 2, pp. 27-34.
- Bozozuk, M., (1972). "Down drag measurement on 160-ft floating pipe test pile in marine clay." Canadian Geotechnical Journal, Vol. 9, No. 2, pp. 127-136.
- Broms, B. B. and Silberman, J. O. (1964). "Skin friction resistance for piles in cohesionless soil." Sols-Soils, No. 10, pp. 33-41.
- Canadian Geotechnical Society (1992). Canadian Foundation Engineering Manual, CFEM, third edition, BiTech Publishers, Vancouver. 512 p.
- Dumas, C. (2000). "Soil downdrag on deep foundations." An overview perspective proceeding of the 18<sup>th</sup> ASCE/PennDOT Geotechnical Seminar, Hershey, PA, 19p.
- Davisson, M. T. (1993). "Negative skin friction in piles and design decisions." International Conference on Case Histories in Geotechnical Engineering. 7.
- Fellenius, B.H. and Broms, B. B. (1969). "Negative skin friction for long piles driven in clay." Proc. 7th ICSMFE, Mexico City, Vol. 2, pp. 93-98.
- Fellenius, B.H. (1972). "Reduction of negative skin friction with bitumen slip layers." Discussion. Journal of the Geotechnical Engineering Division, ASCE, 101(GT4): 412-414.
- Fellenius, B.H. (1979). "Downdrag on bitumen coated piles." Journal of Geotechnical Engineering, ASCE, 105 (GT10): 1262-1265.
- Fellenius, B.H. (1988). "Unified Design of Piles and Pile Groups." TRB Washington, Record 1169, pp. 75 82.
- Fellenius, B.H. (1991). Foundation Engineering Handbook, Chapter 13 - Pile Foundations. Second Edition. Van Nostrand Reinhold Publisher, New York, NY, pp. 511-536.
- Fellenius, B. H. (2004). "Unified Design of Piled Foundations with Emphasis on Settlement Analysis." Proceedings of ASCE Conference Deep Foundations 2004, pp. 253-275.
- Fellenius, B.H. (2006). "Results from long-term measurement in piles of drag load and downdrag" Canadian Geotech. J., April 2006 43(4), 409-430.
- Fellenius, B. H. and Siegel, T.C. (2008). "Pile drag load and downdrag in a liquefaction event." J. Geotech. and Geoenviron. Engrg. ASCE, Reston, Virginia, 134 (9), 1412-1416.

- Hannigan, P.J., Goble, G.G., Thendean, G., Linkins, G.E. and Rausche, F. (2005). "Design and Construction, Vol. I and II. Federal Highway Report No. FHWA-HI-05, Federal Highway Administration, Washington, D.C.
- Hannigan, P.J., Robinson, B. R., Goble, G.G., Linkins, G.E. & Rausche, F., Becker, M. L. (2016). "Design and construction of driven pile foundations." FHWA-NHI-16-009, National Highway Institute, Federal Highway Administration, U.S. Department of Transportation, Washington, D.C.
- Hong Kong Geotechnical Office. (2006). "Foundation design and construction." Geo Publication No.1/2006, the Government of Hong Kong, Hong Kong.
- Idriss, I.M. and Boulanger, R.W. (2008). Soil Liquefaction during Earthquakes. Earthquake Engineering Research Institute MNO-12, 235p.
- Ishihara, K. (1990). "Liquefaction and flow failure during earthquakes." Géotechnique, ICE, London, England, 43(3), 351-451.
- Johnston, A.C., and Schweig, E.S. (1996). "The enigma of the New Madrid earthquakes of 1811–1812." Annual Review of Earth and Planetary Sciences, Vol. 24, pp. 339-384.
- Kulhawy, F. H., and Mayne, P. W. (1990). "Manual on estimating soil properties for foundation design." Electric Power Research Institute, EL-6800 Research Project 1493-6 Final Rep., 2-24 and 2-33.
- Kulhawy, F.H. and Chen, J. R. (2007). "Discussion of 'Drilled Shaft Side Resistance in Gravelly Soils' by Kyle M. Rollins, Robert J. Clayton, Rodney C. Mikesell, and Bradford C. Blaise," Journal of Geotechnical and Geoenvironmental Engineering, ASCE, Vol. 133, No. 10, pp. 1325-1328.
- Long, R. L, Healy, K. A. (1974). "Negative Skin Friction on Piles." Final Report, JHR74-77. Project 73-1.
- Meyerhof, G. G. (1956). Penetration Tests and Bearing Capacity of Piles, American Society of Civil Engineers (ASCE), Journal of the Soil Mechanics and Foundation Division, Vol. 82, No. 1, Paper 886, pp. 1-29.
- MODOT (Missouri Department of Transportation) (2005). "LRFD Bridge Design Specifications. 18p.
- Muhunthan, B., vijayathanan, N. V., and Abbasi, B., (2017). "Liquefaction-induced downdrag on drilled shafts." Washington State Department of Transportation. Final Research Report.
- ODOT (Oregon Department of Transportation) (2015), "Standard Specifications for Highway Construction", 2015 Edition and related Standard Special Provisions.

- O'Neill, M.W., and Reese, L.C. (1999). "Drilled Shafts: Construction Procedures and Design Methods," Publication No. FHWA-IF-99-025, Federal Highway Administration, Washington, D.C., 758 p.
- Poulos, H. G. (1997). "Piles subjected to negative friction." A procedure for design, Geotechnical Engineering, 23-44.
- Race, M. L., Coffman, R. A., (2013), "Effect of Uncertainty in Site Characterization on the Prediction of Liquefaction Potential for Bridge Embankments in the Mississippi Embayment." ASCE Geotechnical Special Publication No. 231, Proc. GeoCongress 2013: Stability and Performance of Slopes and Embankments III, San Diego, California, March, pp. 888-897.
- Race, M.L., Coffman, R.A., (2015). "Response of Drilled Shaft Foundation Constructed in Redrilled Shaft Excavation Following Collapse." Deep Foundations Institute Journal. Vol. 9, No. 2, pp. 60- 73.
- Race, M.L., Bey, S.M., Coffman, R.A., (2015). "Statistical Analysis to Determine Appropriate Design Methodologies for Drilled Shafts Foundations." Geotechnical and Geological Engineering. Vol. 33, Issue 3, pp 713-726.
- Race, M.L. (2015) "Amount of Uncertainty in the Methods Utilized to Design Shaft Foundations." PhD. Thesis, University of Arkansas, Fayetteville, Arkansas, pp.325
- Robertson, P.K. and Cabal, K.L. (2012). "Guide to Cone Penetration Testing for Geotechnical Engineering", Prepared for Gregg Drilling & Testing Inc., 5th Edition, 2012, 130 p.
- Robertson, P.K. and Wride, C.E., (1998), "Evaluating cyclic liquefaction potential using the cone penetration test," Canadian Geotechnical Journal, Vol.35, pp.442-459.
- Rollins, K. M. and S. R. Strand (2006). Downdrag Forces Due to Liquefaction Surrounding a Pile. Proceedings of the 8<sup>th</sup> U.S. National Conference on Earthquake Engineering. Paper No. 1646, San Francisco, CA, April 18-22.
- Rollins, K.M. (2004). "Liquefaction Mitigation Using Vertical Composite Drains: Full Scale Testing." Final Report for Highway IDEA Project 94. Transportation Research Board, February 2004, 105 p.
- Rollins, K.M., Lane, J.D., Nicholson, P.G., and Rollins, R.E. (2004). "Liquefaction Hazard Assessment using Controlled-Blasting Techniques." Proc. 11th International Conference on Soil Dynamics & Earthquake Engineering. Vol. 2, pp. 630-637.
- Rollins, K.M., Lane, J.D., Dibb, E., Ashford, S.A., and Mullins, A.G. (2005a). "Pore Pressure Measurement in Blast-Induced Liquefaction Experiments." Transportation Research Record 1936, Soil Mechanics 2005, TRB, Washington D.C., pp. 210-220.



- Rollins, K.M. and Anderson, J.K.S. (2008). "Cone Penetration Resistance Variation with Time after Blast Liquefaction Testing." *Procs. Geotechnical Earthquake Engineering and Soil Dynamics-IV*, Geotechnical Special Publication 181, ASCE, 10 p.
- Rollins, K.M. and Hollenbaugh (2015). "Liquefaction Induced Negative Skin Friction from Blast-induced Liquefaction Tests with Auger-cast Piles." 6<sup>th</sup> International Conference on Earthquake Geotechnical Engineering, Christchurch, New Zealand.
- Seed, H.B., Martin, P.P., and Lysmer, J. (1975). "The Generation and Dissipation of Pore Water Pressures during Soil Liquefaction." Report Number UCB/EERC-75/26, University of California at Berkeley, Berkeley, CA.
- Siegel, T.C., Lamb, R., Dasenbrock, D., and Axtell, P.J. (2013). "Alternative Design Approach for Drag Load and Downdrag with the LRFD Framework." *Proceedings of the 38th Annual Conference on Deep Foundations 2013*, Phoenix, AZ, pp. 23-39.
- Skempton, A.W., (1951), "The Bearing Capacity of Clays", *Proc. Building Research Congress*, pp. 180-189
- Strand, S. R. (2008). *Liquefaction Mitigation Using Vertical Composite Drains and Liquefaction induced Downdrag on Piles: Implications for Deep Foundation Design*. Ph.D. thesis, Department of Civil and Environmental Engineering, Brigham Young University, Provo, UT.
- Tan, S. A., and Fellenius, B. H. (2016). "Negative skin friction pile concepts with soil-structure interaction." *Geotechnical Research*, 3(4), 137-147.
- Tomlinson, M.J. (1994). "Pile Design and Construction Practices", Fourth Edition, Taylor & Francis.
- Tokimatsu, K., and Seed, H.B. (1987). "Evaluation of settlements in sands due to earthquake shaking," *Journal of Geotechnical and Environmental Engineering*, 103(8), 861-878.
- Vijayaruban, N. V., Muhunthan, B., and Fellenius, B.H. (2015). "Liquefaction-induced Downdrag on Piles and Drilled Shafts." 6<sup>th</sup> International Conference on Earthquake Geotechnical Engineering. Christchurch, New Zealand.
- WSDOT (Washington State Department of Transportation) (2006). "Geotechnical Design Manual M 46-03.
- Zhang, G., Robertson, P. K., and Brachman R. W.I. (2002). "Estimating liquefaction-induced ground settlements from CPT for level ground." *Canadian. Geotech. J.*, NRC Canada, 39(5), 1168–1180.

## CHAPTER 8: Liquefaction-induced Dragload and Downdrag on Driven Pile Foundations

### 8.1. Chapter Overview

Blast-induced liquefaction tests were also performed on three driven piles foundations installed at the TATS). An increase of side and toe resistances, significant ground and driven piles and drilled shafts top settlements were observed following blasting. Following blasting, the excess porewater pressure, the ground settlement as a function of time, and soil settlements as a function of time and depth were monitored. The results of the ground settlements, caused by porewater pressure dissipation; the pile-settlements measurements are presented and discussed herein. The increase and settlements were attributed to the increase of effective stress as the excess porewater pressure dissipated. The load and resistance distribution curves and pile-settlement distribution curves for each pile during the application of load to the top of each foundation and following liquefaction are discussed. In addition, the liquefaction-induced dragloads that developed around each pile and the corresponding neutral plane locations are presented in this chapter. Finally, a new analytical method of evaluating liquefaction-induced dragload and downdrag is discussed.

The paper enclosed in this chapter will be submitted within Journal of Geotechnical and Geoenvironmental Engineering. The full reference is: Rollins, K.M., Luke, I. K., Ishimwe, E., Coffman, R.A., (2018). “Analysis of Liquefaction-induced Dragload and Downdrag on Driven Pile Foundations.” Journal of Geotechnical and Geoenvironmental Engineering (Under review).

## Analysis of Liquefaction-induced Dragload and Downdrag on Driven Pile Foundations

Kyle M. Rollins<sup>1</sup>, Luke I. Kevan<sup>2</sup>, Elvis Ishimwe<sup>3</sup> and Richard A. Coffman<sup>4</sup>,

<sup>1</sup> Professor, Brigham Young University, Provo, Utah, USA; email: rollinsk@byu.edu

<sup>2</sup> Graduate Student, Brigham Young University, Provo, Utah, USA; email: lkevan40@gmail.com

<sup>3</sup> Graduate Student, University of Arkansas, Fayetteville, Arkansas, USA; email: eishimwe@email.uark.edu

<sup>4</sup> Associate Professor, University of Arkansas, Fayetteville, Arkansas, USA; email: rick@uark.edu

### 8.2. Abstract

The results presented in this paper were obtained from a full-scale field testing program that was performed to evaluate the axial behavior of three types of instrumented piles installed into liquefying soil. Controlled blasting tests were used to induce liquefaction in the soil surrounding each test pile. As was evident from the excess porewater pressure responses and ground settlement measurements, liquefaction has occurred. Post-liquefaction ground settlements ranged from 64 to 90 mm, and the pile settlements ranged from 6.5 to 11 mm. The post-blast soil settlement led to the development of negative skin friction on the piles. In addition, the skin friction within liquefied layer reduced from being 100-percent resisting skin friction to approximately 50-percent contributing shaft resistances. A new analytical method of determining liquefaction-induced dragload and downdrag is presented and discussed.

**Keywords:** Liquefaction, Driven Piles, Blasting, Dragloads, Downdrag, Full-scale Testing, Seismic Design.

### 8.3. Introduction

The current level of understanding regarding the development of dragload and downdrag presented in the literature, is predominately based on the soil settlement as related to consolidation phenomena. Several researchers have investigated the consolidation-induced dragload and downdrag on different types of driven piles and drilled shafts (e.g., Bjerrum et al.

1969, Endo et al. 1969, Bozozuk 1970, 1972, 1981, Fellenius 1972, Long and Healy 1974, Fellenius 1988, Little 1994, Briaud and Tucker 1997, Poulos 1997, Dumas 2005, Hannigan et al. 2005, Fellenius and Siegel 2008, Siegel et al. 2013, Hannigan et al. 2016). The phenomena of liquefaction-induced dragload and downdrag has only been addressed in a few more recent published studies (Boulanger and Brandenburg 2004, Rollins and Strand 2006, Strand 2008, Fellenius and Siegel 2008, Rollins and Hollenbaugh 2015, and Muhunthan et al. 2017). Three types of driven piles were installed to 1) investigate the reduction of skin friction within a liquefied layer, and 2) evaluate the development of liquefaction-induced dragload and downdrag around driven pile. Controlled blast tests were performed to induce liquefaction on the soil surrounding each test pile. The pre-and post-blast load and resistance distribution curves along with pile-soil settlement distribution curves of each test pile are presented and discussed. Based on the test results, a design methodology for estimating the amount of liquefaction-induced dragload is discussed.

#### **8.4. Background**

Liquefaction in loose, saturated, sands has caused extensive damage to infrastructure (e.g., bridges abutments and embankments, roads, buildings, power and water supplies) in nearly every historical earthquake event (Yamada 1966, Seed et al. 1968, Wang et al. 1979, Dobry 1989, and Gallagher et al. 2007). Liquefaction-induced lateral spreading has been considered as the root cause of many pile failures during earthquakes. However, liquefaction-induced dragload and downdrag has also been reported as another possible failure mechanism for piled foundation failure in liquefiable soils (Dash et al. 2008). In the absence of test results, different analytical and empirical methods have been proposed to guide foundation engineers in the design of piles

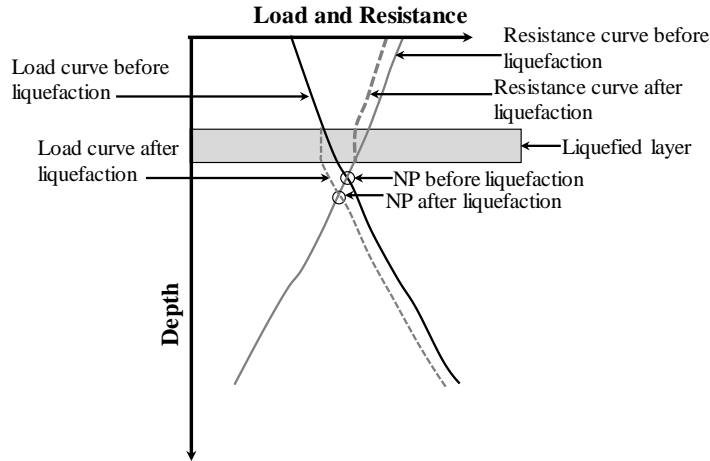
that are subjected to liquefaction-induced dragload and downdrag (e.g., Boulanger and Brandenburg 2004, Fellenius and Siegel 2008, and Muhunthan et al. 2017).

These analytical methods were developed based on the neutral plane method that was originally developed by Fellenius (1972). For example, Boulanger and Brandenburg (2004) modified the traditional neutral plane method (Fellenius 1984) for liquefaction-induced dragload on vertical piles by accounting the variation of excess pore pressures and ground settlements over time as a liquefied layer reconsolidates. Unlike the consolidation-induced dragload, the determination of the post-liquefaction settlements requires 1) the excess porewater pressure isochrones over time, and 2) a relationship between the sand compressibility ( $m_v$ ) and the excess porewater pressure ratio ( $R_u$ ). Boulanger and Brandenburg (2004) provided an empirical relationship to determine the unit skin friction ( $f_s$ ), within a liquefied soil layer, as excess porewater pressure dissipates.

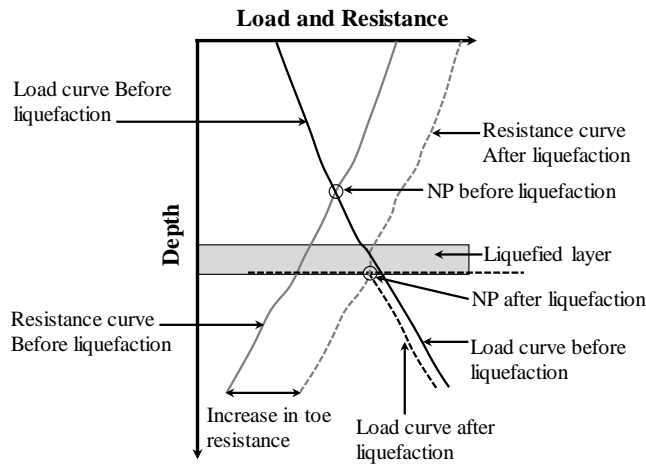
$$f_s = \sigma'_{vo} K_o \tan(\phi)(1 - R_u) \quad \text{Equation 8.1}$$

Where  $\sigma'_{vo}$  is the effective stress,  $\phi$  is the friction angle,  $K_o$  is the coefficient of lateral earth pressure at rest, and  $R_u$  is the excess porewater pressure ratio.

Fellenius and Siegel (2008) applied the unified design method (Fellenius 1984), a method developed for consolidation-induced dragload, to analyze the effect of liquefaction for axially loaded driven pile foundations. Fellenius and Siegel (2008) analyzed the load and distribution curves when the liquefiable layer was located: 1) above the static neutral plane (Figure 1a), and 2) below the static neutral plane (Figure 8.1b). As illustrated in Figure 8.1a, no change occurs in the load and distribution curves when the liquefying layer is located above the static neutral plane. For this case, the loss of negative skin friction within the liquefied zone did not affect the pile performance under axial load



(a)



(b)

**Figure 8.1.** A schematic of load and resistance distribution curves and pile-soil settlement distribution curves when the liquefied layer is located (a) above the neutral plane, and (b) below the neutral plane (modified from Fellenius and Siegel 2008).

When the liquefiable zone was located below the static neutral plane the static neutral plane was re-located to the lower boundary of the liquefiable zone, and an increase in developed dragload was observed (Figure 8.1b). For the latter case (Figure 8.1b), an increase in mobilized toe resistance with the corresponding toe penetration was also observed (Fellenius and Siegel 2008). Fellenius and Siegel (2008) recommended that for designers should consider the liquefaction-induced dragload for the structural design of pile section and settlement evaluation. Boulanger and Brandenburg (2004) and Fellenius and Siegel (2008) agreed that the problem of liquefaction-induced dragload is a settlement (downdrag) issue, not bearing capacity issue. To

validate these analytical methods, Rollins and Hollenbaugh (2015) performed a blast-induced liquefaction tests around three 0.6 m diameter auger-cast piles in Christchurch, New Zealand. Based on the test results, the average negative skin friction resistance values were reported to be approximately 50-percent of the pre-blast positive skin friction, at the end of excess porewater pressure dissipation. This was consistent with the observation obtained by Rollins and Strand (2006).

Most recently, Muhunthan et al. (2017) proposed an analytical method to assess foundation performance for drilled shafts and driven piles installed into liquefiable soils. Muhunthan et al. (2017) applied the method to drilled shafts and driven piles constructed at the Juan Pablo II bridge to evaluate the impact of liquefaction on the foundations after the 2010 Maule earthquake in Chile. Unlike Fellenius and Siegel (2008), who located the neutral plane at a certain depth along the pile under static conditions (before liquefaction), Muhunthan et al. (2017) located the neutral plane at the top of the pile foundation before liquefaction. The analytical method proposed by Muhunthan et al. (2017) allowed to estimate the liquefaction-induced downdrag at the Juan Pablo II bridge; however, full-scale test results are needed to validate this analytical method.

### **8.5. Site Characteristics**

The test site was located in Northeast Arkansas, within the New Madrid Seismic Zone and within the Mississippi Embayment. The generalized soil profile of the TATS is shown in Figure 8.2a. The soil profile consists of high plasticity clay, from the ground surface to a depth of 6.1 m. The clay is underlain by a silty sand layer from 6.1 to 9.8 m. The silty sand layer is underlain by a potentially liquefiable sand deposit. At the time of testing, the groundwater was located approximately 7.0 m below the ground surface. The average measured cone tip resistance

( $q_c$ ) and the average SPT corrected blow count ( $N_{60}$ ) values as a function of depth, are shown in Figures. 8.2b and 8.2c, respectively. The average relative density ( $D_r$ ), as correlated from the CPT soundings data, as obtained using Kulhawy and Mayne (1990) are also shown in Figs. 8.2d. Based on the obtained field investigation data, a liquefiable layer (target zone) was identified from 9.14 to 15.24 m, illustrated in Figure 8.2.

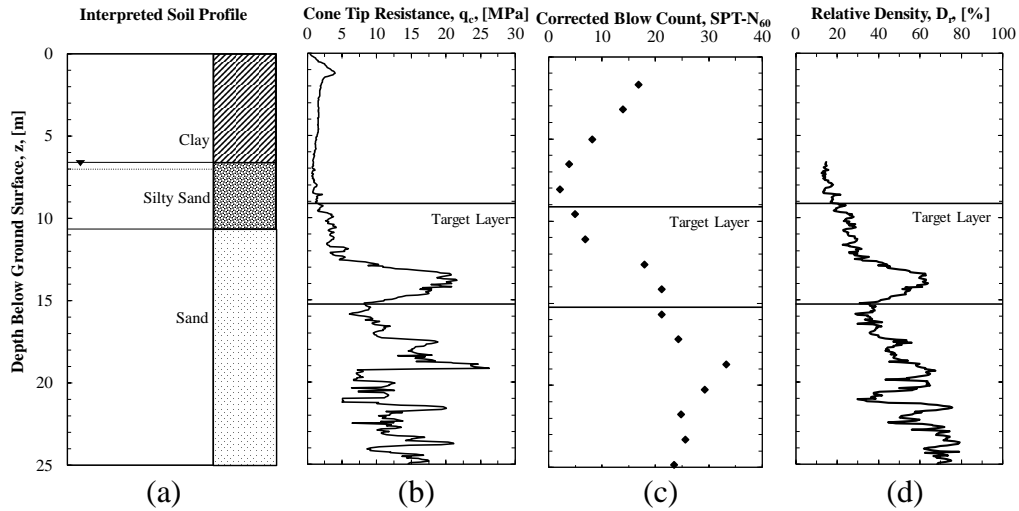


**Figure 8.2.** (a) Interpreted soil profile (b) average cone tip resistance ( $q_c$ ), (c) average SPT blow count ( $N_{60}$ ), and (d) relative density ( $D_r$ ) correlated from CPT soundings.

## 8.6. Testing Program

### 8.6.1. Test Layout and Instrumentation

Three different types of instrumented piles were installed. The test piles consisted of a 457mm by 457mm prestressed concrete pile, a 457-mm diameter closed ended steel pipe pile, and a HP 14x117 section steel H-pile. The steel H-pile, with a total length of 28.0m was installed to a depth of 26.8 m below the ground surface. The steel pipe, with a nominal wall thickness of 14.22mm and a total length of 23.8m was installed to a depth of 22.5 m below the ground surface. The pipe pile was filled with concrete after strain gauges were installed into the annulus of the pipe pile. The prestressed concrete pile, with a total length of 22.6m, was installed to a depth of 21.3m. The pile was prestressed using a total of nine uncoated seven-wire 270 grade



strands. Each strand had a nominal diameter of 13mm. Dynamic load tests were performed during pile installation to 1) monitor each pile during driving, and 2) quantify the axial resistance of each pile at the end of initial drive (EOID) and at the beginning of restrrike (BOR). A pile driving analyzer (PDA) and the Case Pile Wave Analysis Program (CAPWAP) were used to compute the axial resistances of each pile.

A plan view and a cross-sectional view of the testing site are shown in Figure 8.3. The test piles were instrumented with piezoresistive strain gauges at the locations shown in Figure 8.3. These strain gauges were used to measure the axial response of the pile prior to, during, and after controlled blasts. Surveying stakes were installed to monitor the vertical ground surface movement associated with blasting (Figure 8.3). In addition, Sondex tubes were used to measure the amount of soil settlement as a function of depth. As shown in Figure 8.3, Sondex tubes were installed at a distance of 18.58 m away from the center of each tested pile. The digital level indicators were attached on the exposed portion of each pile to measure the pile settlement during pile pre-loading and at various times after blasting.

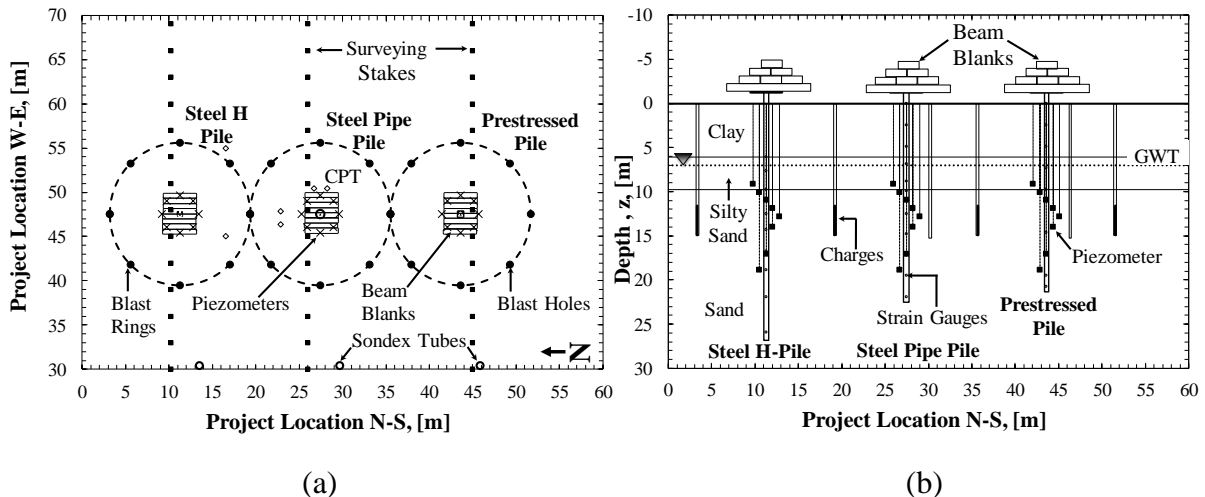


**Figure 8.3.** (a) Plan view, and (b) cross-section of the testing site with locations of driven piles foundations, explosive charges, piezometers, surveying stakes, Sondex tubes, and CPT soundings.

Eight piezometers were also installed around each pile to monitor the generation and dissipation of the excess porewater pressure following blasting. Prior to blasting, an axial load of 523.80 kN was applied at the top of each test pile. This axial load was established using steel beam blanks, as shown in Figure 8.3. The amount of axial load that was transferred from the pile to the surrounding soil was measured using the installed strain gauges. The axial displacements of each pile, as associated with the application of each beam blank, were monitored using a digital level indicator that was mounted at the top of each test pile.

### **8.6.2. Blast-induced Liquefaction Tests**

Three weeks after the completion of pile installation, three separate blast events were performed at the TATS. Eight blast holes were drilled and cased using a 51-mm diameter PVC pipe for each blast event. As shown in Figure 3a, the blast holes were installed in a 16.2-m diameter blast ring around each pile. For the first blast event, performed around the steel H-pile, 3.6kg of explosive charge was placed into each cased blast hole and detonated. For the second blast event, performed around the steel pipe pile, 5.4kg of explosive charge was used per borehole. For the third blast event, performed around the prestressed concrete pile, 6.4 kg of explosive charges were installed into each borehole. The amount of explosive charge was selected based on the results obtained from a pilot liquefaction test that was conducted prior to the series of the blast events. The charges that were utilized consisted of a mixture of ammonium nitrate, sodium nitrate, and aluminum. The explosive charges were centered at a depth of 14.9m for each blast event. The blasts were sequentially detonated with a delay of 500ms between each individual blast hole.

## 8.7. Test Results

### 8.7.1. Pre-Blast Axial Capacities Results

The skin friction resistance ( $R_s$ ), toe resistance ( $R_{toe}$ ), and pile total resistance ( $R_t$ ) estimated using PDA and CAPWAP are summarized in Table 8.1. Specifically, an EOID analysis was performed on the three test piles. Due to the constraint project timeline, restrike was only performed on the pipe pile over a period of 7 days after EOD. Due to the pile setup phenomena, the skin friction resistance of the pipe pile increased by 848.30kN, and the toe resistance decreased by 585.03kN (Table 8.1). This behavior was attributed to the increase of effective stresses caused by the dissipation of excess porewater pressure that was generated during pile installation.

**Table 8.1.** A summary of CAPWAP results.

		<b>Skin Friction Resistance</b>	<b>Toe Resistance</b>	<b>Total Resistance</b>
<b>File Type</b>	<b>Driving Status</b>	<b><math>R_s</math></b>	<b><math>R_{toe}</math></b>	<b><math>R_t</math></b>
		[kN]	[kN]	[kN]
Prestressed Pile	E OID	1014.19	1049.78	2063.97
Steel Pipe Pile	E OID	1047.71	1356.71	2404.42
	BOR (after 7days)	1896.01	771.68	2667.69
Steel H-Pile	E OID	831.82	133.45	965.26

### 8.7.2. Excess Porewater Pressure Ratio Results

The excess porewater pressure ratio ( $R_u$ ) time history and maximum  $R_u$  value for each piezometer installed around the three test piles is shown in Figure 8.4. The obtained  $R_u$  values were determined by dividing the measured excess pore pressure by the initial effective stress at each piezometer depth. The measured  $R_u$  increased above the unity, indicating that soil liquefaction has occurred at the piezometer depth immediately after the series of blasts. Following the first blast event, maximum  $R_u$  of 1.57 and 1.05 were obtained at depths of 9.14 m and 10.06 m respectively. As illustrated in Figure 8.4a, peak  $R_u$  of 0.92 and 0.99 were obtained from the piezometers that were located at depth of 10.97 and 14.02m, respectively.

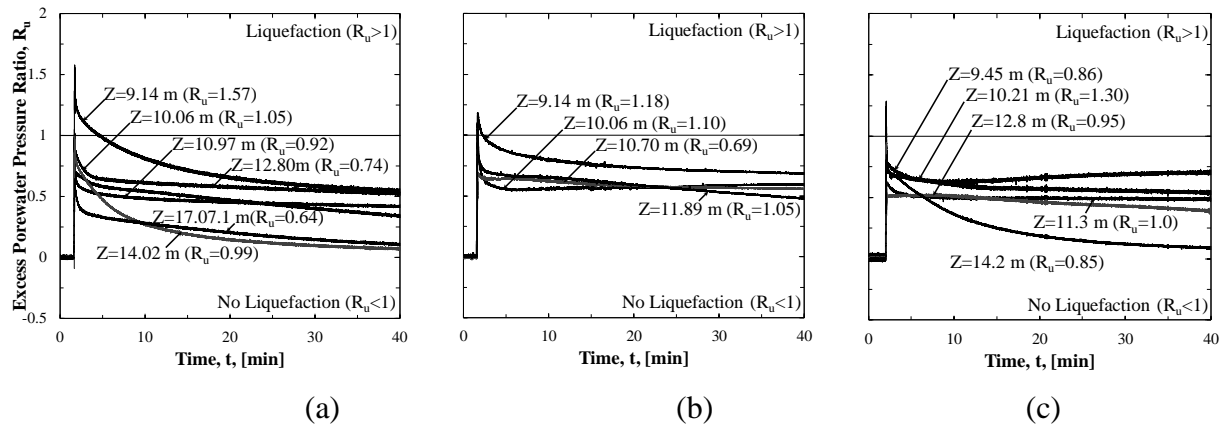


**Figure 8.4.** Measured excess porewater pressure ratio values at different depths, as a function of time, as obtained following the: (a) first (b) second, and c) third blast events surrounding the steel H-pile, pipe pile, prestressed concrete pile, respectively.

Following the second blast event,  $R_u$  values that were greater than unity were observed in three piezometers located at the depths of 9.14, 10.06, and 11.89m (Figure 8.4b). The  $R_u$  values that were measured following the third blast event were all greater than 0.85. The rate of excess porewater pressure dissipation was generally lower for the second blast event than the first and third blast events. These low rates of excess pore water pressure dissipation were attributed to the presence of less permeable soil materials that were observed at this specific location. In addition, the excess porewater pressure dissipated faster for the piezometers located at the bottom of the liquefied zone (Figure 8.4).

### 8.7.3. Post-blast Ground Surface Settlements

The soil surrounding each test pile liquefied, as was evident from the pore water pressure measurements. Following each blast event, the ground surface settled as the blast-induced excess porewater pressure dissipated. The ground surface settlements that were obtained at different times following each blast event are shown in Figure 8.5. In addition to the ground surface settlement, the total pile settlements ranged from 5 to 15 mm, based on the measurements obtained from digital levels indicator that were mounted at the top each pile. Based on these soil

and pile settlements measurements, the soil settled more than each test pile; therefore, negative skin friction (dragloads) were developed.

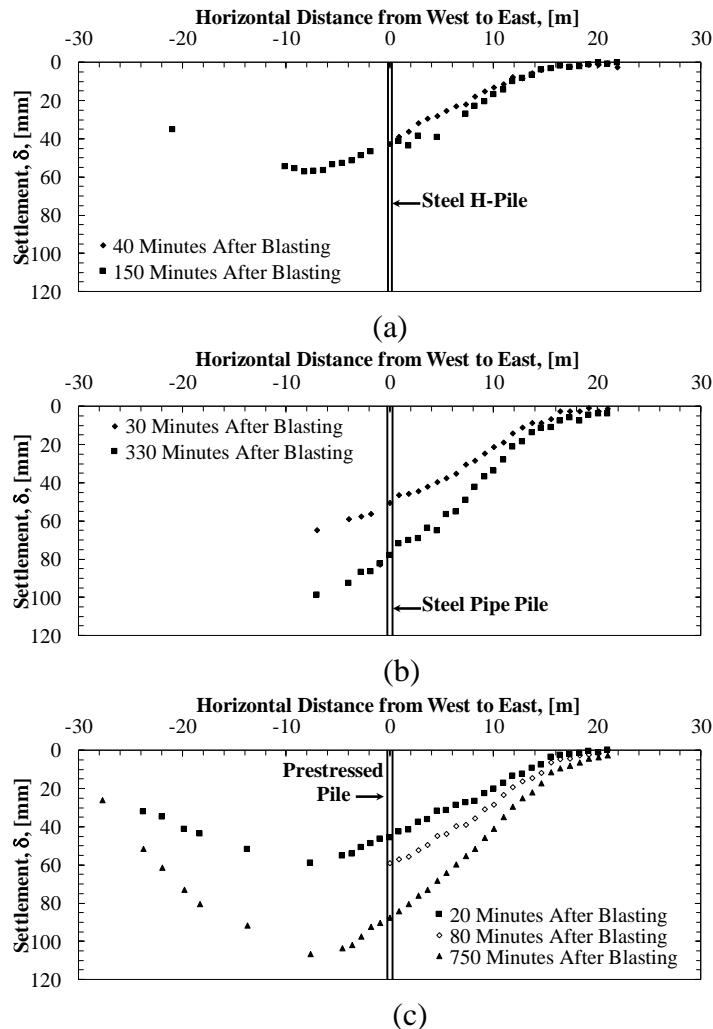


**Figure 8.5.** Post-blast soil settlements following liquefaction, as obtained following the: (a) first, (b) second, and c) third blast events.

#### 8.7.4. Pre-and Post-Blast Loads and Settlements Distribution Curves

The amount of load transfer distributions, as obtained during the application of the static load to the top of each test pile, are shown in Figure 8.6. The axial resistances of each pile were mobilized during the application of the beam blanks. As shown in Figure 8.6, no negative skin friction was developed during the application of the static load, and the neutral plane was observed to be located at the pile head. The soil surrounding each test pile began to settle

immediately after blasting. These post-blast soil settlements produced shear stresses along the interface of the pile and the soil, and an increase of load within the pile was observed. The load and resistance distribution curves that were measured 180 minutes following the blast event that surrounded the steel H-pile are presented in Figure 8.7.

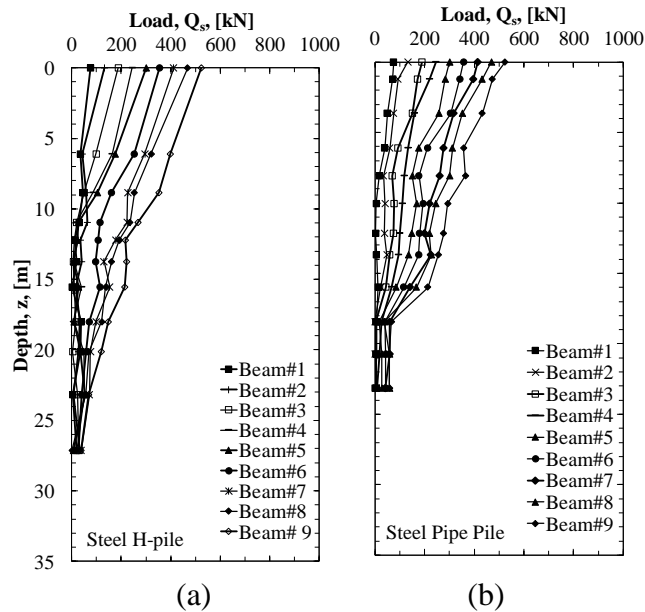


**Figure 8.6.** Load distribution, as a function of depth, as observed for: a) Steel H-pile and b) steel pipe pile during the application of the beam blanks. The imbedded strain gauge data for the square concrete pile was not recovered due to weatherproofing problems within the communication cables for the strain gauges.

The increase in the amount of load between the top of the pile and bottom of the liquefied zone was attributed to an increase in effective stress in response to excess porewater pressure dissipation. As the porewater pressure continued to dissipate, the skin friction along each test pile transitioned from being positive skin friction (upward direction) to negative skin friction (downward) for the top portion of the pile length (to a depth of 17.98m for the H-pile). Therefore, the neutral plane moved from the pile head to a location below the liquefied zone, at the depth of 17.98 m, which corresponded to a dragload of 304.67kN. The downward movement of the neutral plane was attributed to 1) the reduction of the skin friction immediately after blasting, and 2) the rapid development of negative skin friction within the liquefied layer.

The pile and soil settlement distribution curves, as a function of depth, for steel H-pile, are shown in Figure 8.7b. As shown in Figure 8.7b, the settlement within the upper layer was constant from the ground surface to a depth of 9.14 m. The soil settled more than the pile with corresponding values of 63.50 mm and 6.5 mm, respectively. The neutral plane location assessed from the pile-soil settlement distribution curves was located at the depth of 18.20 m. The difference between these two neutral plane locations was attributed to 1) the distance between the Sondex tube and the test pile, and 2) difficulty in determining soil settlement using Sondex tubes.

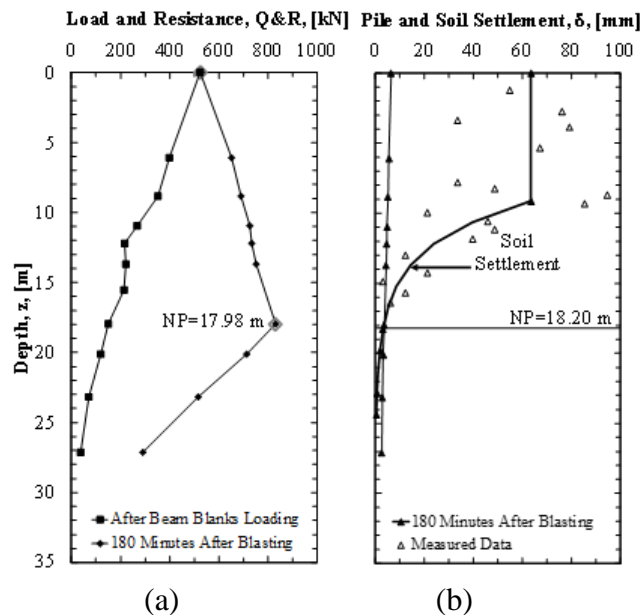


**Figure 8.7.** (a) Pre- and post-blast load and resistance distribution curves and (b) pile and soil settlement distribution curves, as obtained around the H-pile.

For the pipe pile, the load and resistance distribution curve, 86 minutes after blasting are shown in Figure 8.8a. Prior to blasting, the neutral plane was located at the top of the pile; moved to a depth of 18.44m with a corresponding dragload of 413.39kN. From the pile-soil settlement distribution curves, the neutral plane was determined to be located a depth of 18.90m, as determined from the pile-soil settlement distribution curves (Figure 8.8b). For the prestressed concrete pile, the neutral plane was observed to be located at depths of 18.30m and 19.80m, as

obtained from load and resistance curves and pile-settlement curves, respectively, with a corresponding dragload of 304.29 kN for a period of 100 minutes after blasting (Figure 8.9).

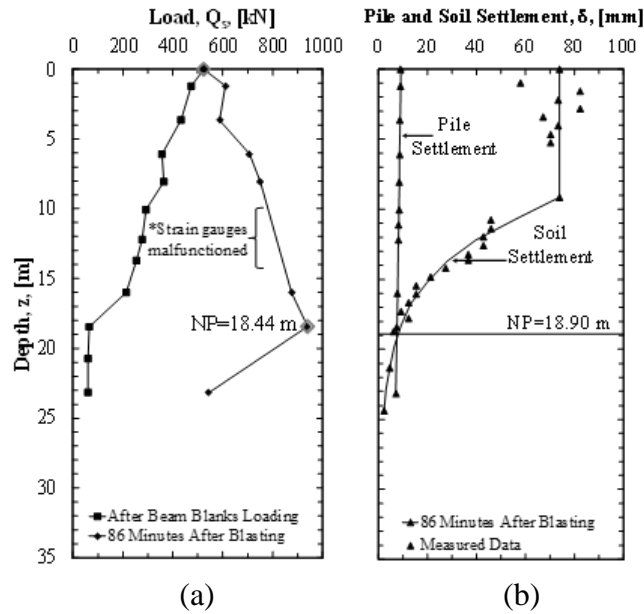


**Figure 8.8.** (a) Pre- and post-blast load and resistance distribution curves and (b) pile and soil settlement distribution curves, as obtained around the steel pipe pile.

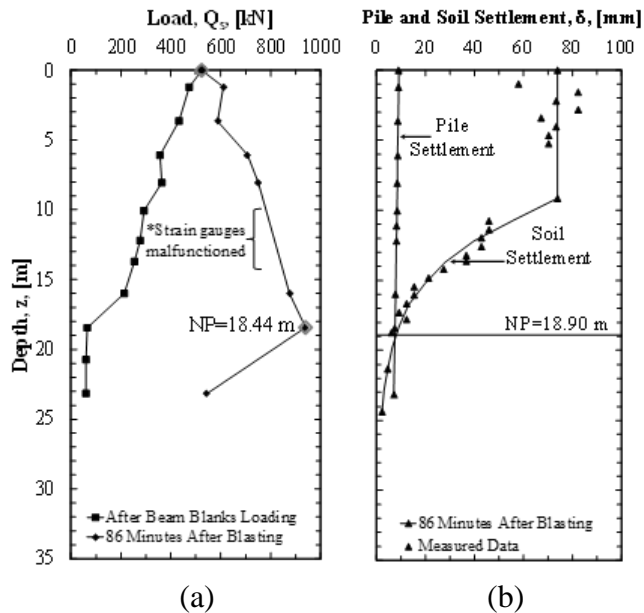


**Figure 8.9.** (a) Pre- and post-blast load and resistance distribution curves and (b) pile and soil settlement distribution curves, as obtained around the pre-stressed pile (No after beam blanks curve due to weatherproofing problems within the communication cables for the strain gauges).



The developed dragload around the steel H-pile, pipe pile and prestressed concrete pile represented about 15, 17, and 32 percent of the total axial resistance that was estimated from CAPWAP analysis. For each pile, the post-blast skin friction measured immediately after blasting were approximately 50-percent of the pre-blast positive shaft resistances. The skin friction with liquefied layer reduced from being 100-percent resisting skin friction to approximately 50-percent contributing shaft resistances. An increase in toe resistance as a function of time was also observed at the toe location of each test pile. It is possible that the developed dragload may have contributed to the settlements (downdrag) by increasing the toe penetration. Specifically, the post-blast soil settlements mobilized the toe resistance with the corresponding toe penetration of 2.62, 6.32, and 9.13 mm for the steel-H pile, pipe pile and prestressed concrete pile, respectively.

### **8.8. Proposed Analytical Method**

The recommended procedure for evaluating liquefaction-induced dragload and downdrag is to use the neutral plane methodology. A new analytical method to evaluate a pile subjected to liquefaction-dragload and downdrag was implemented. The analytical method is based on the obtained experimental data and the traditional neutral plane that was originally developed for consideration-induced dragload and downdrag. The method consisted of determining the load and resistance distribution curves using the unfactored incremental shaft and toe resistances. As shown in Equation 8.2, the load curve is obtained by adding the unfactored structural load (dead load) to the unfactored cumulative 30-percent reduced skin friction at each depth interval, and the pile self-weight within that depth interval. To determine the resistance curve, the resistance at the toe is added to the unfactored reverse non-reduced cumulative skin friction values at each depth interval (Equation 8.3).

$$Q_i = Q_{str} + \Sigma(0.3(f_{s,i} \cdot A_i)) + W_i \quad \text{Equation 8.2}$$

Where,  $Q_i$  = the unfactored load in the pile as a function of depth, for the  $i^{\text{th}}$  element with the first  $i$  element being at the ground surface;  $Q_{str}$  = the unfactored structural load applied on the pile head;  $f_{s,i}$  = the unfactored skin friction of the  $i^{\text{th}}$  element;  $A_i$  = the surface area for the  $i^{\text{th}}$  element; and  $W_i$  = the weight of the  $i^{\text{th}}$  element of the pile.

$$R_j = R_{toe} + \Sigma(f_{s,j} \cdot A_j) \quad \text{Equation 8.3}$$

Where,  $R_j$  = the unfactored resistance in the pile, as a function of depth, for the  $j^{\text{th}}$  element with the first  $j$  element being at the pile toe,  $R_{toe}$  = the unfactored end bearing resistance at the pile toe,  $f_{s,j}$  = the unfactored skin friction of the  $j^{\text{th}}$  element; and  $A_j$  = the surface area for the  $j^{\text{th}}$  element.

The load and resistance curves that were estimated using the proposal empirical equations (Equations 8.2 and 8.3) are presented in Figure 8.10. The neutral plane was located at 17.36, 18.75, 18.97 m for the steel H pile, steel pipe pile and pre-stressed concrete pile, respectively. The difference between the measured and predicted neutral plane locations were attributed to 1) the load within the pile only being measured at the location of the strain gauges, and 2) variability and uncertainty in CPT measurements that were used to calculate the unit shaft toe resistances. The reduction of the skin friction within the liquefied zone may have negligible effect on the axial behavior of a pile. However, the developed negative skin friction (dragload) can be large enough to affect the serviceability conditions of a given pile. Therefore, in this case of liquefaction-induced dragload, an evaluation of serviceability limit states should be completed, and designers should ensure that the induced downdrag are within the acceptable limits. For foundation designers, an evaluation of limit states of a pile under liquefaction-induced

dragload and downdrag should be performed by 1) establishing the location of the neutral plane location, and 2) analyzing load and settlement curves.

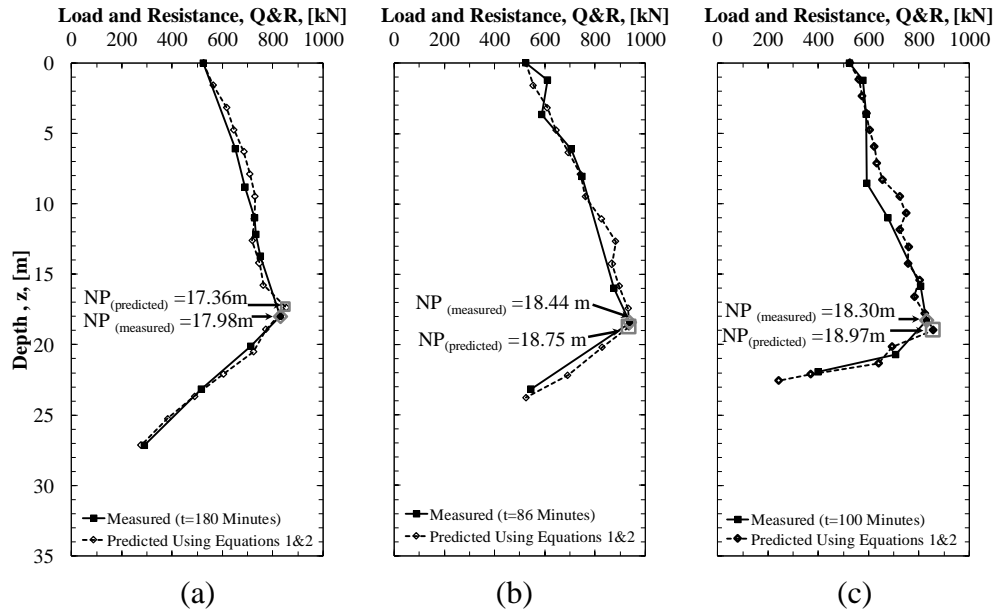


**Figure 8.10.** (a) Predicted and measured load and resistance distribution curves as obtained for: (a) steel H pile, (b) steel pipe pile, and (c) prestressed concrete pile.

## 8.9. Conclusions

In this study, blast-induced liquefaction tests were conducted around three different types of driven piles to investigate the development of dragload and downdrag around a deep foundation. The test piles were instrumented with the strain gauges to measure the load distribution along the piles during the application of an axial load at the pile head, and after liquefaction. The excess porewater pressure responses along with the corresponding ground surface settlement were monitored. The pile settlement as a function of time; the soil settlement as a function of depth were determined. Based on the full-scale load test and blast-induced liquefaction test results discussed herein, following conclusion can be drawn:

1. An increase in skin friction resistance due to the setup behavior was observed after the installation of the pipe pile.

2. As was evident from the excess porewater pressure, soil settlement, and load measurements, liquefaction was successfully induced at the testing test.
3. Prior to blasting, no negative skin friction was developed, and the neutral plane was located at the top of each pile. A close look at the behavior of the loads as the effective stresses increased at various strain gauge locations shows that the neutral plane tends to move below the liquefied zone.
4. The skin friction with liquefied layer reduced from being 100-percent resisting skin friction to approximately 50-percent contributing shaft resistances.
5. For each test pile, toe resistances were increased as the effective stresses increased.
6. Dragloads that were developed represented 15, 17, and 32 percent of the total axial resistance that were estimated from CAPWAP analyses.
7. These significant ground settlements and liquefaction-induced dragloads can affect the performance of a pile, however, further data analysis focusing on the failure mechanics of a pile is needed to support this conclusion.

### **8.10. Acknowledgements**

The authors thank the Arkansas State Highway and Transportation Department, the Missouri Department of Transportation, McKinney Drilling Company, Chris-Hill Construction, Texas Concrete Partners, PDCA, Duane Houkom, Inc., Loadtest, Inc., GEI Consulting Engineers and Scientists, DFI, ADSC, PDCA, Kolb Grading, GRL Engineers, Inc., ICE, AFT Specialty Geotechnical Services, Skyline Steel, W&W AFco Steel, and Nucor-Yamato Steel, for financial and/or in kind contributions to the scope work described herein.

### **8.11. References**

Bjerrum, L., Johannessen, I, J., and Eide, O., (1969). "Reduction of negative skin friction on steel piles to rock." Proc. 7th ICSMFE, Mexico City, Vol. 2, pp. 27-34.

- Boulanger, R.W and Brandenburg, S.J. (2004). "Neutral plane solution for liquefaction-induced downdrag on vertical piles." Proceedings, ASCE Geo-Trans conference, ASCE, Reston, VA, 470-479.
- Bozozuk, M. (1981). "Bearing capacity of a pile preloaded by downdrag." Proceedings of the 10<sup>th</sup> international conference on soil mechanics and foundations engineering, Mexico Cit, Vol. 2: 631-636.
- Bozozuk, M., (1972). "Down drag measurement on 160-ft floating pipe test pile in marine clay." Canadian Geotechnical Journal, Vol. 9, No. 2, pp. 127-136.
- Briaud, J.L., and Tucker, L. (1997). "Design and Construction Guidelines for Downdrag on Uncoated and Bitumen-Coated Piles." NCHRP Report 393, Transportation Research Board, National Academy Press, Washington, D.C., pp. 198.
- Dash, S.R, Bhattacharya, S. and Blakeborough, A.B. (2008): "Bending-Buckling interaction as a failure mechanism in seismically liquefiable deposits", Technical Report of Oxford University. No 2302/08.
- Dobry, R., (1989). Some Basic Aspects of Soil Liquefaction during Earthquakes. Proceedings of the Conference on Earthquake Hazards and the Design of Constructed Facilities in the Eastern United States, Academy of Sciences, New York.
- Dumas, C. (2000). "Soil downdrag on deep foundations." An overview perspective proceedings of the 18<sup>th</sup> ASCE/PennDOT Geotechnical Seminar, Hershey, PA, 19p.
- Endo, M., Minou, A., Kawasaki, T., and Shibata, T. 1969. "Negative skin friction acting on steel piles in clay." In Proceedings of the 8<sup>th</sup> International Conference on Soil Mechanics and Foundation Engineering, Mexico City, 25-29 August 1969. Mexico
- Fellenius, B.H. (1972). "Reduction of negative skin friction with bitumen slip layers." Discussion. Journal of the Geotechnical Engineering Division, ASCE, 101(GT4): 412–414.
- Fellenius, B.H., (1988). "Unified Design of Piles and Pile Groups." TRB Washington, Record 1169, pp. 75 82.
- Fellenius, B. H. and Siegel, T.C. (2008). Pile drag load and downdrag in a liquefaction event J. Geotech. and Geoenviron. Engrg. ASCE, Reston, Virginia, 134 (9), 1412-1416.
- Gallagher, P. M., Pamuk, A. & Abdoun, T., (2007). "Stabilization of Liquefiable Soils Using Colloidal Silica Grout." Journal of Materials in Civil Engineering, Vol. 19, No.1, pp. 33-40.
- Hannigan, P.J., Goble, G.G., Thendean, G., Linkins, G.E. and Rausche, F. (2005). "Design and Construction, Vol. I and II. Federal Highway Report No. FHWA-HI-05, Federal Highway Administration, Washington, D.C.

- Hannigan, P.J., Robinson, B. R., Goble, G.G., Likins, G.E. & Rausche, F., Becker, M. L. (2016). "Design and construction of driven pile foundations." FHWA-NHI-16-009, National Highway Institute, Federal Highway Administration, U.S. Department of Transportation, Washington, D.C.
- Little, J. A. (1994). "Downdrag of Piles: Review and Recent Experimentation, ASCE GSP 40." Vertical and Horizontal Deformations of Foundations and Embankment", pp.1805-1826.
- Long, R. L, Healy, K. A. (1974). "Negative Skin Friction on Piles." Final Report, JHR74-77. Project 73-1.
- Muhunthan, B., vijayathanan, N. V., and Abbasi, B., (2017). "Liquefaction-induced downdrag on drilled shafts." Washington State Department of Transportation. Final Research Report.
- Poulos, H. G. (1997). "Piles subjected to negative friction." A procedure for design, Geotechnical Engineering, 23-44.
- Race, M. L., Coffman, R. A., (2013), "Effect of Uncertainty in Site Characterization on the Prediction of Liquefaction Potential for Bridge Embankments in the Mississippi Embayment." ASCE Geotechnical Special Publication No. 231, Proc. GeoCongress 2013: Stability and Performance of Slopes and Embankments III, San Diego, California, March, pp. 888-897.
- Race, M.L., Coffman, R.A., (2015). "Response of Drilled Shaft Foundation Constructed in Redrilled Shaft Excavation Following Collapse." Deep Foundations Institute Journal. Vol. 9, No. 2, pp. 60- 73.
- Race, M.L., Bey, S.M., Coffman, R.A., (2015). "Statistical Analysis to Determine Appropriate Design Methodologies for Drilled Shafts Foundations." Geotechnical and Geological Engineering. Vol. 33, Issue 3, pp 713-726.
- Race, M.L. (2015) "Amount of Uncertainty in the Methods Utilized to Design Shaft Foundations." PhD. Thesis, University of Arkansas, Fayetteville, Arkansas, pp.325.
- Rollins, K. M. and S. R. Strand (2006). Downdrag Forces Due to Liquefaction Surrounding a Pile.Proceedings of the 8th U.S. National Conference on Earthquake Engineering. Paper No. 1646, San Francisco, CA, April 18-22.
- Rollins, K.M. and Hollenbaugh (2015). "Liquefaction Induced Negative Skin Friction from Blast-induced Liquefaction Tests with Auger-cast Piles." 6<sup>th</sup> International Conference on Earthquake Geotechnical Engineering, Christchurch, New Zealand.
- Seed, H.B., Martin, P.P., and Lysmer, J. (1975). "The Generation and Dissipation of Pore Water Pressures during Soil Liquefaction." Report Number UCB/EERC-75/26, University of California at Berkeley, Berkeley, CA.

- Siegel, T.C., Lamb, R., Dasenbrock, D., and Axtell, P.J. (2013). "Alternative Design Approach for Drag Load and Downdrag with the LRFD Framework." Proceedings of the 38th Annual Conference on Deep Foundations 2013, Phoenix, AZ, pp. 23-39.
- Strand, S. R. (2008). Liquefaction Mitigation Using Vertical Composite Drains and Liquefaction induced Downdrag on Piles: Implications for Deep Foundation Design. Ph.D. thesis, Department of Civil and Environmental Engineering, Brigham Young University, Provo, UT.
- Wang, R., and Brandenburg, S. J. (2013). "Beam on Nonlinear Winkler Foundation and Modified Neutral Plane Solution for Calculating Downdrag Settlement." J. Geotech. Geoenviron. Eng. Journal of Geotechnical and Geoenvironmental Engineering, 139(9), 1433–1442.
- Yamada, G. (1966). "Damage to earth structures and foundations by the Niigata Earthquake, June 16, 1964." Soils and Foundations, 6(1), 1-13.

## CHAPTER 9: Conclusions and Recommendations

### 9.1. Chapter Overview

The intent of the research study, that was documented herein, was to investigate the impact of liquefaction-induced dragload and dragload on the axial performance of deep foundations installed into a liquefiable soil. The conclusions and recommendations that were developed based on the results obtained from the test results are presented in this chapter. Specifically, the conclusions from controlled blast test (pilot liquefaction test), are discussed in Section 9.2 The overall conclusions drawn from the blast-induced liquefaction test results, for the tests involving the drilled shaft and driven pile foundations, are described in Section 9.3. Finally, the recommendations that were drawn from this research study are outlined in Section 9.4.

### 9.2. Conclusion on Controlled Blast Testing (Pilot Liquefaction Test)

Based on the results obtained from the pilot liquefaction tests conducted at the TATS, lower than expected peak excess porewater pressure ratios values were measured. These low values of the measured peak excess porewater pressure ratio were associated with 1) the presence of deep, denser, and siltier sand deposits being present at the pilot testing location, and 2) improper detonation (low PPV) of four of the charges, and 3) an inadequate amount of explosive charge weight that was utilized during blasting (as initially specified based on literature obtained empirical equations). It was concluded that the in-situ properties (vertical effective stress, particle size distribution, relative density, permeability and drainage) affected the generation and dissipation of excess porewater pressure. A modified empirical model for  $R_u$  was developed to account for the in-situ properties (relative density and vertical effective stress). Although blast-induced liquefaction may contribute to the changes of both tip cone resistance and sleeve friction, no evidence of increase of tip cone resistance and sleeve friction due densification.



### 9.3. Conclusion on Liquefaction-induced Dragload around Deep Foundations

The neutral plane method was evaluated using the data from the tests presented herein. Prior to blasting and after applying an axial load at the top of each deep foundation, the neutral plane was located at the ground surface, and no negative shaft resistance was observed. This observation was not consistent with Fellenius and Siegel (2008) method, by which a static neutral plane is developed along the foundation prior to liquefaction. Based on the excess porewater pressure measurements and ground surface settlement measurements, the soil surrounding the installed deep foundations was liquefied. Following blasting, the effective stresses were increased, resulting the transition from positive shaft resistance (upward direction) to negative shaft resistance (downward direction). As the soil settled due to the dissipation of the excess porewater pressure, the neutral plane moved from the top of each foundation to a location below the liquefied zone. The depended progression of the location of the neutral plane at various times was identified from post-liquefaction load distribution and/ or from the drilled shaft and settlement distribution curves. The movement of the neutral plane from the top of each foundation to the bottom of the liquefied layer resulted the development of dragloads.

For the drilled shaft foundations, the shaft resistance with the liquefied layer reduced from being 100-percent resisting shaft resistance to approximately 70-percent contributing shaft resistance. For the driven piles, the shaft resistance with liquefied layer reduced from being 100-percent resisting skin friction resistance to approximately 50-percent contributing skin friction resistance. These observations are consistent with test results presented by Rollins and Strand (2006), and Rollins and Hollenbaugh (2015). The dragloads that were developed following blasting, represented more between 5 to 15-percent, and 15 to 30-percent of the pre-blast total resistance around each drilled shaft and driven pile foundations, respectively. Based on the analysis of the test results, a new empirical method was proposed to the amount of dragloads

development following liquefaction. The proposed method was developed from the obtained experimental data and the traditional neutral plane approach that was originally developed for consolidation-induced dragload and downdrag.

#### 9.4. Recommendations

The research study that is presented in this document has identified the limitations of the existing empirical methods for controlled blast tests and for deep foundations installed into liquefiable soils. Based on the tests results discussed herein, several recommendations are provided.

- The in-situ conditions-based equations for liquefaction that were presented herein, are recommended to be used in determining the blasting layout (e.g., the appropriate amount of explosive charges, detonation delays, and blast holes spacing).
- Due to the geometry of the blast holes at this site, it is recommended that the charges in the holes be one charge deck instead of two charge decks to avoid improper detonations. In the case of verifying ground improvement or post-blast densification, it is recommended to measure pre-and post-blast ground settlements instead of penetration test results.
- The proposed equations (Equations 6.2 and 6.3 for PPV and the  $R_u$ , respectively), for the sites within the NMSZ and other sites with similar soil conditions.
- The effective stress based empirical methods (the  $\alpha$ -method and  $\beta$ -method are for cohesive and cohesionless soils, respectively) are recommended for use when designing drilled shafts or driven piles in liquefiable areas.
- For a deep foundation elements installed in earthquake prone areas, procedures similar to Hannigan et al. (2016), and outlined in Chapter 7 should be utilized to determine the load

and resistance distribution curves. The location and progression of the neutral plane should be confirmed using the pile/drilled shaft-soil settlement distribution curves.

- Due to difficulties associated with measuring the soil settlement as a function and time using a Sondex tube, it is recommended to use extensimeters instead of Sondex tube for the future research project.
- The research study that is documented herein only focused on single drilled shafts and driven piles, and most of the driven piles are typically installed into groups. Therefore, an extensive study on liquefaction-induced dragload and downdrag for pile groups is recommended, and the behavior of pile groups subjected to liquefaction-induced dragloads should be evaluated at the TATS. The liquefaction-induced dragload and downdrag should have less effect on the axially behavior pile group.
- The post-liquefaction settlements and liquefaction-induced dragloads and/or downdrag can affect the performance of a drilled shaft foundation, however, further data analysis is needed to support this conclusion.
- For further research, possible mechanisms of pile and/or drilled shaft failure in liquefiable soils, including: bending, buckling, and punching failure should be evaluated. These mechanisms may be caused by the 1) loss of shaft/skin friction resistance during the generation of the excess porewater pressure, and 2) development of negative shaft resistance (dragloads) during the excess porewater pressure dissipation.

## **APPENDIX A: Construction Procedures and Blasting Tests around Drilled Shafts and Driven Piles**

### **A.1. Overview**

An overview of the general construction methods used for drilled shaft and driven pile foundations at the TATS is presented in this chapter. Specifically, the procedures for the design, construction and installation of the steel H pile, closed ended steel pipe pile, and pre-stressed concrete piles at the TATS is presented in Section A.2. The design and construction methods discussed include, the selection of appropriate drilled shaft or pile sections, lengths, embedment lengths, strain gauge installation techniques, pile installation stages, and the application of a static load on top of each foundation. A detailed description of the construction techniques utilized to instrument the soil at the TATS, and various methods used to acquire data during testing are documented in this chapter. The methods used to confirm the pile driving system and suitable equipment was used at the TATS are discussed Section A.3. A description on test instrumentation used at the TATS, and the top down load test is presented in Sections A.4, and A.5, respectively. In addition, a detailed description on blast-induced liquefaction tests on the soil surrounding each deep foundation is discussed in Section A.6.

### **A.2. Construction of Drilled Shafts**

The three drilled shaft foundations that were investigated during the research study that is documented herein, were constructed as a part of another research project conducted by Bey (2014) and Race (2015). The constructed drilled shaft consisted of: two, quantity four-foot diameter by 88-ft long and 86.5-ft long drilled shafts; one, quantity, six-foot diameter by 66.5-ft long drilled shaft. The drilled shafts weredesigned to support an unfactored design load of 1974 kips (987 tons) of an existing bridge located in the vicinity of the testing site. The design length and the diameter of each drilled shaft were established using the O'Neill and Reese (1999)

methods. The appropriate drilled shaft diameter, number of rebar, the rebar size, clear spacing, and spiral reinforcement that satisfied the design requirements were selected using the ACI 318 (2008), AASHTO (2012) and the O'Neill and Reese (1999) design manual. A detailed discussion regarding the design process and the construction techniques of the drilled shafts at the TATS can be found in Bey (2014) and Race (2015). A photograph of a rebar cage, the concrete being poured into the pre-drilled and cased hole, and a constructed drilled shaft foundation at the TATS is shown in Figure A.1.

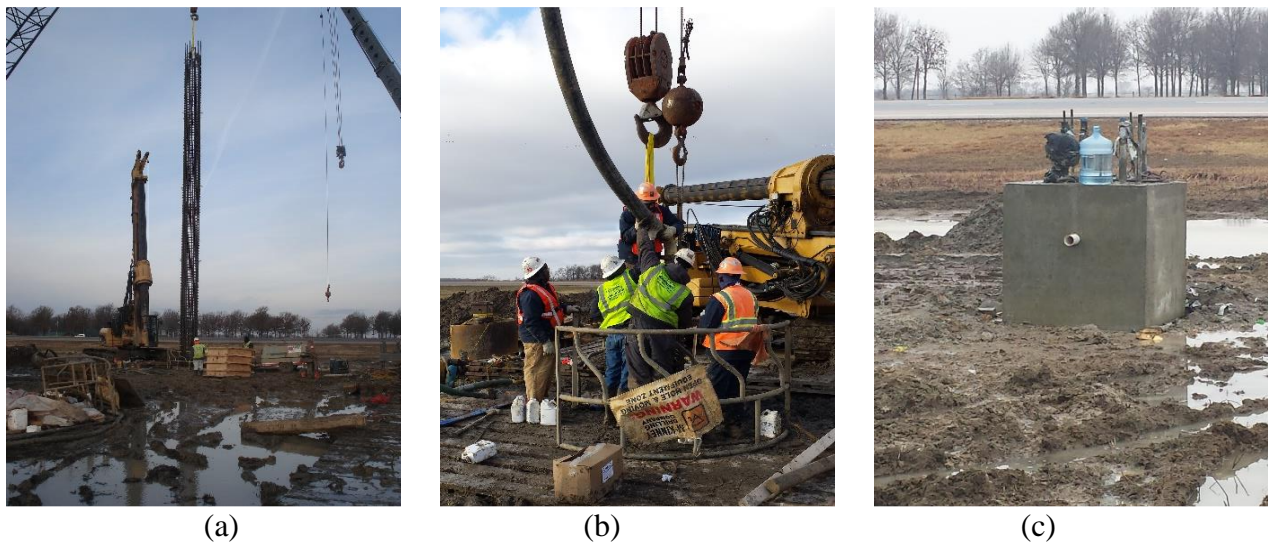


**Figure A.1.** Photographs of (a) the installation of the rebar cage (b) the concrete being placed into a cased hole, and (c) a constructed drilled shaft foundation (north drilled shaft) at the Turrell Arkansas Test Site (Courtesy of Morgan Race).

### A.3. Construction and Installation of Driven Piles

As previously discussed in Chapter 8, three different types of driven piles were installed at the TATS. The pre-stressed, pre-cast concrete pile was fabricated at the Texas Concrete plant in Victoria, Texas. A detailed schematic of the pre-stressed pile is shown in Figure A.2. The pre-stressed concrete pile was designed with a factored load nominal compression strength of about 230kips. The pile was pre-stressed using a total of nine uncoated seven strands. Each of pre-stressing strands were 0.5-inch diameter, uncoated, seven-wire, low-relaxation strand, with an

ultimate strength ( $f_{pu}$ ) of 270ksi or grade 270. The pre-stressing strands conformed to ASTM A416 (2017). The W4.0 spiral wires were used to provide a transverse reinforcement within the pile.

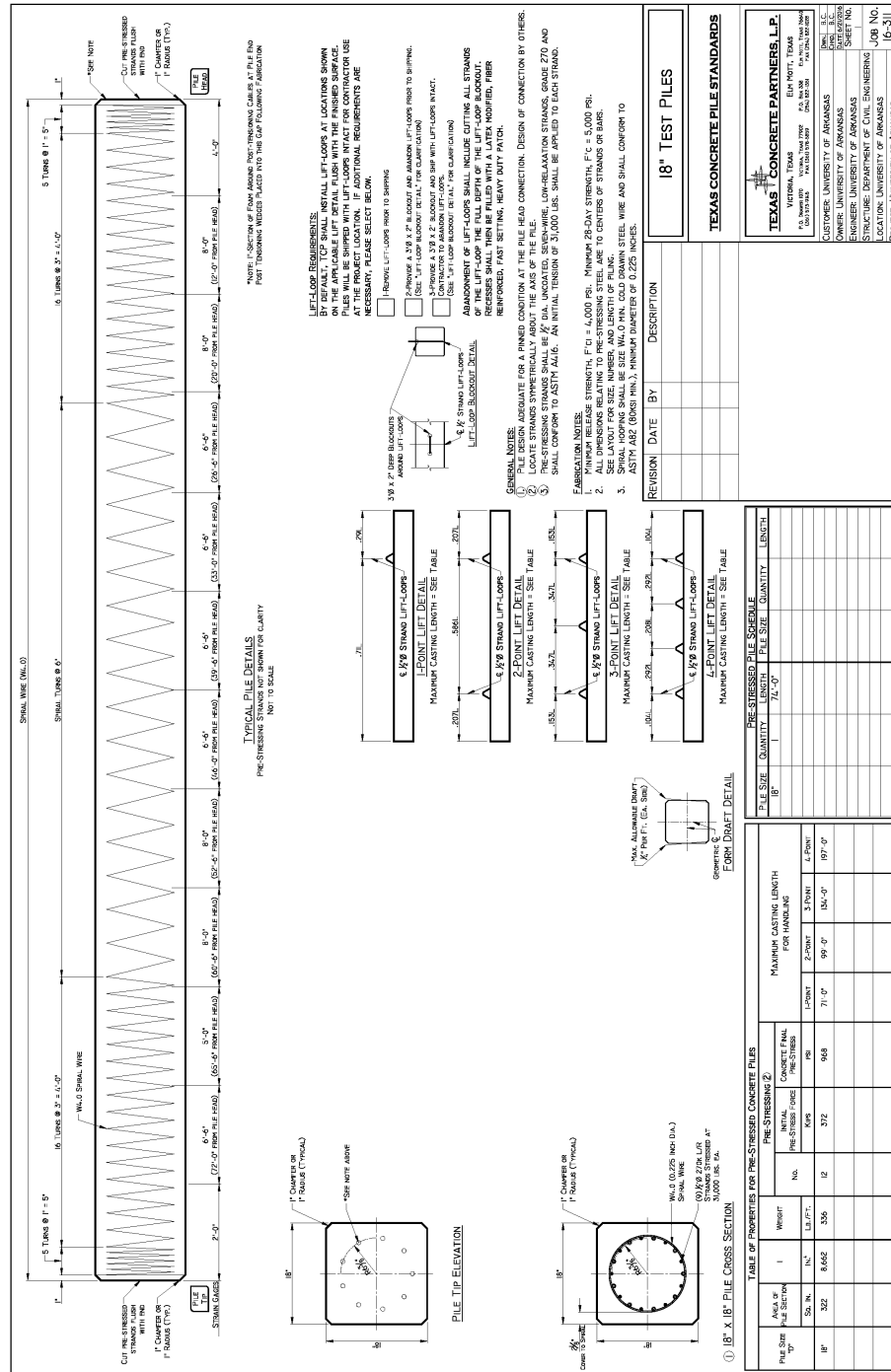
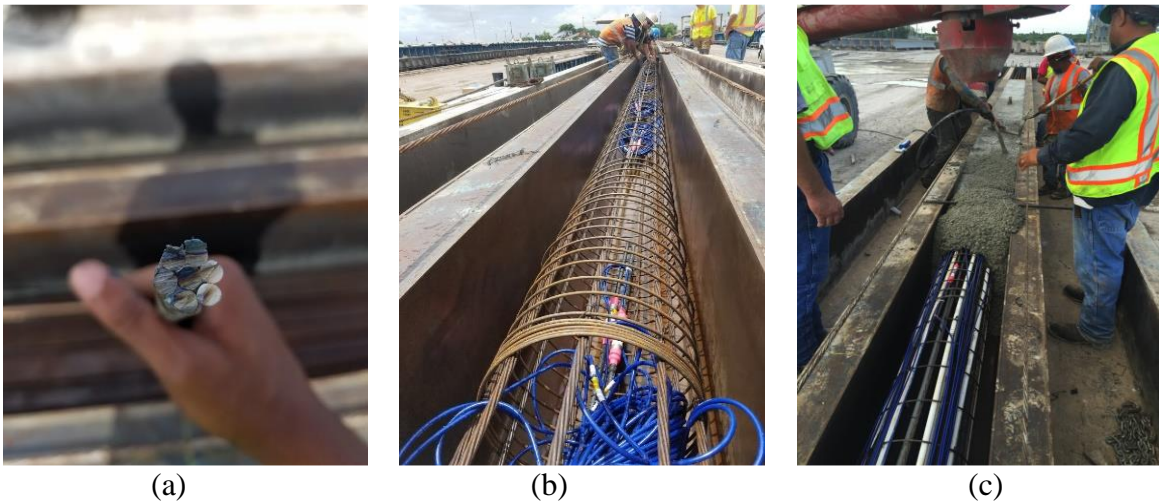
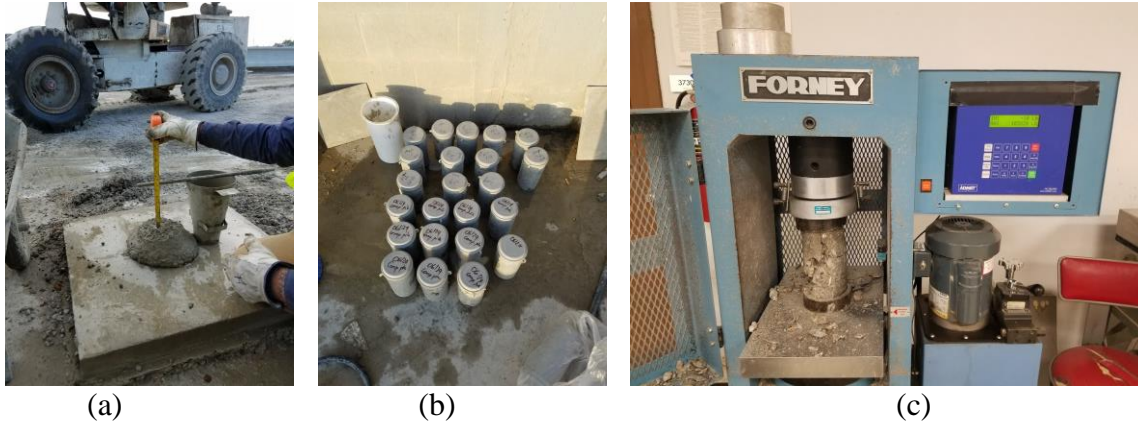


Figure A.2. Schematic of the reinforcement details of the square pre-stressed, pre-cast concrete pile.

Each spiral hooping conformed to ASTM A82 (2017), with a yield strength of 80ksi. Prior to concrete placement, an initial tension of 31,000 pound (16 tons) was applied to each individual strand using a pre-stressing machine. Photographs of the seven-wire strand, the spiral, and concrete mixture being poured into the pre-stressed bed at the Texas Concrete plant is presented in Figure A.3. The workability of the concrete mixture was verified by performing several conventional slump tests on the concrete sampled at the placement. As shown in Figure A.4a, a slump of about 8.25 inches was measured. In addition, several compressive strength tests were performed on the test cylinders that were acquired during concrete placement (Figure A.4b). The test specimens were kept in moist storage for twenty-eight (28) days, and broken using a Forney F series standard compression test machine, as shown in Figure A.4c. At twenty-eight days following concrete placement, the compressive strengths ( $f'_c$ ) varied from 8909 to 10,413psi (61 to 72Mpa), with corresponding modulus of elasticity ( $E_c$ ) values ranging from 5438 to 5880ksi (38 to 41GPa).



**Figure A.3.** Photographs of (a) a seven-wire 270 grade strand, (b) the W4.0 spiral wires being installed around the pre-stressed strands within the square pre-stressing bed prior to pre-stressing process and concrete placement, and (c) the concrete being placed into the pre-stressing bed (Photo by author).



**Figure A.4.** Photographs of (a) a slump test being conducted on the concrete mix, (b) the collected concrete cylinders (four-inch diameter and 8-inch long) acquired immediately after pouring the concrete into the pre-stressing bed, and (c) a test specimen (at failure) within a compression testing machine. (Photo by author).

A steel pipe pile with an outside diameter (OD) of 18 inches (457mm) and a wall thickness of 0.56inches (14mm) was also installed at the testing site. The steel conformed to the ASTM A252 (2010) Grade 1, with a yield strength of 30ksi (205MPa), and pipe weight of 93.54 lbs/ft (139.3kg/m). Likewise, a steel H-pile was installed at the TATS. The 92-foot long HP 14x117 section H pile had a flange width of 0.805inches (20.4mm) and web width of 0.805inches (20.4mm) was installed at the TATS. According to the ASTM A572 (2010), the steel for the H pile was specified as grade 50 (yield strength =50ksi), which is the most commonly used steel H-Pile grade in the Northeast Arkansas region. After the fabrication, the test piles were safely transported and delivered to the TATS, as shown in Figure A.5.



**Figure A.5.** Photographs of (a) the steel pipe pile , and (b) pre-stressed pile being delivered at the TATS.



All the pile handling and installation were performed using a Kobelco crane. Photographs of a Kobelco crane components (e.g., crane, boom and swinging leads), hammer and helmet components used at the TATS are presented in Figure A.6. The piles were driven using an International Construction Equipment (ICE) I-30 diesel hammer at desired embedment lengths, with each pile sticking up approximately 1.2m (4ft) above the ground elevation. A photograph of the I-30 diesel hammer is presented in Figure A.7a. A driving system that included crane, leads, hammer, pile cushion and helmet was selected based on a driveability analysis that was completed using the FHWA-Driven 1.2 program. The analysis was conducted by AHTD personnel (Dr. Jabo Joseph) using the CPT data that were acquired at the location of the respective pile. The hammer had an efficiency of 80%, sufficient energy was developed to drive the piles into the soil at the specified depths. For the pre-stressed concrete pile, a pile cushion made of a plywood with the same cross sectional as the pile head was utilized to prevent pile damage and overstressing of the pile during pile driving.

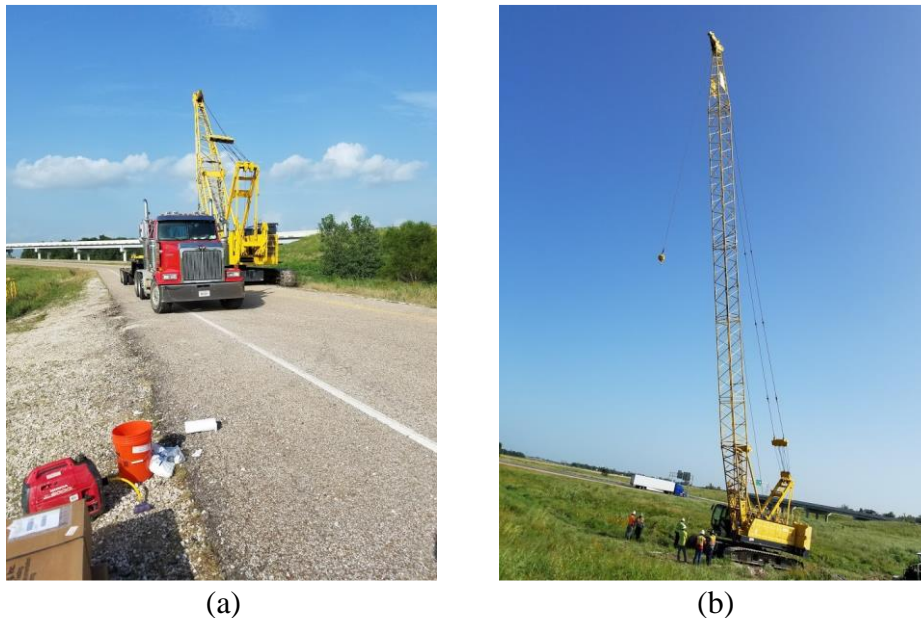


**Figure A.6.** Photographs of (a) Kobelco crane parts being delivered at the TATS, (b) a completed Kobelco crane with a boom before attaching the swinging leads and hammer system.

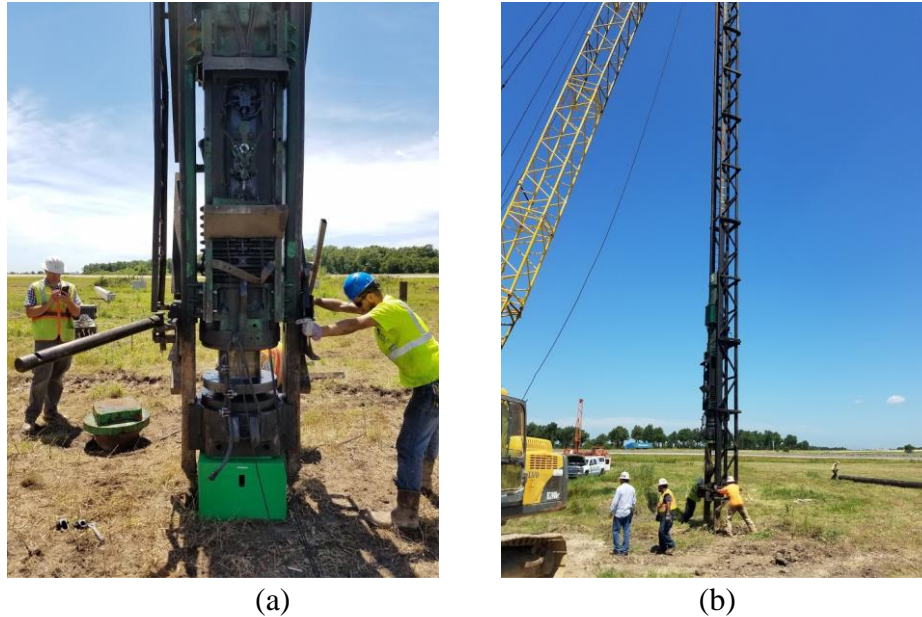


**Figure A.7.** Photographs of (a) a helmet being mounted to the ICE I-30 diesel hammer, and (b) the ICE-I-30 hammer being mounted to the swinging leads attached to the crane.

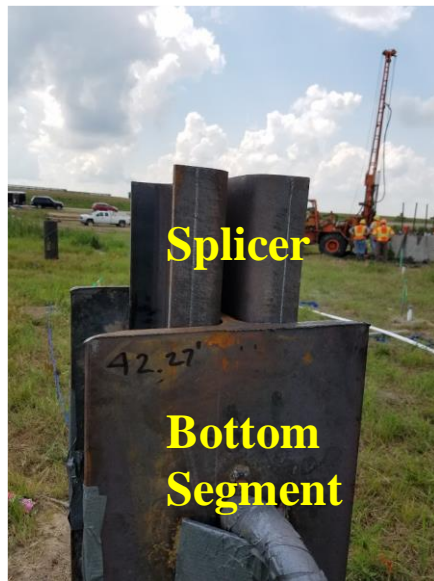
As shown in Figure A.8a, the steel H-pile was delivered to the testing site into two segments. The bottom segment with a total length of 42.27ft was first delivered to the pile location, and driven into the soil (Figure A.8). A mechanical splicer plates was then welded to the bottom segment, and used to connect both segment, as shown in Figures A.8c and A.8d. High strain dynamic load tests were performed during pile installation and during restrike. The dynamic measurements, including strain and acceleration were acquired using a strain transducer and accelerometer that were attached near the pile head, as shown in Figure A-9a. The strain transducer and accelerometer measurements were collected using a WIFI transmitter that was remotely connected to the Pile Driving Analyzer (PDA), as shown in Figure A.9b. During driving, the diesel hammer operated on various fuel settings depending upon the driving resistances (Figures A.9c and A.9d). Following driving, CAPWAP analyses were then performed on selected hammer blows records acquired at the end of initial driving and at the beginning of restrike using the PDA to determine the pile capacity.



(a)



(b)

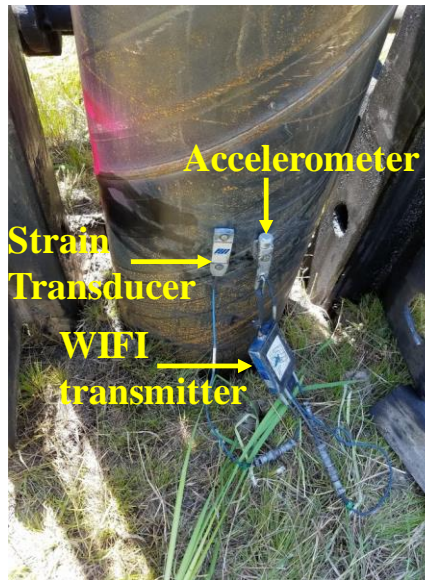


(c)



(d)

**Figure A.8.** Photographs of (a) two HP 14x117 sections being delivered on the testing site, (b) HP 14x117 being unloaded from the truck using the crane, (c) the mechanical splicer, and (d) the top segment of the H-pile being placed into the splicer and the welded to the bottom segment of the H-pile.



(a)



(b)



(c)



(d)

**Figure A.9.** Photographs of (a) the strain transducer, accelerometer, and WIFI transmitter utilized during pile dynamic load tests, (b) the Pile Driving Analyzer (PDA) being performed while driving the HP section. Fuel settings being changed during the installation of (c) the pipe pile and (d) the pre-stressed pile.

#### A.4. Test Instrumentation

##### A.4.2. Strain Gauge Measurements

As previously mentioned in Chapters 7 and 8, linear vibrating wire and piezoresistive strain gauges were used to measure strain in the drilled shafts and driven piles, respectively. The

reason for using a piezoresistive type gauge for the piles instead of a vibrating wire type gauge was because the piezoresistive gauges can be read much faster than the vibrating wire gauges. For dynamic (statnamic) measurements, near instantaneous readings can be required because the impact wave rapidly propagates through driven piles during the test (Coffman 2018). For the drilled shafts, the strain gauges were mounted on sister bars that were then attached to the reinforcement cage, as illustrated in Figure A.10. Detailed discussion on the installation of the strain gauges in the drilled shaft foundation are presented in Bey (2014).



**Figure A.10.** Photograph of the linear vibrating wire strain gauge being mounted on the reinforcement cage (Photo courtesy of Sarah Bey, Bey 2014).

To prevent instrumentation damage, the pipe pile and H piles were instrumented at the test site. For the steel H pile, the piezoresistive strain gauges were installed using two end blocks that were welded in the middle of the flange, as shown in Figure A.11a. The completed assembly of the strain gauge and the electric wires were covered with angle iron to prevent instrumentation damage to the gauges during pile driving (Figure A.11b). The strain gauges on the top segment of the H-pile were installed in the similar fashion as the button segment. For the pipe pile, the strain gauges that were attached to sister bars that were zip-tied on a 12.7-mm (2-inch) diameter

PVC pipe, as shown in Figure A.12. The PVC pipes were then placed inside the pipe pile, and, concrete mixture was poured around the gauges and inside of the close ended pipe pile (Figure A.12b). Unlike the drilled shafts, the strain gauges that were embedded within the pre-stressed pile were mounted to sister bars that were attached to the spirals, before concrete placement within the pre-stressing bed (Figure A.13). For all the drilled shafts and driven piles, two strain gauges were installed diametrically opposed, at each desired depth: 1) to obtain the average strain measurements within pile can be used during data reduction, and 2) for redundancy.

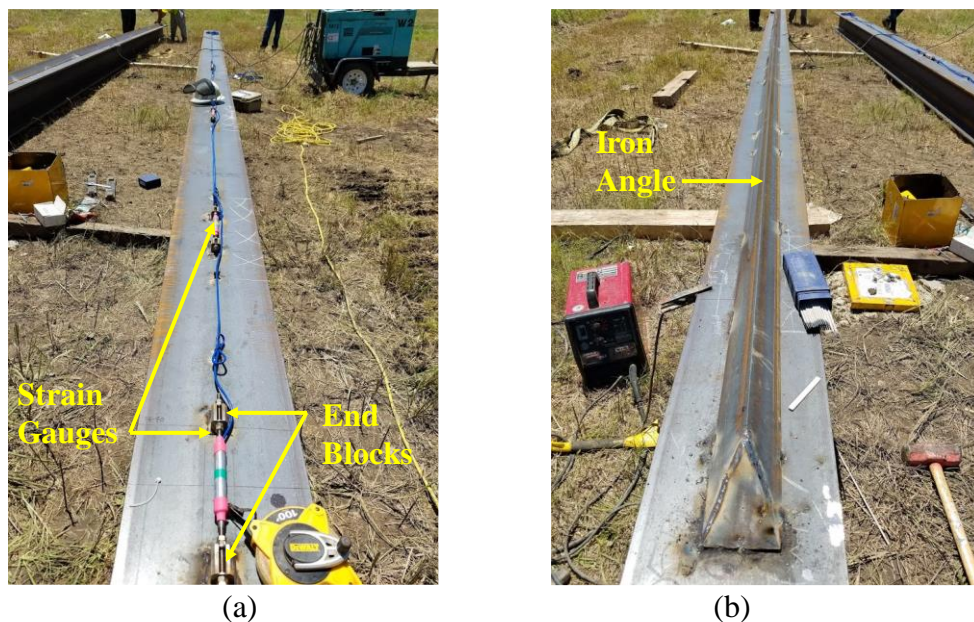


**Figure A.11.** Photographs of (a) the piezoresistive strain gauges assembly with end blocks and strain gauge cables attached on flange of the bottom segment of the H-pile, and (b) the protection angle iron covering the strain gauges (Photo courtesy by the author)..

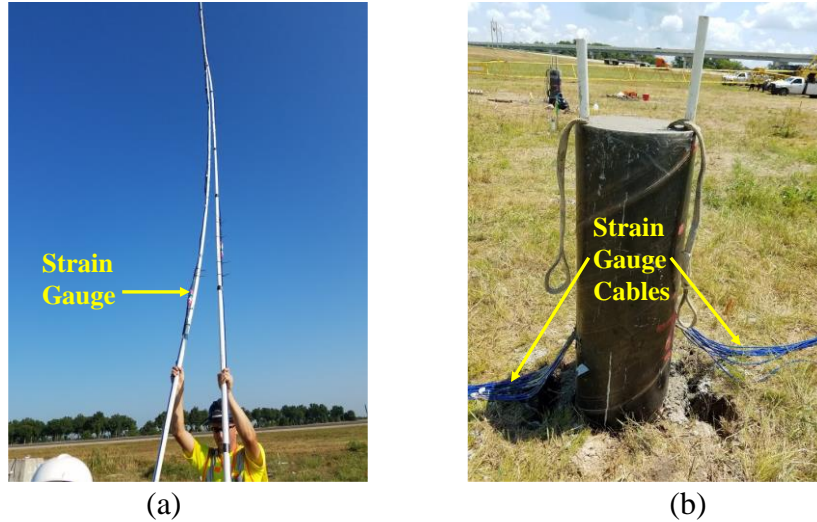


**Figure A.12.** Photographs of (a) the strain gauge attached to sister bar and zip-tied on the 2-inch diameter PVC pipes, and (b) the strain gauge cables exiting from the completed pipe (Photo courtesy by the author).

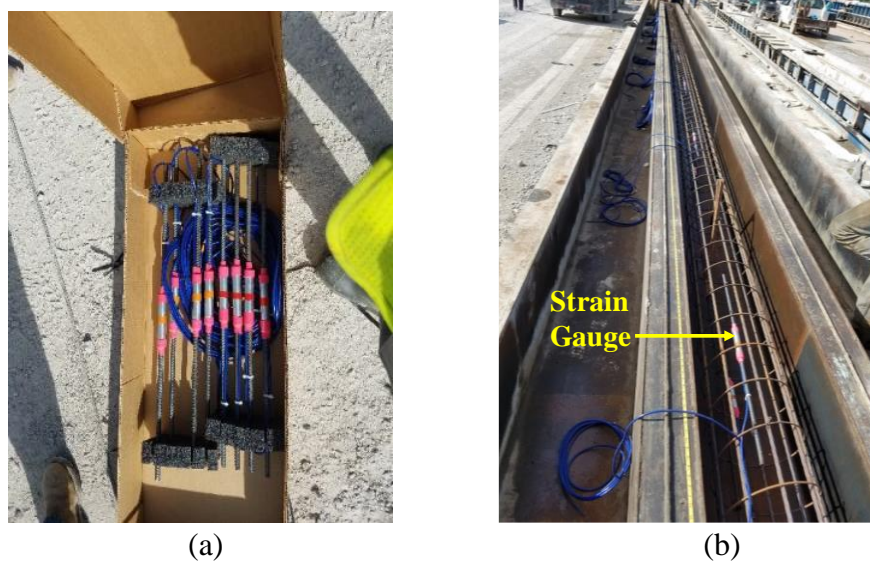


**Figure A.13.** Photographs of (a) the piezoresistive strain gauges utilized for driven piles at the TATS, and (b) the sister bar strain gauge tied to a sister bar and attached to the spirals prior to the concrete pouring (Photo courtesy by the author).

#### **A.4.2. Excess Porewater Pressure Measurements**

Following the completion of pile installation, eight pore pressure transducers (piezometers) were installed around each deep foundation. The piezoresistive piezometer sensor utilized at the TATS are shown in Figure A.14a. The piezoresistive piezometers were installed following the step-by-step procedures provided by Rollins et al. (2015). Prior to installation, each

piezometer sensor was inserted into a nylon cone tip housing with an electrical cable and steel-wire retrieval cables (Figure A.14b). The nylon cone tip housing was utilized to protect the sensor during installation. As reported in Rollins et al. (2005), the nylon casing was also used to minimize the difference between the unit weight of the soil and the sensor.

As shown in Figure A.14b, the piezometers were submerged in water 1) to ensure a full saturated of a sensor and 2) to remove air bubble trapped inside the sensor prior to installation. A retrieval cable was attached to the head of the casing. The retrieval cable was utilized to facilitate the installation and retrieval process of the piezometer, as shown in Figure A.14c. The piezometers were attached to a push rod that was connected to a drill rig, and then pushed into a pre-drilled, grouted borehole at various depths (Figure A.14c). Because of the high cost of each piezometer and time consumption associated with the preparation and installation of each piezometer, the piezometers were retrieved following each blast event and re-used for the next blast events. Therefore, some of the installed piezometers were damaged during the retrieval and re-installation process, and the damaged transducers were discarded.

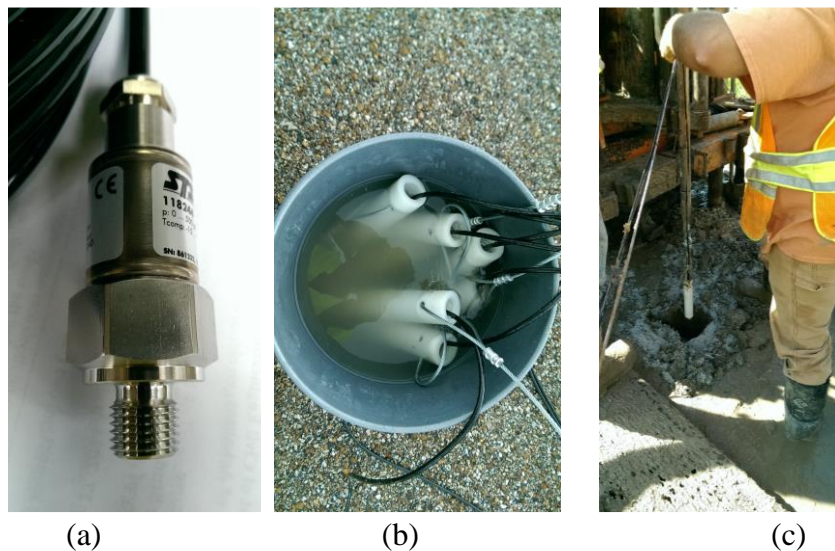


**Figure A.14.** Photographs of (a) a typical piezoresistive piezometer utilized at the TATS, (b) the piezometers inserted within nylon cone tip and being saturated prior to installation, and (c) the piezometer component that includes, nylon cone tip, a retrieval cable, and an electric cable, attached on a push rod (Photo courtesy by the author).



#### ***A.4.2. Post-liquefaction Settlements and PPV Measurements***

As discussed in Chapters 6, 7, and 8, the amount of soil settlement, as a function of depth was monitored using a Sondex tube. The Sondex tube assembly consisted of a 2-inch diameter PVC pipe, a flexible 4-inch diameter corrugated drain pipe, metal clamps, and a Sondex probe. Prior to installation, a PVC pipe was inserted inside the corrugated pipe to ensure a smooth pathway for the Sondex probe. As shown in Figure A.15a, the metal clamps were placed tightly around the corrugated pipe at two-foot increments. The Sondex tube assembly (corrugated pipe, PVC pipe, and metal clamps) was then pushed into the pre-drilled hole at a depth of 50ft using a drill rig, as shown in Figure A.15a. Sondex measurements were obtained as follows. The Sondex probe containing a magnetic sensor was inserted into the PVC pipe within the corrugated pipe. The measurements were recorded as the probe descended into the Sondex tubes and detected the distance between the installed metal clamps.

The amount of ground surface settlement before and after blasting were measured using string potentiometers and level survey, as shown in Figures A.15b and A.15c, respectively. In addition, Leica digital indicators were mounted at the top of each foundation to monitor the downward movement of each foundation during the application of the static load, and movement associated with blasting. A photograph of a Leica digital rod mounted to a drilled shaft is shown in Figure A.15d. The peak particle velocity induced by blasting at the TATS was measured using two Instantel Minimate seismographs. A photograph of an Instantel Minimate seismographs is shown in Figure A.16. The seismograph devices were placed at the ground surface, and 150ft away from each blast ring.



(a)



(b)



(c)



(d)

**Figure A.15.** Photographs of (a) the installation of Sondex tube components, including the corrugated pipe metal clamps, PVC pipe (inserted within the corrugated pipe), (b) installed string potentiometers, (c) surveying stakes and automatic level utilized at the TATS, and (d) Leica digital level rods being attached at the top of the North drilled shaft foundation (Photo courtesy by the author).



**Figure A.16.** Photographs of the instantel minimate blast seismographs installed before blast-induced liquefaction tests (Photo courtesy by the author).

#### **A.5. Top Down Load Application**

As discussed in Chapters 6 and 7, an axial load of 352.40 and 117.76kips was applied to the top of each drilled shaft and driven pile, respectively, prior to the performance of the blast-induced liquefaction tests at the TATS. The axial load was accumulated through the use of BB-4 beam blanks, as shown Figure A.17a. Each blank beam was 20-inches by 16-inches by 20.02-ft long and weighed 12,584 pounds. For drilled shafts, the static load was applied directly onto drilled shaft head, and twenty-eight beam blanks were stacked on the top of the each drilled shaft foundation using a crane (Figure A.17). A photograph of twenty-eight BB-4 beam blanks on to the top of the north drilled shaft is presented in Figure A.17b. For the driven piles, the beam blanks were placed onto a load distribution cap that was attached to the top of each respective test pile using a snoop crane, as shown in Figures A.18a and A.18b. The load distribution cap weighed 4,500 pounds, and nine beam blanks were placed at the top of each pile (Figure A.18c and A.18d).



**Figure A.17.** Photographs of (a) beam blanks being placed at the top of the north drilled shaft, and (b) an axial load of 352.40 kips placed at the top of the North drilled shaft (Photo courtesy by the author).



**Figure A.18.** Photographs of (a) the crane that was used to move the beam blanks from a truck to the H pile, (b) the steel load distribution plate being reloaded from a truck, (c) the load distribution plate being place at the top of the H-pile, and (d) the beam blanks being place at the top of the H-pile (courtesy of Richard Coffman).

## A.6. Controlled Blasting around Drilled Shafts and Driven Piles

The soil surrounding each drilled shaft and driven pile was subjected to liquefaction by detonating explosive charges that were placed in the soil around each foundation. The methodology and procedures described by Rollins et al. (2005), Ashford et al. (2004), Ashford et al. (2000), Weaver et al. (2005), Rollins et al. (2001), Rollins et al. (2004). Rollins and Hollenbaugh (2015) regarding full-scale blast induced liquefaction testing, were followed. The charges that were utilized at the TATS were “DYNO AP emulsion explosives,” as shown in Figure A.19. The charges were consisted of a mixture of ammonium nitrate, sodium nitrate, and aluminum. The installation of the explosive charges started by drilling a 3-inch diameter hole at specified locations and depths using a rotary mud drilled technique. Due to the site conditions (loose sands) at the TATS, each blast hole was cased with a 2-inch diameter PVC pipe to keep the hole open below the groundwater table (Figure A.19b).



**Figure A.19.** Photographs of (a) the Dyno emulsion explosive, and (b) the charge being placed into the pre-drilled and cased hole (Photo courtesy by the author).

As previously discussed in Chapters 6 and 7, the explosive charges were placed in a circular array around each installed foundation, as shown in Figure A.20a. Prior to detonation,

each blast hole was filled with gravel for stemming and sand bags were placed over the charge holes. Within each blast hole, gravels were loaded on the top of the explosive charges 1) to provide a confinement of the blast gases, 2) to prevent the escape of the explosion gases after detonation, and 3) allow the energy produced by explosion to propagate in radial directions. As shown in Figure A.20a, three separate blast events were performed for this project. A total of 3.63kg (8lbs) of explosive charges were placed into the pre-drilled and cased blast holes around the North drilled shaft and steel H-pile during the first blast test.

For the second blast test, a total of 5.44kg (12lbs) per borehole of explosive charges were detonated around the center drilled shaft and closed ended steel pipe pile. For the South drilled shaft and pre-stressed pile concrete pile, an explosive charge weight of 6.35kg (14lbs) per borehole was detonated. The explosive charges were detonated sequentially around each blast ring with a 200ms delay between each individual blast hole following the pattern illustrated in Figure A.20a. In addition, five sand bags were also placed to the top of each blast hole to prevent the escape of PVC pipe and gravel during blasting (Figure A.20b). For safety and quality control, a licensed blaster assisted following proper installation and detonation procedures of the explosive charges. All of the installed instrumentation was monitored with a data acquisition system (DAQ) that was located approximately 50ft away from the blast ring. A photograph of the TATS layout prior to the third blast event is presented in Figure A.20b.

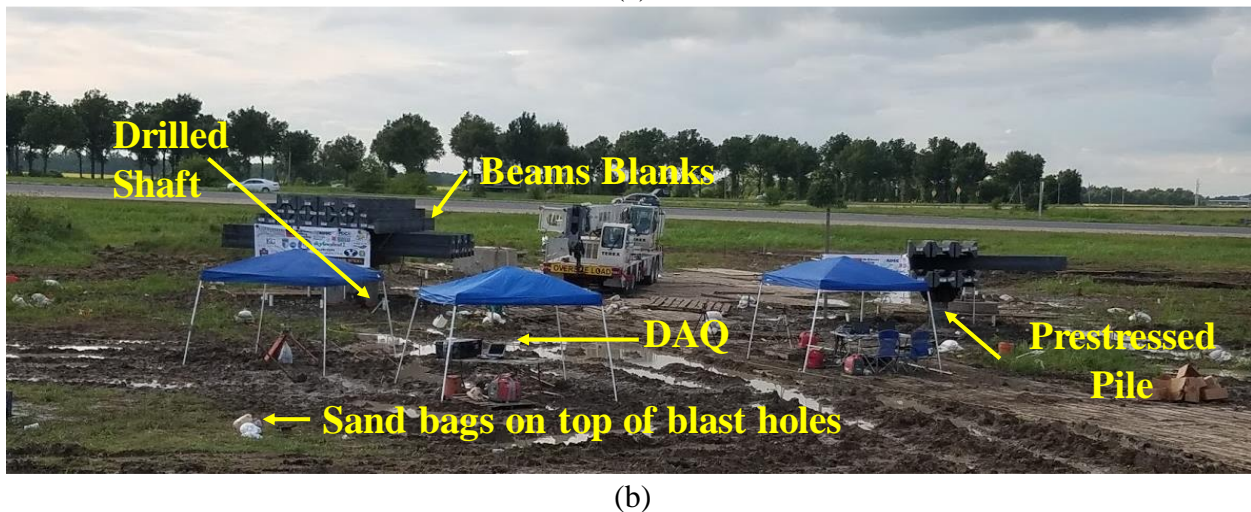
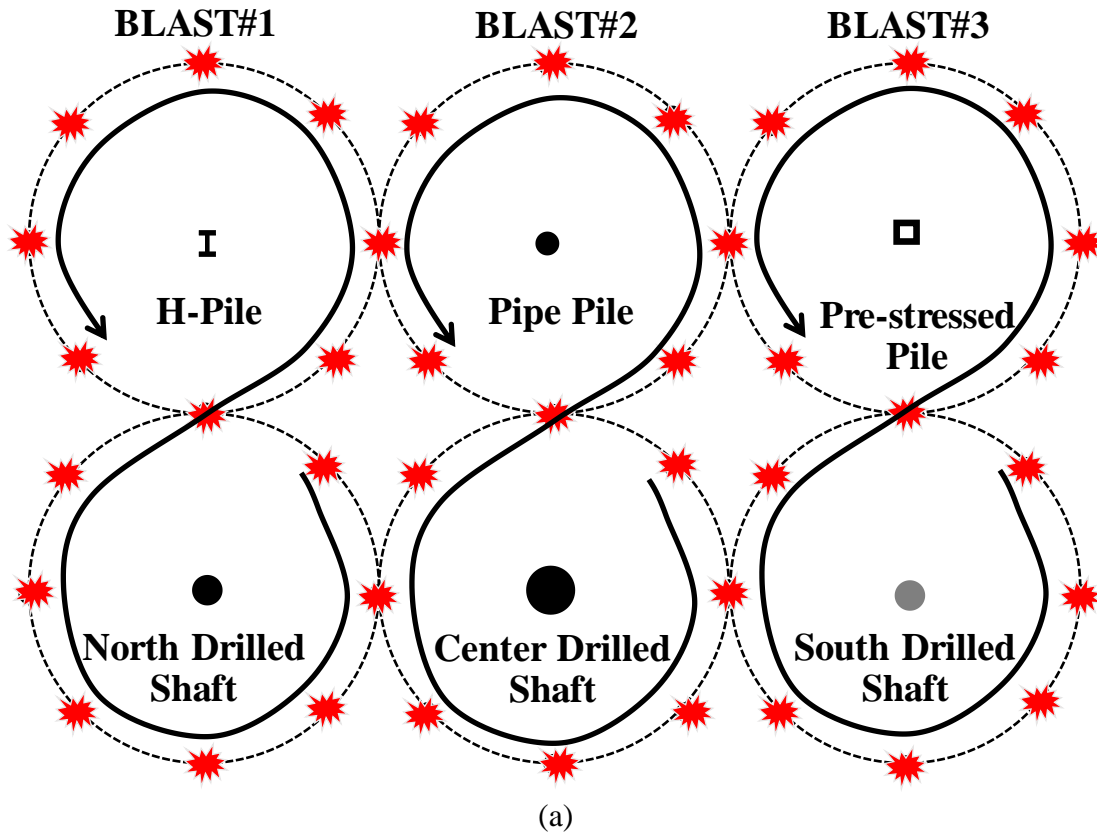


**Figure A.20.** (a) Explosive charge pattern for the three blast events, and (b) a photograph of the TATS before blasting the soil around the Center drilled shaft and the closed ended steel pipe pile.

#### A.7. References

Ashford, S.A. and Rollins, K.M. (2002). "TILT: Treasure Island Liquefaction Test: Final Report." Report SSRP-2001/17, Department of Structural Engineering, University of California, San Diego.

- Ashford, S.A., Rollins, K.M., and Lane, J.D. (2004). "Blast-induced Liquefaction for Full-Scale Foundation Testing." *Journal of Geotechnical and Geoenvironmental Engineering*. Vol. 130, No. 8, pp 798-806.
- Race, M. L., Coffman, R. A., (2013), "Effect of Uncertainty in Site Characterization on the Prediction of Liquefaction Potential for Bridge Embankments in the Mississippi Embayment." ASCE Geotechnical Special Publication No. 231, *Proc. GeoCongress 2013: Stability and Performance of Slopes and Embankments III*, San Diego, California, March, pp. 888-897.
- Race, M.L., Coffman, R.A., (2015). "Response of Drilled Shaft Foundation Constructed in Redrilled Shaft Excavation Following Collapse." *Deep Foundations Institute Journal*. Vol. 9, No. 2, pp. 60- 73.
- Race, M.L., Bey, S.M., Coffman, R.A., (2015). "Statistical Analysis to Determine Appropriate Design Methodologies for Drilled Shafts Foundations." *Geotechnical and Geological Engineering*. Vol. 33, Issue 3, pp 713-726.
- Rollins, K.M. (2004). "Liquefaction Mitigation Using Vertical Composite Drains: Full Scale Testing." Final Report for Highway IDEA Project 94. Transportation Research Board, February 2004, 105 p.
- Rollins, K.M., Lane, J.D., Nicholson, P.G., and Rollins, R.E. (2004). "Liquefaction Hazard Assessment using Controlled-Blasting Techniques." *Proc. 11th International Conference on Soil Dynamics & Earthquake Engineering*. Vol. 2, pp. 630-637.
- Rollins, K.M., Lane, J.D., Dibb, E., Ashford, S.A., and Mullins, A.G. (2005a). "Pore Pressure Measurement in Blast-Induced Liquefaction Experiments." *Transportation Research Record 1936, Soil Mechanics 2005*, TRB, Washington D.C., pp. 210-220.
- Rollins, K.M. and Anderson, J.K.S. (2008). "Cone Penetration Resistance Variation with Time after Blast Liquefaction Testing." *Procs. Geotechnical Earthquake Engineering and Soil Dynamics-IV*, Geotechnical Special Publication 181, ASCE, 10 p.
- Rollins, K.M. and Hallenbaugh (2015). "Liquefaction Induced Negative Skin Friction from Blast-induced Liquefaction Tests with Auger-cast Piles." *6<sup>th</sup> International Conference on Earthquake Geotechnical Engineering*, Christchurch, New Zealand.



## APPENDIX B: Geotechnical Site Investigation Information

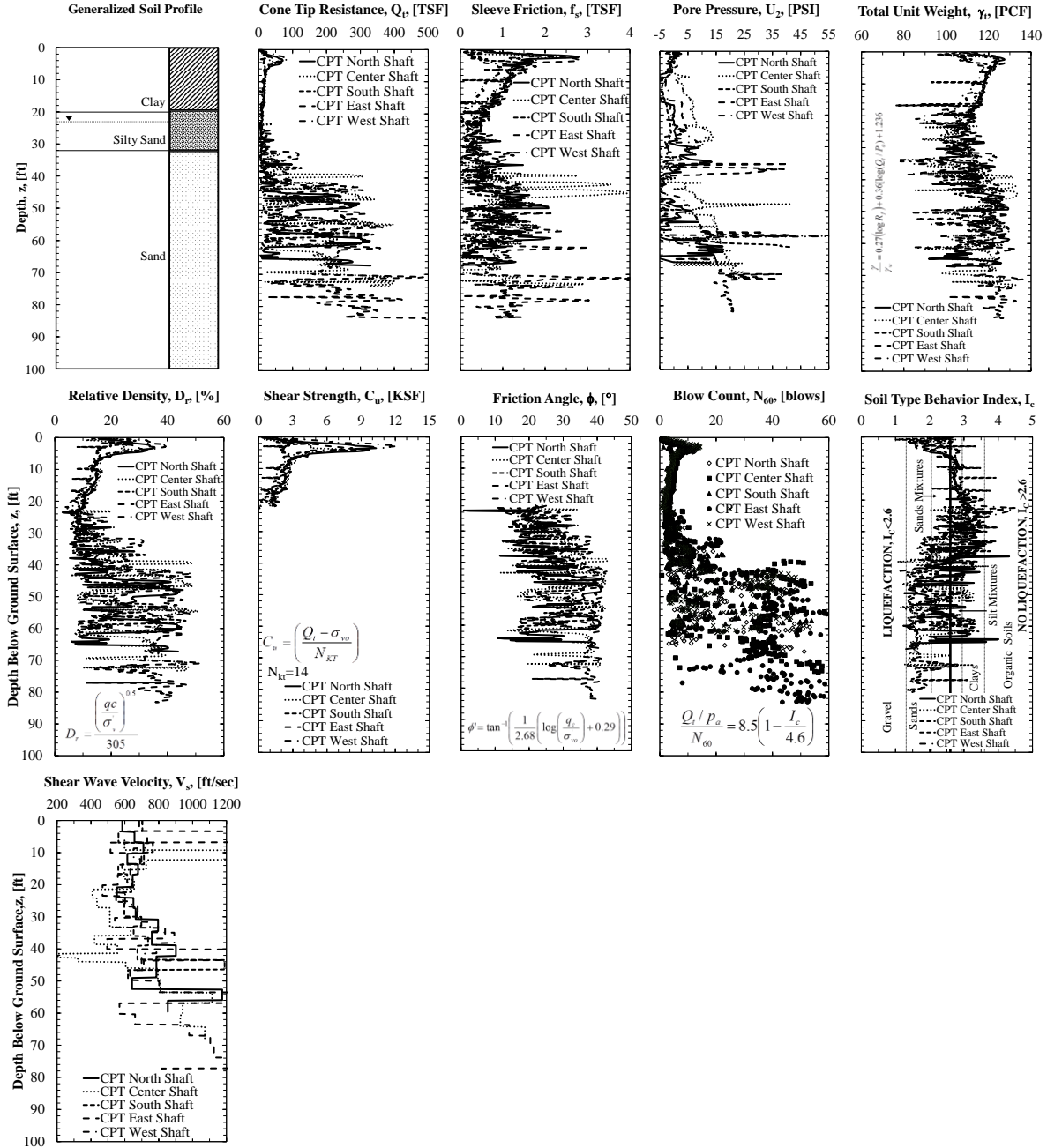


**Figure B.1.** Generalized soil profile, CPT measurements, total unit weight, relative density, shear strength, friction angle, SPT- $N_{60}$  and the soil index behavior correlated from these CPT measurements at the drilled shaft locations (data from Bey 2014).

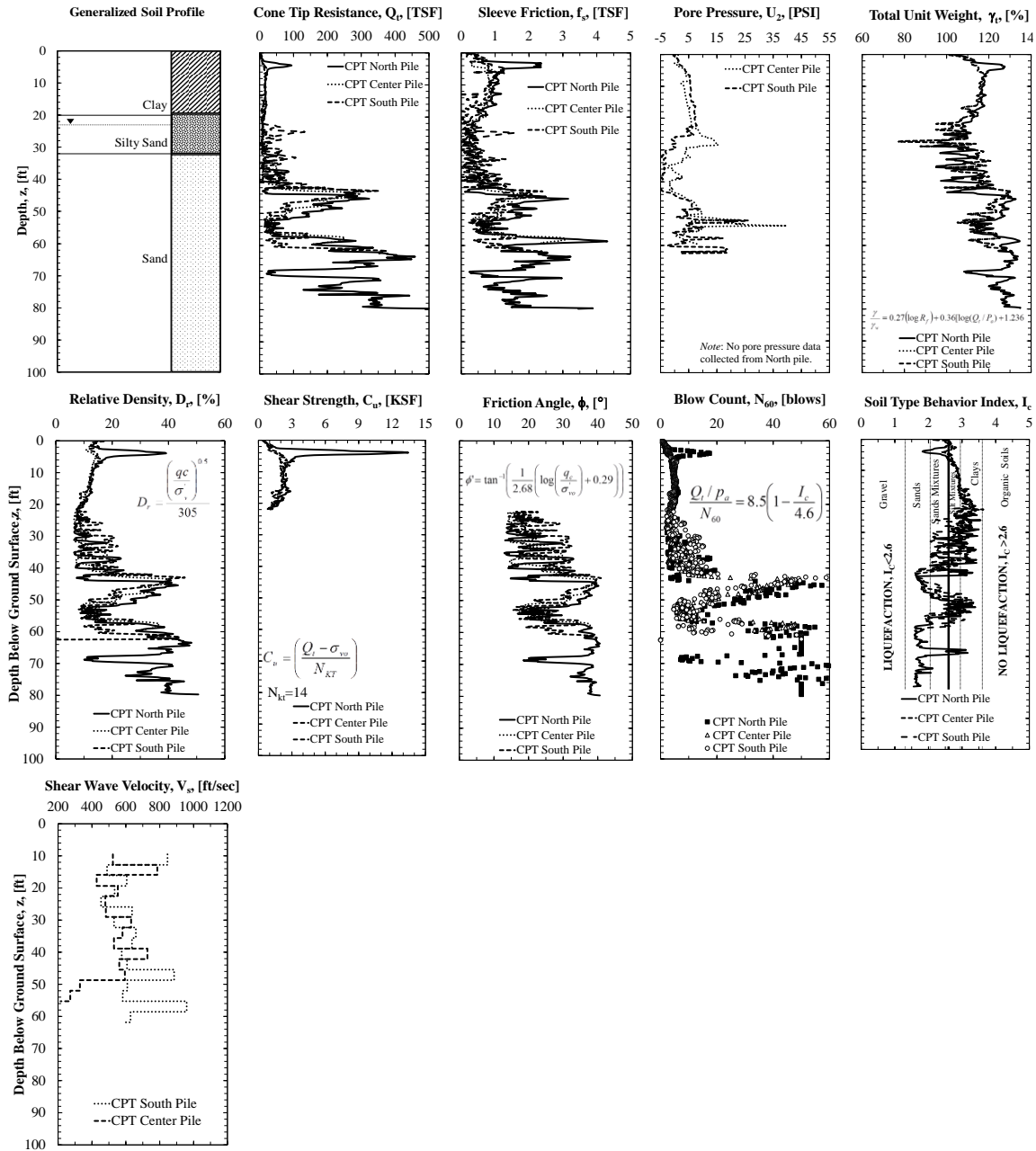


**Figure B.2.** Generalized soil profile, CPT measurements, total unit weight, relative density, shear strength, friction angle, SPT- $N_{60}$  and the soil index behavior correlated from these CPT measurements at the driven piles locations.

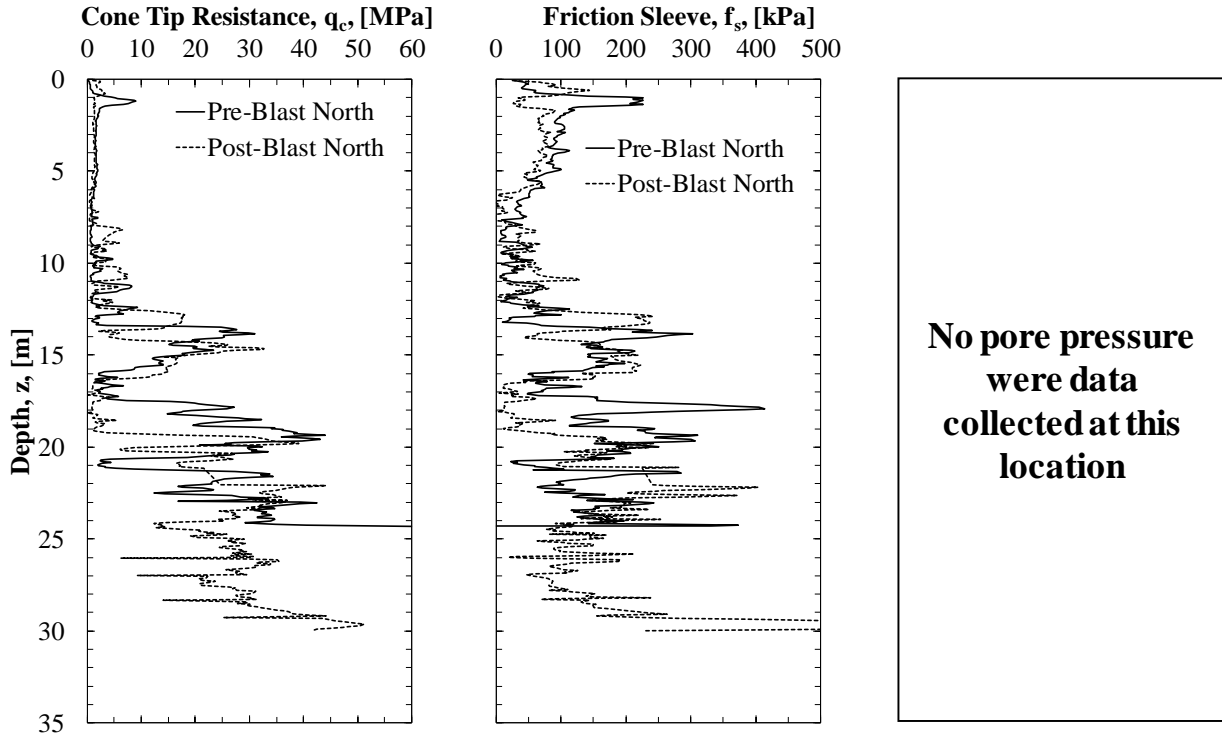


**Figure B.3.** Pre-and post-blast CPT measurements from the northern testing location.

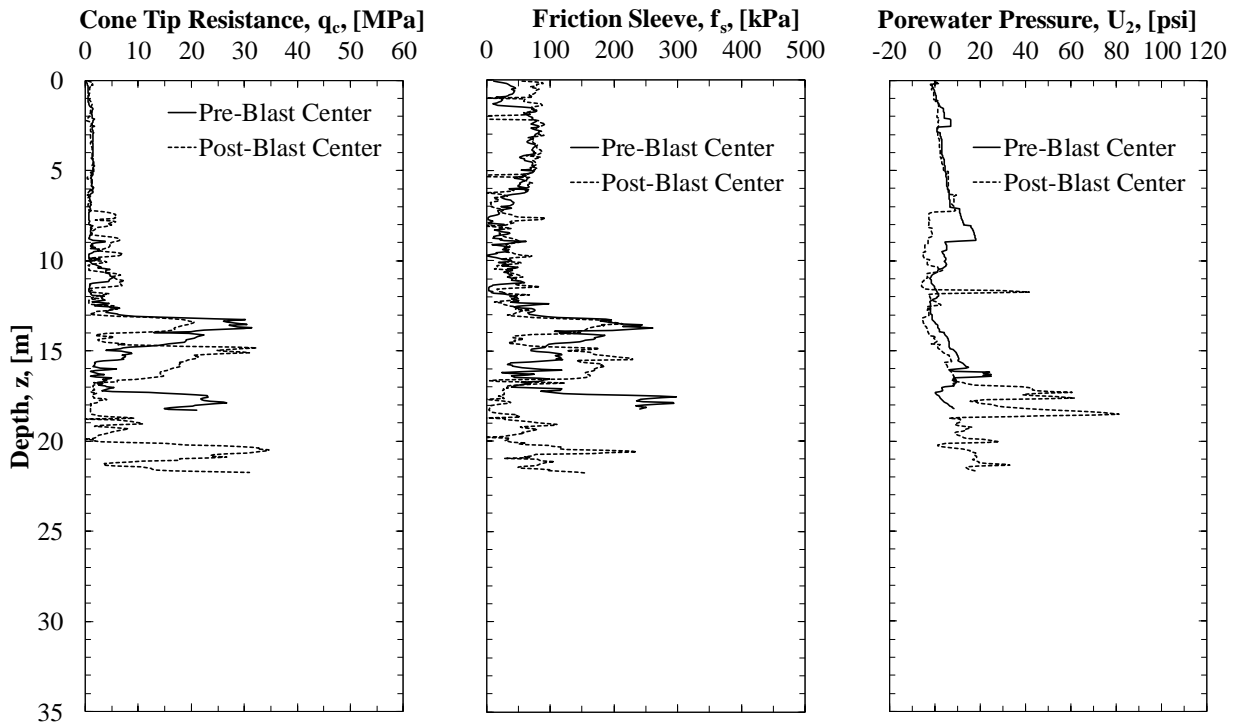


**Figure B.4.** Pre-and post-blast CPT measurements from the center testing location.

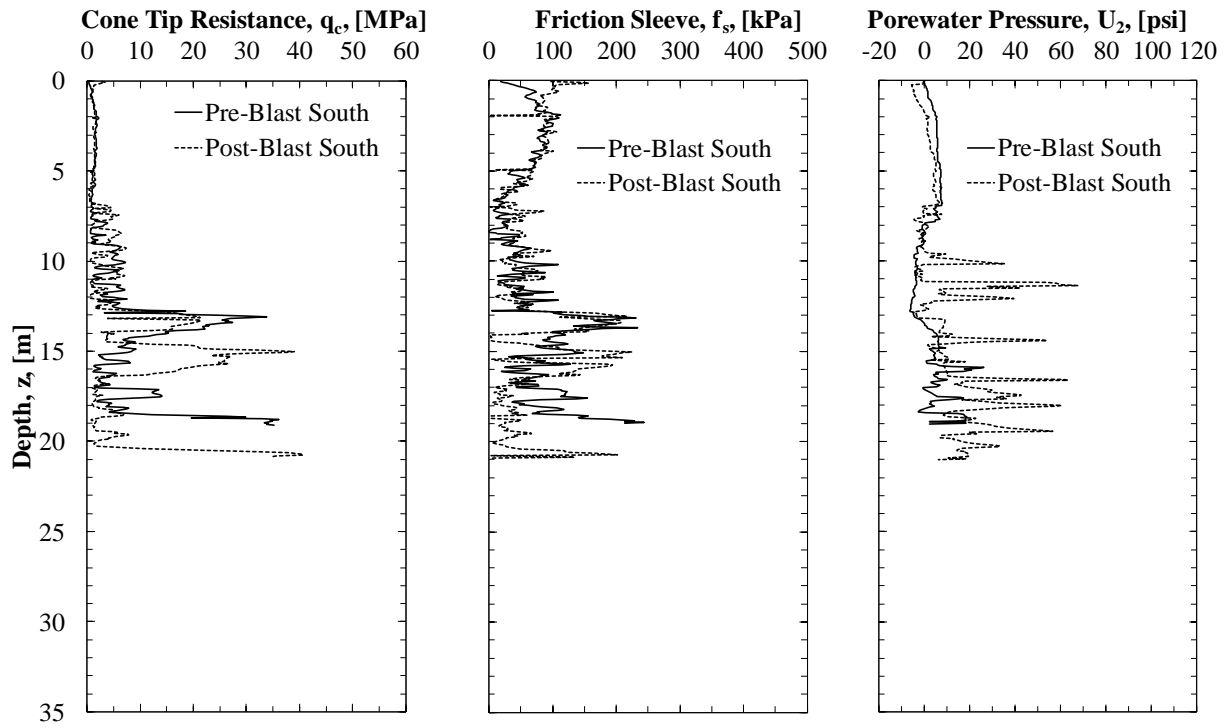


**Figure B.5.** Pre-and post-blast CPT measurements from the southern testing location.

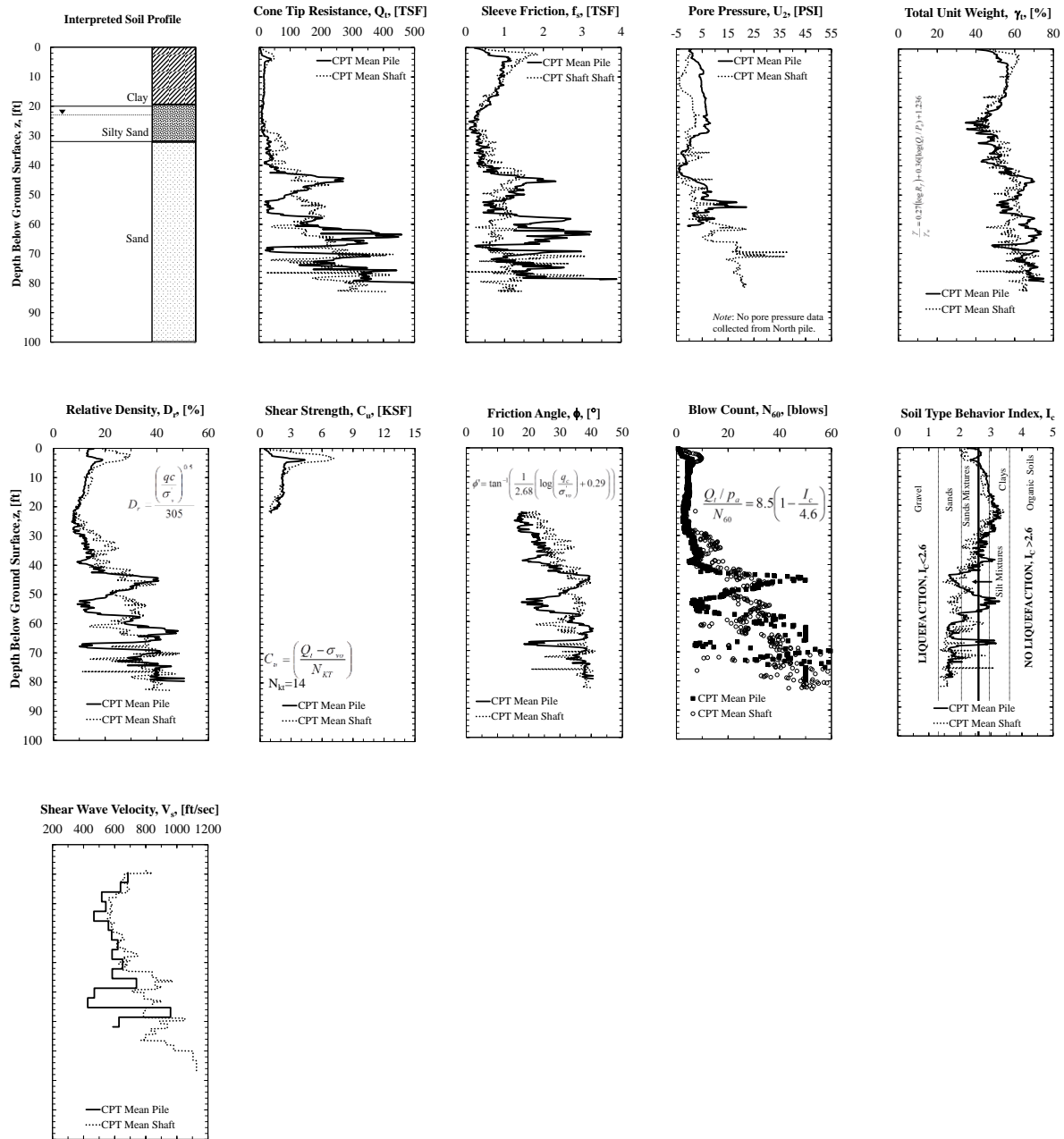


**Figure B.6.** Generalized soil profile of the TATS and comparison between CPT data collected around drilled shaft and driven pile foundations.

## APPENDIX C: Porewater Pressure Data

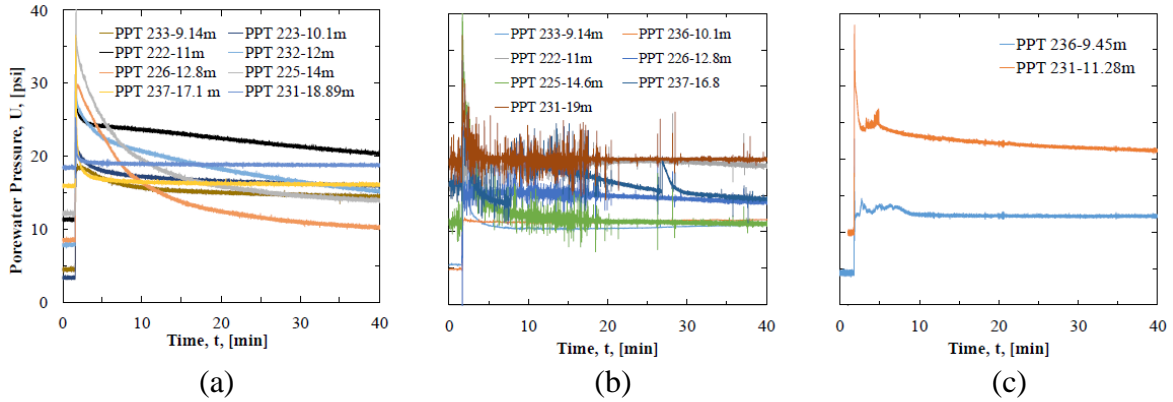


**Figure C.1.** Measured excess porewater pressure as a function of time, as obtained from: (a) north, (b) center (c) south drilled shafts, respectively.

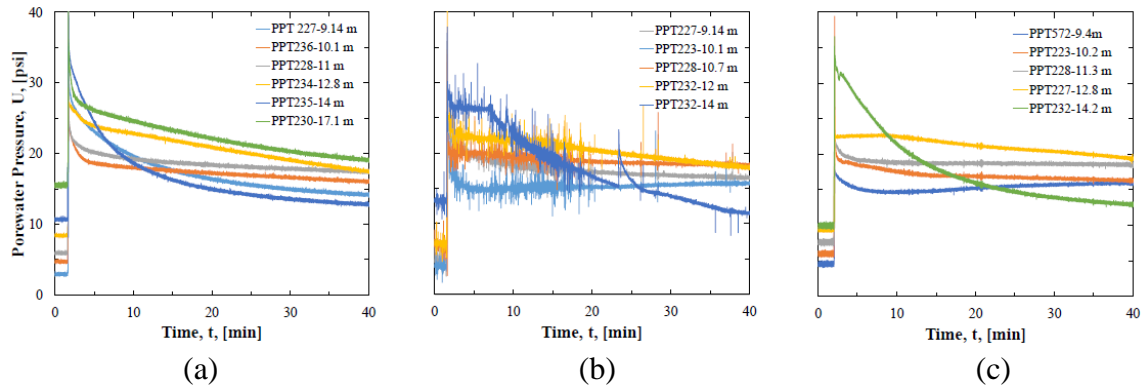


**Figure C.2.** Measured excess porewater pressure as a function of time, as obtained from: (a) steel H-pile, (b) Steel pipe (c) prestressed concrete pile, respectively.

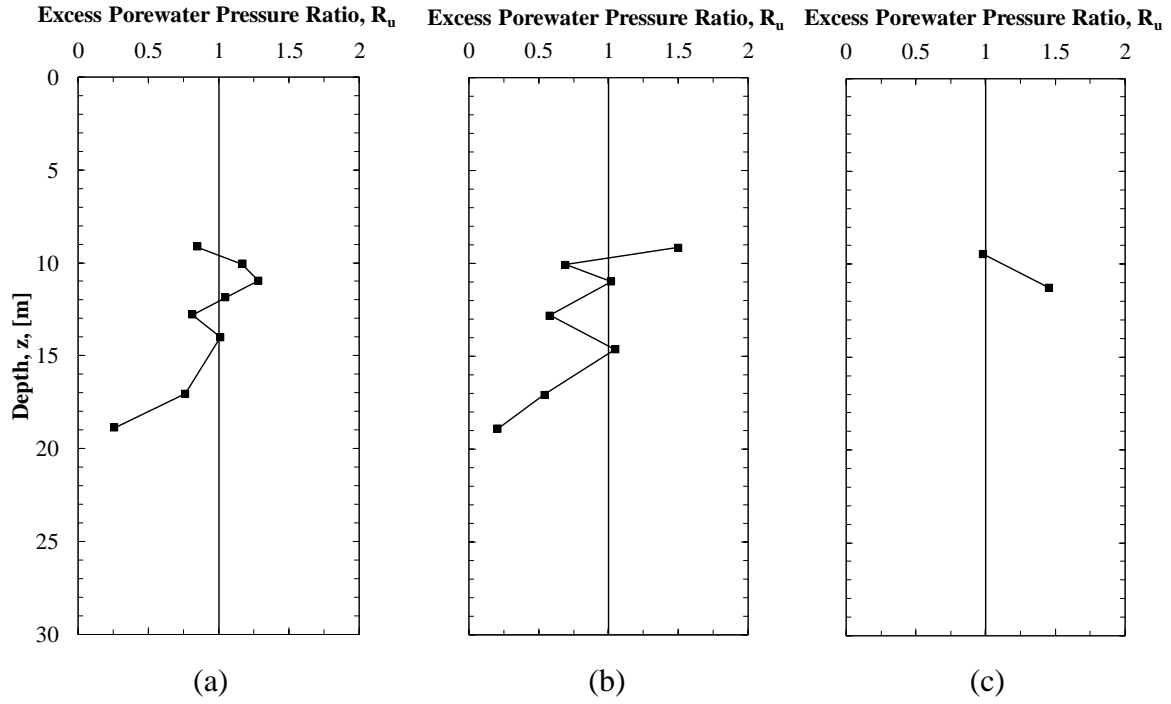


**Figure C.3.** Measured excess porewater pressure ratio as a function of depth, as obtained from: (a) north, (b) center (c) south drilled shafts, respectively.

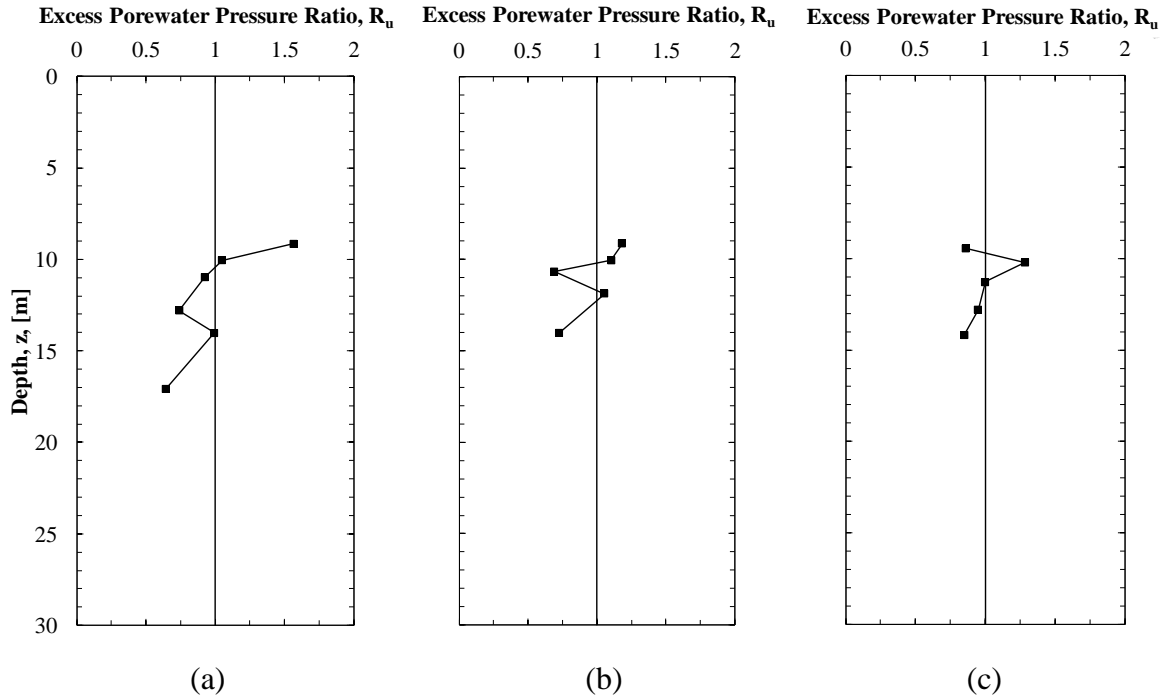


**Figure C.4.** Measured excess porewater pressure ratio as a function of depth, as obtained from: (a) steel H-pile, (b) Steel pipe (c) prestressed concrete pile, respectively.



## APPENDIX D: Alternative Approach for Liquefaction-induced Dragload

The following alternative approach is suggested for calculating dragload when a full-scale load test has been previously performed on piles or shafts at a project site. The measured Q-z and t-z curves are utilized to determine the amount of load/resistance per unit length of the foundation for a given amount of soil and pile settlement that have been predicted. The soil settlement should be predicted using the Lee (2007) approach and the pile settlement is predicted using the Briaud and Tucker (1997) approach. After the relative amount of settlement between the foundation and soil is determined, the amount of end bearing resistance is determined from the Q-z curve, as shown in Figure D.1. This aforementioned amount of settlement is also used to determine the amount of side resistance for the bottom segment using the obtained t-z curve. Using compatibility and accounting for elastic compression ( $\delta_{el}$ ), the amount of elastic compression within this interval is determined and added to the amount of relative settlement to compute the amount of side resistance for the next segment.

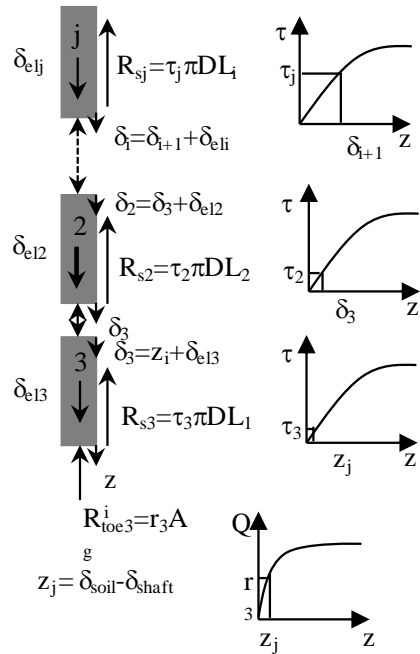


**Figure D.1.** A schematic of the alternative approach for liquefaction-induced dragloads.

The process is repeated until the top of the foundation is reached. The resistance curve is determined by adding the summation of the side resistance to the end bearing from the bottom of the shaft to the top of the shaft. Likewise, the load curve is developed by adding the summation of the side resistance to the structural load that is applied to the top of the shaft. For the North drilled shaft, the side shear component of the load and resistance curves that were produced using this methodology were 25-percent larger than the measured curves Figure . For the Center drilled shaft, the side shear component of the load and resistance curves that were predicted using this methodology were 20-percent larger than the measured curves. These predicted curves are anticipated to be larger than measured curves because of the time-dependent nature of the consolidation process. The developed Q-z and t-z curves along with the , the amount of toe resistance, side resistance and the settlement for each segment for the North and Center drilled shafts are shown in Figure D.2, and D.3, respectively. Further details regarding the development of Q-z and t-z curves can be found in Race (2015). The post-liquefaction load and resistance curves that were predicted using this alternative approach are shown in Figures D.4, D.5, for the North and Center drilled shafts, respectively.

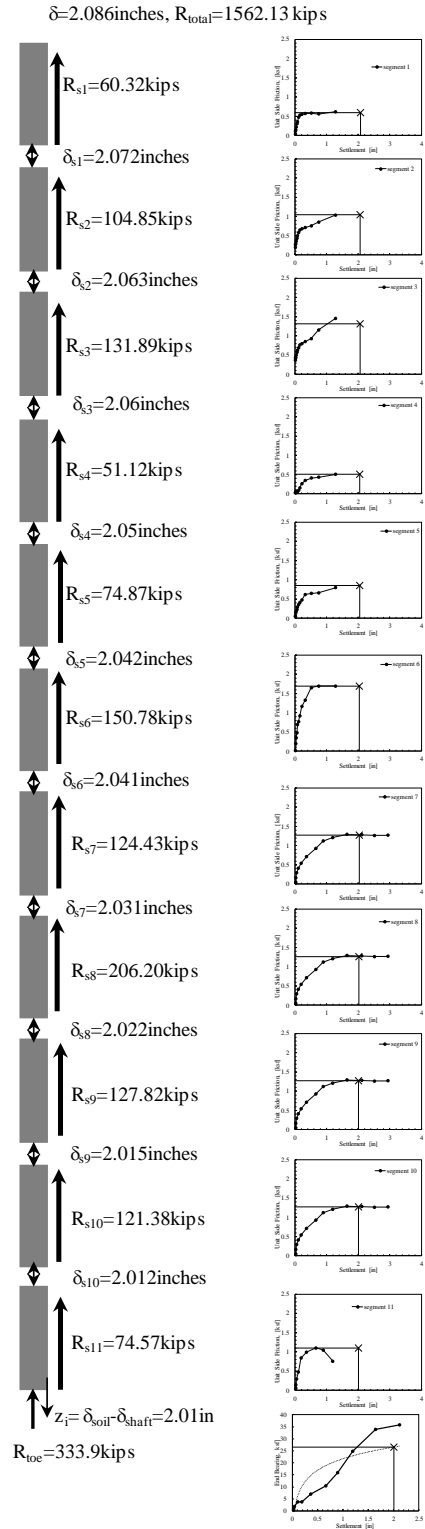


**Figure D.2.** Developed Q-z, t-z curves, the amount of toe resistance, side resistance and the settlement developed around the North drilled shaft.

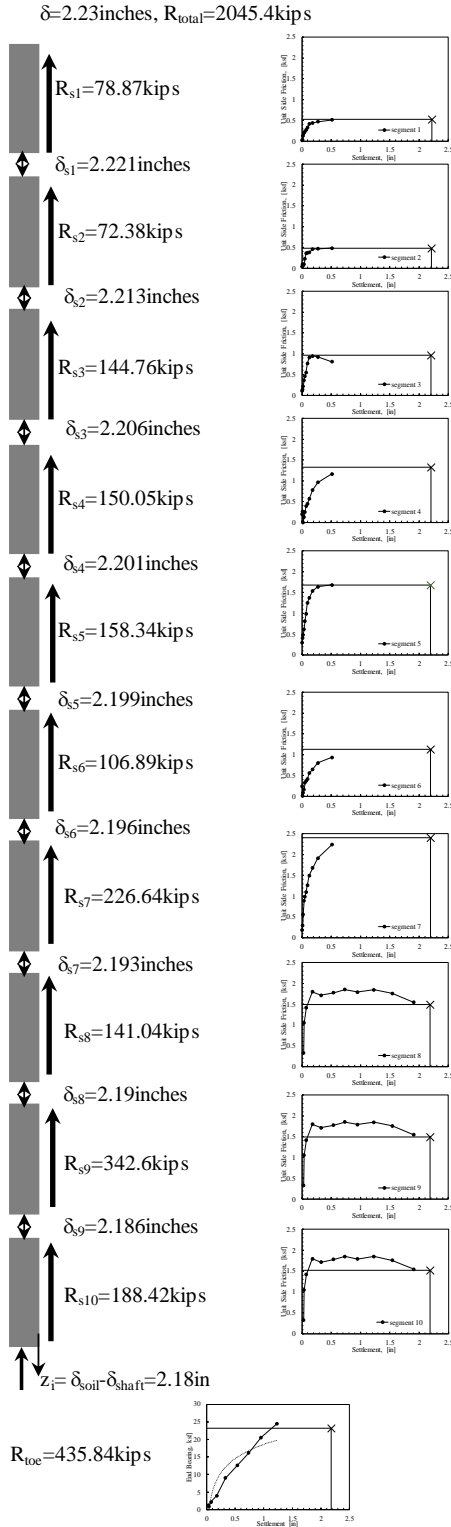


**Figure D.3.** Developed Q-z, t-z curves, the amount of toe resistance, side resistance and the settlement developed around the Center drilled shaft.

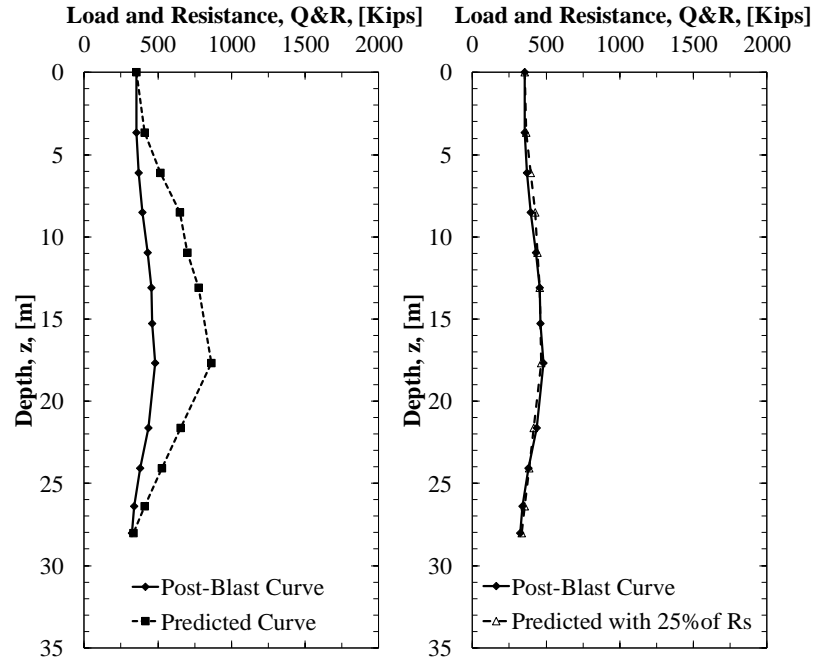


**Figure D.4.** A comparison between the post-blast and predicted load and resistance distribution curves, as obtained for North drilled shaft.

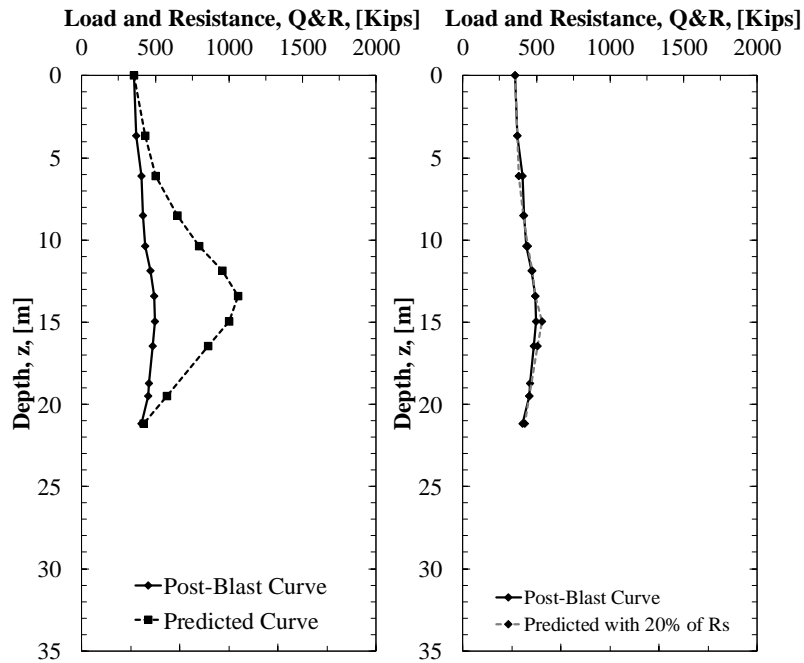


**Figure D.5.** A comparison between the post-blast and predicted load and resistance distribution curves, as obtained for Center drilled shaft.